



City Research Online

City, University of London Institutional Repository

Citation: Parker, S. J. (1985). Electric spark ignition of gases and dusts. (Unpublished Doctoral thesis, The City University)

This is the accepted version of the paper.

This version of the publication may differ from the final published version.

Permanent repository link: <https://openaccess.city.ac.uk/id/eprint/35456/>

Link to published version:

Copyright: City Research Online aims to make research outputs of City, University of London available to a wider audience. Copyright and Moral Rights remain with the author(s) and/or copyright holders. URLs from City Research Online may be freely distributed and linked to.

Reuse: Copies of full items can be used for personal research or study, educational, or not-for-profit purposes without prior permission or charge. Provided that the authors, title and full bibliographic details are credited, a hyperlink and/or URL is given for the original metadata page and the content is not changed in any way.

A THESIS ENTITLED
ELECTRIC SPARK IGNITION OF GASES AND DUSTS

Assumptions, by crude and vain,
Full oft to use will Science bring;
The conqueror shall soon be cast away,
The swimmer soon shall cast away.

A.J.L. Clough, Poem.

Submitted for the degree of Doctor of Philosophy at the City University, London

The City University
Department of Chemistry
August 1985

dedicated to the memory of my mother.

CONTENTS

	<u>Page</u>
Contents	i
List of figures and illustrations	ii
List of photographs	iv
List of tables	vi
Acknowledgements	vii
Abstract	viii
I General Introduction	1
II Experiments	3
Part 1	3
Part 2	95
Part 3	131
III General Conclusions	267
References	231
Appendix 1 Component values	A1
Appendix 2 Spark energy calculation programme and listing of variables	A4
Appendix 3 Notes on spark discharge tests	A13
Appendix 4 Schlieren techniques used in this work	A17
Appendix 5 Details of the powders used in the dust-ignition tests	A33

A.H. Clough, Poem.

Dedicated to 

CONTENTS

	<u>Page</u>
CONTENTS	i
List of figures and illustrations	ii
List of photographs	v
List of tables	vi
Acknowledgements	vii
Abstract	viii
I General Introduction	1
II Experimental work	5
Part 1 The electric spark generator	5
Part 2 Gas ignition studies	95
Part 3 Dust ignition studies	131
III General Conclusions	247
References	251
Appendix 1 Component values	A1
Appendix 2 Spark energy computation programme and listing of variables	A6
Appendix 3 Notes on spark discharge form	A13
Appendix 4 Schlieren techniques used in this work	A17
Appendix 5 Details of the powders used in the dust-ignition tests	A33

LIST OF FIGURES AND ILLUSTRATIONS

	<u>Page</u>	
<u>PART 1</u>		
I-1	Block diagram of a typical modulator circuit	14
I-2	Block diagram of the basic spark generator circuit	16
I-3	Lumped circuit analogue of an equivalent transmission line	19
I-4	Terminated transmission line	22
I-5,6,7	Current and voltage pulses for a lossless transmission line discharging into a resistance load	26, 27
I-8,9,10	Measured spark voltage and current pulses for a 4 mm spark gap	30
I-11	Block diagram of the spark generator system	35
I-12	Schematic diagram of 1st thyatron (T1) circuitry	39
I-13	Schematic diagram of 2nd thyatron (T2) circuitry	40
I-14	'Heater supply' circuitry	41
I-15	'Thyatron supply' circuitry	42
I-16	Basic thyatron trigger circuit	45
I-17	Modified thyatron trigger circuit	45
I-18,19	Measured trigger pulses	45
I-20	'Transformer supply' circuitry	47
I-21	Clock system and common power supply for the ACS and ACPU units	50
I-22	Channel one circuitry for the ACS timing unit	51
I-23	Triggering circuitry for the ACS timing unit	52
I-24	Pulse timing and triggering circuitry for the ACPU timing unit	53
I-25	Output interface switching circuitry for each ACPU channel	54
I-26	The optical transmitter circuit	56
I-27	The optical receiver circuit	56
I-28	The gap arrangement showing matching resistor	58
I-29	Simulated spark voltage pulse	67
I-30	Measured pulse	67
I-31-34	Measured waveforms showing the effects of using ferrite cores in the ground return path	69
I-35,36	Spark measurements showing separation of circuit noise	72
I-37	Calibration test results using fixed voltage sources	75
I-38	Open-circuit voltage measurements	81
I-39	Short-circuit voltage measurements	81
I-40,41	Spark energy and duration as functions of line voltage for a chosen PFN	83
I-42,43	Spark energy and duration as functions of matching resistance for three chosen PFN's	83
I-44,45	Spark energy and duration as a function of the number of PFN sections for a chosen PFN configuration	84-85
I-46,47	Relationship between spark energy and gap width using two PFN configurations	87
I-48-50	Gap voltages and spark measurements for three gap widths and one PFN	88
I-51,52	Spark measurements showing the effect of increasing circuit resistance, causing a change in discharge type, for a chosen PFN	90
I-53-57	Spark voltage measurements for a capacitive-discharge circuit, showing the effect of increasing circuit resistance	91
I-58	Physical limitations on spark energy as a function of spark duration and gap width	92

PART 2

II-1,2	Spark data acquisitions showing 'square' and 'decaying' power \rightarrow time relationships	102
II-3	Schematic diagram of the gas mixing system	104
II-4	Cross section of the gas mixer	106
II-5	Ignition results using a 2 mm gap	109
II-6	Ignition results using a 4 mm gap	110
II-7	Ignition results using a 7 mm gap	111
II-8	Kernel sizes for two sparks in the gas mixture using a 2 mm gap	114
II-9	Kernel sizes for three sparks in air using a 4 mm gap	117
II-10	Kernel sizes for a 2.35 mJ spark both in air and in the gas mixture	117
II-11	Kernel sizes for three sparks in the gas mixture using a 7 mm gap	119
II-12	Figure showing basis of comparison of kernel sizes	119
II-13	Kernel sizes for three sparks of similar energies and durations in the gas mixture	121
II-14	Figure showing the effect of altering spark energy and duration on the kernel expansion for a 7 mm gap width	123
II-15	A comparison of MIE curves using capacitive and pulse circuits	127

PART 3

III-1	Dispersion tube assembly for dust-cloud ignition experiments	142
III-2	Cross-section of dust cloud ignition apparatus	143
III-3	Schematic diagram of the dust dispersion system	144
III-4	Spark triggering and dust dispersion timing diagram	145
III-5	Complete timing diagram showing schlieren camera triggering	148
III-6	Ignition probabilities using three sparks as a function of mass of dispersed powder	153
III-7-10	Ignition probabilities as a function of three values of mass of dispersed powder for one spark	154
III-11	Ignition probabilities as a function of ignition delay time t for three sparks	155
III-12	Timing diagram for the second (double) dispersion method	156
III-13	Ignition probabilities using three sparks as a function of mass of dispersed powder	157
III-14	Ignition probabilities as a function of ignition delay time t and second dispersion duration t_D	158
III-15-16	Distributions of dust particles in the explosion vessel for both dispersion methods	160
III-17-22	Check-point comparisons of ignition probabilities using both dispersion methods	161,162
III-23-25	Spark energy measurements using single and double dispersion	165
III-26-27	Measured spark energies and durations as a function of dispersion for three gap widths	166
III-28-30	Spark energy measurements for three gap widths	167
III-31-36	Results of ignition tests for the stabiliser powder, for three gap widths and both dispersion methods	168-170
III-37-39	Results of ignition tests for the stabiliser powder, showing 'ignition uncertainty regions' for three gap widths	172,174,176

LIST OF FIGURES AND ILLUSTRATIONS cont.

	<u>Page</u>
PART 3 cont.	
III-40	Second explosion vessel for studying downstream ignition 179
III-41	Simplified model of ignition for both dispersion methods 206
III-42-43	Kernel sizes and expansion velocities for three sparks and two gap widths 210
III-44-45	Kernel sizes and expansion velocities for three sparks and a 4 mm gap width 212
III-46-47	Kernel sizes and expansion velocities for three sparks and a 4 mm gap width 215
III-48	Ignition results for Benzanthron 218
III-49	Ignition results for Lycopodium 218
III-50	Ignition results for PAN 220
III-51-52	Kernel sizes and expansion velocities for one spark and the four tested powders 222
III-53	The three-electrode capacitive spark discharge circuit 228
III-54	Generalised results for the stabiliser, lycopodium and PAN, showing the 'ignition boundary' 233
III-55	Generalised results for the stabiliser and Benzanthron, showing the 'ignition boundary' 234
III-56	A generalised model of the spark kernel to flame kernel transition, showing the increase in temperature at the kernel front due to combustion 235
III-57	Minimum stored energy for ignition of magnesium and aluminium clouds (results from Boyle and Llewellyn) 237
III-58	Minimum ignition energy for tapioca and flour clouds (results from Van Laar) 237
III-59	Minimum ignition energy for melamin, peameal and lycopodium clouds (results from Glarner) 237
APPENDICES	
A1-A2	Discharge voltages and currents showing the various discharge phases A14
A3	Basic schlieren set-up A18
A4	Schlieren set-up using a still camera A20
A5	Circuit diagram of light-flash schlieren system A21
A6	Schlieren set-up using a high-speed camera A25
A7	Interference test set-up A27
A8	Effects of schlieren lens L3 aberrations A31
A9	Test set-up showing the appearance of interference lines A32
A10	Coulter-counter results for the stabiliser powder A36
A11	Coulter-counter results for the PAN powder A36
A12	Coulter-counter results for the Benzanthron powder A37
A13	Coulter-counter results for the Lycopodium powder A37
A-1.2	Scanning electron microscope photographs for the stabiliser powder A39
A-3.4	Scanning electron microscope photographs for the PAN powder A39
A-5.6	Scanning electron microscope photographs for the Benzanthron powder A40
A-7.8	Scanning electron microscope photographs for the Lycopodium powder A40

LIST OF PHOTOGRAPHS

Page

PART 1

I-1	Thyratron supply and triggering equipment	61
I-2	Timing units	61
I-3	Optical transmitter	61
I-4-6	Examples of the use of the clipping circuitry	78

PART 2

II-1	The explosion bomb used for gas ignition tests	105
II-2	The explosion bomb and gas mixture	105
II-3-4	Schlieren photographs of two sparks in 2.7 % propane-air using a 2 mm gap	113
II-5-6	Schlieren photographs of two sparks in air using a 4 mm gap	116
II-7	Schlieren photographs of one spark in 2.7 % propane-air using a 4 mm gap	118
II-8-9	Schlieren photographs of two sparks in 2.7 % propane-air using a 7 mm gap	118

PART 3

III-1-4	Layout of experimental apparatus for the dust ignition work	146,147
III-5-6	High-speed photographs of dust distribution in the spark gap	152
III-7-9	Schlieren photographs of a 4 mJ spark in air and in the stabiliser cloud	184
III-10-11	High-speed photographs of ignition of the stabiliser powder using a 4 mJ spark	186
III-12	Schlieren photographs of two sparks in the stabiliser cloud of similar energies and durations using 2 mm and 4 mm gaps	188
III-13	Schlieren photographs of two sparks in the stabiliser cloud using a 2 mm gap	190
III-14	Schlieren photographs of three sparks in air using a 4 mm gap	192
III-15	Schlieren photographs of three sparks in the stabiliser cloud using a 4 mm gap	193
III-16	Schlieren photographs of two sparks in the stabiliser cloud using 2 mm and 4 mm gaps	195
III-17	Schlieren photographs of a single spark in the stabiliser cloud where ignition is successful and unsuccessful	197
III-18	Schlieren photographs of a single spark in the stabiliser cloud and in Benzanthron, lycopodium and PAN, for a 4 mm gap	221
III-19-21	Current traces for capacitive discharges with and without added series inductance	230

APPENDICES

A-1,2	Scanning electron microscope photographs for the stabiliser powder	A39
A-3,4	Scanning electron microscope photographs for the PAN powder	A39
A-5,6	Scanning electron microscope photographs for the Benzanthron powder	A40
A-7,8	Scanning electron microscope photographs for the Lycopodium powder	A40

LIST OF TABLES

ACKNOWLEDGEMENTS

Page

PART 3

III-1	Ignition results using a capacitive discharge circuit and the stabiliser powder	228
III-2	Ignition results using a capacitive discharge circuit and the Benzanthron powder	229

APPENDICES

A1	Coulter-counter undersize measurements	A35
A2	Ströhlein and density measurements	A35
A3	Hartmann-bomb results	A38

I wish to acknowledge the financial support from The Royal Norwegian Council for Scientific and Industrial Research and the Swedish Fire Research Board, and thank Ing. Braathen from FFJ for the loan of the high-speed camera. Furthermore, I wish to thank Doc. R.S. Sigmond from NTNI for helpful discussions and my supervisors Professor Cullis and Professor Burgoyne at City University for their help and interest.

Finally, I wish to acknowledge a good friend, Anastasios Simos, for his moral support.

I hereby grant powers of discretion to the University Librarian to allow this thesis to be copied in whole or in part without further reference to me. This permission covers only single copies made for study purposes, subject to normal conditions of acknowledgment.

This thesis describes a study of the effect of independent variation of spark energy and duration on measured minimum ignition energies, spark-to-flame kernel expansion times, and four dust clouds.

ACKNOWLEDGEMENTS

This research was conducted at the Christian Michelsen Institute in Bergen, and I am indebted to the staff of the Institute for their help and support. In particular I would like to acknowledge [redacted] for having suggested the topic, and for his help as the work progressed. I would also like to thank [redacted] for her endless patience when typing the manuscript, and [redacted] for her help with some of the drawings. Thanks are also due to [redacted] [redacted] for his help with the SEM-photographs.

I wish to acknowledge the financial support from The Royal Norwegian Council for Scientific and Industrial Research and the Swedish Fire Research Board, and thank [redacted] from FFI for the loan of the high-speed camera. Furthermore, I wish to thank [redacted] from NTH for helpful discussions and my supervisors Professor Cullis and Professor Burgoyne at City University for their help and interest.

Finally, I wish to acknowledge [redacted], for his moral support.

I hereby grant powers of discretion to the University Librarian to allow this thesis to be copied in whole or in part without further reference to me. This permission covers only single copies made for study purposes, subject to normal conditions of acknowledgement.

ABSTRACT

This thesis describes a study of the effect of independent variation of electric spark energy and duration on measured minimum ignition energies, for a quiescent gas mixture, and four dust clouds.

To enable such a study, a spark generator was designed and constructed, based on a pulse-modulator principle, that could produce arc-type discharges, of controlled energy and duration, and on a reproducible basis. Particular emphasis was placed on the so-called 'low-energy' range, from 0.1 mJ to 20 mJ, where the control of discharge parameters has often been difficult with other discharge circuits.

The fuels chosen for this study were 2.7 % propane-air, a commercial stabiliser powder, Benzanthron, lycopodium and polyacrylonitrile. Of these, the first three were found to ignite below 1 mJ. The ability to ignite dust clouds with spark energies as low as those for hydrocarbon gas-air mixtures was therefore confirmed.

Ignition tests using the gas mixture, where spark-to-flame kernel expansion was studied with a schlieren technique, showed that ignition could be achieved using energies that were an order of magnitude lower than those using traditional capacitive circuits. This result was explained in terms of the increased efficiency in the thermalisation of spark energy using a pulse-circuit, where the rate of energy release in the gap was higher than for a capacitive circuit, for which spark duration is increased using resistive elements.

Ignition tests using the four dust clouds, dispersed in a specially constructed explosion vessel, were made together with high-speed schlieren photographs of the spark-to-flame kernel expansion. Results showed that for a given dust, an optimum spark duration existed at which ignition energy was at a minimum. This was found to coincide with an optimum rate of spark-kernel expansion following discharge. The differences in optimum values of minimum spark ignition energies and durations, between the four powders, were interpreted in terms of the 'induction times' of the constituent particles. These times depended upon the chemical composition and physical size and shape of the particles.

The dust-ignition work concludes with a simplified model of the spark-ignition process, assuming that a critical energy density in the spark/flame kernel is required for ignition. Both the present results and those from the literature are discussed on the basis of this model. This is shown to account for the general observation that 'pure' capacitive discharges must be of higher energies than those produced when using series resistance or inductance in a capacitive circuit.

The existence of an optimum rate of kernel expansion, at which spark ignition energy was at a minimum, indicated an optimum rate of energy release in the spark gap. As a unique relationship between rate of energy release and spark duration does not exist when comparing different discharge circuit configurations, it was proposed that 'rate of energy release', rather than 'spark duration', be used as a criterion for measuring minimum ignition energies.

Finally, it is suggested that a fuel be designated two values of minimum ignition energy, one representing a 'hazard assessment' value based on capacitive discharges, and one representing the 'absolute sensitivity' to ignition by a spark discharge.

... every word or concept, clear as it may seem to be, has only a limited range of applicability."

Werner Heisenberg

The electric spark has been widely exploited as an ignition source in combustion studies and applications since around the turn of this century. But just as an electric spark may be harnessed as an ignition source, so it can also cause ignition where this is undesirable. Potential fire and explosion risks are known to exist, for example, where a combustible medium is present and where an electric spark may develop in its vicinity.

I GENERAL INTRODUCTION

The term 'electric spark' has come to describe a great number of naturally-occurring processes of electrostatic origin, and also describes discharges produced from breaks in electrical circuits (so-called 'inductive break-flashes'). The extreme difficulty experienced in studying spark phenomena has meant that no universally accepted definition exists of an 'electric spark'. It can best be thought of as the transition between two more or less stable forms of gaseous conduction, involving a transient transfer of electric charge. Because of this rather loose definition, it has been used to describe a wide variety of phenomena from 'brush', 'corona', and 'arc' discharges, for example, through to lightning strokes.

Despite the widespread occurrence of various forms of electric sparks, their efficiency as ignition sources, or their 'incendivity', has not been critically defined. Thus, the risk (or success) of ignition of a given combustible medium, also lacks a clear definition. The most commonly used term that defines a spark's incendive nature is the 'minimum ignition energy' (MIE). This refers to the least value of energy discharged in a spark that will just cause ignition of a given fuel. This term does not, however, directly represent the incendive feature of a spark, but rather defines the sensitivity to ignition of a fuel under a given set of conditions, which would include the manner in which the spark energy is discharged in time and space. Such conditions would also include the physical state of the fuel at the moment the spark occurs. This means that, if one is to be more specific, one should categorically state the electrical and physical features of an electric spark that cause it to be incendive. Only when such measures are taken can one state the usefulness of a spark as an ignition source.

GENERAL INTRODUCTION

" . . . every word or concept, clear as it may seem to be, has only a limited range of applicability."

Werner Heisenberg

The electric spark has been widely exploited as an ignition source in combustion studies and applications since around the turn of this century. But just as an electric spark may be harnessed as an ignition source, so it can also cause ignition where this is undesirable. Potential fire and explosion risks are known to exist, for example, where a combustible medium is present and where an electric spark may develop in its vicinity.

The term 'electric spark' has come to describe a great number of naturally-occurring processes of electrostatic origin, and also describes discharges produced from breaks in electrical circuits (so-called 'inductive break-flashes'). The extreme difficulty experienced in studying spark phenomena has meant that no universally accepted definition exists of an 'electric spark'. It can best be thought of as the transition between two more or less stable forms of gaseous conduction, involving a transient transfer of electric charge. Because of this rather loose definition, it has been used to describe a wide variety of phenomena from 'brush', 'corona', and 'arc' discharges, for example, through to lightning strokes.

Despite the widespread occurrence of various forms of electric sparks, their efficiency as ignition sources, or their 'incendivity', has not been critically defined. Thus, the risk (or success) of ignition of a given combustible medium, also lacks a clear definition. The most commonly used term that defines a spark's incendive nature is the 'minimum ignition energy' (MIE). This refers to the least value of energy discharged in a spark that will just cause ignition of a given fuel. This term does not, however, directly represent the incendive feature of a spark, but rather defines the sensitivity to ignition of a fuel under a given set of conditions, which would include the manner in which the spark energy is discharged in time and space. Such conditions would also include the physical state of the fuel at the moment the spark occurs. This means that, if one is to be more specific, one should categorically state the electrical and physical features of an electric spark that cause it to be incendive. Only when such measures are taken can one state the usefulness of a spark as an ignition source.

In the field of risk and hazard assessment, the 'sensitivity to ignition' of a combustible medium is studied almost exclusively with the aid of electric sparks. The reasons for this include their ease of production (compared to other ignition sources), their highly localised heating effect in short durations as well as over a wide energy range, and their relevance to practically-occurring discharges.

It is undoubtedly the last of these factors that has led to the widespread acceptance of the electric spark as an ignition source in the laboratory. For these purposes, a simple capacitive-discharge circuit is traditionally used, where a spark's 'incendivity' is determined in terms of the energy stored in the capacitor, or that discharged in the spark gap. However, because of the wide range of naturally-occurring discharges, it is unreasonable to suppose that a single, simple circuit such as this can establish the absolute sensitivity to ignition of a combustible by 'electric sparks' generally. Despite this clearly unsatisfactory situation, capacitive-type circuits still form the basis of ignition sensitivity tests today. The term 'minimum ignition energy' has, as a result, become internationally accepted as a measure of ignitability, whereas in fact it only reflects one aspect of an electric spark. It may be thought of as the only common factor that may readily be determined for various forms of discharge that expresses the efficiency of a given spark, even though the actual processes of ignition may be unknown.

Had the processes of ignition by electric discharges been easier to study, one might expect that other terms associated with the discharge would have been adopted to describe the 'sensitivity to ignition' by electric sparks. In particular, there has not been, until very recently, any attempt at investigating the thermalisation process of electric sparks when they are produced in combustible mixtures. This has meant that any observations relating the electric spark to the ignition process have usually been made without considering the conversion of electrical energy to the heat energy required for ignition. It has also meant the continued use of 'MIE' and other terms associated with the discharge circuit and its layout.

One aspect of spark discharges that has been found to influence incendivity, and thus MIE, is the discharge duration. This has been found using both gas mixtures and dust clouds. This, in turn, is often expressed as a function of the added circuit impedance in a capacitive-discharge circuit. The explanation of such a duration dependence has usually assumed that increased energy losses from the spark during its formation and expansion lead to higher ignition energies at short durations, but the reasons for, and means of, energy loss have

not been properly quantified. Such assumptions have led to widely varying subjective opinions within the field.

The question of whether 'sensitive' dusts can be ignited by spark energies below 1 mJ has also been raised, as in such cases one would need to handle such materials with the same precautions as one would an hydrocarbon gas-air mixture. A study of this problem has relied upon the ability to produce, and reproduce, very low energy discharges in the laboratory under controlled conditions. A prevalent problem that has usually been raised, however, has not been the production of such low energies, but the ability to quantify and measure them.

The present work was, therefore, begun in an attempt to study the roles of 'minimum ignition energy' and 'discharge duration' on the spark ignition process, using a single gas mixture (2.7% propane-air) and four dust clouds, one of which was thought to be ignitable using energies as low as ~1mJ. This would hopefully lead to a more precise identification of the influential physical aspects of laboratory-generated electric sparks when utilised as ignition sources using these media. This, in turn, would lead to a more complete description of the properties of electric sparks that influence their igniting power, and hence, their application to the assessment of ignition hazards.

For these purposes, a spark generator was designed and constructed that could produce low energy arc discharges (0.1 mJ to 20 mJ), whereby energy and duration could be varied independently, while maintaining the rate of energy release approximately constant over the discharge duration. This task also required a careful analysis of the methods used to measure spark energy. Schlieren systems were also constructed to study the spark ignition process using the five combustible mixtures.

The experimental work is divided into three 'parts' which constitute Section II of this thesis. The first part describes the electric spark generator. The second part describes a study of spark duration and MIE using the gas mixture, where the success of ignition was related to the spark kernel development with time, as observed using Schlieren techniques. The third part describes similar tests using four dusts dispersed as clouds. Most of this work concentrated on the one particularly 'sensitive' dust, a commercially produced polymer powder, which was examined systematically, enabling comparative observations to be made on the other three. Each of these ignition studies concludes with a discussion of the spark ignition process, and how this is affected by varying the physical parameters associated with a spark discharge. Finally, Part III of the thesis brings together some general conclusions drawn from the experimental work.

CONTENTS

Page

I. INTRODUCTION	0
1.1 The demands placed on the new spark generator	8
1.2 Previous design limitations	9
1.3. Overcoming previous limitations using the new generator	9
1.3.1 Independent variation of duration and energy on a reproducible basis	9
1.3.2 Producing and controlling effects of stray capacitances	10
1.3.3 Operating voltage and timing	11
II EXPERIMENTAL WORK	
2. THE BASIS FOR THE DESIGN OF THE SPARK GENERATOR	14
2.1 PART I: THE ELECTRIC SPARK GENERATOR	14
2.2 Theory of operation	18
2.2.1 The equivalent transmission line	18
2.2.2 The terminated equivalent transmission line	21
2.2.3 The impedance transformation	23
2.2.4 Discharging a transmission line into a resistive load	24
2.2.5 Summary of theory	28
2.2.6 Applying the theory to the current work	28
2.2.6.1 Simulating an equivalent transmission line	28
2.2.6.2 Producing spark discharges based on the transmission line model	31
3. DETAILS OF THE GENERATOR CIRCUIT	34
3.1 Thyratrons and associated circuitry	34
3.1.1 The thyratrons	34
3.1.2 Thyatron 1, cathode end circuitry	37
3.1.3 Thyatron 1, anode end circuitry	37
3.1.4 Thyatron 2, cathode end circuitry	38
3.1.5 Thyatron 2, anode end circuitry	38
3.1.6 Thyatron triggering	38
3.1.6.1 Development and testing of the trigger circuit	38
3.1.6.2 The T1 and T2 trigger circuits	43
3.1.7 The grounded heater supply boxes	44
3.1.8 The grounded thyatron supply box	44
3.2 The isolation transformers and windings	46
3.2.1 The transformers	46
3.2.2 The transformer supplies	46
3.3 The main supply and grounding system	48
3.4 The timing units	48
3.5 The optical links	54
3.6 The gap arrangement	57
3.7 The PFD components	59
4. CONSTRUCTION AND LAYOUT	60

CONTENTS

Page

1. INTRODUCTION	8
1.1 The demands placed on the new spark generator	8
1.2 Previous design limitations	8
1.3. Overcoming previous limitations using the new generator	9
1.3.1 Independent variation of duration and energy on a reproducible basis	9
1.3.2 Producing low energy discharges and controlling effects of stray capacitances	10
1.3.3 Operating voltage and timing	11
2. THE BASIS FOR THE DESIGN OF THE SPARK GENERATOR	14
2.1 The generator principle	14
2.2 Theory of operation	18
2.2.1 The equivalent transmission line	18
2.2.2 The terminated equivalent transmission line	21
2.2.3 The impedance transformation	23
2.2.4 Discharging a transmission line into a resistive load	24
2.2.5 Summary of theory	28
2.2.6 Applying the theory to the current work	28
2.2.6.1 Simulating an equivalent transmission line	28
2.2.6.2 Producing spark discharges based on the transmission line model	31
3. DETAILS OF THE GENERATOR CIRCUIT	34
3.1 Thyratrons and associated circuitry	34
3.1.1 The thyratrons	34
3.1.2 Thyatron 1, cathode end circuitry	37
3.1.3 Thyatron 1, anode end circuitry	37
3.1.4 Thyatron 2, cathode end circuitry	38
3.1.5 Thyatron 2, anode end circuitry	38
3.1.6 Thyatron triggering	38
3.1.6.1 Development and testing of the trigger circuit	38
3.1.6.2 The T1 and T2 trigger circuits	43
3.1.7 The grounded heater supply boxes	44
3.1.8 The grounded thyatron supply box	44
3.2 The isolation transformers and supplies	46
3.2.1 The transformers	46
3.2.2 The transformer supplies	46
3.3 The mains supply and grounding system	48
3.4 The timing units	48
3.5 The optical links	54
3.6 The gap arrangement	57
3.7 The PFN components	59
4. CONSTRUCTION AND LAYOUT	60

I. INTRODUCTION

1.1 The demands placed on the new spark generator

A new system for producing and measuring electric sparks was built because of the limitations of many previous designs. Before these are discussed, demands that were made upon the present system are presented. The (ide Page should be able to:

5.	THE SPARK ENERGY MEASUREMENT SYSTEM	62
5.1	Background	62
5.2	The measurement equipment	64
5.2.1	The digitising system	64
5.2.2	Software for the digitising system	64
5.2.3	The probes	65
5.3	Features of the complete measurement system	66
5.3.1	Voltage waveform recording	66
5.3.1.1	Choice of voltage amplifier	66
5.3.1.2	Ground loops	68
5.3.2	Equipment calibrations	68
5.3.3	Waveform timing	70
5.3.4	Noise and shielding	71
5.3.5	Influence on generator circuit	73
5.4	System errors and accuracy	73
5.5	Calibration tests	74
6.	GENERATOR CALIBRATION TESTS	76
6.1	Introduction	76
6.1.1	Description of tests	76
6.1.2	Defining discharge duration	76
6.2	Example of circuit operation using the clipper circuitry	77
6.3	Open and short circuit tests	79
6.3.1	Description of tests	79
6.3.2	Open circuit test	79
6.3.3	Short circuit test	80
6.4	PFN tests	82
6.5	Gap-width tests	85
6.6	Physical limitations of the spark circuit	89
7.	CONCLUSIONS	93

1.2 Previous design limitations

The limitations of some previous generator designs, which the design of the present system intended to overcome, are listed below:

- a) An inability to trigger gap-breakdown at a specified moment in time.
- b) An inability to vary operation voltage (breakdown voltage) over a wide range.

1. INTRODUCTION

1.1 The demands placed on the new spark generator

A new system for producing and measuring electric sparks was built because of the limitations of many previous designs. Before these are discussed, demands that were made upon the present system are presented. The (ideal) system should be able to:

- a) Produce a single electric spark at a given instant.
- b) Produce electric sparks between fixed electrodes, whereby electrode-gap distance may be varied from 0 to 10 mm.
- c) Produce electric sparks of various nett energies, which can be varied from fractions of a millijoule to some joules.
- d) Produce electric sparks of any fixed energy but with durations that can be varied from fractions of a microsecond to some milliseconds.
- e) Produce electric sparks of any fixed energy and duration whereby the spark current either oscillates or is unidirectional, and where the rate of discharge of energy may be varied to some degree.
- f) Be capable of measuring the discharged spark energies to within an experimental accuracy of 10%.

These demands were made specifically with the current ignition work in mind, but were aimed at producing a generating/measuring system that was versatile enough to be used beyond the range of tests in this work. The complete system was therefore constructed as a general laboratory tool for spark ignition studies. In the tests that follow, only part of the complete system was used.

1.2 Previous design limitations

The limitations of some previous generator designs, which the designs of the present system intended to overcome, are listed below:

- a) An inability to trigger gap-breakdown at a specified moment in time.
- b) An inability to vary operation voltage (breakdown voltage) over a wide range.

- c) A limited ability to vary spark energy and duration independently.
- d) An inability to accurately reproduce spark-discharge parameters from one spark to the next.
- e) An inability to produce low energy sparks (0.1 - 10 mJ) with various durations.
- f) A lack of full control over circuit losses and effects of stray capacitances.
- g) Difficulties in accurately measuring the discharged spark energies in the spark gap, particularly for energies below 10 mJ.

Of these, the most significant limitation has been the control and measurement of spark energies, particularly below ~ 10 mJ. The reason for this has often been the over-simplification of the measurement circuit, which has not been carefully adapted to the spark generator. The matter of accurately measuring spark energies to give meaningful measurements is such a time-consuming exercise that many workers in the field^{1,2,3} have simply not analysed the problem in sufficient depth.

1.3 Overcoming previous limitations using the new generator

1.3.1 Independent variation of duration and energy on a reproducible basis

Most other previous designs of spark generators used for ignition tests have been severely limited by their dynamic range of operation. The ability to vary independently either energy or duration has been restricted, primarily due to the nature of the circuit. This has led to difficulties, for example, in making a comprehensive study of the effects upon ignition, of energy and duration, either for gas mixtures or dust clouds.

Some few workers studying the effects of duration on minimum ignition energy, have used 'pulse-modulator' principles for the generation of reproducible discharges. Wolf and Burkett⁴ first used a modulator-type circuit for ignition studies of a neo-pentane-air mixture, where current wave-shape was nearly square. This approach was repeated later by Ballal and Lefebvre⁵ when studying the ignition of liquid fuel sprays and flowing gases. Bartels and Riddlestone⁶ have also used charged artificial transmission lines for studying the ignition of gas mixtures.

The success of these techniques was so clear that a similar approach was taken in the design of the present circuit. This used a pulse-modulator principle and artificial, or bulked-parameter, transmission lines, which lent itself very well to the demands listed in section 1.1. Using such a circuit, energy and duration could be varied independently within wide limits, and in a pre-determined manner. Many other previous designs have tended to produce a wide variety of electric sparks with various energies and durations, but these have generally been produced quite arbitrarily. For example, a capacitive discharge circuit may yield various spark energies and durations by adding circuit inductance and/or resistance. By changing the values of these added components, different spark energies and durations can be produced. Most workers using this circuit^{1,7,8,9}, have altered these component values in order to produce 'longer' or 'shorter' sparks, but have not usually been able to choose, and therefore predict, the kind of discharge that will result. In addition, secondary effects, such as an arbitrary alteration of rate of discharge of spark energy, are also introduced, making individual effects, such as spark duration, difficult to study.

The present system was based upon simple transmission-line theory and produced discharges in accordance with this theory. A comprehensive measurement system was also designed so that a given spark type could be both produced and measured.

1.3.2 Producing low energy discharges and controlling effects of stray capacitances

One of the most significant difficulties experienced by other workers has been the reduction of stray capacitance and the control and quantification of circuit losses. This has been a prime factor in limiting the ability to produce low energy sparks below 1 mJ. Some workers, such as Lewis and von Elbe¹⁰ and Priede¹¹, overcame this difficulty by modifying the gap arrangement so that the gap itself acted as the circuit capacitance. In these cases it was possible to produce low energy discharges, but because of the very nature of the circuit, it was not possible to insert resistive or inductive elements to alter spark duration.

In this circuit, the dual role played by circuit series resistance overcame this limitation to some extent. Resistance was used not only as an indirect means

of varying spark duration, but also as a means of reducing the effects of unwanted circuit stray capacitances. This was achieved by building the resistance into the gap itself so that the circuit 'sees' the resistance and gap together as the load. One of the basic principles of a pulse-type circuit such as this is that the spark gap must be 'matched' to the circuit impedance, in order to produce a well-defined, rectangular spark current pulse. After breakdown, the gap will tend to assume a dynamic impedance which itself is dependent upon the external circuit. By adding series resistance to the gap, the external circuit will be modified and thus so will the gap impedance. If the series resistance is large compared with the gap impedance, then effects of stray circuit capacitances located on the circuit-side of the resistance will be reduced accordingly. It is only the stray capacitances on the gap-side of the resistance (i.e. between resistor and gap) that contribute to the gap capacitance and therefore limit the production of very low energy discharges.

In order to reduce the effects of circuit stray capacitances, the series resistance should be placed as near to the gap as possible. The present circuit used special resistor-types that screwed into the gap-anode. This meant that resistor-to-gap-capacitance was significantly reduced. If circuit impedance was high, the matching resistance will also be high, and the gap will be 'isolated' from the rest of the circuit. Discharge energy therefore consisted of the gap capacitance energy plus the additional energy fed in by the circuit. By careful choice of the electrode geometries, gap capacitance was reduced to a minimum, so that the discharge was almost completely controlled by the external circuit.

The resistance therefore played two important roles. The first was that of matching, to give a well-defined current pulse, and the second was to isolate the effects of stray circuit capacitances. A careful choice of the value of the resistor was thus essential. More details regarding this circuit principle are to be found in sections 2 and 6.

1.3.3 Operating voltage and timing

If electrode distance is to be varied over a wide range, as point b) in section 1.1 suggests, then according to Paschen's law, so must the gap-breakdown voltage. Some previous designs of spark generator, e.g. those of Lewis and von Elbe¹⁰ and Riddlestone¹², used a wide range of operating voltages, but

have relied upon 'natural-breakdown' methods for discharging the energy. Such methods charge the spark gap capacitance up to the static breakdown voltage; breakdown is either allowed to occur naturally, or is assisted, for example by illuminating the gap with UV light. The disadvantage with this method of triggering energy release is that for a given operating voltage, neither a larger or smaller gap may be used than that corresponding to the static-breakdown value. When gap voltage V is fixed in this way, so is the minimum energy that can be dissipated in the gap, according to V^2 .

More important, when the spark is being used in ignition tests, the time of its passage may be critical. When quiescent gas mixtures are used, the time of breakdown is not important simply because the mixture is non-turbulent. When either turbulent gas, dust or vapour mixtures are used however, the spark must be produced at a given time. Natural breakdown methods are not suitable for these applications because breakdown time is difficult to control.

A recent solution to this problem was given by Franke¹³ who used a three-point gap. This method has also been adopted as a standard in the current 'mindestzündenergie' working group¹⁴. Precise breakdown timing is obtained by triggering a weak discharge from a third point to the gap-cathode which leads to breakdown of the main gap. The original limitation of gap voltage variation still holds, although operating voltage can be reduced slightly below the static-breakdown value for a given gap length.

A further problem regarding operating voltage using static-breakdown methods is the premature breakdown of the gap. This often happens when dispersing dust clouds towards and around the gap. Some dusts cause breakdown as they reach the gap, before the dust itself is fully dispersed. Optimum and repeatable conditions for ignition are therefore impossible to achieve, as the state of the cloud at the time of ignition cannot be readily defined.

The present system 'pulsed' the gap so that breakdown could be triggered using any voltage above a fixed lower value (the impulse breakdown value for the specific gap arrangement). The gap could therefore be triggered at any time after a combustible mixture had been admitted into the ignition test vessel. 'Pulsing' the gap not only overcame problems of timing, but also

2. ensured that the electrodes were initially at ground potential, rendering them safe for handling and adjusting. This conditional zero-start voltage also meant that premature breakdown was avoided should dust be present in the gap before the chosen instant of discharge. A further advantage of using a pulsing method was that, when point electrodes are used, operating voltage may be considerably reduced below the static breakdown value for the gap. This reduction was typically greater than 50% for the method used here, and depended primarily on the speed of pulsing. This meant that minimum discharge energies could be significantly lowered, compared with standard breakdown methods.

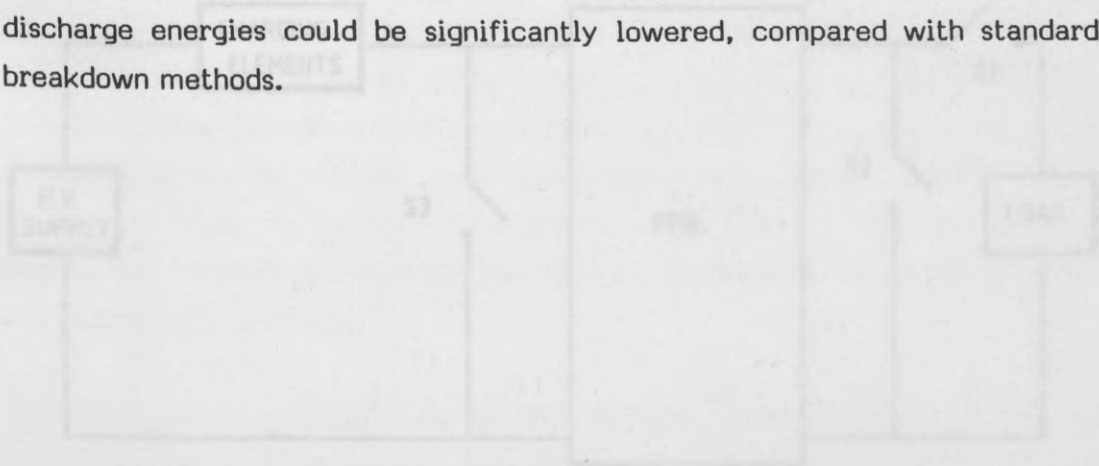


Figure 1-1. Block diagram of a typical modulator circuit.

A pulse forming network (PFN) is charged up to a specific high voltage and discharged into the load by triggering the first high voltage switch (S1). The amplitude and duration of the pulse(s) discharged in the load may be varied by clipping the fed pulse using the second switch (S2); excess PFN energy due to load mismatch may then be dumped into a matched dump resistor using the third switch (S3). This prevents PFN reverse voltage and subsequent charging to an overvoltage. The load in this case is typically a magnetron or other crowding device.

The charging elements in this circuit may be relatively complicated, depending mainly on the required pulse repetition frequency (p.r.f.). When high p.r.f.'s are needed, triggered charging mechanisms may be used, whereby the h.v. switches are allowed to recycle before the PFN begins to recharge. For low p.r.f.'s and single shots, the charging elements may simply be resistors.

2. THE BASIS FOR THE DESIGN OF THE SPARK GENERATOR

2.1 The generator principle

The generator was based on a radar modulator circuit, which resembles that shown in Figure I-1.

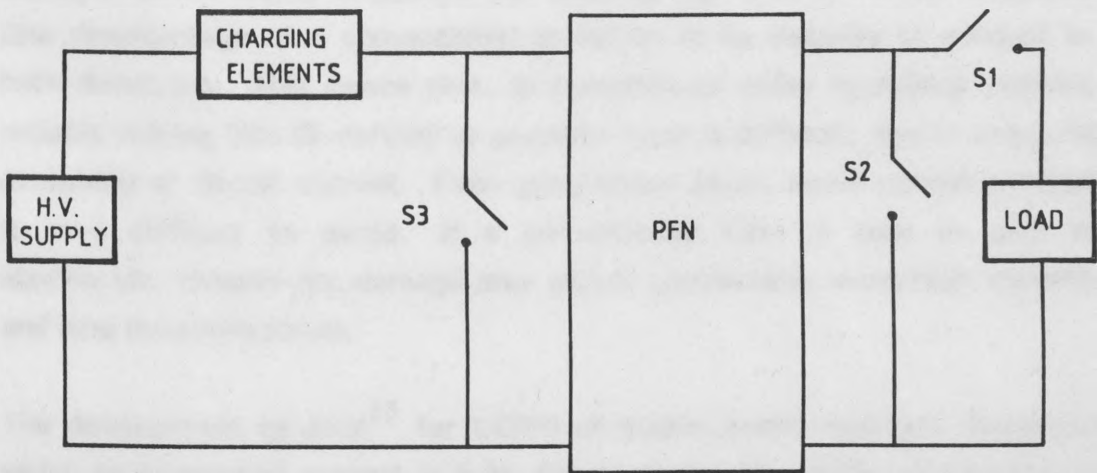


Figure I-1. Block diagram of a typical modulator circuit.

A pulse forming network (PFN) is charged up to a specific high voltage and discharged into the load by triggering the first high voltage switch (S1). The squareness and duration of the pulse(s) discharged in the load may be altered by clipping the fed pulse using the second switch (S2); excess PFN energy due to load mismatch may then be dumped into a matched dump resistor using the third switch (S3). This prevents PFN inverse-voltage and subsequent charging to an overvoltage. The load in this case is typically a magnetron or other transmitting device.

The charging elements in this circuit may be relatively complicated, depending mainly on the required pulse repetition frequency (p.r.f.). When high p.r.f.'s are needed, triggered charging techniques may be used, whereby the h.v. switches are allowed to recover before the PFN begins to recharge. For low p.r.f.'s and single shots, the charging elements may simply be resistors.

The pulse forming network usually consists of an arrangement of inductors and capacitors with a characteristic impedance equal to the load impedance. It is this part of the circuit that discharges the energy in a pre-determined manner into the load.

The elements of greatest interest in this circuit are the high voltage switches. These are usually thyratrons, which are capable of holding off high voltages before being triggered, yet passing high currents once triggered. One disadvantage of a conventional thyatron is its inability to conduct in both directions. This means that, in conventional pulse modulator circuits, reliable pulsing into ill-defined or unstable loads is difficult, due to inductive overshoot of circuit current. Even using stable loads, some voltage reversal is very difficult to avoid. If a conventional tube is used in such an application, reverse-arc damage may occur, particularly using high currents and long duration pulses.

The development by EEV¹⁵ for CERN of double-ended multigap thyratrons which could conduct current in both directions led to significant advances in pulse-modulator design. Load mismatching could easily be tolerated, and a single double-ended tube could be used to replace two conventional ones. A simplified modulator circuit using two such devices is shown in Figure I-2. This circuit has been rearranged so as to provide a common earth to both thyratrons (which are double ended types). PFN-load mismatching and overshoot can now be tolerated due to the nature of the switch-tubes. This is essential when this circuit is used as a spark generator whereby spark current may be either oscillatory or unidirectional.

The circuit shown in Figure I-2 formed the basis of the spark generator. The load in this application was the spark gap itself with associated stray reactance. Since this could not be defined in terms of a fixed impedance, it was difficult to match the gap directly to the PFN (circuit) impedance. Matching was achieved by connecting fixed high voltage resistors to the gap-anode. This is discussed in section 3.6.

This circuit is essentially a line-type pulser¹⁶ and its mode of operation is based on transmission line theory. This is presented in section 2.2. The basic operation is as follows:

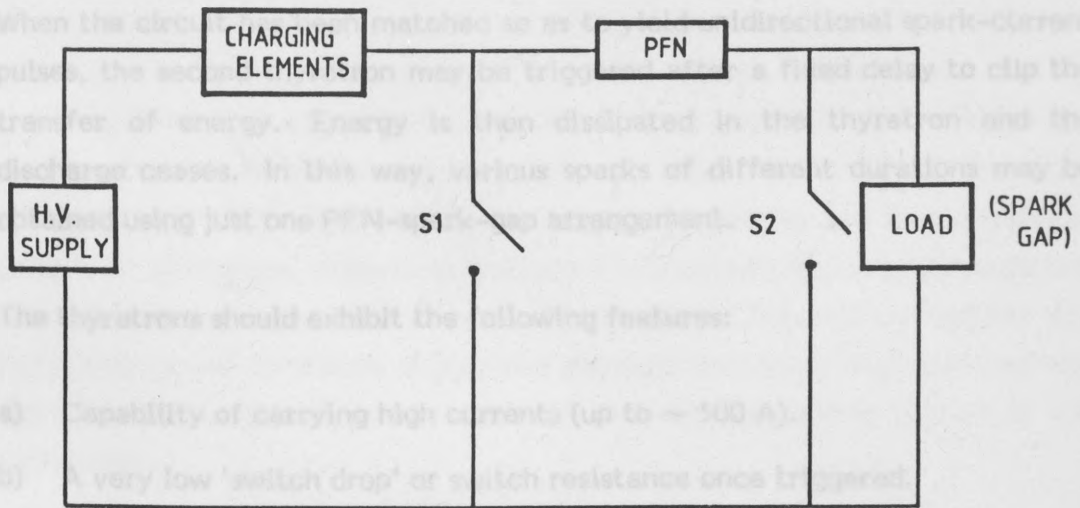


Figure I-2. Block diagram of the basic spark generator circuit.

First, the PFN is charged to a fixed voltage by the high voltage supply (HML type 421) and charging element, which in this case is a resistor. This resistance has a high value of the order of $10^9 \Omega$ in order to avoid the supply contributing energy during the passage of a spark. The PFN may be regarded in its simplest form as a lossless transmission line of fixed impedance to which the spark gap is matched. When the first thyatron is triggered, the spark-gap anode-voltage is lowered to the negative PFN voltage, and the gap breaks down. The PFN then discharges its energy in the closed circuit. Assuming a lossless PFN and thyatron, and perfect matching between the spark gap and the PFN, all the stored PFN energy will be discharged in the spark gap and matching resistor.

In practice, the PFN and thyatron are not lossless and some of the stored energy will be lost in these parts of the circuit. For example, Molyneux-Berry¹⁷ has measured tube drop as being ~ 150 V using similar thyatron devices for pulse modulator design. Furthermore, if the spark gap is not matched to the load, only a fraction of the energy will be transferred. In practice it is not necessary to evaluate these losses because matching is done empirically by varying gap-anode resistance, in order to obtain the best pulse shape. A perfect rectangular current pulse is not absolutely essential, and nor is complete energy transfer. However, because losses are usually low, a first approximation may be made by ignoring them, so as to obtain an indication of discharge energy.

When the circuit has been matched so as to yield unidirectional spark-current pulses, the second thyatron may be triggered after a fixed delay to clip the transfer of energy. Energy is then dissipated in the thyatron and the discharge ceases. In this way, various sparks of different durations may be obtained using just one PFN-spark-gap arrangement.

The thyatrons should exhibit the following features:

- a) Capability of carrying high currents (up to ~ 500 A).
- b) A very low 'switch drop' or switch resistance once triggered.
- c) The ability to withstand or 'hold off' high voltages.
- d) A fast 'on' switching time.
- e) An ability to conduct current in both directions.

English Electric thyatrons, type CX 1168 B, with the following properties, were chosen for this application:

- a) A maximum allowable peak anode current of 3kA, and average anode current 3A.
- b) An estimated switch drop of less than 200 V when on.
- c) A 70 kV peak forward anode hold-off.
- d) A typical switching time of less than 100 ns and a rate of rise of anode current of 5000 A/ μ s.
- e) A double-ended design enabling current to flow in both directions.

Full specifications for these devices are to be found in Reference 18.

It is a property of all thyatrons that, once they are triggered and conduction begins, the triggered grid loses control due to a sheath of ions forming around it. The tube returns to a non-conducting state only when the anode voltage has been removed or reversed for a time sufficient to allow the charge density in the tube to decay to a low value. In the case of double-ended types, a reversal of anode voltage will only mean a reversal in the direction of current flow. Therefore the only criterion for switch-off is that the magnitude of anode current falls below a limiting holding value for a specific time. Typical values for single-ended devices are about 100 mA d.c. for a few μ s, but these are estimated values only, and are not given by the

manufacturer. One may assume that these values represent the orders of magnitude to be expected using the 1168B devices. This means that in practice, there is a lower limit of circuit current together with a limitation on the current duration. Low currents of long durations are therefore difficult to conduct. In practice, for low spark energies and long durations, using 'arc' discharges, a physical limitation existed whereby current could not decrease below a lower limit at a specific duration. This was termed the 'arc limit' and as will be shown, it was this physical limitation that governed the operation of the circuit at low currents, and not the holding current of the thyratrons.

Figure I-3. Lumped circuit analogue of an equivalent transmission line.

In this application, current typically varied from about 0.1 amp to about 100 amps, and durations varied from about 0.1 microsecond to several milliseconds. To keep the tubes conducting when using low currents and long durations, recovery time was prolonged by suitable design of the grid trigger circuit (see section 3.1.6), which in turn prolonged the maximum allowable duration for a fixed current. This is poor pulse modulator design, when high p.r.f.'s are being used, but is quite permissible for single shot and crowbar applications.

The thyratrons were operated at or near their lower limits and not their upper limits, which are those quoted by the manufacturer. These lower limits, found by experimentation, governed the operation of the generator at low spark energies.

2.2 Theory of operation

This treatment is a simplified version of transmission line theory that may be found in most standard text books dealing with the subject.¹⁹

2.2.1 The equivalent transmission line

By a suitable choice of normalisation, all forms of practical transmission lines, be they wire types or waveguides, may be reduced to the equivalent transmission line represented by a parallel wire line. This form of line is associated with continuous parameters, but in order to analyse its electrical performance, a lumped circuit analogue may be used (see figure I-3).

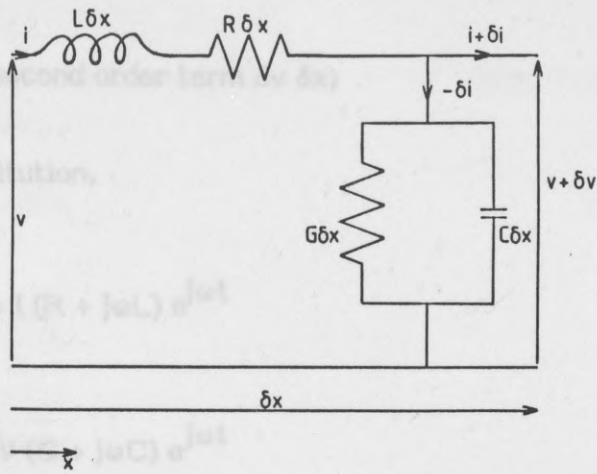


Figure I-3. Lumped circuit analogue of an equivalent transmission line.

Typically, the line will possess an inductance, resistance and capacitance per unit length which are represented by bulked parameters in the above circuit. In this circuit,

L = inductance per unit length

R = resistance per unit length

G = conductance per unit length

C = capacitance per unit length

Assuming that a high frequency generator is connected to the left of the line, the instantaneous voltage and current are given by

$$v = \text{Re } V e^{j\omega t} \quad (2.1)$$

$$i = \text{Re } I e^{j\omega t} \quad (2.2)$$

where V and I are amplitude terms, ω is angular frequency and t is time.

For the above section, the voltage drop and shunt current are given by

$$-\delta v = i (R + j\omega L) \delta x \quad (2.3)$$

and
$$-\delta i = (v + \delta v) (G + j\omega C) \delta x$$

$$\approx v (G + j\omega C) \delta x \quad (2.4)$$

(ignoring the second order term $\delta v \delta x$) on an infinitely long line, and where γ is its general constant.

Then by substitution,

$$V = Ae^{\gamma x} + Be^{-\gamma x} \quad (2.17)$$

$$\frac{-\delta (Ve^{j\omega t})}{\delta x} = I (R + j\omega L) e^{j\omega t} \quad (2.5)$$

$$\frac{-\delta (Ie^{j\omega t})}{\delta x} = V (G + j\omega C) e^{j\omega t} \quad (2.6)$$

As $\delta x \rightarrow 0$,

$$\frac{dV}{dx} = -I (R + j\omega L) \quad (2.7)$$

$$\frac{dI}{dx} = -V (G + j\omega C) \quad (2.8)$$

The time factor $e^{j\omega t}$ will now be implied in the following treatment.

By differentiating equation 2.7 w.r.t. x , and by substitution,

$$\frac{d^2V}{dx^2} = (R + j\omega L) (G + j\omega C) V \quad (2.9)$$

which simplifies to

$$\frac{d^2V}{dx^2} - \gamma^2 V = 0 \quad (2.10)$$

where $\gamma^2 = (R + j\omega L) (G + j\omega C)$ load, the voltage and current at any distance from the load, can be derived as follows:

The general solution of 2.10 is given by

$$V = Ae^{-\gamma x} + Be^{\gamma x} \quad (2.12)$$

where A and B are constants.

B may be shown to be neglected for an infinitely long line, and since γ is in general complex,

$$V = Ae^{-\alpha x} e^{-j\beta x} \tag{2.13}$$

where $\gamma = \alpha + j\beta$

Using 2.12 in 2.7,

$$I = \frac{Y}{(R + j\omega L)} (Ae^{-\gamma x} - Be^{\gamma x}) \tag{2.14}$$

By substitution,

$$I = A \left(\frac{G + j\omega C}{R + j\omega L} \right)^{1/2} e^{-\alpha x} e^{-j\beta x} \tag{2.15}$$

The ratio of voltage to current, or the characteristic impedance, is then given by

$$\frac{V}{I} = Z_0 = \left(\frac{R + j\omega L}{G + j\omega C} \right)^{1/2} \tag{2.16}$$

At high frequencies, where ω is large,

$$Z_0 \approx \sqrt{\frac{\omega L}{\omega C}} \approx \sqrt{\frac{L}{C}} \tag{2.17}$$

2.2.2 The terminated equivalent transmission line

When an infinitely long equivalent transmission line is terminated in an impedance Z_R , which represents a load, the voltage and current at the load or at any distance from the load, can be derived as follows:

If 'd' is the distance from Z_R to any point on the line, as shown in Figure I-4, then x in equation 2.12 may be replaced by -d, i.e.

$$V = Ae^{\gamma d} + Be^{-j\gamma d} \tag{2.18}$$

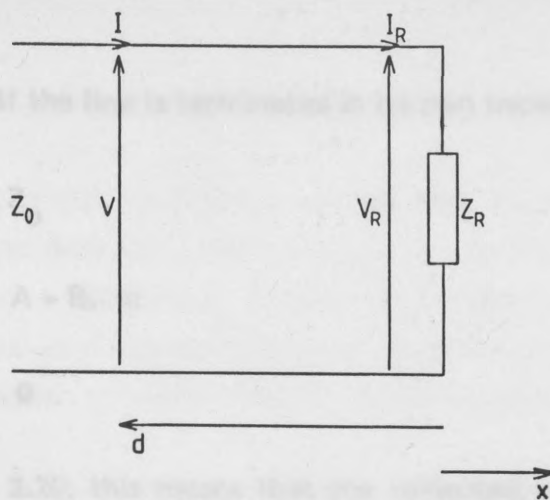


Figure I-4. Terminated transmission line

If the line is considered to be loss-free, then

$$V = Ae^{j\beta d} + Be^{-j\beta d} \quad (2.19)$$

The first term in this expression represents an incident voltage wave, whilst the second represents a reflected wave, seen from the generator end.

The current is given by

$$I = \frac{Ae^{j\beta d}}{Z_0} - \frac{Be^{-j\beta d}}{Z_0} \quad (2.20)$$

from (2.14).

Thus at any point on the line, the impedance is given by

$$Z = \frac{V}{I} = Z_0 \left(\frac{Ae^{j\beta d} + Be^{-j\beta d}}{Ae^{j\beta d} - Be^{-j\beta d}} \right) \quad (2.21)$$

When $d = 0$, $Z = Z_R$, and

$$Z_R = Z_0 \left(\frac{A + B}{A - B} \right) \quad (2.22)$$

2.2.4 In particular, if the line is terminated in its own impedance, then

The $Z_R = Z_0$ has been concerned with an equivalent transmission line terminated in an arbitrary impedance Z_R . In the present work, the load may be i.e. $A + B = A - B$, or $B = 0$, a resistive load R_L is first assumed. (2.23)

From 2.19 or 2.20, this means that the reflected wave at the load is zero, so that the line is matched.

$$Z = Z_0 \coth j\beta d \quad (2.28)$$

2.2.3 The impedance transformation

θ has not yet been defined, and from equation 2.11

The reflection coefficient for the impedance equation given by equation 2.22, is defined as

$$\rho_o = \left(\frac{B e^{-j\beta d}}{A e^{j\beta d}} \right)_{d=0} = \frac{B}{A} \quad (2.24)$$

Expanding the bracket terms gives
Substituting this in 2.22 gives

$$\rho_o = \frac{B}{A} = \frac{Z_R - Z_0}{Z_R + Z_0} \quad (2.25)$$

From which, at high frequencies,

By dividing numerator and denominator of equation 2.21 by A and substituting $\frac{B}{A}$ with ρ_o , we arrive at

$$Z = Z_0 \left(\frac{[Z_R + Z_0] e^{j\beta d} + [Z_R - Z_0] e^{-j\beta d}}{[Z_R + Z_0] e^{j\beta d} - [Z_R - Z_0] e^{-j\beta d}} \right) \quad (2.26)$$

which may be reduced to

$$Z = Z_0 \left(\frac{Z_R + jZ_0 \tan \beta d}{Z_0 + jZ_R \tan \beta d} \right) \quad (2.27)$$

$$\text{where } \delta = d \sqrt{LC} \quad (2.28)$$

2.2.4 Discharging a transmission line into a resistance load

The above treatment has been concerned with an equivalent transmission line terminated in an arbitrary impedance Z_R . In the present work, the load may be assumed to be a resistance, although in practice it is complex due to the physical formation of the spark channel. In order to build a model of the circuit operation, however, a resistive load R_L is first assumed.

By ignoring any terminating impedance, the general a.c. impedance Z of the equivalent transmission line, as given by equation 2.27, is

$$Z = Z_0 \coth j\beta d \quad (2.28)$$

β has not yet been defined, and from equation 2.11

$$\begin{aligned} \gamma = \alpha + j\beta &= (R + j\omega L)^{1/2} (G + j\omega C)^{1/2} \\ \text{or } \gamma &= (-\omega^2 LC)^{1/2} \left(1 + \frac{R}{j\omega L}\right)^{1/2} \left(1 + \frac{R}{j\omega C}\right)^{1/2} \end{aligned} \quad (2.29)$$

Expanding the bracket terms gives

$$\gamma = j\omega \sqrt{LC} \left(1 + \frac{jR}{2\omega L} + \dots\right) \left(1 + \frac{jG}{2\omega C} + \dots\right) \quad (2.30)$$

From which, at high frequencies,

$$\begin{aligned} \gamma &= \left(\frac{R}{2} \sqrt{\frac{C}{L}} + \frac{G}{2} \sqrt{\frac{L}{C}}\right) + j\omega \sqrt{LC} \\ \text{i.e. } \beta &= \omega \sqrt{LC} \end{aligned} \quad (2.31)$$

Substituting this in equation 2.28 and introducing the one-way transmission time δ ,

$$Z = Z_0 \coth j\omega \delta \quad (2.32)$$

$$\text{where } \delta = d \sqrt{LC} \quad (2.33)$$

The Laplace-transform impedance is found by substituting $j\omega$ by s , where s is the transform parameter, i.e.

$$Z(s) = Z_0 \coth s\delta \quad (2.34)$$

The current transform is then

$$i(s) = \frac{V}{s(R_L + Z_0 \coth s\delta)} \quad (2.35)$$

$$= \frac{V(1 - e^{-2s\delta})}{s(Z_0 + R_L)} \left[1 - \frac{Z_0 - R_L}{Z_0 + R_L} e^{-2s\delta} + \left(\frac{Z_0 - R_L}{Z_0 + R_L} \right)^2 e^{-4s\delta} - \dots \right] \quad (2.36)$$

The inverse transform yields

$$i(t) = \frac{V}{Z_0 + R_L} \left[1 - U(t-2\delta) - \frac{Z_0 - R_L}{Z_0 + R_L} \{ U(t-2\delta) - U(t-4\delta) \} \right. \quad (2.37)$$

$$\left. + \left(\frac{Z_0 - R_L}{Z_0 + R_L} \right)^2 [U(t-4\delta) - U(t-6\delta) - \dots] \right] \quad (2.37)$$

In this equation Δt may be introduced as

$$\Delta t = (t - n\delta) \text{ where } n = 2, 4, 6 \dots$$

and $U(\Delta t) = 1$ for $\Delta t > 0$

$$U(\Delta t) = 0 \text{ for } \Delta t < 0$$

When the line is matched ($R_L = Z_0$), current is given by

$$i(t) = \frac{V}{2Z_0} \quad (2.38)$$

over a duration 2δ , as shown below in Figure I-5.

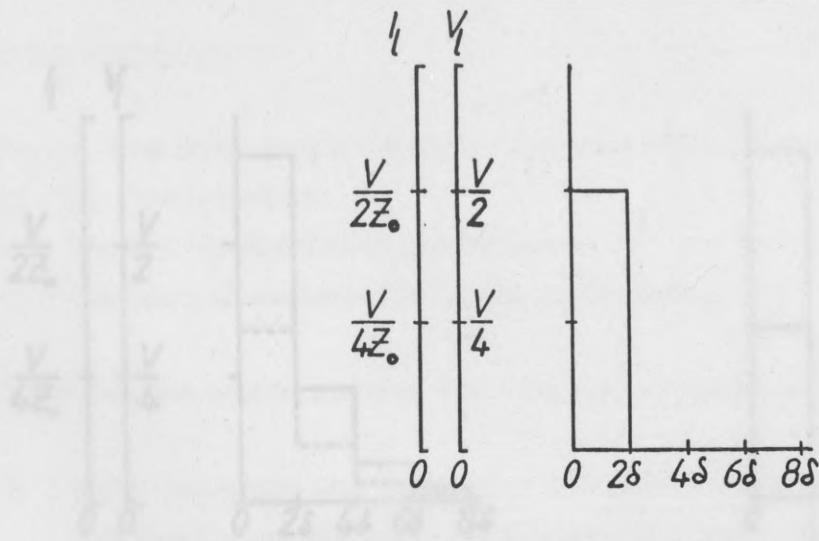


Figure I-5. Current and voltage pulses for a lossless transmission line discharging into a resistance load equal to the characteristic impedance of the line.

The voltage at the load is $\frac{V}{2}$ and the energy is given by

$$E = \int_0^{2\delta} \frac{V}{2} i(t) dt \quad (2.39)$$

$$= \int_0^{2\delta} \frac{V}{2} \cdot \frac{V}{2Z_0} dt$$

$$\text{so that } E = \frac{2V^2}{4} \cdot \frac{d\sqrt{LC}}{\sqrt{\frac{L}{C}}}$$

$$= \frac{d}{2} CV^2 \quad (2.40)$$

(where C is the capacitance per unit line length).

In a similar manner, conditions of overmatching and undermatching may be used to show the variation in line current with time. Current and voltage pulses for $R_L = 2Z_0$ and $R_L = \frac{Z_0}{2}$ are shown below.¹⁶

2.2.5 Summary of theory

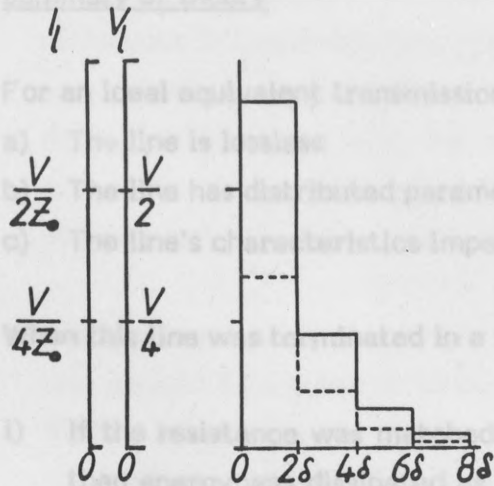


Figure I-6.

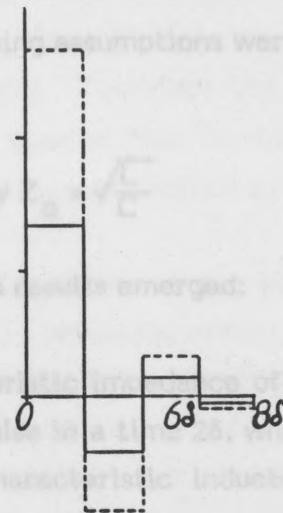


Figure I-7.

Current and Voltage pulses for a lossless transmission line discharging into a resistance load, where in Figure 6 $R_L = 2Z_0$ and in Figure 7 $R_L = Z_0/2$. Load current is shown by the dotted line and voltage by the solid line.

2.2.6 Applying the theory to the current work

By deliberately mismatching the load a series of steps is introduced into the current and voltage waveforms, which is caused by reflections at the load resistance. Each reflection traverses the line and is reflected back to the load in time 2δ . Reflections continue, diminishing in amplitude until all the line energy has been dissipated in the load resistor.

The capacitive line energy is discharged in a manner which depends upon the degree of matching. Clearly the most efficient energy transfer, in terms of time, is obtained under conditions of perfect matching, where a rectangular pulse is produced (see Figure I-5). Duration is then at a minimum.

When the line is mismatched, the energy in each reflected step may be obtained by integrating equation 2.39 over intervals of 2δ . By a suitable choice of δ (length of line) and R_L , various energy-time configurations may be produced.

2.2.5 Summary of theory

For an ideal equivalent transmission line, the following assumptions were made:

- a) The line is lossless
- b) The line has distributed parameters
- c) The line's characteristic impedance is given by $Z_0 = \sqrt{\frac{L}{C}}$

When this line was terminated in a resistance, these results emerged:

- i) If the resistance was matched to the characteristic impedance of the line, then energy was dissipated as a rectangular pulse in a time 2δ , which was a function only of the line length and its characteristic inductance and capacitance.
- ii) If the resistance was mismatched to the characteristic impedance of the line, then energy was dissipated as a series of steps, in a time greater than 2δ . The steps, of duration 2δ , were positive or negative according to the mismatch ratio. Energy was therefore expended over a longer time than 2δ .

2.2.6 Applying the theory to the current work

2.2.6.1 Simulating an equivalent transmission line

Assumption a) given above stated that the line was lossless, which reduces the original model given in Figure I-1 to a simple inductor-capacitor chain. As stated in b), these parameters tend to be distributed, and continuous, rather than bulked values. This distributed phenomenon of inductance and capacitance per unit length can be simulated by using lumped components in the form of a pulse forming network (PFN). In its simplest form, a PFN may consist of a network of conductors and capacitors as shown in Figure I-3. More complex arrangements may be derived in order to produce various pulse shapes or to closer approximate an ideal transmission line. In the current work, it was necessary to use lumped components because for the long duration discharges that were being produced, excessively long lengths of line would have been needed. The use of a PFN, or artificial transmission line, was therefore a more practical proposition, and by changing the PFN parameters, various transmission line lengths and impedances could be simulated.

Theoretical treatment of the operation of the PFN follows that of the continuous transmission line. No network having a finite number of elements can, however, exactly simulate a transmission line, although the degree of simulation increases with the number of elements. Therefore the treatment described above becomes more accurate the greater the number of PFN sections. (One section comprises one inductive and one capacitive element).

In the present work, this simple L-C simulation was used and the above theory was applied as a guide to circuit operation and to producing various discharge shapes, by varying the degree of circuit matching. Since a lumped system is not lossless, and switching time in the circuit has a finite value, the pulses at the load were not rectangular, as shown in Figures I-5 - I-7. In addition, the load was complex due to the spark gap and was not a simple resistance, as was assumed in the above treatment. This led to an additional mismatch between circuit and load. The net result was that the current produced at the load was often a distorted rectangular pulse instead of being of rectangular form. This was, however, quite acceptable for the present application, where the necessary requirement was to produce sparks of a known energy, duration and approximate pulse shape on a reproducible basis.

Some results using one PFN, varying the resistive loading about the point of matching using a 4 mm gap are shown in Figures I-8 - I-10. These show the spark current and voltage pulses for matched, overmatched and undermatched conditions respectively, which may be directly compared with Figures I-5 - I-7. In this case the δ time is $\sim 15 \mu\text{s}$.

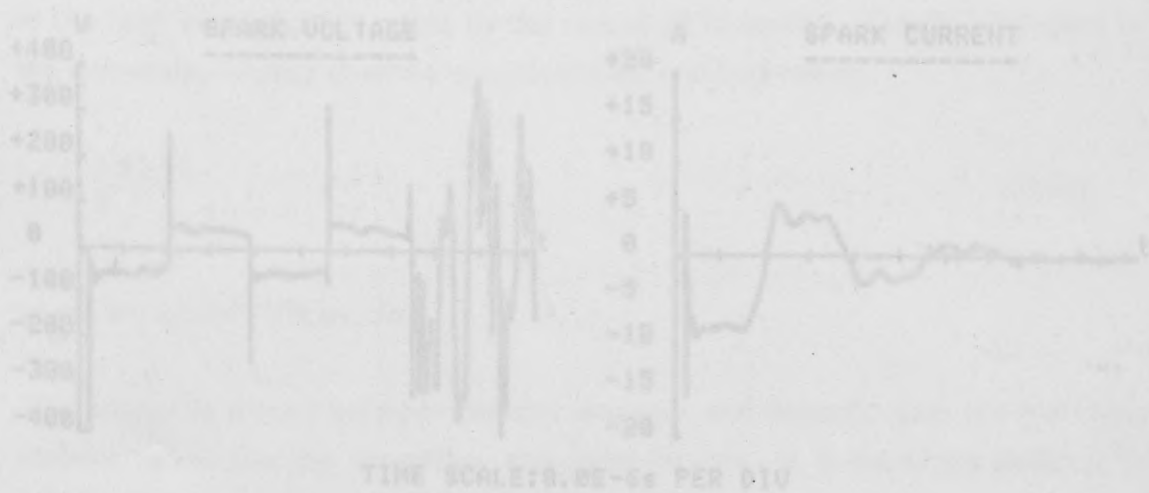


Figure I-10. Spark energy = 10.1 mJ.

Figures I-8 - I-10. Measured spark voltages and current pulses for a 4 mm gap and one PFN, showing first matched conditions, second overmatched conditions, and finally undermatched condition.

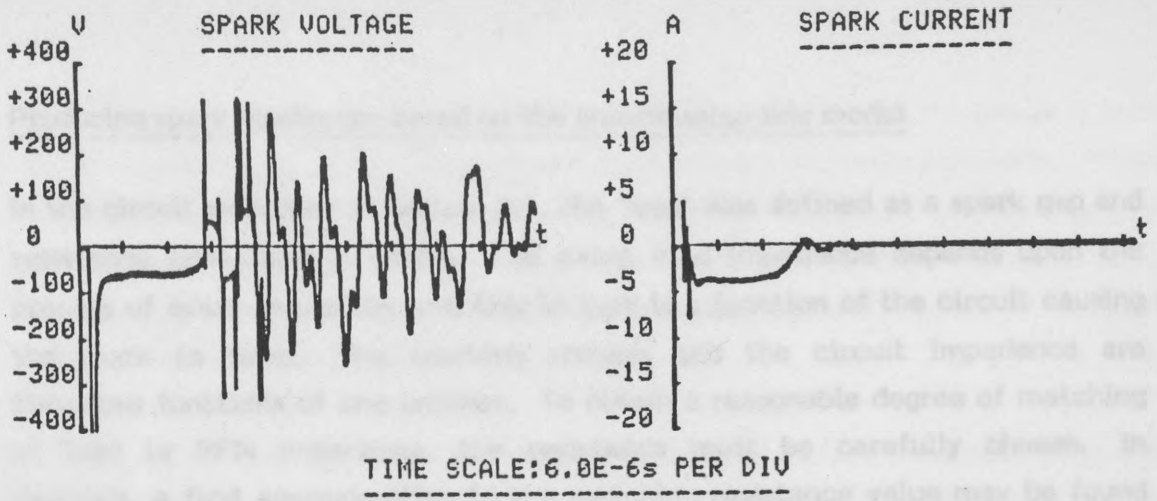


Figure I-8. Spark energy = 3 mJ.

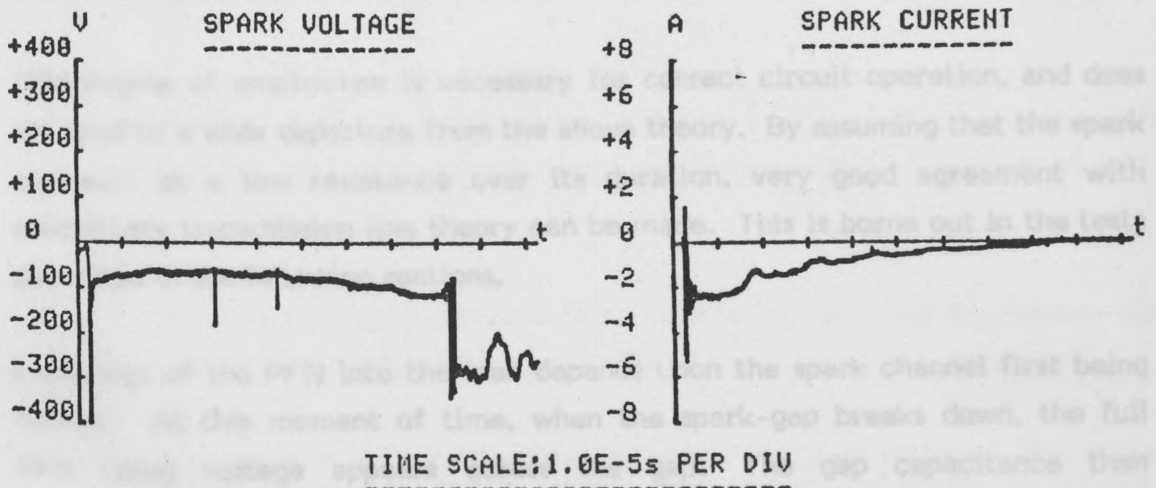


Figure I-9. Spark energy = 5.4 mJ.

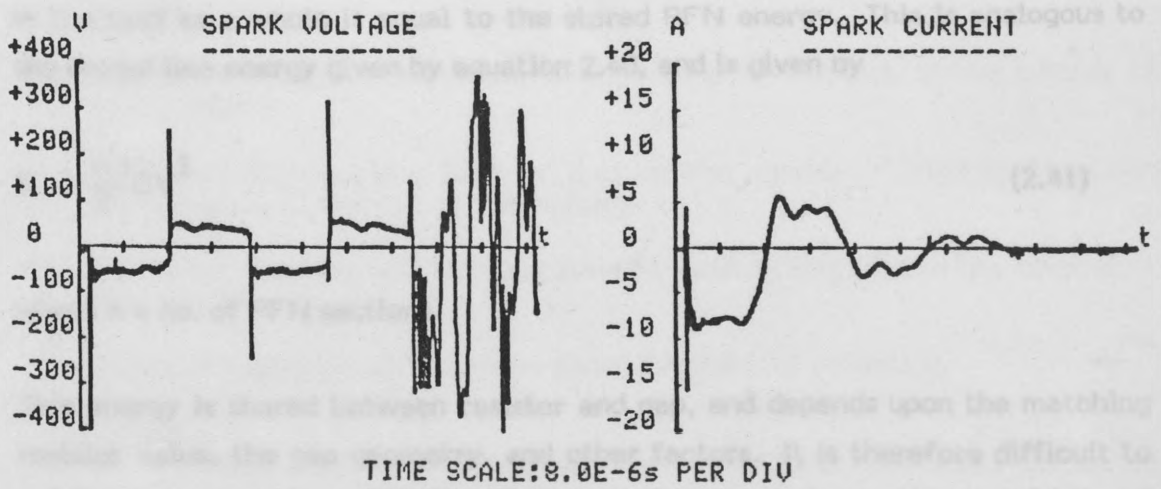


Figure I-10. Spark energy = 10.1 mJ.

Figures I-8 - I-10. Measured spark voltages and current pulses for a 4 mm gap and one PFN, showing first matched conditions, second overmatched conditions, and finally undermatched conditions.

2.2.6.2 Producing spark discharges based on the transmission line model

In the circuit described in section 2.1, the 'load' was defined as a spark gap and resistance connected in series. The exact load impedance depends upon the process of spark formation, and this in turn is a function of the circuit causing the spark to form. The sparking process and the circuit impedance are therefore functions of one another. To obtain a reasonable degree of matching of load to PFN impedance, the resistance must be carefully chosen. In practice, a first approximation to the matching resistance value may be found by ignoring the presence of the spark gap. 'Matching' is usually achieved by slightly reducing this resistor value, so that the dynamic load impedance, which is principally resistive, is matched to the theoretical PFN impedance.

This degree of empiricism is necessary for correct circuit operation, and does not lead to a wide departure from the above theory. By assuming that the spark gap acts as a low resistance over its duration, very good agreement with elementary transmission line theory can be made. This is borne out in the tests described in the following sections.

Discharge of the PFN into the load depends upon the spark channel first being formed. At this moment of time, when the spark-gap breaks down, the full PFN (line) voltage appears across the gap. The gap capacitance then discharges, breaking the gap down, and the PFN energy is dissipated in the gap and matching resistor. Since gap voltage is practically independent of line voltage, gap energy is a function of the circuit current. The energy dissipated in the load as a whole is equal to the stored PFN energy. This is analogous to the stored line energy given by equation 2.40, and is given by

$$E = \frac{n}{2} CV^2 \quad (2.41)$$

where n = no. of PFN sections.

This energy is shared between resistor and gap, and depends upon the matching resistor value, the gap geometry, and other factors. It is therefore difficult to predict the gap energy using the above circuit theory, due to the complexity of the spark channel. For this reason, spark energy values must be measured using a suitable probing system.

A rough guide to the gap energy value may be obtained by assuming that it acts as a resistance, whose value depends upon the matching resistance. When the latter is high (at and above matching for example), most of the energy will be dissipated in the matching resistor. At low values of matching resistance, gap current is high and a higher relative energy will be dissipated in the gap. This is shown later in section 6.

Duration and waveshape, on the other hand, may be readily predicted using the above theory. It may be shown, using a similar treatment to that above, that the one way circuit transmission time is given by

$$\delta \propto n \sqrt{LC} \quad (2.42)$$

so that duration may be varied by a suitable variation of inductance and capacitance, and increases linearly with an increase in the number of PFN sections.

By approximating the spark gap as a fixed resistance following breakdown, the following results emerge from the circuit theory:

- a) Discharge energy will increase linearly with PFN (line) voltage. This is due to a linear increase in circuit current, and a roughly constant gap voltage, as line voltage increases.
- b) Discharge energy will increase when the load is undermatched due to the relative increase in the ratio of gap energy to energy dissipated in the matching resistance.
- c) Discharge energy will increase linearly with an increase in the number of PFN sections.
- d) Discharge duration is a function only of the number of PFN sections and the product LC, and not of line voltage.
- e) Discharge duration will increase linearly with an increase in the number of PFN sections.
- f) Discharge duration will increase about the point of matching.

Because the spark gap does not usually act as a fixed resistance, deviations from these results are expected. This is particularly relevant using low impedance PFN's. At certain other points of the circuit's operation, other limitations will also influence these results when using a spark gap as part of

the load. For example, when line voltage approaches the thyatron cut-off voltage, discharge duration may no longer be given by the number of PFN sections. Also, if spark current is reduced, by increasing the matching resistance, the spark may eventually extinguish, independent of the PFN configuration and line voltage. Furthermore, should current be reduced so as to promote a transition in discharge type, the discharge energy may not necessarily increase with increase in line voltage.

For the range of spark energies and gap widths used in the ignition tests described later, the circuit operation followed the above results very closely, when using arc discharges. The circuit theory was therefore used as a guideline for producing discharges of a given energy and duration.

The thyatrons were housed in ceramic tubes and it was important to keep these within a specific temperature range during operation. These tubes are usually oil-immersed in order to hold the ceramic envelopes at a constant temperature. This method also increases the insulation around the tube. In this application, however, the thyatrons were air-cooled by electric fans about 40 cm from the anode and cathode ends. This was sufficient to keep the ceramic envelope temperatures below the maximum rated value of 200°C.

This method also allowed necessary access to the tubes. This was particularly important in the case of the first thyatron, T1, where PFN components had to be placed beside the tube and changed from time to time.

Each thyatron required the following supplies at each tube end:

- a) Heater (H) Voltage 6.5 ± 5% V @ approx. 22A
- b) Reservoir (R) " Voltage marked on tube @ approx. 7A
- c) Grid 1 (G1) " When D.C. primed, 75-150 V. @ 25-50 mA

Although a tolerance of 5% for the heater voltage was quoted by the manufacturer, this was for high p.f. applications only. In this work the thyatrons were working at a very low p.f. and were essentially connected as crowbar devices. A higher heater voltage of 6.8 V was therefore used. Similar r.m.s. heater voltages were used at each end in order to avoid unwanted transfer of hydrogen within the tube. The reservoir values were marked on each tube end for T1 and T2 were 5.9 and 6.0 V respectively.

3. DETAILS OF THE GENERATOR CIRCUIT

A block diagram of the generator circuit based on Figure I-2 is shown in Figure I-11. This shows the supplies and peripheral biasing and triggering units for the thyratrons, T1 and T2. Each part of this circuit will now be broken down and analysed in greater detail.

3.1 Thyratrons and associated circuitry

3.1.1 The thyratrons

The thyratrons were housed in ceramic tubes and it was important to keep these within a specific temperature range during operation. These tubes are usually oil-immersed in order to hold the ceramic envelopes at a constant temperature. This method also increases the insulation around the tube. In this application, however, the thyratrons were air-cooled by electric fans about 40 cm from the anode and cathode ends. This was sufficient to keep the ceramic envelope temperatures below the maximum rated value of 200°C.

This method also allowed necessary access to the tubes. This was particularly important in the case of the first thyatron, T1, where PFN components had to be placed beside the tube and changed from time to time.

Each thyatron required the following supplies at each tube end:

- | | | |
|------------------|---------|---|
| a) Heater (H) | Voltage | $6.3 \pm 5\% \text{ V @ approx. } 22\text{A}$ |
| b) Reservoir (R) | " | Voltage marked on tube @ approx. 7A |
| c) Grid 1 (G1) | " | When D.C. primed, 75-150 V, @ 25-50 mA |

Although a tolerance of 5% for the heater voltage was quoted by the manufacturer, this was for high p.r.f. applications only. In this work the thyratrons were working at a very low p.r.f. and were essentially connected as crowbar devices. A higher heater voltage of 6.8 V was therefore used. Similar r.m.s. heater voltages were used at each end in order to avoid unwanted transfer of hydrogen within the tube. The reservoir values were marked on each tube and for T1 and T2 were 5.9 and 6.0 V respectively.

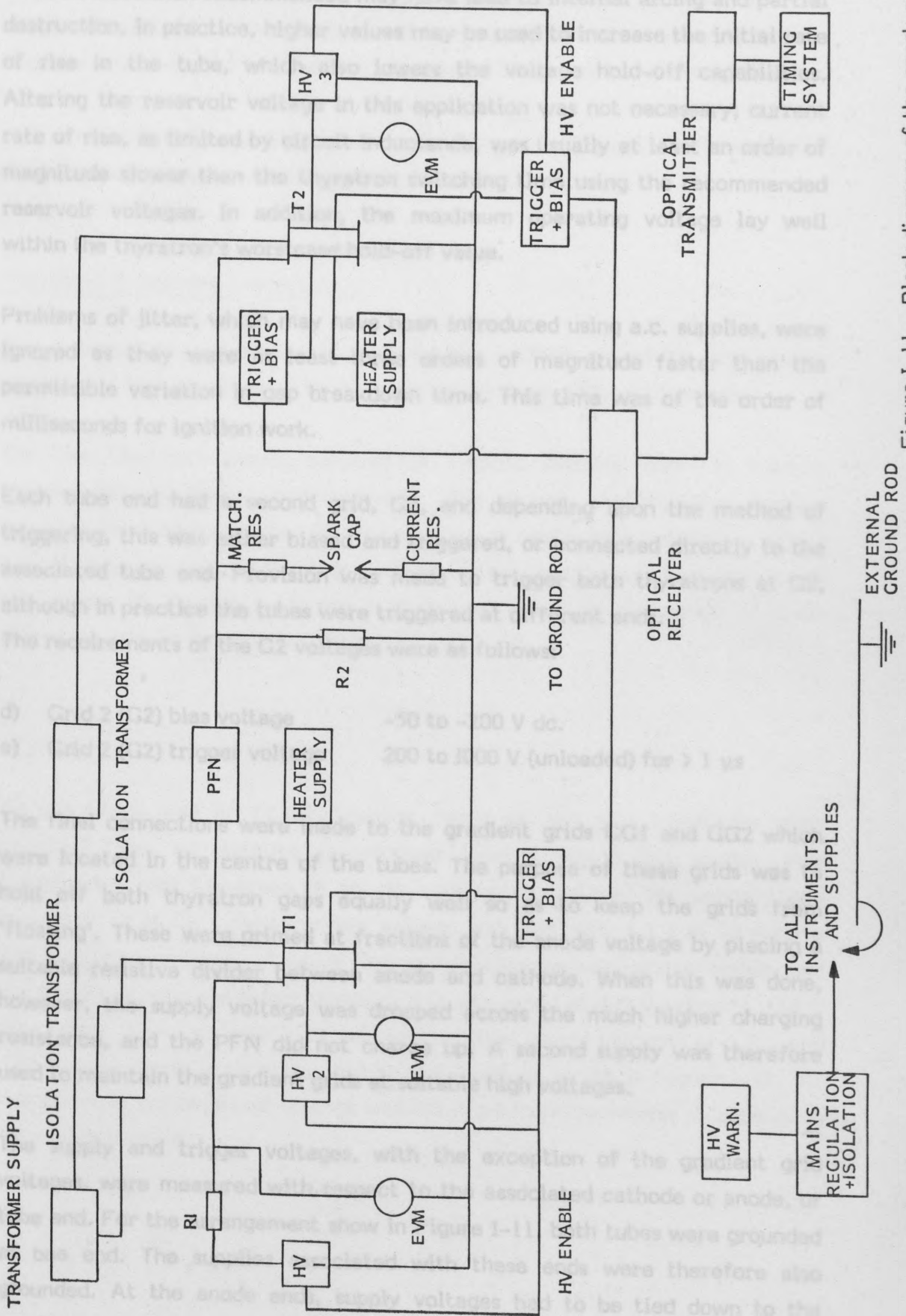


Figure I-11. Block diagram of the spark generator system.

It was very important to match these voltages at each end of the tubes. Lower values than recommended may have lead to internal arcing and partial destruction. In practice, higher values may be used to increase the initial rate of rise in the tube, which also lowers the voltage hold-off capabilities. Altering the reservoir voltage in this application was not necessary; current rate of rise, as limited by circuit inductance, was usually at least an order of magnitude slower than the thyatron switching time using the recommended reservoir voltages. In addition, the maximum operating voltage lay well within the thyatron's worstcase hold-off value.

Thyatron I, cathode and circuitry

Problems of jitter, which may have been introduced using a.c. supplies, were ignored as they were at least three orders of magnitude faster than the permissible variation in gap breakdown time. This time was of the order of milliseconds for ignition work.

The first the heater supply, supplied two outputs, variable from 0 to 7 V a.c.

Each tube end had a second grid, G2, and depending upon the method of triggering, this was either biased and triggered, or connected directly to the associated tube end. Provision was made to trigger both thyatrons at G2, although in practice the tubes were triggered at different ends.

The requirements of the G2 voltages were as follows:

- d) Grid 2 (G2) bias voltage -50 to -200 V dc.
- e) Grid 2 (G2) trigger voltage 200 to 1000 V (unloaded) for $> 1 \mu\text{s}$

The final connections were made to the gradient grids GG1 and GG2 which were located in the centre of the tubes. The purpose of these grids was to hold off both thyatron gaps equally well so as to keep the grids from 'floating'. These were primed at fractions of the anode voltage by placing a suitable resistive divider between anode and cathode. When this was done, however, the supply voltage was dropped across the much higher charging resistance, and the PFN did not charge up. A second supply was therefore used to maintain the gradient grids at suitable high voltages.

The supply and trigger voltages, with the exception of the gradient grid voltages, were measured with respect to the associated cathode or anode, or tube end. For the arrangement show in Figure I-11, both tubes were grounded at one end. The supplies associated with these ends were therefore also grounded. At the anode ends, supply voltages had to be tied down to the anode, and therefore isolated from earth.

In the case of T2, the end marked 'cathode' was the end that was grounded, despite the fact that it was positive with respect to the opposite tube end whilst conducting. This was because of tube conditioning - a process used by the tube manufacturer to condition the respective polarities of the tube ends.

The circuits for T1 and T2 are shown in Figures I-12 and I-13 respectively. Each part of these circuits will now be discussed.

3.1.2 Thyratron 1, cathode end circuitry

Two external supply boxes were built for the cathode end of T1. These were termed the 'grounded heater supply' and the 'grounded thyratron supply'.

The first, the heater supply, supplied two outputs, variable from 0 to 7 V a.c. for the cathode heater and reservoir. The second, the thyratron supply, provided three variable d.c. voltage outputs, a grid 1 bias voltage, a grid 2 bias voltage, and a grid 2 trigger voltage. The circuits for these two boxes are shown in Figures I-14 and I-15 respectively. A discussion of their operation may be found in Sections 3.1.7 and 3.1.8.

3.1.3 Thyratron 1, anode end circuit

At the anode end of T1, the heater, reservoir and grid 1 voltages were obtained from an isolating transformer located beside the anode. This transformer was immersed in an oil bath which isolated the primary and secondary to 40 kV. The secondary voltage was nominally 6.3 V at 30 A for a 220 V primary voltage. A small step up transformer was located beside, and connected to, the secondary winding, and was rated at 6.3 V primary, 110 V secondary. The 'oil bath' thus supplied nominal supply voltages of 6.3 V and 110 V, a.c. These were connected to the anode as shown in Figure I-12. As can be seen, the reservoir voltage was obtained from the heater voltage using a suitable dropper.

3.1.4 Thyratron 2, cathode end

Since the second thyratron clips a negative going pulse, its cathode was positive with respect to the anode throughout the duration of the pulse. The cathode was, however, connected to ground. This is shown in Figure I-13. The thyratron must in this case be triggered at the anode end, meaning that only G1 required biasing at the cathode end. G2 was connected directly to the cathode as shown.

A 'grounded thyratron supply' box provided the bias for G1 and its G2 outputs were redundant. They were left available should T2 be used for positive-going pulses, whereby it would be triggered at the cathode end. Dotted lines in Figure I-13 show the G2 wiring which is similar to that used for T1.

3.1.5 Thyratron 2, anode end circuitry

The anode end lay at a negative high voltage throughout the duration of the spark pulse. The trigger circuitry used for the anode end also had to lie at the anode potential. The circuit was similar to that used for cathode-end triggering and is shown schematically in Figure I-13. This circuitry was located beside the anode and was powered by a second oil-immersed isolation transformer which provided heater, reservoir and G1 voltages in a similar manner to the T1 anode supply.

3.1.6 Thyratron triggering

3.1.6.1 Development and testing of the trigger circuit

The trigger circuit should provide a trigger pulse of approximately 200 - 1000 V amplitude superimposed upon a negative bias of about -150 V d.c. The duration of the pulse should be much greater than 1 μ s to help to inhibit thyratron recovery.

Figure I-12. Schematic diagram of 1st thyratron (T1) circuitry.

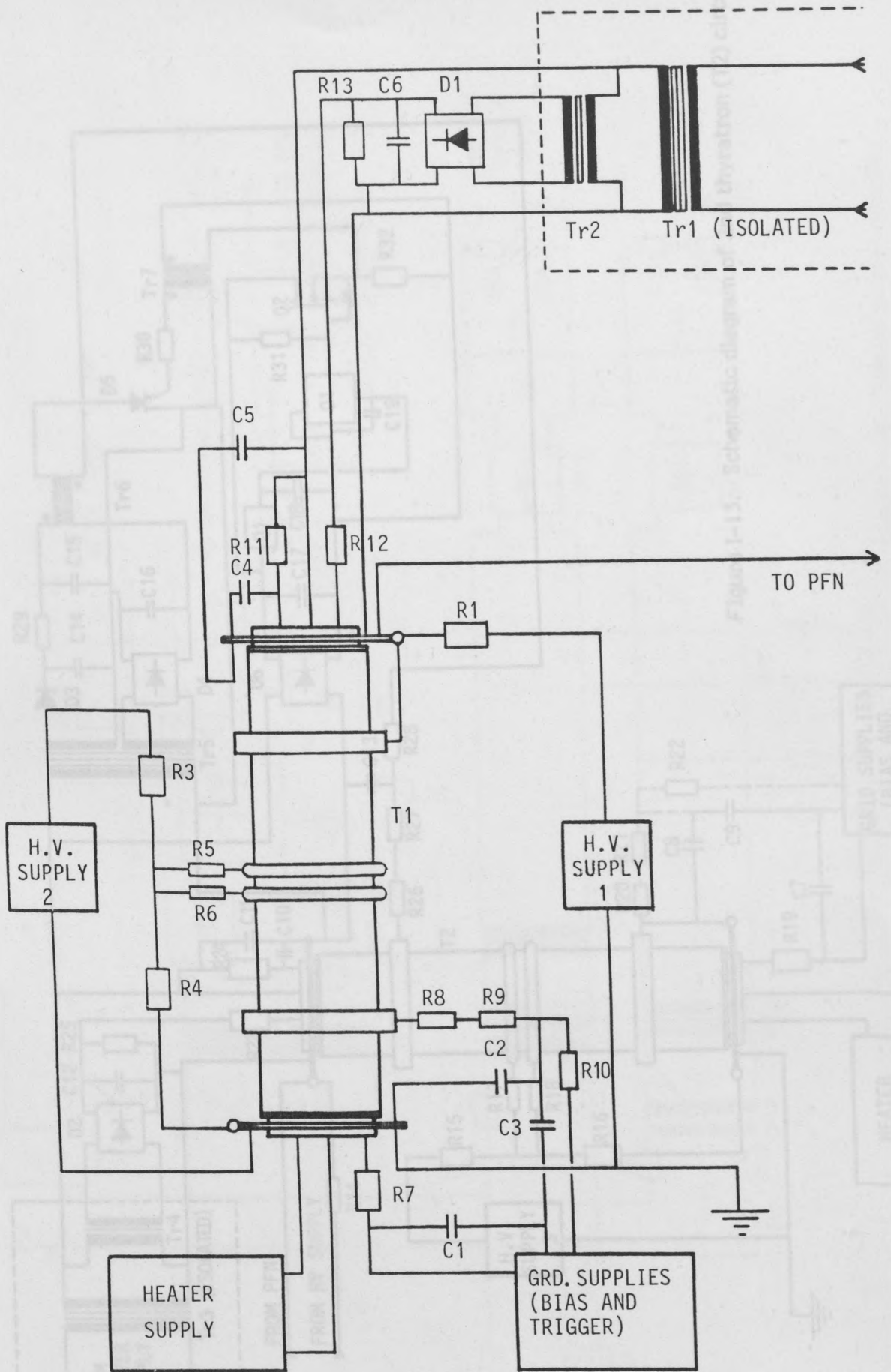


Figure I-12. Schematic diagram of 1st thyatron (T1) circuitry.

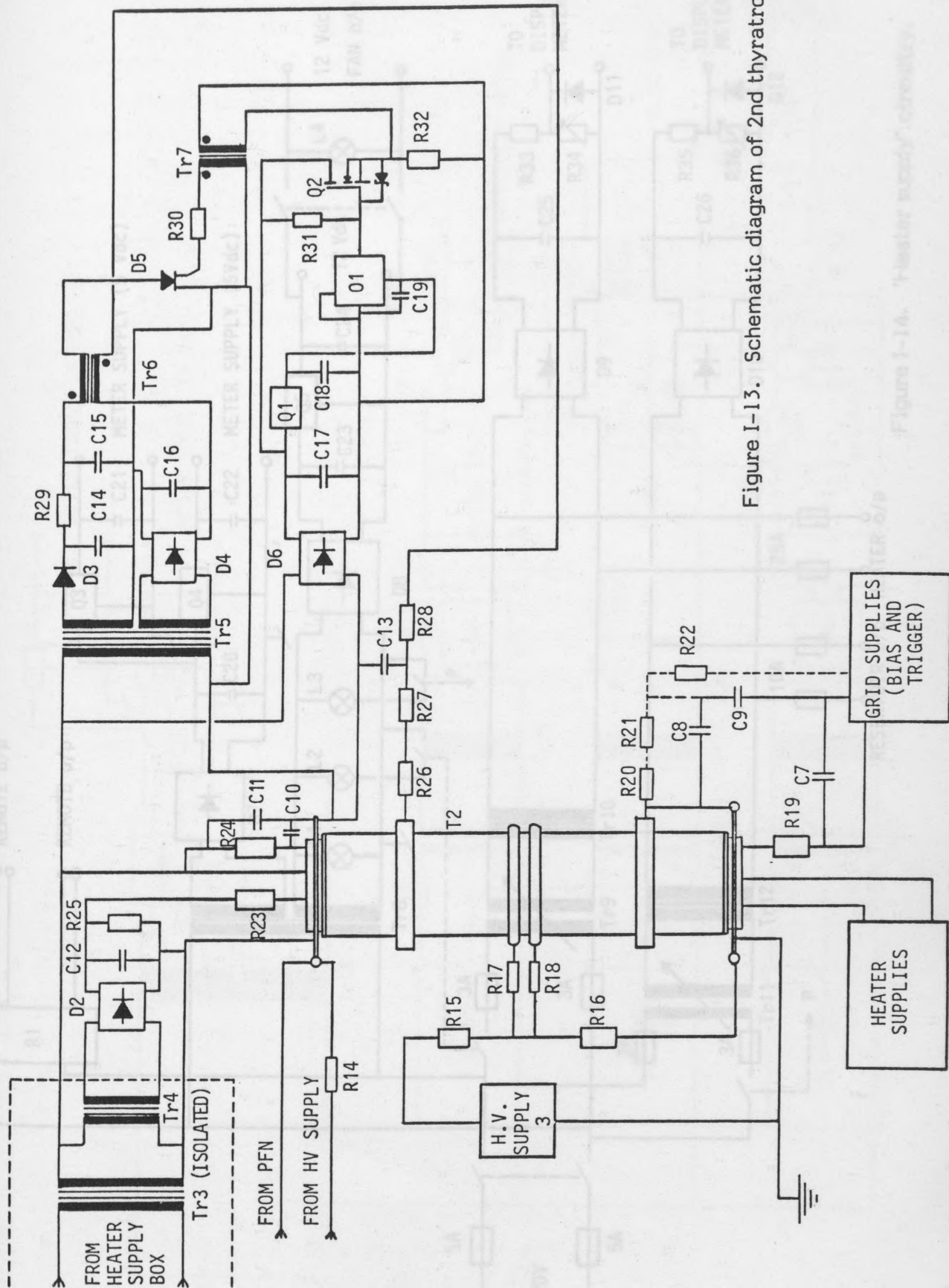


Figure I-13. Schematic diagram of 2nd thyratron (T2) circuitry.

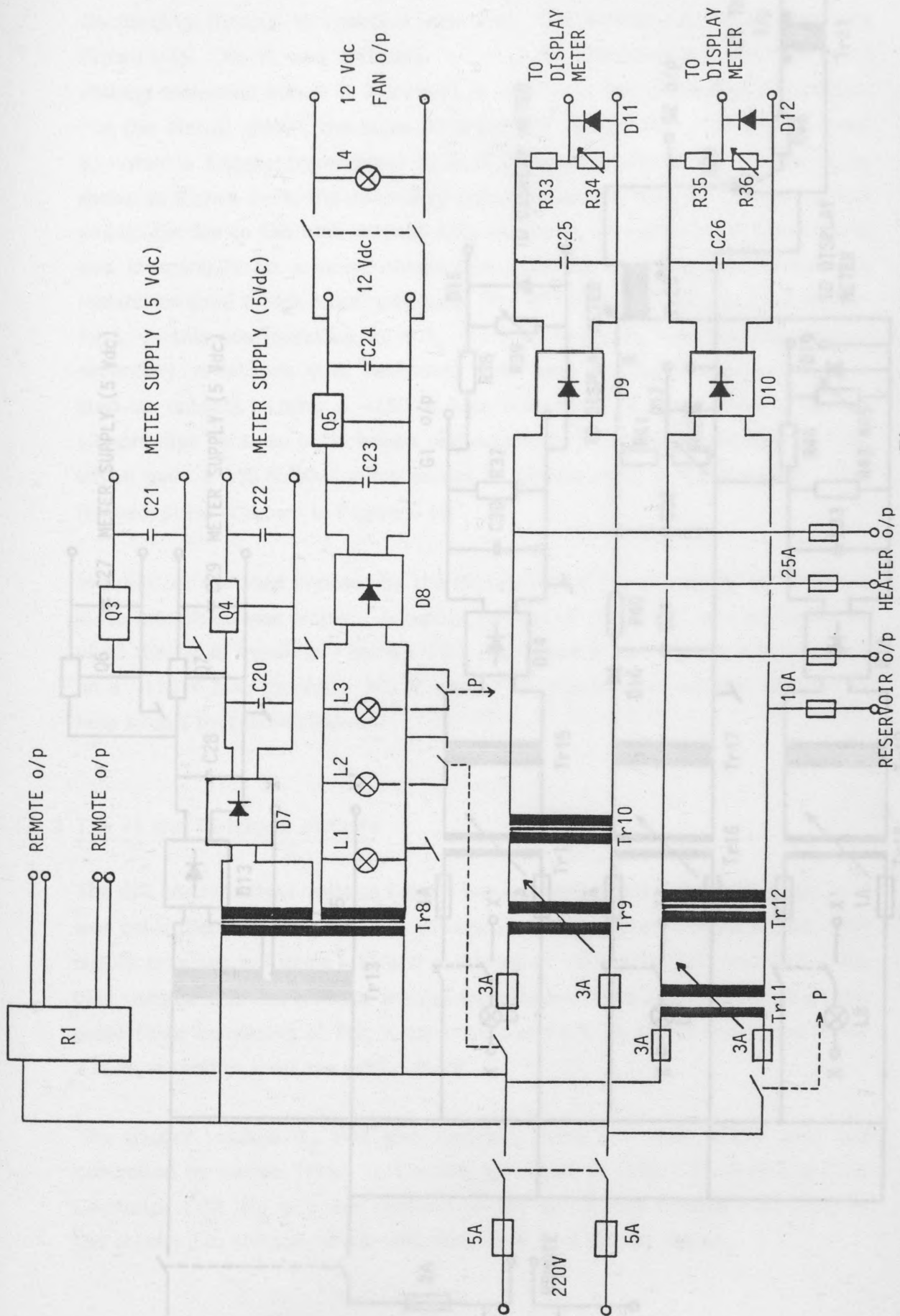


Figure I-14. 'Heater supply' circuitry.

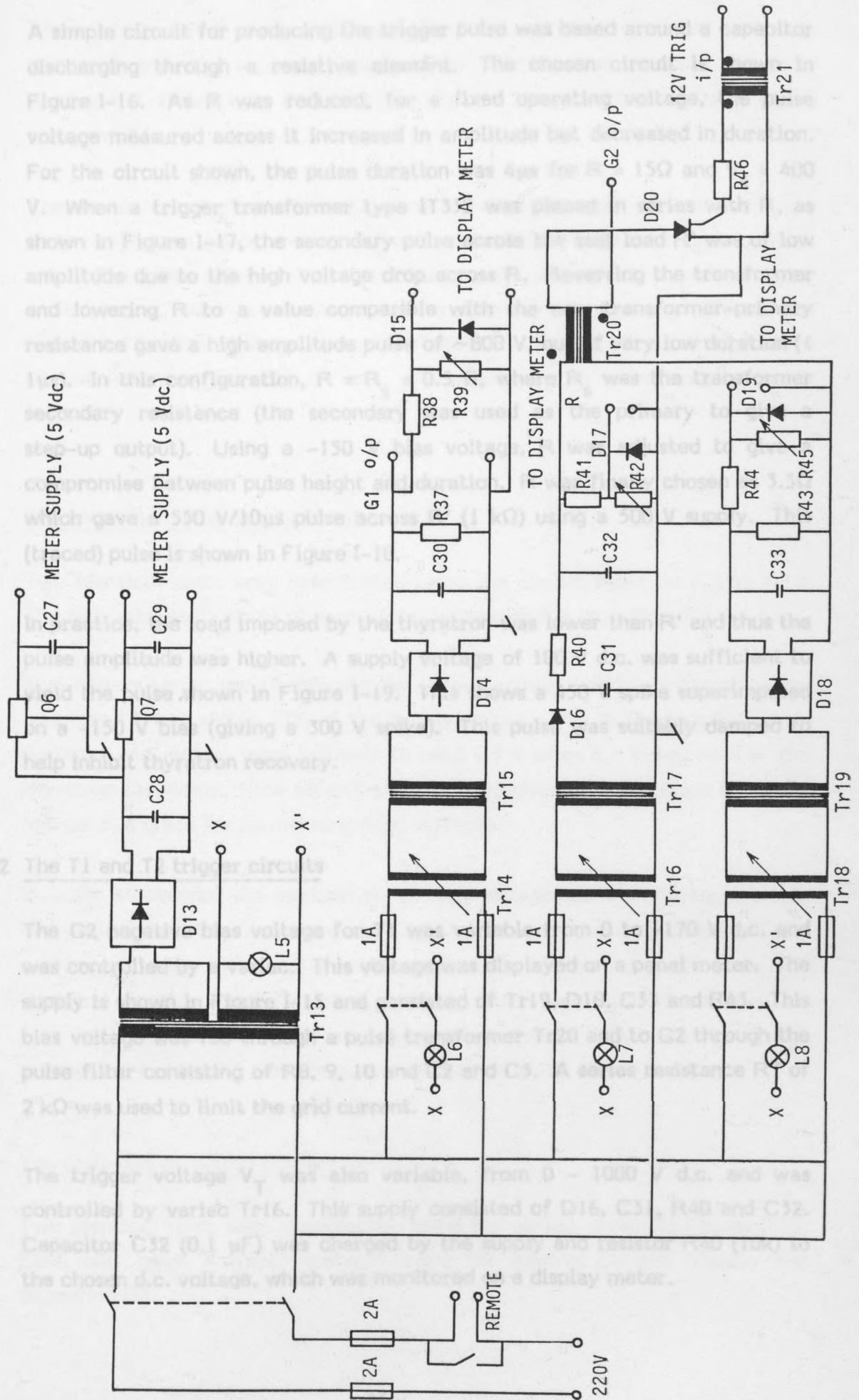


Figure I-15. 'Thyatron supply' circuitry.

A simple circuit for producing the trigger pulse was based around a capacitor discharging through a resistive element. The chosen circuit is shown in Figure I-16. As R was reduced, for a fixed operating voltage, the pulse voltage measured across it increased in amplitude but decreased in duration. For the circuit shown, the pulse duration was $4\mu\text{s}$ for $R = 15\Omega$ and $V_s = 400\text{ V}$. When a trigger transformer type IT332 was placed in series with R , as shown in Figure I-17, the secondary pulse across the test load R' was of low amplitude due to the high voltage drop across R . Reversing the transformer and lowering R to a value comparable with the new transformer-primary resistance gave a high amplitude pulse of $\sim 800\text{ V}$, but of very low duration ($< 1\mu\text{s}$). In this configuration, $R = R_s = 0.5\Omega$, where R_s was the transformer secondary resistance (the secondary was used as the primary to give a step-up output). Using a -150 V bias voltage, R was adjusted to give a compromise between pulse height and duration. R was finally chosen as 3.3Ω which gave a $550\text{ V}/10\mu\text{s}$ pulse across R' ($1\text{ k}\Omega$) using a 500 V supply. This (traced) pulse is shown in Figure I-18.

Two identical units were constructed using the circuit shown in Figure I-16.

In practice, the load imposed by the thyratron was lower than R' and thus the pulse amplitude was higher. A supply voltage of 180 V d.c. was sufficient to yield the pulse shown in Figure I-19. This shows a 450 V spike superimposed on a -150 V bias (giving a 300 V spike). This pulse was suitably damped to help inhibit thyratron recovery.

Fine adjustment of the supplies was then made using the meters as a guide for loaded operating voltages.

3.1.6.2 The T1 and T2 trigger circuits

In order to prevent the application of high voltages to the thyratron anode

The G2 negative bias voltage for T1 was variable from 0 to -170 V d.c. and was controlled by a variac. This voltage was displayed on a panel meter. The supply is shown in Figure I-15 and consisted of Tr19, D18, C33 and R43. This bias voltage was fed through a pulse transformer Tr20 and to G2 through the pulse filter consisting of R8, 9, 10 and C2 and C3. A series resistance R7 of $2\text{ k}\Omega$ was used to limit the grid current.

The trigger voltage V_T was also variable, from $0 - 1000\text{ V d.c.}$ and was controlled by variac Tr16. This supply consisted of D16, C31, R40 and C32. Capacitor C32 ($0.1\mu\text{F}$) was charged by the supply and resistor R40 (10k) to the chosen d.c. voltage, which was monitored on a display meter.

When a 6 - 20 V pulse triggered the Tr21 primary, thyristor D20 was triggered and V_T appeared across Tr20 primary and resistor R. Tr20 produced a stepped-up impulse superimposed upon the bias voltage which triggered T1.

The circuit was duplicated for T2, except that this circuit was built adjacent to the thyatron anode and lay at anode potential. The pulse trigger voltage was 9 V and the supply voltage was fixed at 180 V d.c. This was obtained by recitifying a 120 V a.c. voltage from a step-up transformer Tr5 shown in Figure I-13. Bias voltage was also fixed at -150 V d.c., obtained from a similar secondary winding on Tr5. All voltages were referenced to anode potential.

3.1.7 The grounded heater supply boxes

Two identical units were constructed using the circuit shown in Figure I-14. The two unloaded outputs of each supply were variable from 0 to 7.0 V a.c.

Two meters were used to indicate the output voltage levels. Meter accuracy was found to lie within 10% of the supply output. Due to the high operating currents, the meters were adjusted to read 6.3 V when 6.3 V was read at the thyatron terminals. Fine adjustment of the supplies was then made using the meters as a guide for loaded operating voltages.

In order to prevent the application of high voltages to the thyatron anode and grids before the thyatrons reached their stable operating temperatures, a timer unit was activated when the heater box was switched on. This unit inhibited the high voltage supply and the thyatron supply for fifteen minutes, thus avoiding the possibility of premature operation. The two timer unit outputs were open and close relay contacts rated at 10 A, 220 V a.c.

3.1.8 The grounded thyatron supply box

Two identical units were constructed using the circuit shown in Figure I-15. Each unit gave 3 output voltage levels for biasing G1 and biasing and triggering G2.

Figure I-18.

Measured trigger pulse with a resistive load.

Figure I-19.

Measured trigger pulse and bias with a thyatron load.

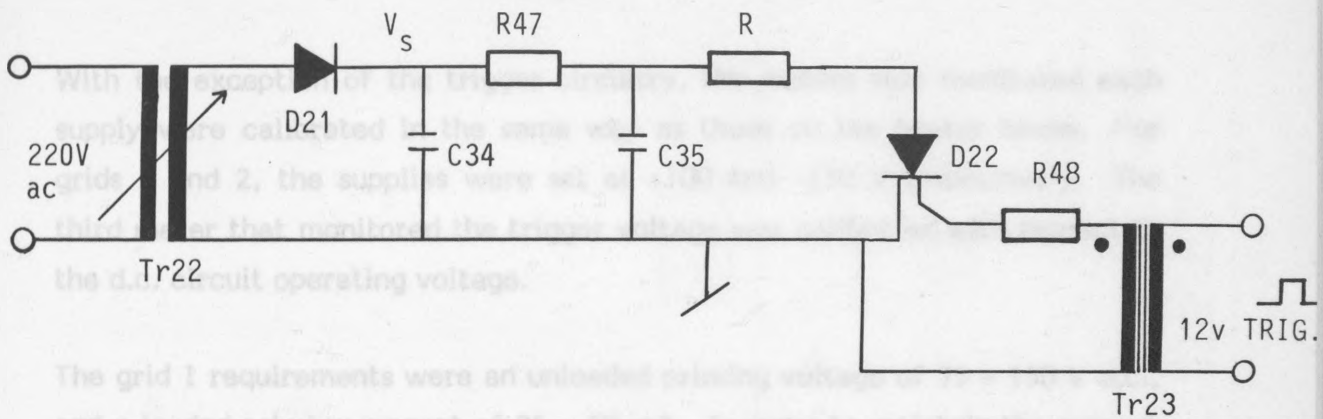


Figure I-16. Basic thyatron trigger circuit.

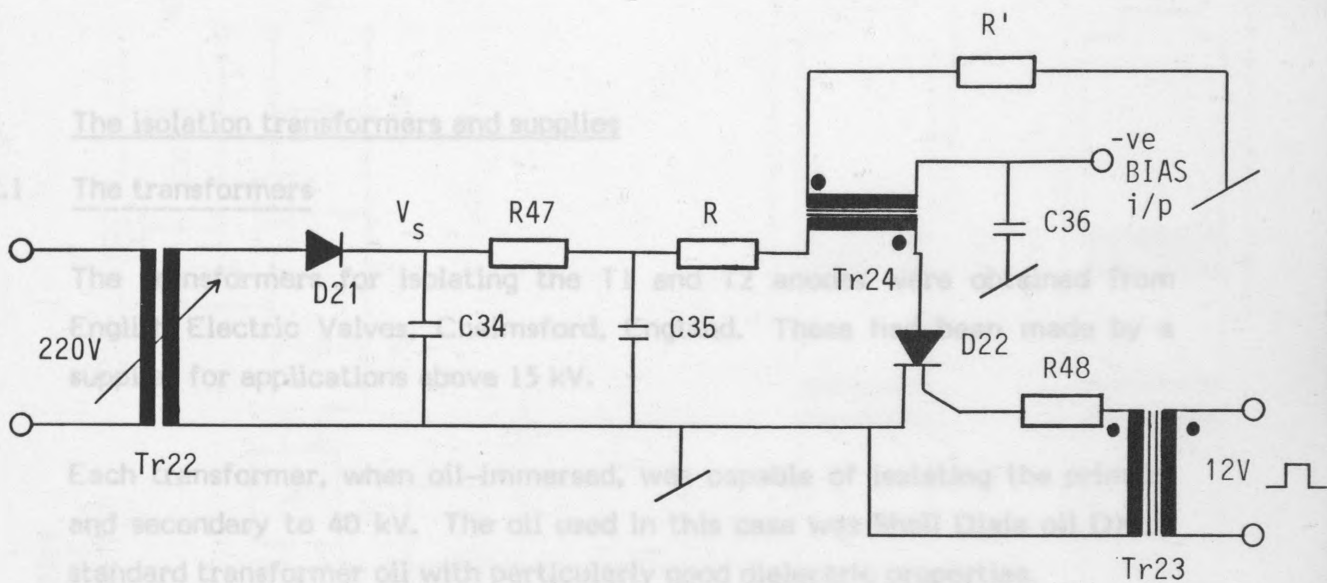


Figure I-17. Modified thyatron trigger circuit.

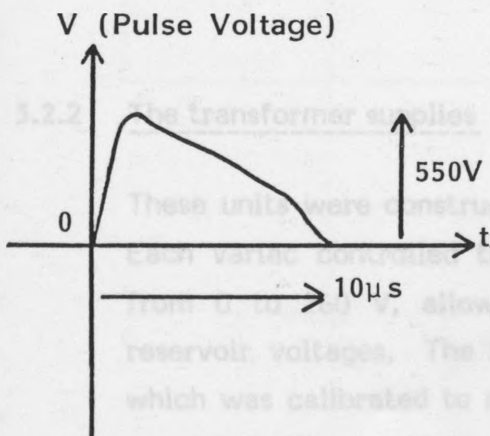


Figure I-18.

Measured trigger pulse with a resistive load.

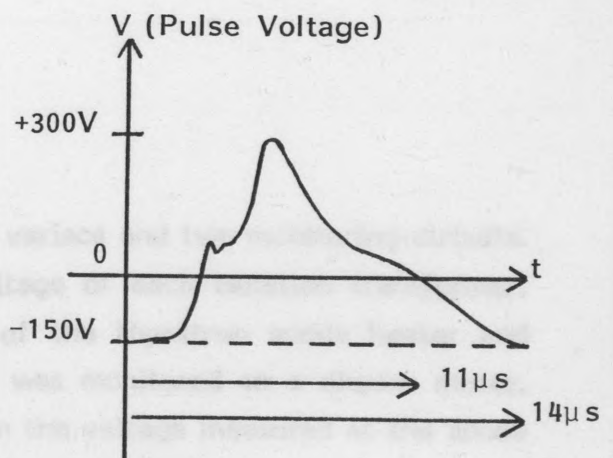


Figure I-19.

Measured trigger pulse and bias with a thyatron load.

With the exception of the trigger circuitry, the meters that monitored each supply were calibrated in the same way as those on the heater boxes. For grids 1 and 2, the supplies were set at +100 and -150 V respectively. The third meter that monitored the trigger voltage was calibrated with respect to the d.c. circuit operating voltage.

The grid 1 requirements were an unloaded priming voltage of 75 - 150 V d.c., and a loaded priming current of 25 - 50 mA. In order to maintain the current in the grid circuits, priming resistors were placed beside the grids G1 and G2 as shown in Figure I-12. Also shown is a pulse filter consisting of R8, 9, 10 and C2 and C3. This served to reduce any effects of high voltage transients, produced upon triggering, from reaching the bias circuitry.

3.2 The isolation transformers and supplies

3.2.1 The transformers

The transformers for isolating the T1 and T2 anodes were obtained from English Electric Valves, Chelmsford, England. These had been made by a supplier for applications above 15 kV.

Each transformer, when oil-immersed, was capable of isolating the primary and secondary to 40 kV. The oil used in this case was Shell Diala oil DX, a standard transformer oil with particularly good dielectric properties.

The transformer primaries were wound for 220 V and the secondaries were wound for 6.3 V at 30 A. A 50 VA step-up transformer was located beside the secondary to give a 110 V grid voltage, which was led to the anode together with the heater (6.3 V) voltage.

3.2.2 The transformer supplies

These units were constructed using two variacs and two monitoring circuits. Each variac controlled the primary voltage of each isolation transformer, from 0 to 260 V, allowing variation of the thyatron anode heater and reservoir voltages. The heater voltage was monitored on a display meter, which was calibrated to read 6.3 V when the voltage measured at the anode was 6.3 V. The complete circuit is shown in Figure I-20.

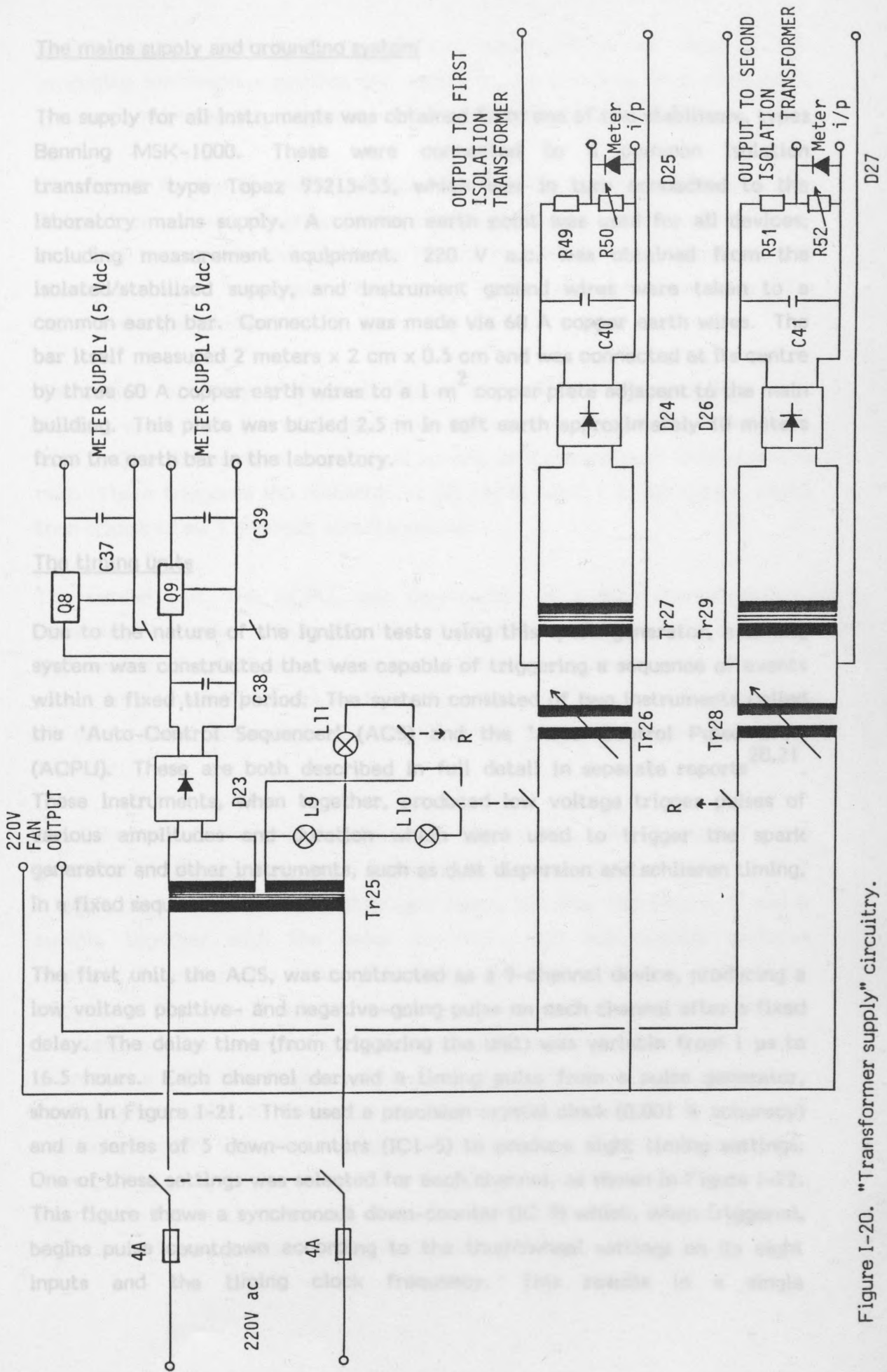


Figure I-20. "Transformer supply" circuitry.

3.3 The mains supply and grounding system

The supply for all instruments was obtained from one of two stabilisers, types Benning MSK-1000. These were connected to a common isolation transformer type Topaz 95215-53, which was in turn connected to the laboratory mains supply. A common earth point was used for all devices, including measurement equipment. 220 V a.c. was obtained from the isolated/stabilised supply, and instrument ground wires were taken to a common earth bar. Connection was made via 60 A copper earth wires. The bar itself measured 2 meters x 2 cm x 0.5 cm and was connected at its centre by three 60 A copper earth wires to a 1 m² copper plate adjacent to the main building. This plate was buried 2.5 m in soft earth approximately 10 meters from the earth bar in the laboratory.

3.4 The timing units

Due to the nature of the ignition tests using this spark generator, a timing system was constructed that was capable of triggering a sequence of events within a fixed time period. The system consisted of two instruments called the 'Auto-Control Sequencer' (ACS) and the 'Auto Control Pulse Unit' (ACPU). These are both described in full detail in separate reports^{20,21}. These instruments, when together, produced low voltage trigger pulses of various amplitudes and duration which were used to trigger the spark generator and other instruments, such as dust dispersion and schlieren timing, in a fixed sequence.

The first unit, the ACS, was constructed as a 9-channel device, producing a low voltage positive- and negative-going pulse on each channel after a fixed delay. The delay time (from triggering the unit) was variable from 1 μ s to 16.5 hours. Each channel derived a timing pulse from a pulse generator, shown in Figure I-21. This used a precision crystal clock (0.001 % accuracy) and a series of 5 down-counters (IC1-5) to produce eight timing settings. One of these settings was selected for each channel, as shown in Figure I-22. This figure shows a synchronous down-counter (IC 9) which, when triggered, begins pulse countdown according to the thumbwheel settings on its eight inputs and the timing clock frequency. This results in a single

negative pulse output, which triggers the monostable output stage (IC 10), producing synchronous positive and negative output pulses. The monostable also served to reset the trigger input for each channel (IC 7).

The circuit for the channel shown was identical for the first eight channels. Channel nine served either as a reset channel, to avoid further countdown, or as a re-trigger channel, whereby each channel was re-triggered and countdown was resumed. This last mode of operation was the 'auto-sequence' mode.

The trigger circuitry is shown in Figure I-23. Three trigger options were possible apart from the re-trigger mode (shown as 'auto-reset'). These were 12 V or 24 V pulses, from an external source, or a manual push-button on the unit. These triggered the monostables (IC 13) at point T in the figure, which then triggered all 9 channels simultaneously.

The second unit, the ACPU, was constructed as a four channel device, producing four pulse outputs per channel. The delay circuitry was similar to that used for the ACS, except that each channel was independently triggered, either from another channel, or from the ACS. This gave a very wide range of delay times with high resolutions, when both units were connected together.

One channel of the unit is shown in Figure I-24. An 8-channel pulse generator similar to that shown in Figure I-21 was also used. When a 12 V trigger pulse arrives at the first trigger input, flip-flop channels A, C and D switch, together with the delay circuitry, with subsequently switches channels B and resets channel C. Each channel creates a pulse upon triggering. Channels A and B create a fixed duration pulse of 100 μ s, channel C creates a pulse dependent upon the time delay setting of IC 14 and channel D creates a pulse the duration of which is dependent upon the reception of a second trigger pulse 2. Thus, four operations in all, are carried out for each channel. Facility was provided for each channel to switch on either positive or negative going trigger pulses and for output pulse amplitude level to be selected as 5 V or 12 V for each of the four operations. The output stages for each channel were as shown below in Figure I-25.

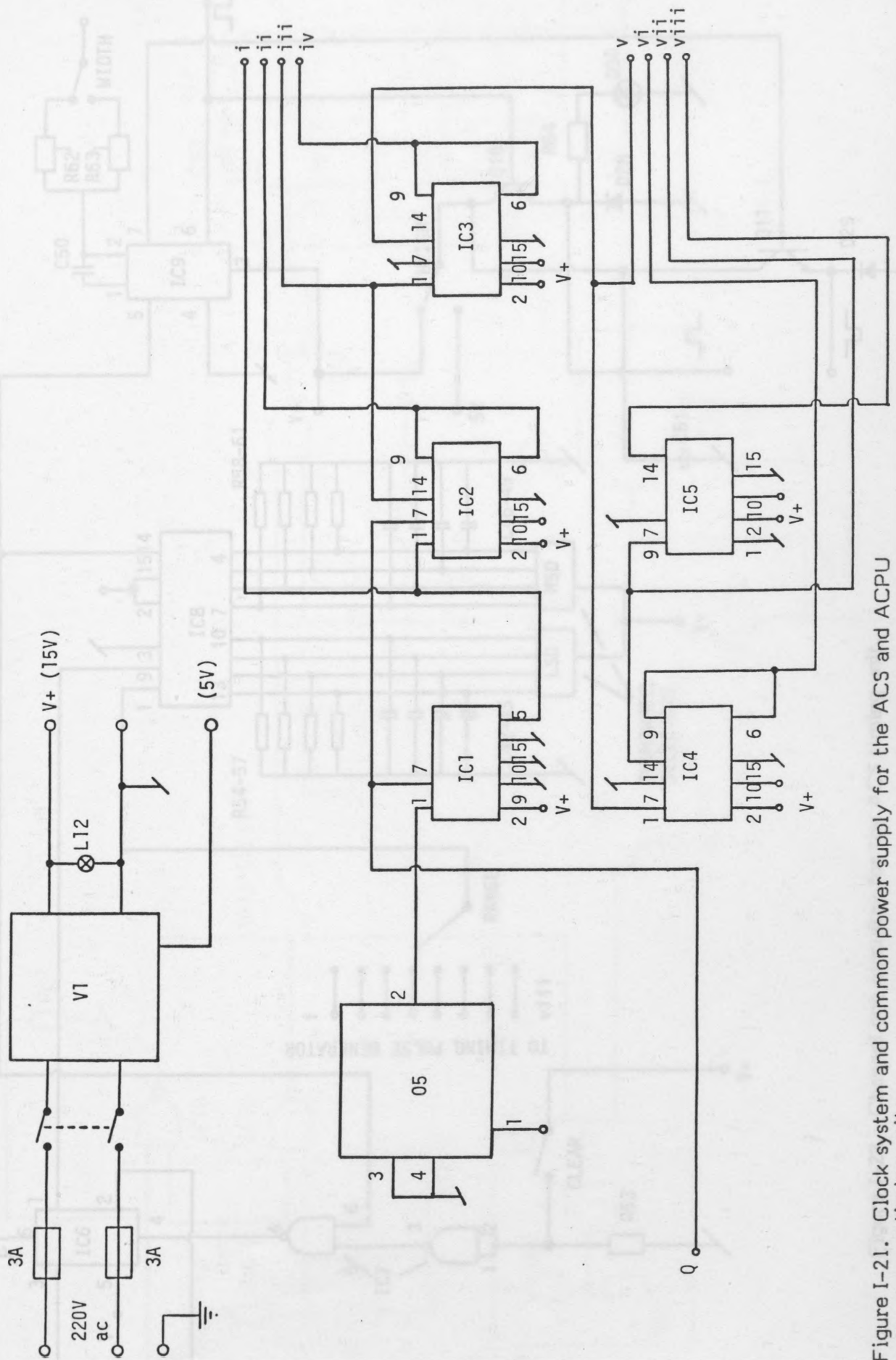


Figure I-21. Clock system and common power supply for the ACS and ACPU timing units.

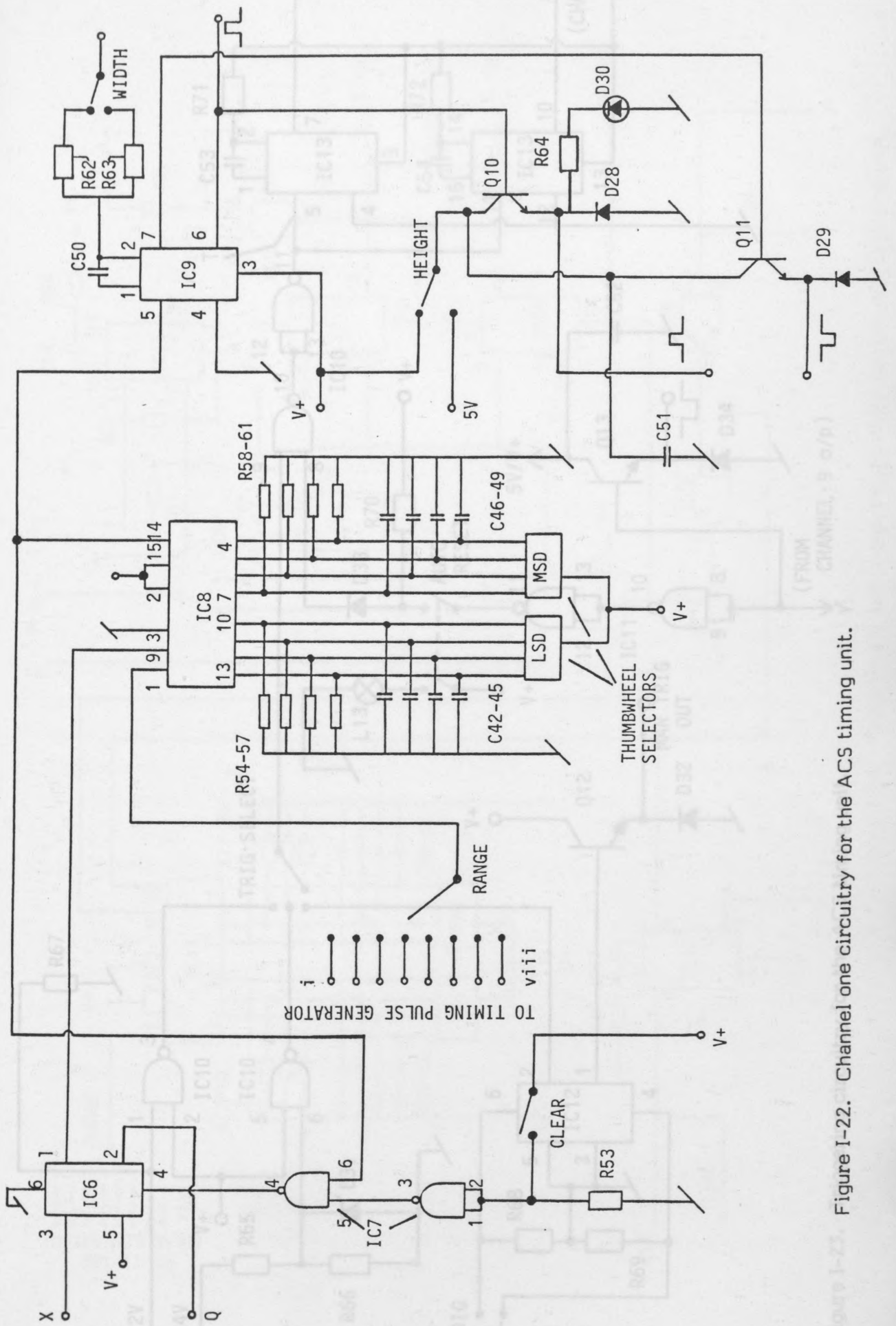


Figure I-22. Channel one circuitry for the ACS timing unit.

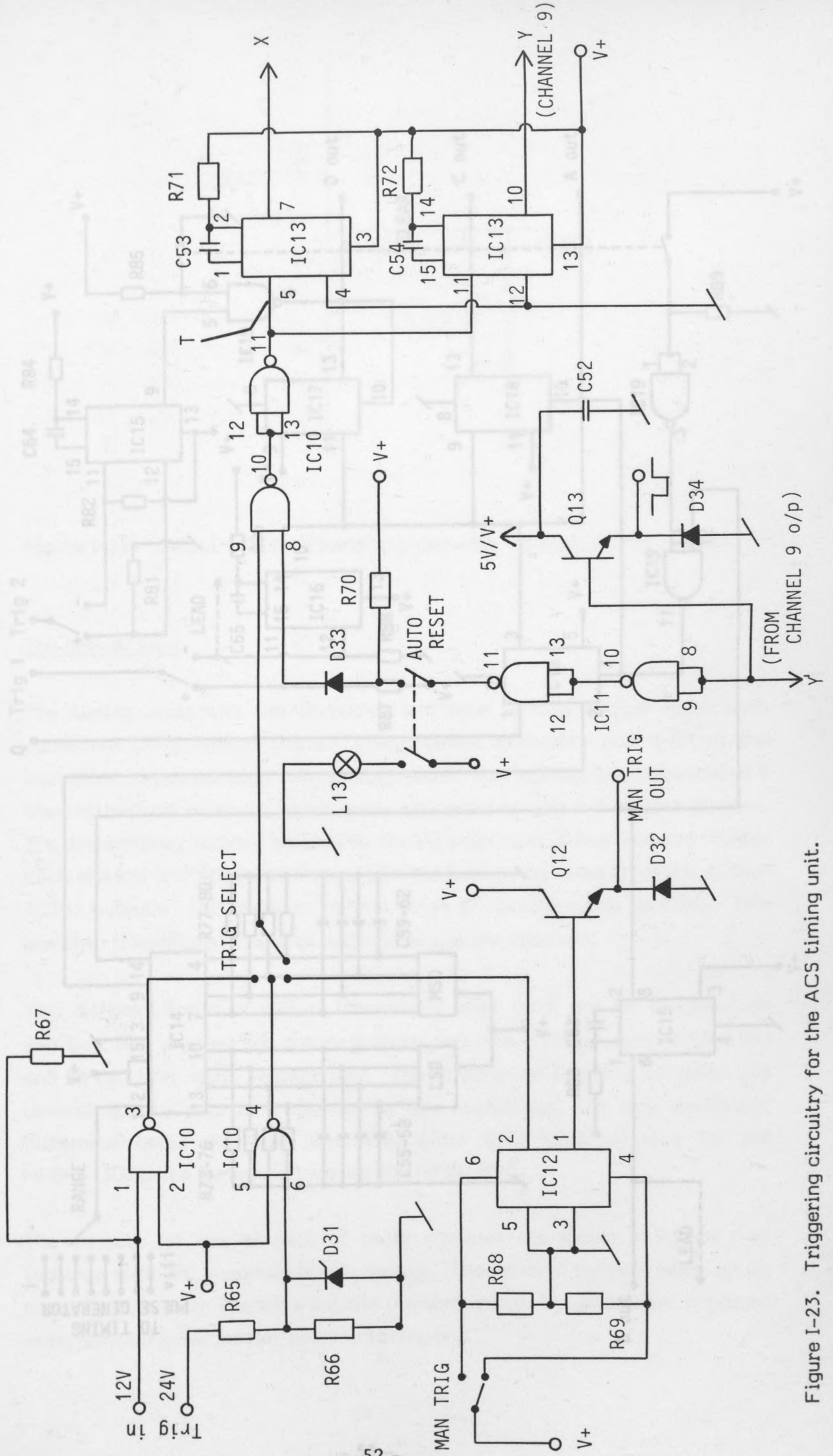


Figure I-23. Triggering circuitry for the ACS timing unit.

Figure I-24. Pulse timing and triggering circuitry for the ACS timing unit.

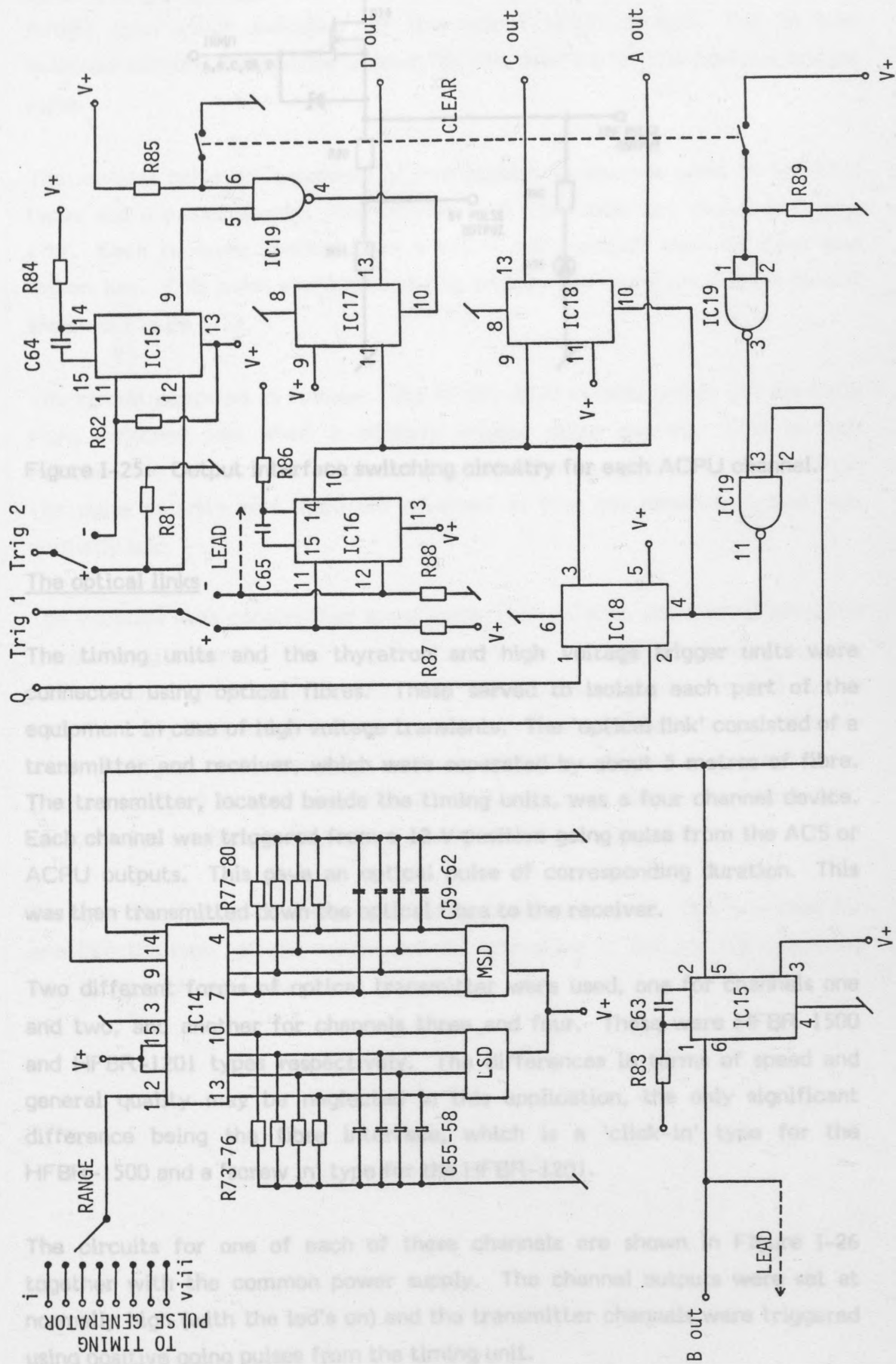


Figure I-24. Pulse timing and triggering circuitry for the ACPU timing unit.

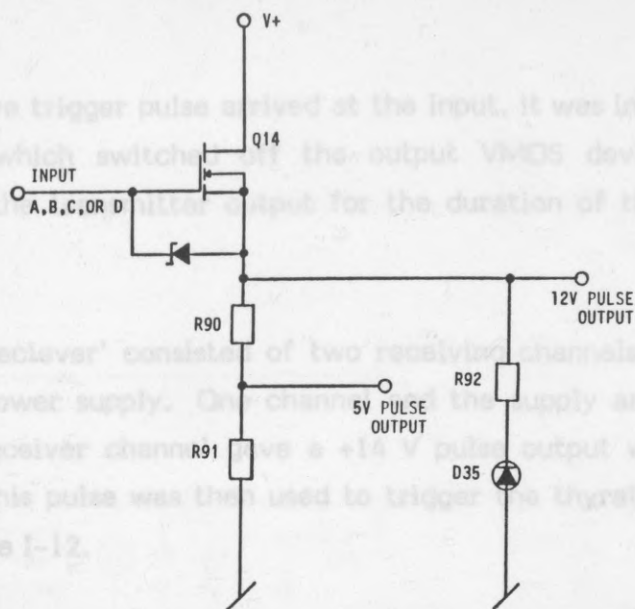


Figure I-25. Output interface switching circuitry for each ACPU channel.

3.5 The optical links

The receiver was constructed specifically for use with the two HFBR-2500. The timing units and the thyatron and high voltage trigger units were connected using optical fibres. These served to isolate each part of the equipment in case of high voltage transients. The 'optical link' consisted of a transmitter and receiver, which were separated by about 5 metres of fibre. The transmitter, located beside the timing units, was a four channel device. Each channel was triggered from a 12 V positive going pulse from the ACS or ACPU outputs. This gave an optical pulse of corresponding duration. This was then transmitted down the optical fibre to the receiver. One was used for enabling the high voltage supply, one for triggering T1 and one for triggering Two different forms of optical transmitter were used, one for channels one and two, and another for channels three and four. These were HFBR-1500 and HFBR-1201 types respectively. The differences in terms of speed and general quality may be neglected in this application, the only significant difference being the fibre interface, which is a 'click-in' type for the HFBR-1500 and a 'screw in' type for the HFBR-1201.

The circuits for one of each of these channels are shown in Figure I-26 together with the common power supply. The channel outputs were set at normally high (with the led's on) and the transmitter channels were triggered using positive going pulses from the timing unit.

When a positive trigger pulse arrived at the input, it was inverted through the NAND gate which switched off the output VMOS device. This in turn switched off the transmitter output for the duration of the positive trigger pulse.

The 'optical receiver' consisted of two receiving channels using HFBR-2500 types and a power supply. One channel and the supply are shown in Figure I-27. Each receiver channel gave a +14 V pulse output when its input was driven low. This pulse was then used to trigger the thyatron trigger circuit shown in Figure I-12.

The circuit operated as follows: The HFBR-2500 output, which was normally high, switched low when a positive trigger pulse arrived. This in turn switched the output VMOS high and triggered the thyatron trigger circuitry. The pulse polarity was therefore reversed so that the receiver output was normally low.

The receiver was constructed specifically for use with the two HFBR-2500 transmitting channels. The receiver for the one HFBR 1201 transmitter was mounted with the trigger circuitry for T2. The power supply for this device (D6, C17, Q1, C18) was obtained directly from the 6.3 V isolation transformer shown in Figure I-13. The 6.3 V heater supply was rectified as shown, to give approximately 9 V d.c. (instead of 14 V) so that when the HFBR-2201 receiver was triggered, a 9 V pulse was produced for triggering T2.

Three of the four optical transmitting channels were used. One was used for enabling the high voltage supply, one for triggering T1 and one for triggering T2. The fourth was redundant.

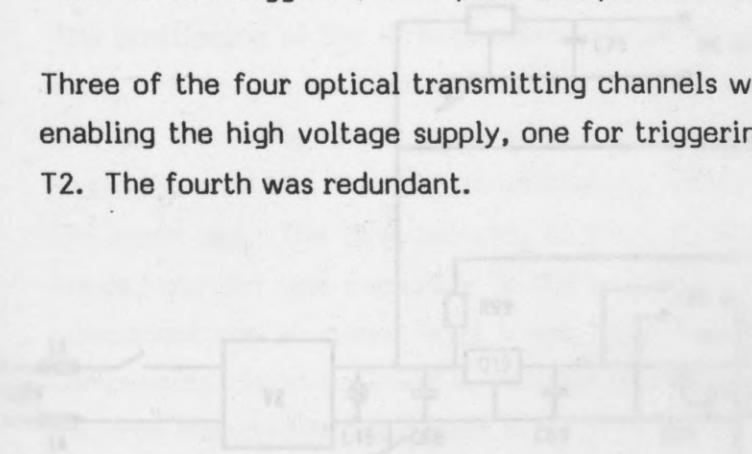


Figure I-27. The optical receiver circuit. One channel of two is shown.

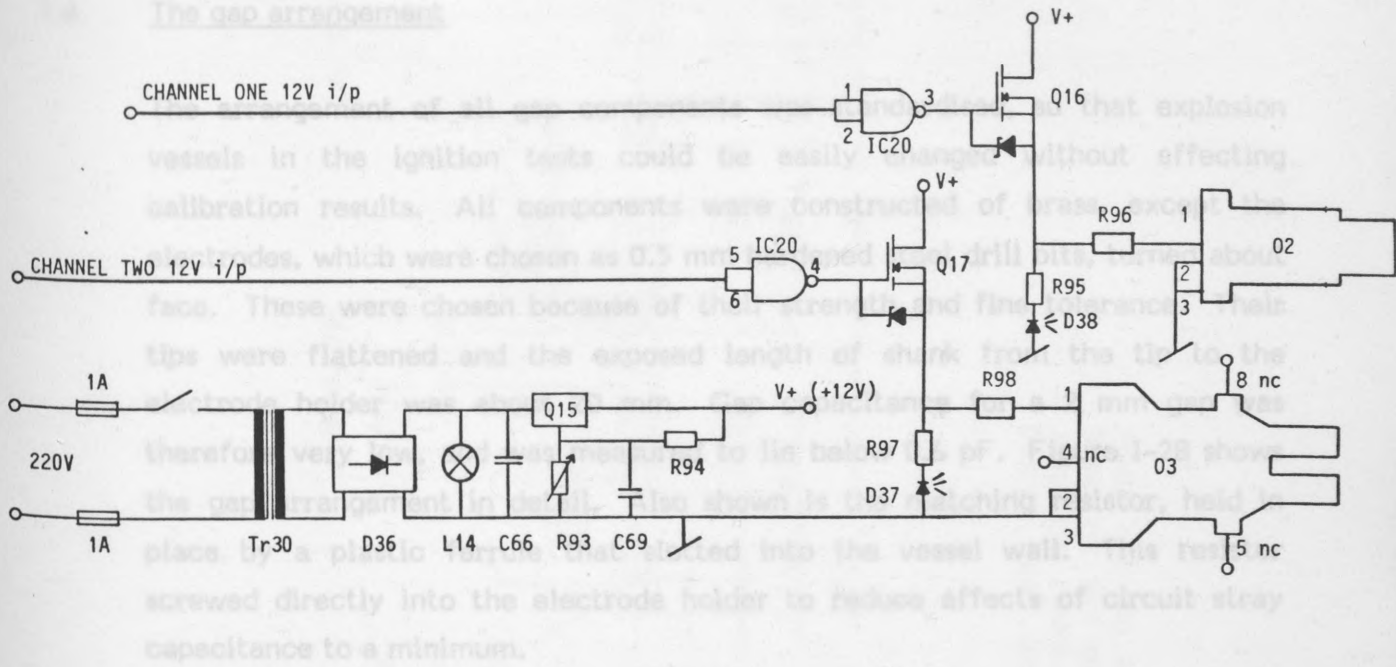


Figure I-26. The optical transmitter circuit. Two channels of four are shown.

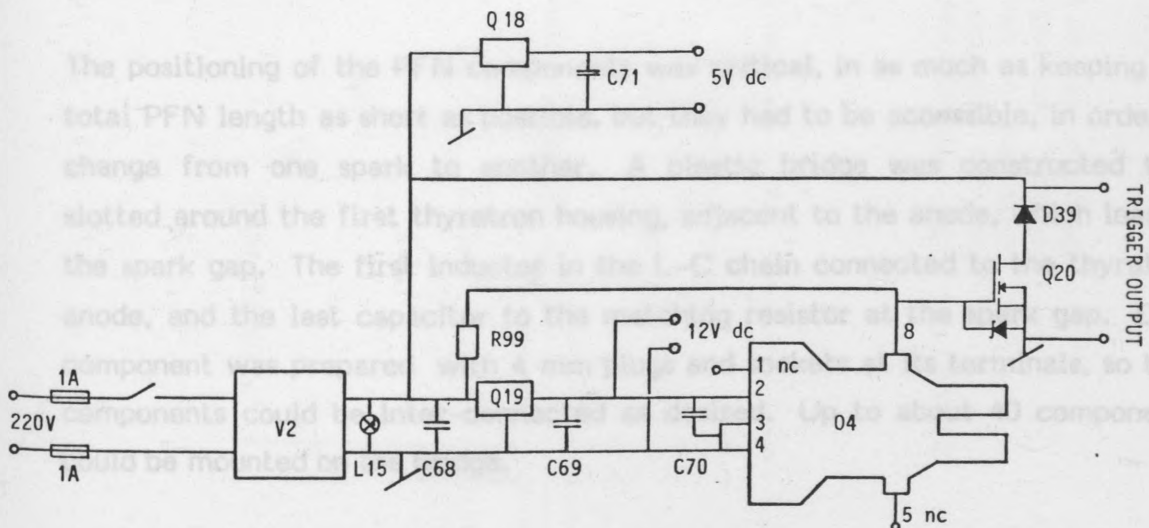


Figure I-27. The optical receiver circuit. One channel of two is shown.

3.6 The gap arrangement

The arrangement of all gap components was standardised, so that explosion vessels in the ignition tests could be easily changed without affecting calibration results. All components were constructed of brass, except the electrodes, which were chosen as 0.5 mm hardened steel drill bits, turned about face. These were chosen because of their strength and fine tolerance. Their tips were flattened and the exposed length of shank from the tip to the electrode holder was about 20 mm. Gap capacitance for a 2 mm gap was therefore very low, and was measured to lie below 0.6 pF. Figure I-28 shows the gap arrangement in detail. Also shown is the matching resistor, held in place by a plastic ferrule that slotted into the vessel wall. This resistor screwed directly into the electrode holder to reduce effects of circuit stray capacitance to a minimum.

The resistors were hand-made items produced by Welwyn, UK, types T44TUL. These resistors were constructed to withstand high current transients of about 100A for some several hundreds of microseconds, and were also flame-retardant. Worst-case inductance values for these resistors were below 0.1 μ H.

3.7 The PFN components

The positioning of the PFN components was critical, in as much as keeping the total PFN length as short as possible, but they had to be accessible, in order to change from one spark to another. A plastic bridge was constructed that slotted around the first thyatron housing, adjacent to the anode, which lead to the spark gap. The first inductor in the L-C chain connected to the thyatron anode, and the last capacitor to the matching resistor at the spark gap. Each component was prepared with 4 mm plugs and sockets at its terminals, so that components could be inter-connected as desired. Up to about 40 components could be mounted on the bridge.

The capacitors were manufactured by Leclanche, and were polystyrene types Pht, rated at 40 kV with a tolerance of $\pm 10\%$. The values were 20 pF, 50 pF, 100 pF, 150 pF, 200 pF, 390 pF, 500 pF, 680 pF, 1 nF, 2 nF and 2.5 nF.

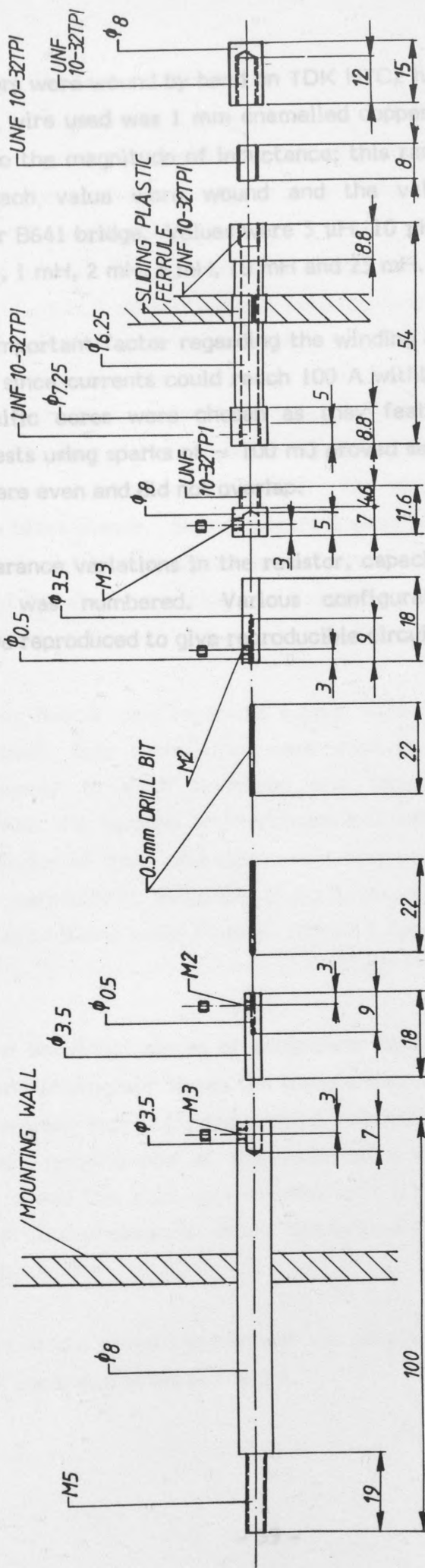


Figure I-28. The gap arrangement showing matching resistor (with sliding ferrule). Electrodes (drill bits) are of hardened steel. All other parts are of brass. The adjacent electrode to the matching resistor connects to the measuring resistor via the M5 screw thread on the far left of the figure.

The inductors were wound by hand on TDK H7C2 high-permeability soft-ferrite cores. The wire used was 1 mm enamelled copper. Four core sizes were used according to the magnitude of inductance; this ranged from 5 μ H to 25 mH. 10 coils of each value were wound and the values were checked using a Wayne-Kerr B641 bridge. Values were 5 μ H, 10 μ H, 20 μ H, 50 μ H, 100 μ H, 200 μ H, 500 μ H, 1 mH, 2 mH, 5 mH, 10 mH and 25 mH.

The most important factor regarding the winding of the inductors was the core saturation, since currents could reach 100 A within a fraction of a millisecond. These specific cores were chosen as they featured a high saturation flux density. Tests using sparks of ~ 100 mJ proved satisfactory, providing that the windings were even and did not overlap.

Due to tolerance variations in the resistor, capacitor and inductor values, each component was numbered. Various configurations of components could therefore be reproduced to give reproducible circuit conditions.

High current heater and reservoir supply wires were 1.3mm². To reduce resistive losses, four such wires were used to connect each heater and reservoir supply to each thyatron and lamp. High voltages were conveyed from the supplies to thyatrons and tubes using RS 223 U-coaxial cable. Soldering of these and other short connecting cables carrying HT was carried out carefully to avoid any sharp edges, which would promote corona leakage. Connections were Fletcher 27A017 type, laboratory rated to 80 kV.

Some of the individual pieces of equipment are shown in photographs 1.1 to 1.5. The first photograph shows the transformer supply (1), the heater supply (2), the thyatron supply (3) and vacuum receiver (4). Figure 1.2 shows one can see the bath housing one of the tubular transformers (1). The second photograph shows the auto-control plate with 221 and 222 control relays (2), and the third photograph shows the vacuum thyatron, which is connected to the timing units.

Photographs of the remaining parts of the apparatus are shown together with the ignition apparatus in parts 2 and 3.

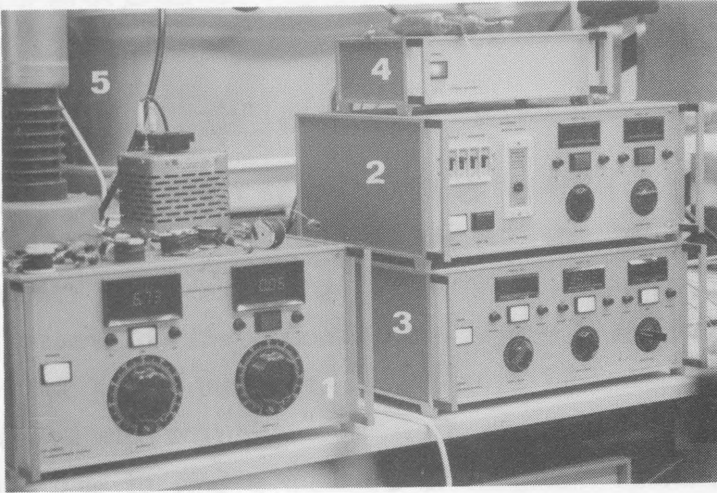
4. CONSTRUCTION AND LAYOUT

The grounded thyatron supplies, heater supplies, transformer supply, optical units and trigger units were constructed independently using metal 'Elra' cases. Apart from the optical triggering fibres, all connecting leads, whether high voltage or low voltage, were kept as short as possible. The trigger units (the ACS and ACPU) were physically isolated from the thyatrons by about 4 m to avoid unwanted triggering due to the E.M.I. generated by the thyatrons. Otherwise, the positioning of the various items of equipment was such as to maintain low lead lengths and facilitate the fan-cooling of the thyatrons. The first thyatron lay in an oil bath with its anode accessible for connection and changing of the PFN. The second device was vertically mounted on brass stands. Both thyatrons were placed adjacent to the spark gap, but their relative positions were found to be critical due to spurious triggering of T2 when triggering T1. Careful screening of the devices served to eliminate this problem.

High current heater and reservoir supply wires were 1.5mm^2 . To reduce resistive losses, four such wires were used to connect each heater and reservoir supply to each thyatron end terminal. High voltages were conveyed from the supplies to thyatrons and EVM's using RS 223 U coaxial cable. Soldering of these and other short connecting cables carrying HT was carried out carefully to avoid any sharp edges, which would promote corona leakage. Connections were Fischer 107A017 types, laboratory tested to 80 kV.

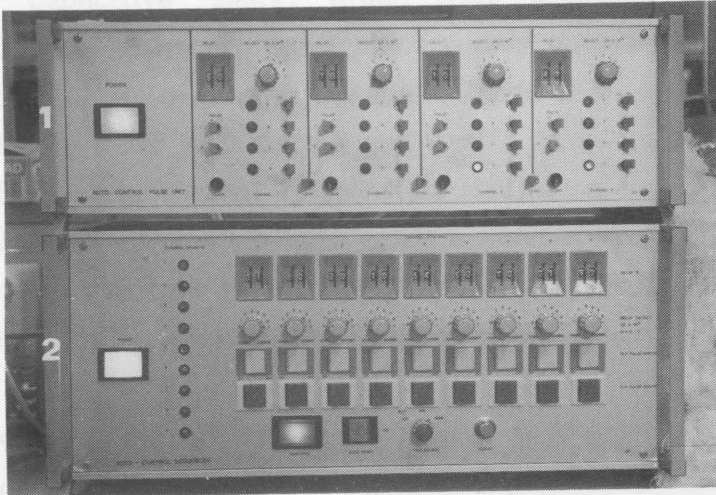
Some of the individual pieces of equipment are shown in photographs I-1 to I-3. The first photograph shows the transformer supply (1), the heater supply (2), the thyatron supply (3) and optical receiver (4). Behind these one can see the bath housing one of the isolation transformers (5). The second photograph shows the auto-control pulse unit (1) and auto control sequencer (2), and the third photograph shows the optical transmitter, placed adjacent to the timing units.

Photographs of the remaining parts of the generator are shown together with the ignition apparatus in parts 2 and 3.



Photograph I-1.

Thyatron supply and triggering equipment.



Photograph I-2.

Timing units.



Photograph I-3.

Optical transmitter.

5. THE SPARK ENERGY MEASUREMENT SYSTEM

5.1 Background

Since the days of the earliest work in the field of spark ignition^{22,23}, a variety of methods have been used to evaluate the incendivity of an electric spark, usually by measuring energy or charge dissipated in the spark gap. There were two reasons for this, according to the type of spark ignition work being carried out. For safety purposes, i.e. where a laboratory-produced spark was being compared with possible electrostatic or break-flash discharges in practice, the reason was to find a measure of minimum spark incendivity, for which an ignition hazard existed. A number of workers soon found, however, that incendivity could be expressed in a variety of ways, depending upon the circuit producing the spark. For example Morgan²⁴ and Finch²⁵ spoke of 'inductive' and 'capacitive' sparks which were produced under different electrical conditions, both of which yielded widely different incendivities. The problem then arose as to whether the spark should be 'measured' in terms of the circuit producing it, or in the spark gap itself. This also applied to the second area of ignition work, that of deliberately igniting a fuel, for example in an internal combustion engine. In both cases a need arose to classify the spark, be it in terms of a certain aspect of the spark itself, or the circuit producing it, to give a minimum 'measure' of the ignitability of a given fuel medium.

A confused picture emerged as early as the 1920's, because various workers defined 'spark intensity' in terms of the circuit producing the spark, very often using arbitrary experimental conditions such as gap width settings and inclusion of various circuit reactances.

A major attempt to clarify this was made by Finch and Sutton²⁶ in 1932, who used an oscilloscope camera to 'catch' the spark current and voltage curves as the spark passed. This gave way to the concept of 'minimum ignition spark energy' as obtained by integrating the spark voltage and current curves over the spark duration. Thus the term 'spark intensity' was replaced by 'spark energy', which has been used ever since.

The method of measuring spark energies has remained virtually unchanged since 1932. Typically, the spark gap voltage is measured using a high voltage probe and the gap current is measured using a precision resistor or current probe. Although probing methods vary from laboratory to laboratory, the general

principle of calculating spark energy is the same. Once the spark voltage $V(t)$ and spark current $I(t)$ have been recorded, over the duration of the spark (t), the spark energy (E) is obtained from

3.2 The measurement equipment

$$E = \int_0^t V(t) I(t) dt$$

3.2.1 The digitising system

Due to the transient nature of a spark discharge, whose duration may vary from fractions of a microsecond to many milliseconds, the voltage and current curves must be retained in some manner for integration. Finch and Sutton's simple camera method, for example, is still widely in use. More recently, as both phosphorescent cathode ray tube screens and digital storage methods have become available, waveform storage has become possible and photographs can be taken after the spark had passed. In these cases, spark energies have to be evaluated manually. First, points are read off the $V(t)$ and $I(t)$ curves, and a power-versus-time curve is plotted. Then the curves are either cut out using scissors and weighed, or their areas are measured geometrically. These methods are quite often subject to appreciable errors, and are also laborious. Some however, are still in use today.

The apparent simplicity of the method of measuring spark energies using probing techniques, has often led a large number of workers into believing that this aspect of spark ignition work can be studied with the minimum of effort. Unfortunately, this is not the case, particularly when measuring low energy discharges (typically below ~ 10 mJ). This is because at such low energies, radiated circuit noise and high speed of events limit the precision with which normal measurements may be made. The measurement circuit as a whole, and its interaction with the spark generator circuit, must be studied carefully, as a UHF circuit. Simple and arbitrary probe/oscilloscope connection is unlikely to yield correct results.

3.2.2 Because of the intricacies of reliable measurement of low spark energies, a significant effort was made to tackle the problem in the present work. This resulted in a computerised oscilloscope system that was carefully built around the spark generator circuit. The system was based on the Tektronix 7612D/4052 instruments, and formed an accurate, operator-independent method

of spark-energy measurement, based on the digitisation of the spark voltage and current signal waveforms.

5.2 The measurement equipment

5.2.1 The digitising system

This system consisted of the Tektronix 4052 computer and 7612D dual-channel digitiser. The 7612D is a fast two-channel digitiser with a 200 MHz sampling rate and a GPIB port for data communication. The 4052 desk-top controller links with the 7612D using the GPIB bus and is used to read and process data from the 7612D according to the operator's demands.

The digitising system simultaneously converted the $V(t)$ and $I(t)$ analogue signals into digital codes using an analogue-to-digital conversion technique especially developed by Tektronix. They were then sent in code form over the GPIB bus to the 4052 controller. This manipulated the voltage and current curves to give plots of spark power and energy as functions of discharge time. With this system, errors were significantly reduced, as compared to conventional analogue systems, because the need to photograph the curves from a screen was obviated. Accuracy was also improved, particularly at low spark durations, due to the high sampling rate (200 MHz) of the 7612D. This meant that even when spark durations were as low as 0.1 μ s, total accuracy could be kept to within an estimated 5%.

Integration was performed by the 4052 computer by multiplying and summing the voltage and current waveforms. A set of programmes was written for this purpose, which also featured a range of functions to optimise the accuracy of the complete system. These are described in the following section.

5.2.2 Software for the digitising system

The software for addressing, polling and reading data from the 7612D digitiser, and for computation and display of data by the 4052, had to be developed, as no such software existed for this application. A number of

different programmes were written to read and display the data in several ways. Provision was also made to allow various input-amplifier configurations to be used with the 7612D. Special programmes were written for these configurations.

The task of the system software was to perform the following functions:

- a) Read and display the 'spark voltage' curve $V(t)$ or any part of it.
- b) Read and display the 'spark current' curve $I(t)$ or any part of it.
- c) Align the voltage and current waveforms to allow for phase differences between the two.
- d) Compute and display the 'spark power' curve $I(t) \cdot V(t)$ or any part of it.
- e) Compute and display the 'spark energy' curve $\int_0^t I(t) V(t) dt$ or any part of it.
- f) Begin integration following spark breakdown in order to eliminate effects of spurious noise signals prior to breakdown.
- g) Compute the net 'spark energy' from the 'spark energy' curve.
- h) Compute and display the 'dynamic impedance' (variation in spark voltage/spark current ratio with time).

A number of additional sub-programmes were also written, which included auto-zeroing of the waveforms and saturation warning, should either signal exceed the input amplifier range of the 7612D. These are described in detail in a separate report²⁷. In all some 12 programmes were written to cover the various configurations of input amplifiers used with the 7612D, and the use of break-points in the recordings. Programme language was TEK-BASIC.

One of these programmes, that used most widely for the acquisition and display of data in this work, is shown in Appendix 2 together with its flow-chart. Also shown is a glossary of symbols used in the programmes.

5.2.3 The probes

The current probe was a precision $10 \text{ m}\Omega$ resistor manufactured by HILO and the voltage probe a Tektronix P6015 type. These were chosen primarily for their wide-frequency range of operation. The voltage probe was used

because of its low tip capacitance (ca. 3 pF), high input resistance (100 M Ω), and its fast response time (< 5 ns). The current shunt was used because of its low inherent inductance and wide bandwidth (up to the order of 1GHz).

For spark energy measurements, the voltage probe was connected to the spark electrodes. The current resistor was permanently coupled to the ground electrode, and formed part of the generator circuit. The connection of the resistor is shown in section 3.6 and in the work describing ignition tests (see parts 2 and 3).

5.3 Features of the complete measurement system

5.3.1 Voltage waveform recording

5.3.1.1 Choice of voltage amplifier

A typical transient discharge gives a very fast voltage fall from the breakdown value to the arc-drop value. For example, this voltage may fall from 10 kV to about 50 V within about 10 ns. This change in the magnitude of the voltage must be recorded accurately, particularly at low durations of arc drop. The voltage probe itself is quite capable of responding to such a change, but a typical oscilloscope amplifier input stage may not be. Thus for voltage measurements following spark breakdown, a problem usually exists due to an overloading effect of the breakdown pulse on the voltage amplifier input. For example, when measuring an arc drop of ~ 50 V an input scale setting of 20 mV/div might be used, assuming a probe ratio of 1000. This means that for an operating voltage of 10 kV the input amplifier is overloaded by a factor of up to ~ 120 prior to breakdown. Under such conditions, where the amplifier input capacitance becomes charged prior to breakdown, the precise accuracy of the amplifier is difficult to predict. An indication of its response may be gained from the 'recovery time' quoted by the manufacturer. If this time is longer than the spark-signal duration, then a significant recording error may occur.

For this application an input amplifier was selected with a wide bandwidth (75 MHz) and fast risetime (4.7 ns), with a particularly fast recovery time. This was a Tektronix 7A13 type, with an effective screen height of up to 40.000 divisions. This becomes overdriven at an input setting of 0.1 V/div

when the input voltage exceeds about 40V. This would imply a wide enough dynamic range to faithfully record spark voltage signals. A check was made, however, to ensure no significant errors at low signal durations, using this input sensitivity without a probe, and a signal generator to simulate the spark voltage.

Spark voltage was simulated using an HP3343A signal generator, which produced a step pulse from 10 V to 0.05 V in 10 nS. This corresponded to a step pulse from 10 kV to 50 V using a 1000:1 probe. The step looked like that shown below in Figure I-29.

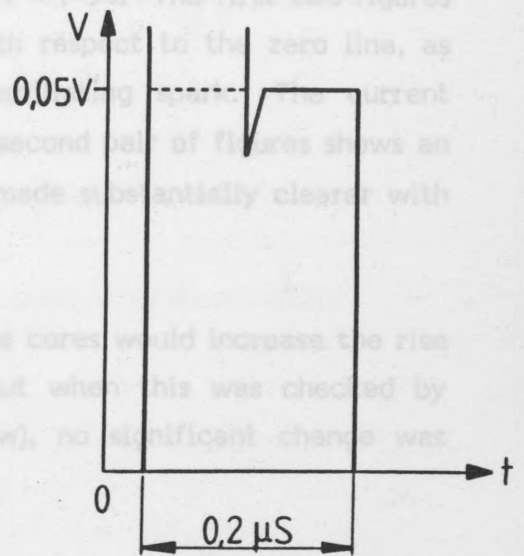
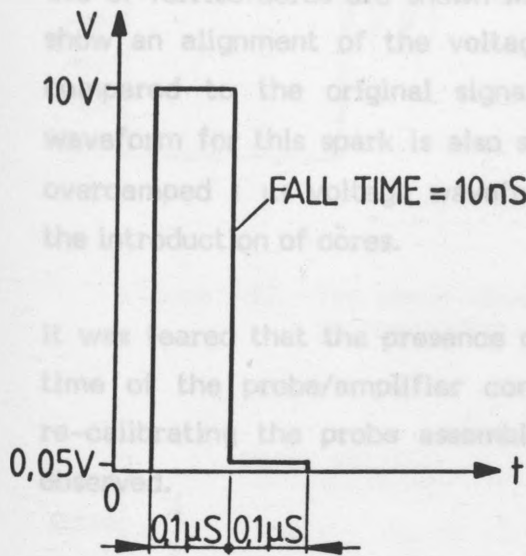


Figure I-29 Simulated spark voltage pulse. Figure I-30. Measured pulse.

The signal was then recorded using a 3' length of coaxial cable and the recorded signal viewed on the 4052 terminal. In this way the overall distortion of the signal could be calculated after passing through the digitizing system.

The results showed a faithful reproduction of the recorded signal over the period of the step change ($0.2 \mu\text{s}$), as shown in Figure I-30. The slight overshoot that was observed was probably due to the upper bandwidth limitation of the 7A13 amplifier.

5.3.1.2 Ground loops

Due to the probe lead length and its connection to the grounded input amplifier, the effects of high frequency fields, or ground loops, were sometimes evident at the digitiser input. This is a typical problem where fast transients are being measured and currents may be induced in the ground paths between the probe-circuit connection and the vertical amplifier input. To counteract these effects, ferrite cores were placed over the probe return cable to induce losses in the ground path. The exact number and positioning of these was found by trial and error. The problem was most acute using high gap widths and 'undervoltages', where a slight displacement of the signal with reference to the zero line was observed. Some typical results showing the use of ferrite cores are shown in Figures I-31 - I-34. The first two figures show an alignment of the voltage curve with respect to the zero line, as compared to the original signal, for an oscillating spark. The current waveform for this spark is also shown. The second pair of figures shows an overdamped 1 μ s voltage waveform that is made substantially clearer with the introduction of cores.

It was feared that the presence of the ferrite cores would increase the rise time of the probe/amplifier combination, but when this was checked by re-calibrating the probe assembly (see below), no significant change was observed.

5.3.2 Equipment calibrations

These included square-wave checks of the digitiser input amplifiers at regular intervals, and the weekly calibration check of the high voltage probe. For the latter tests, the probe/amplifier combination was used with an analogue mainframe (type 7834) and then checked again using the 7612D. The signal source was a HP8082A signal generator. Signals of 1 kHz and 1 MHz were used with rise times from 1 to 10 ns. 'Matching' of the 8082A output to the probe tip was achieved by shunting the tip with a 50 Ω carbon resistor.

No other calibration checks on the system were made, apart from an initial series of energy checks. These are described in section 5.5.

Measured waveforms showing the effects of using ferrite cores in the ground return path.

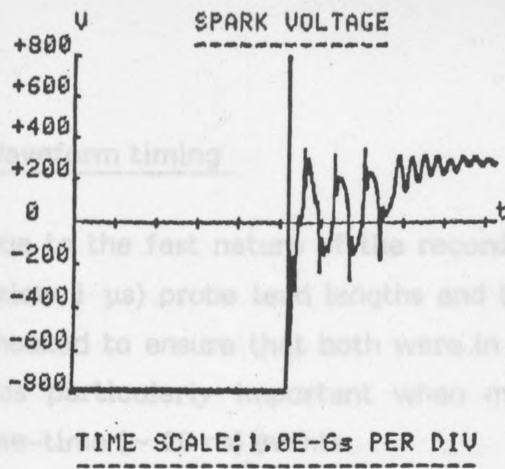


Figure I-31.

A measured oscillatory voltage waveform without cores.

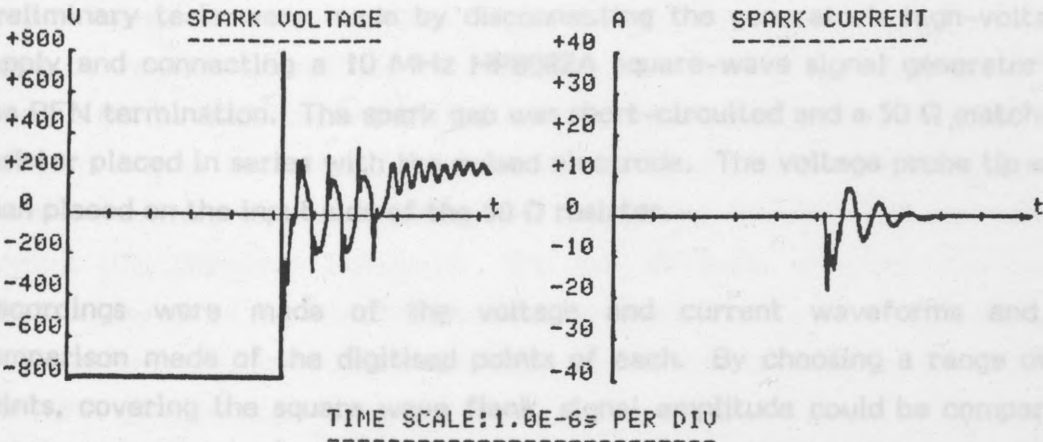


Figure I-32. The above waveform using cores. Also shown is the corresponding current waveform.

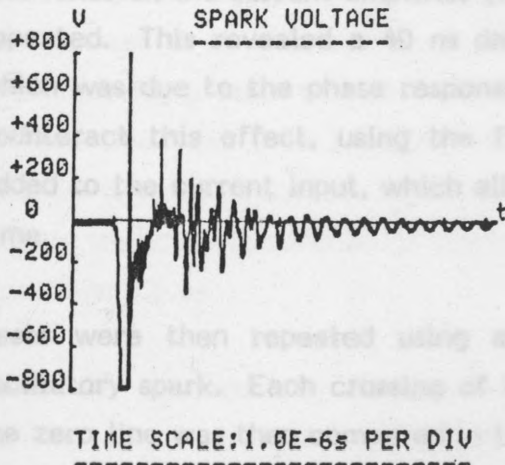


Figure I-33.

A measured unidirectional voltage waveform without cores.

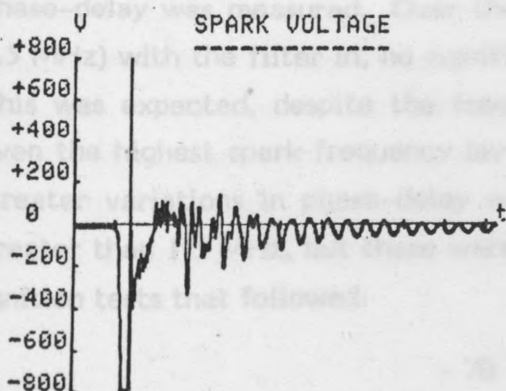


Figure I-34.

The above waveform using cores.

5.3.3 Waveform timing

Due to the fast nature of the recorded voltage and current signals (typically below 1 μs) probe lead lengths and terminations at the digitiser inputs were checked to ensure that both were in phase with respect to one another. This was particularly important when measuring low duration ($\sim 0.1 \mu\text{s}$) fast rise-time ($\sim 20 \text{ ns}$) events.

Preliminary tests were made by disconnecting the generator's high-voltage supply and connecting a 10 MHz HP8082A square-wave signal generator to the PFN termination. The spark gap was short-circuited and a 50 Ω matching resistor placed in series with the pulsed electrode. The voltage probe tip was then placed on the input side of the 50 Ω resistor.

Recordings were made of the voltage and current waveforms and a comparison made of the digitised points of each. By choosing a range of 5 points, covering the square wave flank, signal amplitude could be compared and the relative phase delay computed. Using the fastest digitising speed of the 7612D (200 MHz), no error was visible, meaning that delay was well within 5 ns.

The filter on the current amplifier (7A13) was then switched in, and the tests repeated. This revealed a 40 ns delay between current and voltage flanks, which was due to the phase response of the filter (not the probe leads). To counteract this effect, using the filter, an 8-point pre-trigger delay was added to the current input, which aligned the two waveforms with respect to time.

Tests were then repeated using a mis-matched PFN and producing an oscillatory spark. Each crossing of the current and voltage waveforms with the zero line was then compared in terms of the digitised array numbers. By varying the frequency of the spark current, the dependancy of frequency on phase-delay was measured. Over the range of frequencies used ($\sim 10 \text{ kHz} - 1.5 \text{ MHz}$) with the filter in, no significant change in delay time was observed. This was expected, despite the frequency-dependent delay of the filter, as even the highest spark frequency lay well below the filter cut-off frequency. Greater variations in phase-delay would be expected for spark frequencies greater than 1.5 MHz, but these were not used either in these tests, or in the ignition tests that followed.

5.3.4 Noise and shielding

Due to the very fast switching time of the thyatron T1, and the stray reactance associated with the supply circuits, a certain amount of radiated noise was inevitably produced in this part of the circuit. In addition, above about 16 kV, the thyatron tube began to radiate x-rays. The net result was that a burst of high frequency noise was recorded by the voltage and current probes. This lasted some microseconds and had a frequency of between 10 and 20 MHz. The noise was most problematic in the case of the current trace because recording-amplifier sensitivities were so high. Noise could then swamp the actual recorded current pulse, meaning that the calculated value of spark energy became quite inaccurate. In theory, it should be possible to screen this noise out by isolating the probes and the radiative part of the circuit (the thyatron circuitry). This was difficult, however, due to the physical layout of the circuit; distances between the thyatron and gap were necessarily small, and screens would have interfered with the accessibility to the PFN components. The problem was partly overcome by enclosing T1 in a metal-bath. Noise was, however, still picked up by the current probe and the measured amplifiers, both of which were located beside the bath.

Noise was further reduced by reducing the length of signal lead between the current probe and the input amplifier. This lead tended to pick up radiated noise, even at its shortest length of 35 cm, and so was double-screened. An analogue filter operating at 5 MHz on the input current amplifier helped to reduce this noise even further. The use of this filter however, reduced the fastest recordable current rise time to about 100 nS, meaning that significant errors would be introduced in spark energy calculation for spark durations of less than 0.5 μ s.

This did not normally become a problem, however, because the sparks produced by the circuit at such low durations were always low energy sparks (≤ 1 mJ). These were produced by 'undervolting' the gap to keep dissipated energy low, which in turn meant that time lag from thyatron triggering to gap breakdown was dramatically increased above the statistical time lag of the gap. This meant that radiated noise, which appeared upon thyatron triggering, occurred prior to gap breakdown, i.e. energy dissipation in the gap. The filter therefore became unnecessary at these durations where computed energy errors would otherwise occur.

Figure I-36. The same spark measurement as above, but where breakdown is delayed and the current pulse is separated from the circuit noise. A more accurate energy calculation results.

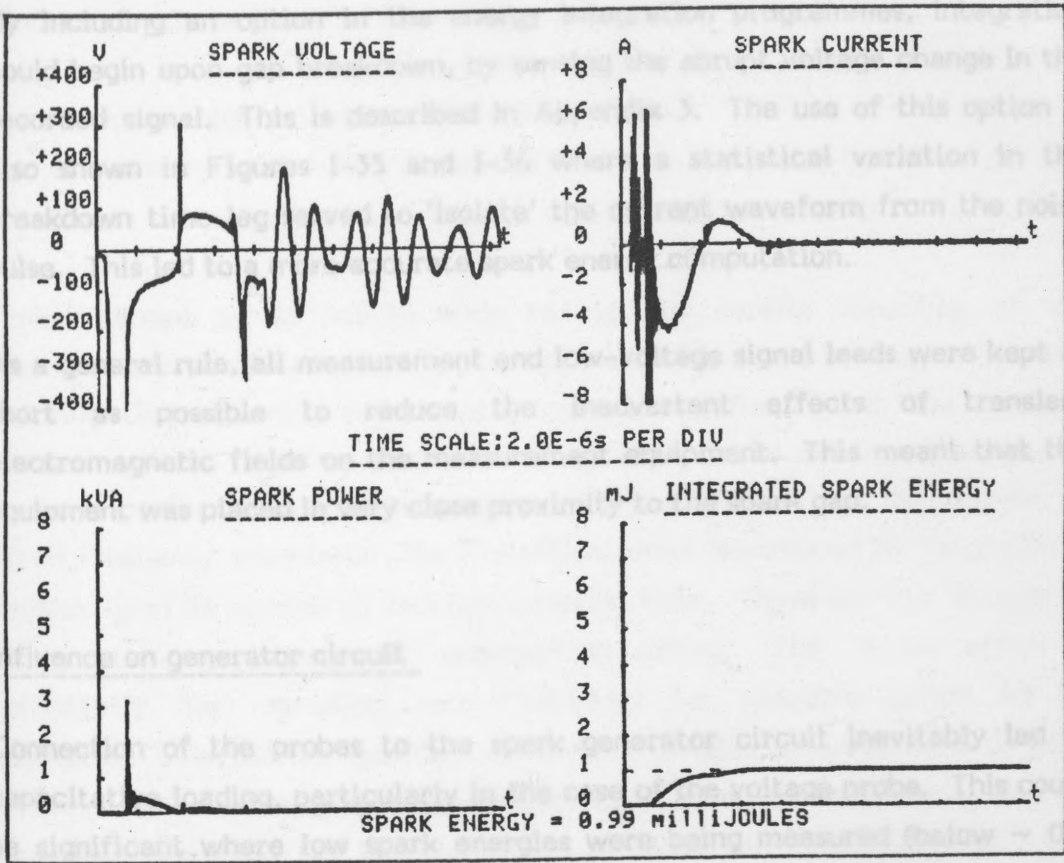


Figure I.35 A typical spark measurement where breakdown occurs rapidly and circuit noise is superimposed on the current pulse, which leads to errors in the energy calculation.

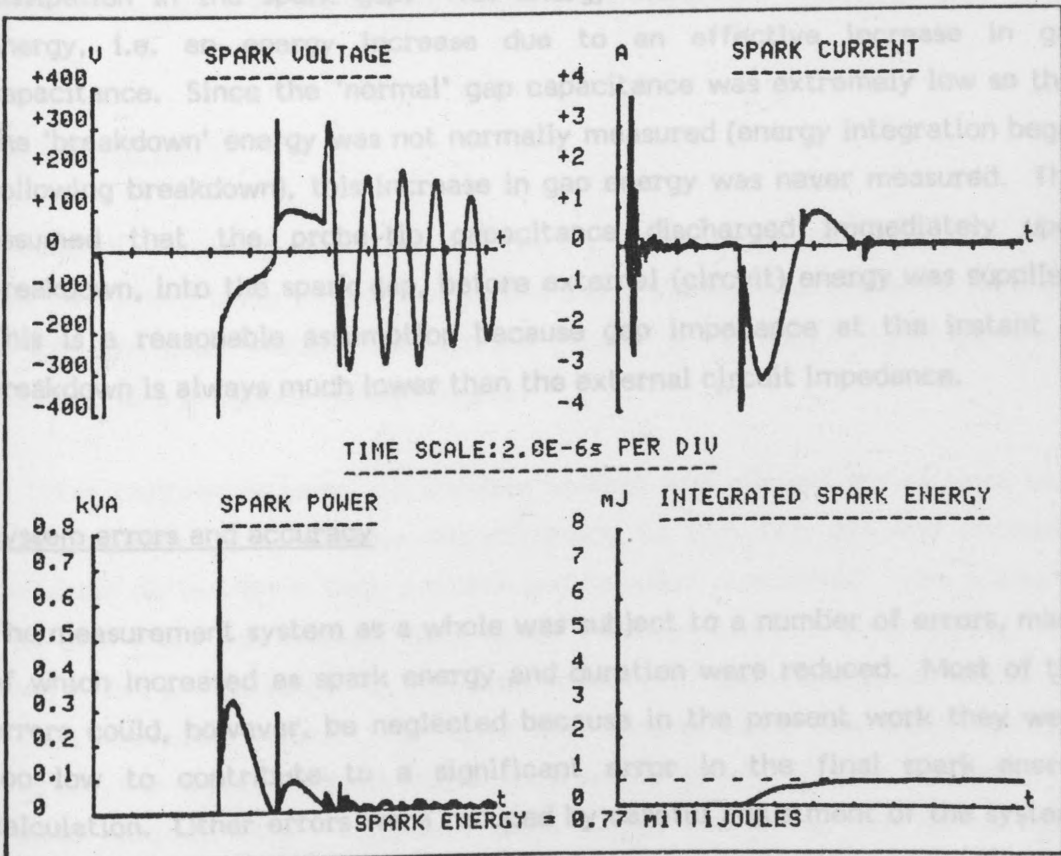


Figure I-36. The same spark measurement as above, but where breakdown is delayed and the current pulse is separated from the circuit noise. A more accurate energy calculation results.

By including an option in the energy integration programmes, integration could begin upon gap breakdown, by sensing the abrupt voltage change in the recorded signal. This is described in Appendix 3. The use of this option is also shown in Figures I-35 and I-36 where a statistical variation in the breakdown time lag served to 'isolate' the current waveform from the noise pulse. This led to a more accurate spark energy computation.

As a general rule, all measurement and low-voltage signal leads were kept as short as possible to reduce the inadvertent effects of transient electromagnetic fields on the measurement equipment. This meant that the equipment was placed in very close proximity to the spark gap.

5.3.5 Influence on generator circuit

Connection of the probes to the spark generator circuit inevitably led to capacitive loading, particularly in the case of the voltage probe. This could be significant where low spark energies were being measured (below ~ 0.5 mJ). This is principally due to the probe-tip capacitance (~ 3 pF). For a 10 kV operating voltage, this represented an additional 0.15 mJ energy dissipation in the spark gap. This energy manifests itself as 'breakdown' energy, i.e. an energy increase due to an effective increase in gap capacitance. Since the 'normal' gap capacitance was extremely low so that the 'breakdown' energy was not normally measured (energy integration began following breakdown), this increase in gap energy was never measured. This assumed that the probe-tip capacitance discharged immediately upon breakdown, into the spark gap, before external (circuit) energy was supplied. This is a reasonable assumption because gap impedance at the instant of breakdown is always much lower than the external circuit impedance.

5.4 System errors and accuracy

The measurement system as a whole was subject to a number of errors, many of which increased as spark energy and duration were reduced. Most of the errors could, however, be neglected because in the present work they were too low to contribute to a significant error in the final spark energy calculation. Other errors were reduced by careful adjustment of the system, as has already been described.

The errors may be listed as follows:

- a) Errors in signal acquisition by the probes
- b) Errors introduced by the presence of noise on the probe signals
- c) Errors in the computation of spark energy (digitiser errors)

Errors caused by a) and b) were reduced by careful screening of the measurement equipment, taking precautions as discussed in section 5.3, and ensuring that incoming signals gave maximum deflection on the digitiser input amplifiers. Possible errors caused by c) would be due to the digitiser's dynamic performance and resolution, which would tend to deteriorate as signal frequency increased. The theoretical error introduced by the digitiser depends upon its number of bits and sampling time. There are two sources of error; sampling errors and quantisation errors. The 7612D offers a sufficiently high sampling rate (200 MHz) for sampling errors to be negligible. Unavoidable quantisation errors, or general errors due to poor dynamic performance, are so low in this instrument that these may also be neglected, assuming the correct choice of input sensitivity settings. Any errors in the dynamic performance of the 7612D were therefore neglected in this work, even at high signal frequencies and without the use of averaging techniques. Spark energies were calculated to two significant figures.

5.5 Calibration tests

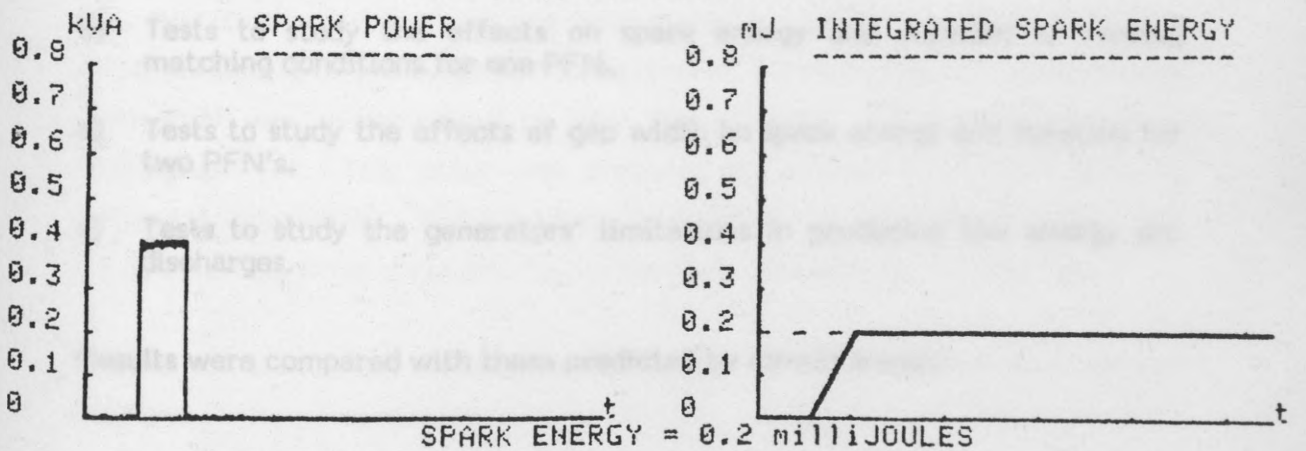
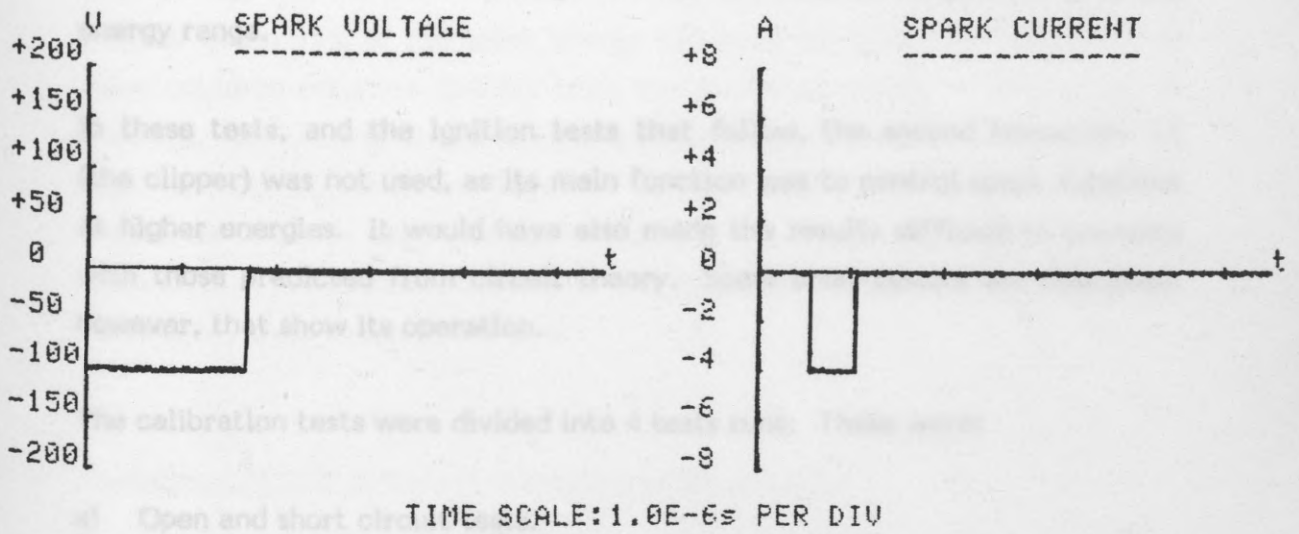
Instead of recording spark waveforms, an initial series of calibration tests was performed using single-shot pulsed input voltages, which were recorded to simulate spark voltage and current values. A HP 8082A signal generator was used as a precision voltage source.

In these calibration tests, all possible voltage and current scales were used together with input voltages corresponding to 1/4, 1/2, 3/4 and complete full-scale deflection in both positive and negative directions. Time scales of 1 μ s and 1 ms per division were used. Position controls were varied between \pm 3/4 of full-scale. In all cases, readings of spark energy lay within 1% of the expected values. The error was largest using low input voltages whereby the input signal-to-noise ratio was highest. Figure I-37 shows a typical printout, where computed spark energy lies at 0.2 mJ, for an input voltage of 100 V and a 0.5 μ s square current pulse of 4A amplitude.

No significant computation error was recorded. For lower amplitude current pulses of longer duration and where input sensitivity was too low, errors appeared due to poor bit resolution of the signal. Increasing sensitivity to fill the effective screen height of the input amplifiers eliminated this problem.

Description of tests

Before ignition tests were begun, a series of calibration tests were run to check the operation of the spark generator. First, all these tests were run under conditions that produced low energy discharges, in the range 0.1 to 0.2 mJ, that would be used in the subsequent ignition tests. (These tests were compared with those predicted by elementary transmission line theory (see section 2.2). Limitations of the generator were also investigated by running



Defining discharge duration

When a PFN is over- or under-matched, the wave current may tail off slowly. It is difficult to define from the measured wave current the exact discharge duration, especially visually. Energy expenditure during the tail of the discharge

6. GENERATOR CALIBRATION TESTS

6.1 Introduction

6.1.1 Description of tests

Before ignition tests were begun, a series of calibration tests was run to check the operation of the spark generator. Most of these tests were run under conditions that produced low energy discharges, in the range 0.1 - 10 mJ, that would be used in the subsequent ignition tests. Results were compared with those predicted by elementary transmission line theory (see section 2.2). Limitations of the generator were also investigated in this low energy range.

In these tests, and the ignition tests that follow, the second thyatron, T2 (the clipper) was not used, as its main function was to control spark durations at higher energies. It would have also made the results difficult to compare with those predicted from circuit theory. Some brief results are described, however, that show its operation.

The calibration tests were divided into 4 tests runs. These were:

- a) Open and short circuit tests.
- b) Tests to study the effects on spark energy and duration of varying matching conditions for one PFN.
- c) Tests to study the effects of gap width on spark energy and duration for two PFN's.
- d) Tests to study the generators' limitations in producing low energy arc discharges.

Results were compared with those predicted by circuit theory.

6.1.2 Defining discharge duration

When a PFN is over- or under-matched, the spark current may tail-off slowly following the initial current peak. This makes total discharge duration difficult to define from the recorded voltage or current waveforms, especially visually. Energy expenditure during this phase of the discharge

may be low compared with that at the time the current is at its peak. In this case, the useful duration of the spark, in terms of an ignition source, may be lower than that recorded oscillographically. Therefore, some means had to be devised for quantifying the useful spark duration. The use of a digitiser for recording and processing the waveforms meant that a repeatable method could be chosen.

It is shown later, that an appreciable amount of energy can be dissipated whilst gap current is low and gap voltage is high. As a result, it is not sufficient to define duration in terms of gap current. The most useful method is to define both a gap energy and duration from the energy \rightarrow time relationship. In the present work, the 'spark duration' was defined as the time at which 95% of the spark energy had been dissipated in the gap. This value could be returned directly from the computed energy \rightarrow time array. In practice, the unidirectional, overdamped discharges used in this work were well defined in terms of duration by carefully choosing the matching resistance value so that current did not tail-off slowly with time. This was more difficult to control for some of the oscillatory discharges where current could decay over a significant time.

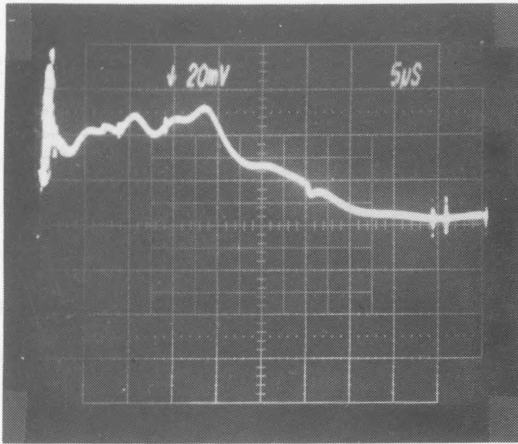
6.2 Example of circuit operation using the clipper circuitry

The first tests used a 10 kV line voltage and a 1210 Ω impedance 8-section PFN, consisting of inductors and capacitors of 1 mH and 680 pF respectively. This PFN was overmatched to give the arbitrary pulse shape shown in Photograph I-4. This pulse was produced by triggering T1 (in Figure 2) without triggering T2. The pulse was then clipped by triggering T2 14 μ s and 25 μ s after T1, which gave the results shown in Photographs I-5 and I-6.

Further tests were not made using this section of the generator, as it was not required in the ignition tests.

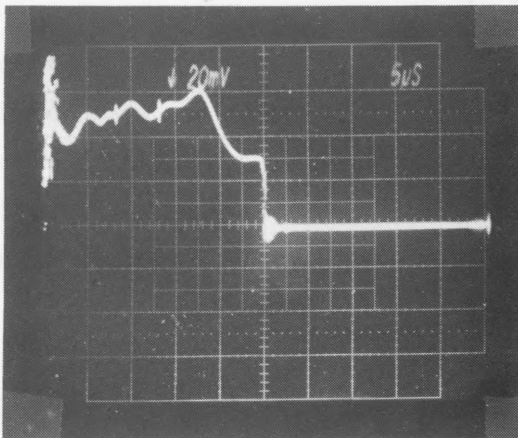
Photographs I-4 to I-6.

Examples of the use of the clipping circuitry.



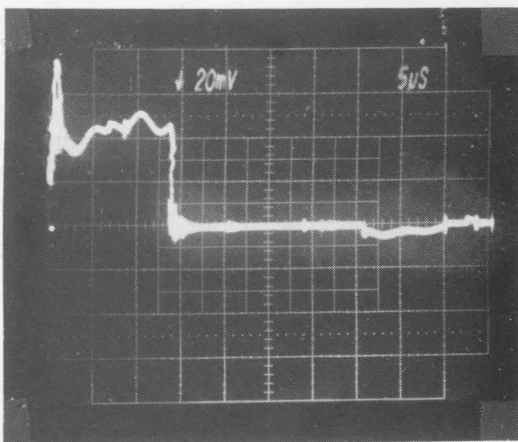
Photograph I-4.

Arbitrary unclipped current pulse.
Horizontal scale $5 \mu\text{s}/\text{div}$.
Vertical scale $2\text{A}/\text{div}$.



Photograph I-5.

Above pulse clipped after $25 \mu\text{s}$.
Scales as above.



Photograph I-6.

Above pulse clipped after $14 \mu\text{s}$.
Scales as above.

6.3 Open and short circuit tests

6.3.1 Description of tests

In this series of tests, a 6 element PFN with $L = 1 \text{ mH}$, $C = 680 \text{ pF}$ was used to check the operation of the T1 circuitry. The spark gap was first open-circuited (i.e. made too large for sparking to occur), then short-circuited, and the operating currents and voltages were measured and compared with predicted values. The operating voltage was arbitrarily set at 8.6 kV. A matching resistor of 1350Ω was used, which roughly corresponded to the theoretical PFN $\sqrt{L/C}$ value of $\sim 1200 \Omega$.

Circuit variables for these tests, and the PFN tests that follow, were set as given below:

6.3.1.1 Short-circuit test

Heater voltages : 7.0 V ac
Reservoir voltages : 5.9 V ac
Grid 1 anode voltage : 100 V dc
Grid 2 bias voltage : - 150 V dc
Grid 2 trigger voltage : 220 V dc

6.3.2 Open circuit test

In this test, the gap was increased to 3 cm to avoid sparking, and the following voltages were monitored:

- The voltage on the thyatron (T1) anode at the moment of switching.
- The voltage across the gap at the moment of switching.
- The voltage at the PFN-matching-resistor junction at the moment of switching.
- The static T1 anode voltage prior to switching.

A HILO PD75 capacitive probe was used to measure the T1 anode voltage on triggering, as a conventional Tektronix probe tended to load the point of measurement. A Sensitive Research ESH80 electrostatic voltmeter gave the static anode voltage. The other (gap and PFN) voltages were measured with a Tektronix P6015 probe. All curves were recorded on a Tektronix 7834 storage oscilloscope.

The voltage variation at the T1 anode and at the gap are shown in Figure I-38. The thyatron switched on after about 200 ns, but because of the extremely low flow of current (through the gap charging resistance of 200 M Ω) it began to recover immediately and charge began to build up on the thyatron capacitance and the PFN. The approximate time of charge recovery was 10 ms; the accuracy of this measurement was limited by the 30 Hz l.f. cut-off of the PD75 probe.

The value of current, measured using the 10 m Ω shunt resistor between the gap cathode and earth, was practically zero. A small current did of course flow through the 200 M Ω gap-shunt resistor when the thyatron was switched, but this was of the order of microamps and was not discernable.

6.3.3. Short-circuit test

In this test, the gap was short-circuited so that the load seen by the circuit was just the matching resistor. The current through the resistor was measured using the current shunt. Using a resistor of 1350 Ω , an almost 'rectangular' current pulse with slight tail-off was observed.

Measurements of voltage during the breakdown period were also made, this time at the thyatron anode and across the load resistor. Traces were obtained of the voltage at these points both at the time of switching and whilst current flowed through the load.

The results for the voltage measurements are shown in Figure I-39. These measurements show that a loss of circuit voltage was incurred at the moment of thyatron switching, which took about 0.2 μ s. A voltage drop of about 1.5 kV was measured, as shown in the top curve in Figure I-39. The circuit operating voltage was thus 7.1 kV, not 8.6 kV. Under these conditions, -4.7 kV was measured across the load resistor and a current of \sim 3.5 A was found. This corresponded to the expected value of 3.5 A, from the ratio 4.7 kV/1350 Ω .

The circuit's operating voltage, which is the breakdown voltage, and the magnitude of the circuit impedance, under a fixed set of operating conditions, could, therefore, be obtained from the short-circuit test.

The final test was made by mismatching the PFN with a 240 Ω resistor. The thyatron anode voltage was then measured to establish the tube-drop as the load current oscillates. This voltage oscillated about zero with an amplitude of about 180 V. No delay or problem occurred in the thyatron current was observed.

4.4 PFN tests

The first series of tests was run to establish the effects of line voltage, number of sections, and degree of matching for a typical PFN configuration. This consisted of an LC ladder with $L = 1 \text{ mH}$ and $C = 680 \text{ pF}$, giving a characteristic impedance of approximately 1200 Ω . These values were chosen as being typical of those used in ignition tests.

The following parameters were varied, using a 2 mm gap width:

- Line voltage. This was varied from 7.5 kV to 15 kV in 2.5 kV steps.
- Number of PFN sections. This was varied from 1, through 3, to 8.
- Degree of matching. This was varied by changing the value of matching resistance, R , above and below the matching point. 7 values of R from 60 Ω to 5.3 k Ω were used.

Figure I-38. Open circuit voltage measurements

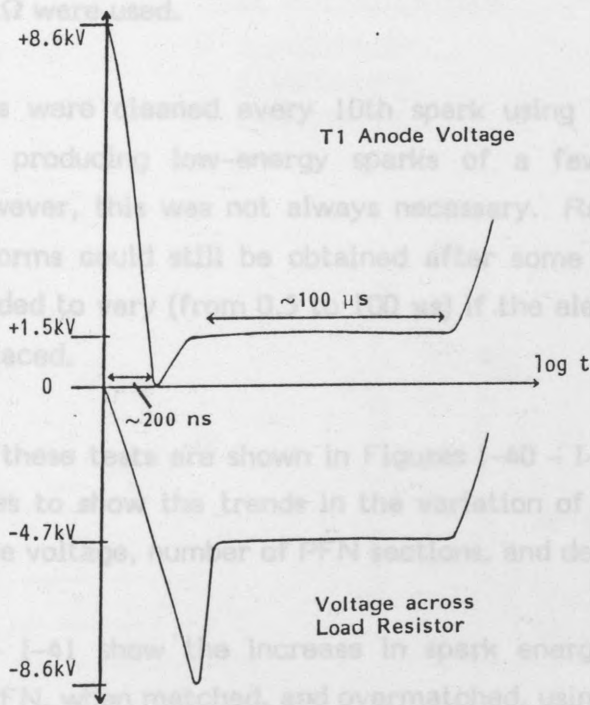


Figure I-39. Short circuit voltage measurements

One final test was made by mismatching the PFN with a $240\ \Omega$ resistor. The thyatron anode voltage was then measured to establish the tube-drop as the load current oscillated. This voltage oscillated about zero with an amplitude of about 180 V. No delay or problem of reversal in thyatron current was observed.

6.4 PFN tests

The first series of PFN tests was run to study the effects of line voltage, number of sections, and degree of matching for a typical PFN configuration. This consisted of an L-C ladder with $L = 1\ \text{mH}$ and $C = 680\ \text{pF}$, giving a characteristic impedance of approximately $1200\ \Omega$. These values were chosen as being typical of those used in ignition tests.

The following parameters were varied, using a 2 mm gap width:

- a. Line voltage. This was varied from 7.5 kV to 15 kV in 2.5 kV steps.
- b. Number of PFN sections. This was varied from 1, through 3, to 8.
- c. Degree of matching. This was varied by changing the value of matching resistance, R , above and below the matching point. 7 values of R from $60\ \Omega$ to $5.3\ \text{k}\Omega$ were used.

The electrodes were cleaned every 10th spark using grade 320 carborundum paper. When producing low-energy sparks of a few millijoules with this apparatus, however, this was not always necessary. Reproducible current and voltage waveforms could still be obtained after some 20 sparks, but time to breakdown tended to vary (from 0.5 to 100 μs) if the electrodes were either not cleaned or replaced.

The results of these tests are shown in Figures I-40 - I-43. These were picked out as examples to show the trends in the variation of energy and duration as functions of line voltage, number of PFN sections, and degree of matching.

Figures I-40 - I-41 show the increase in spark energy and duration for an eight-section PFN, when matched, and overmatched, using a 2 mm spark gap.

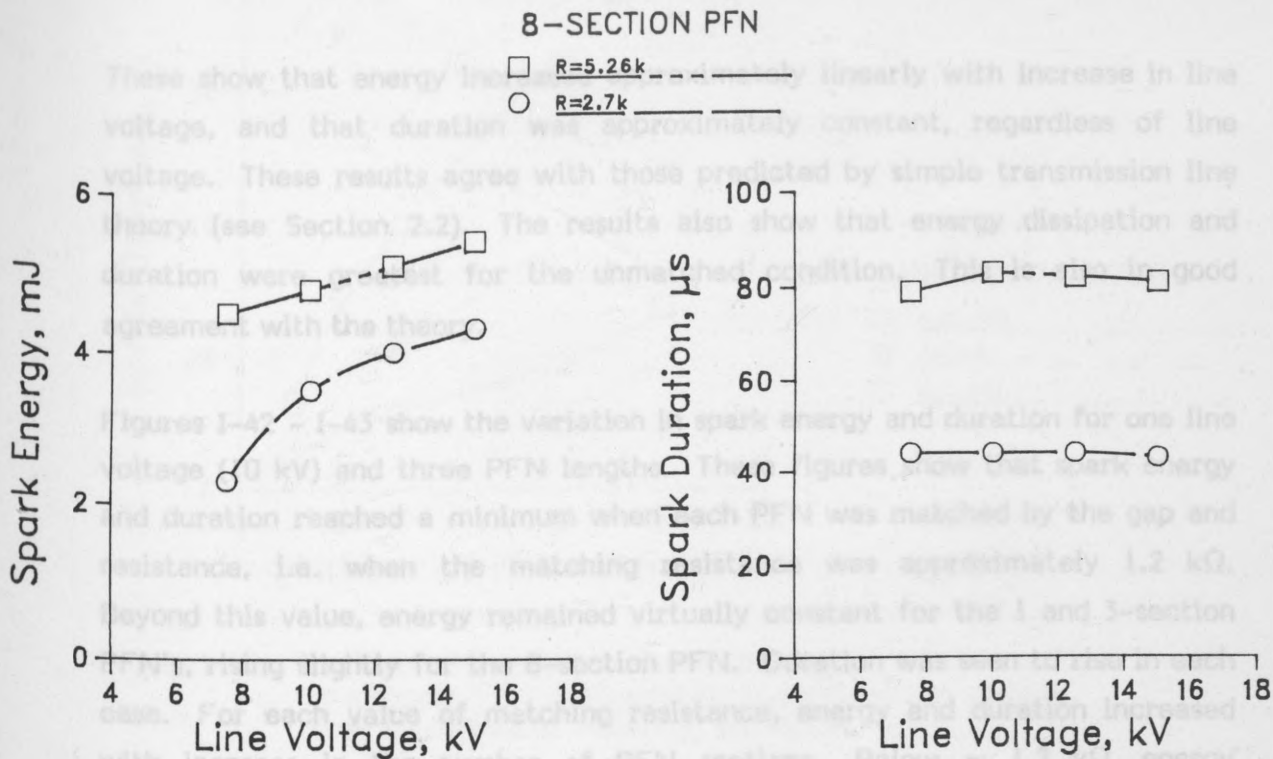


Figure I-40. Spark energy and duration as functions of line voltage for a chosen PFN. Figure I-41. Spark duration as a function of line voltage for a chosen PFN.

Two conditions of matching are shown for a 2 mm gap.

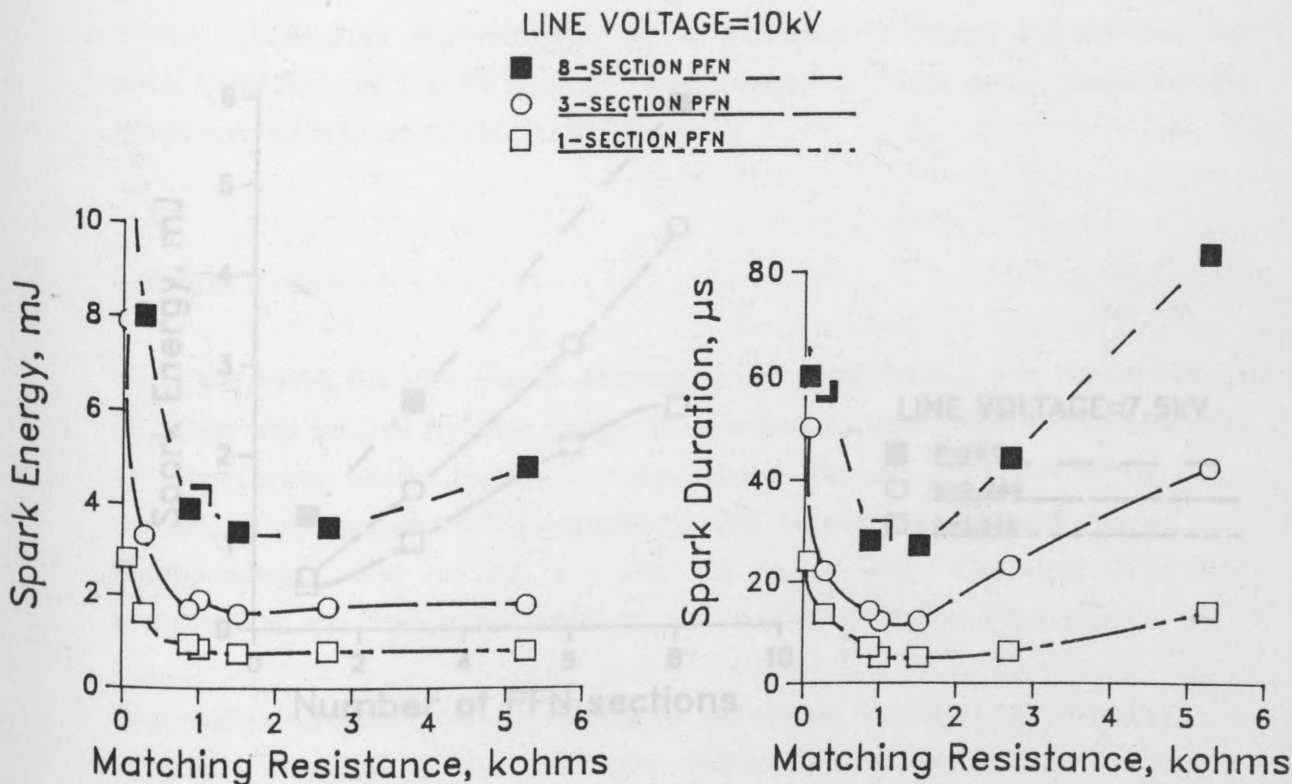


Figure I-42. Spark energy as a function of matching resistance for three chosen PFN's, a fixed line voltage, and a 2 mm gap.

Figure I-43. Spark duration as a function of matching resistance for three chosen PFN's, a fixed line voltage, and a 2 mm gap.

Spark energy and duration as functions of matching resistance for three chosen PFN's, a fixed line voltage, and a 2 mm gap.

These show that energy increased approximately linearly with increase in line voltage, and that duration was approximately constant, regardless of line voltage. These results agree with those predicted by simple transmission line theory (see Section 2.2). The results also show that energy dissipation and duration were greatest for the unmatched condition. This is also in good agreement with the theory.

Figures I-42 - I-43 show the variation in spark energy and duration for one line voltage (10 kV) and three PFN lengths. These figures show that spark energy and duration reached a minimum when each PFN was matched by the gap and resistance, i.e. when the matching resistance was approximately 1.2 k Ω . Beyond this value, energy remained virtually constant for the 1 and 3-section PFN's, rising slightly for the 8-section PFN. Duration was seen to rise in each case. For each value of matching resistance, energy and duration increased with increase in the number of PFN sections. Below ~ 1.2 k Ω , energy dissipation and spark duration increased sharply, because the circuit oscillated. Above ~ 1.2 k Ω the load became more resistive, i.e. the spark became more highly damped. These results are also in good agreement with those predicted by circuit theory.

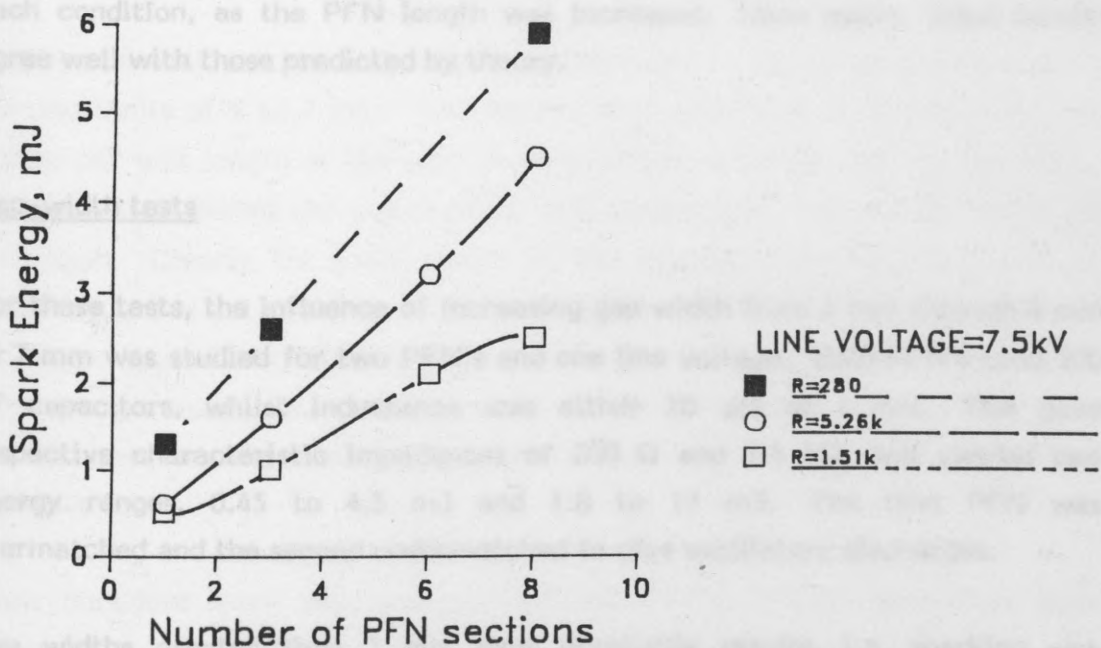


Figure I-44. Spark energy as a function of the number of PFN sections for a chosen PFN configuration and a fixed line voltage. Three conditions of matching are shown, for a 4 mm gap.

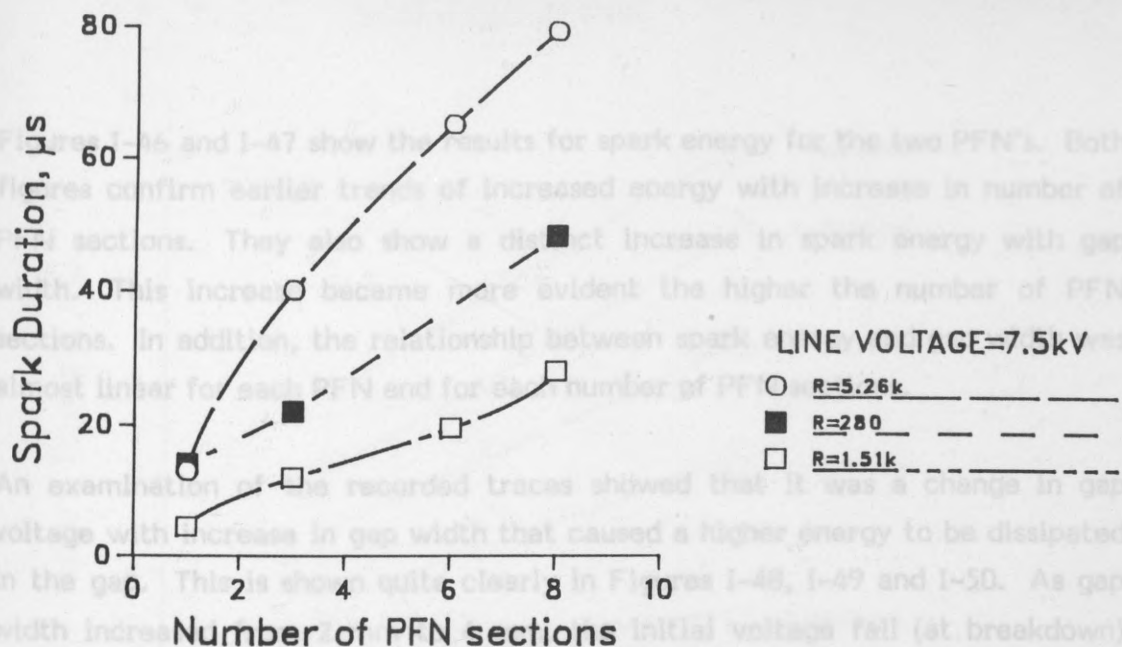


Figure I-45. Spark duration as a function of the number of PFN sections for a chosen PFN configuration and a fixed line voltage. Three conditions of matching are shown.

Finally, Figures I-44 and I-45 show, for a line voltage of 7.5 kV, the increases in spark energy and duration with increase in the number of PFN sections. The three curves in each figure correspond to conditions of undermatching, matching and overmatching, i.e. using three different matching resistor values. These figures show approximately linear increases in energy and duration for each condition, as the PFN length was increased. Once again, these results agree well with those predicted by theory.

6.5 Gap-width tests

For these tests, the influence of increasing gap width from 2 mm through 4 mm to 7 mm was studied for two PFN's and one line voltage. Both PFN's used 500 pF capacitors, whilst inductance was either 20 μH or 1 mH. This gave respective characteristic impedances of 200 Ω and 1.4 kΩ, and yielded two energy ranges, 0.45 to 4.5 mJ and 1.8 to 13 mJ. The first PFN was overmatched and the second undermatched to give oscillatory discharges.

Gap widths greater than 7 mm gave unreliable results, i.e. sparking was irregular, because of the necessary increase in pulse voltage to ensure breakdown. A higher line voltage than 10 kV would have enabled higher gap widths to be used, but this value was chosen because it was typical of the voltages used in the ignition tests, where low energy discharges were produced.

500pF/200V PFN

Figures I-46 and I-47 show the results for spark energy for the two PFN's. Both figures confirm earlier trends of increased energy with increase in number of PFN sections. They also show a distinct increase in spark energy with gap width. This increase became more evident the higher the number of PFN sections. In addition, the relationship between spark energy and gap width was almost linear for each PFN and for each number of PFN sections.

An examination of the recorded traces showed that it was a change in gap voltage with increase in gap width that caused a higher energy to be dissipated in the gap. This is shown quite clearly in Figures I-48, I-49 and I-50. As gap width increased from 2 mm to 4 mm, the initial voltage fall (at breakdown) changed from about -100 V to about -150 V, and then decreased to about -300 V as gap width was increased to 7 mm. This trend was similar for all recorded oscillatory and unidirectional sparks for all the number of sections used. The current curve was identical in all three cases, and is shown in Figure I-50, where power and energy curves are also shown for a 2 section PFN and a 7 mm gap. This was expected on theoretical grounds as under these conditions, the generator acts as a constant current source. Note that Figure I-50 (7 mm gap) shows a delay of some four microseconds to breakdown. The current pulse is now easily discernible from the circuit noise, due to the lower impulse ratio at this gap width.

500pF/1mH PFN

It appeared that voltage was roughly proportional to gap width between these working limits of 2 to 7 mm. This further implied an almost constant value of energy per unit length of the gap. In other words, a certain voltage has had to maintain itself across the gap in order that current will flow and the spark not extinguish. Clearly the early stages of the discharge are vital in terms of maintaining this current flow in the gap. Figure I-50 shows that in this stage, for larger gap widths, both voltage and current are at their peak, meaning a large energy dissipation. This in turn means that the maximum spark duration that is possible when using large gap widths and low energies is lowered significantly.

Spark durations were also recorded for each PFN length. Durations were constant for each length and independent of gap width, for both PFN's.

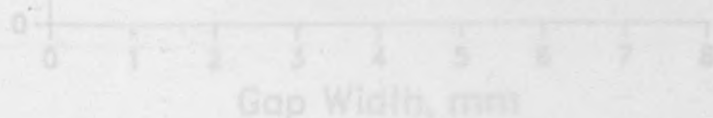


Figure I-47. Relationship between spark energy and gap width using a second PFN configuration.

500pF/20uH PFN

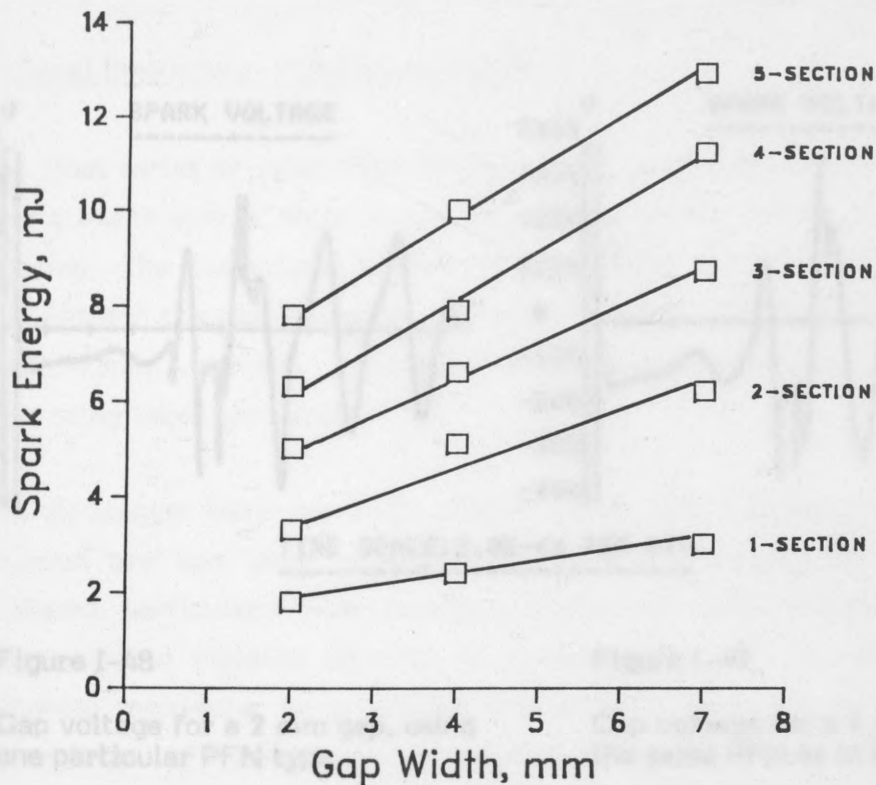


Figure I-46. Relationship between spark energy and gap width using one PFN configuration.

500pF/1mH PFN

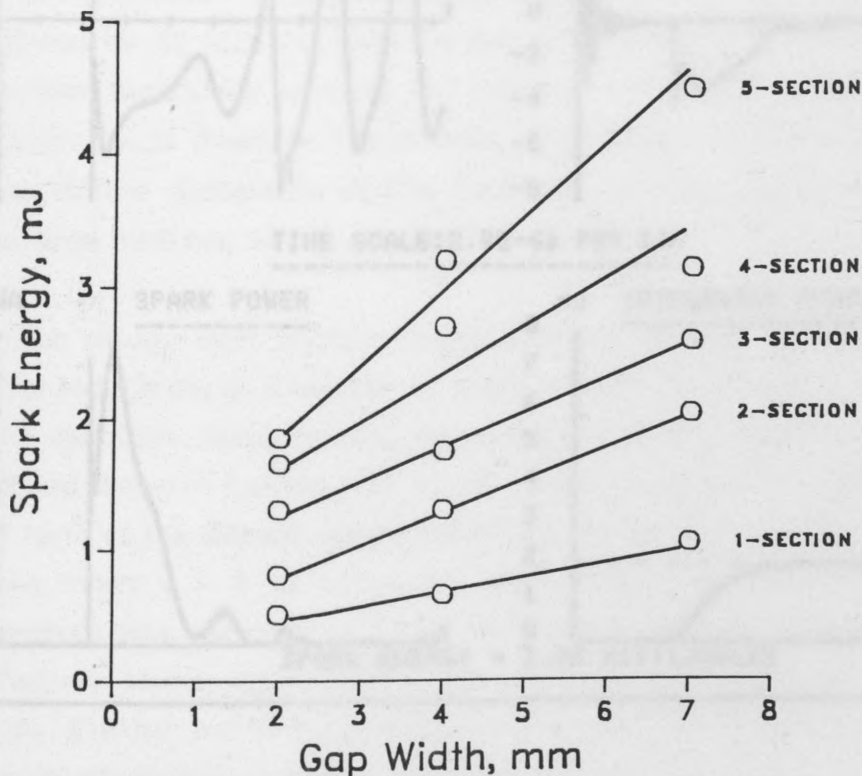


Figure I-47. Relationship between spark energy and gap width using a second PFN configuration.

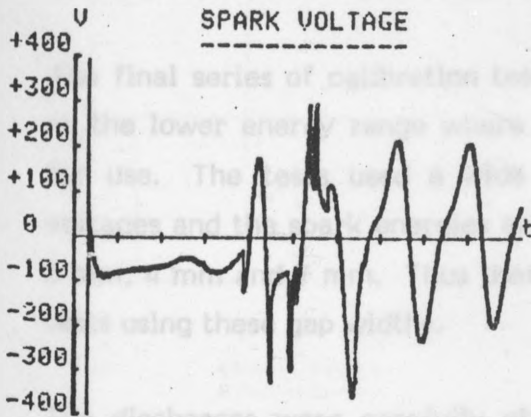


Figure I-48 Increase duration of a spark by increasing gap voltage for a 2 mm gap, using one particular PFN type.

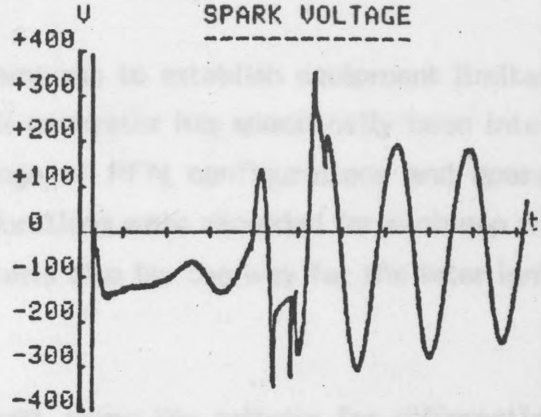


Figure I-49 Gap voltage for a 4 mm gap using the same PFN as in Figure 48.

TIME SCALE: $2.0E-6s$ PER DIV

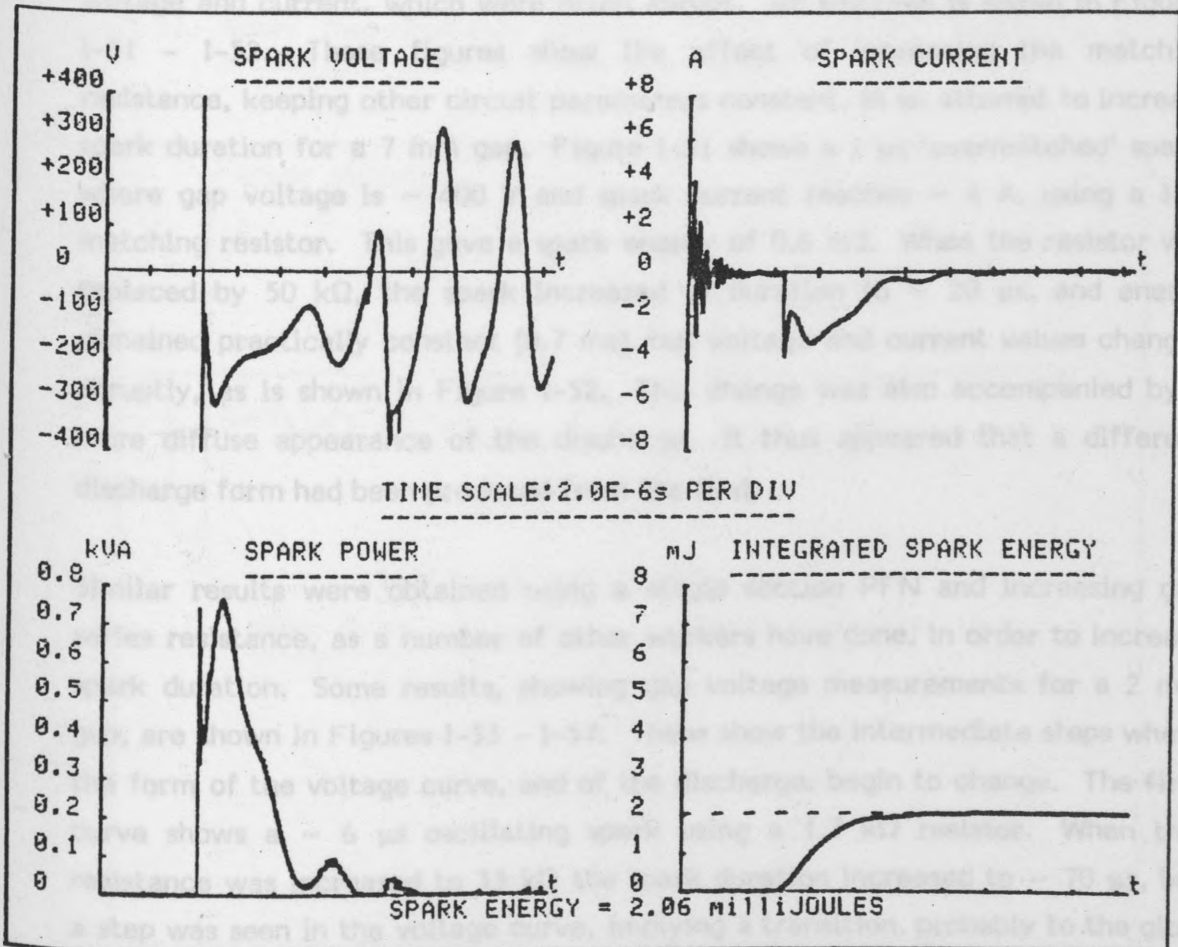


Figure I-50. Spark measurements and calculations for a 7 mm gap, using the same PFN as in the figures above.

6.6 Physical limitations of the spark circuit

The final series of calibration tests was run to establish equipment limitations at the lower energy range where this generator has specifically been intended for use. The tests used a wide range of PFN configurations and operating voltages and the spark energies and durations were recorded for each gap width, 2 mm, 4 mm and 7 mm. Thus these tests also lay the way for the later ignition tests using these gap widths.

The discharges were carefully checked, using the criteria for differentiating between 'arc' and 'glow' types (see Appendix 3) to ensure that 'arc' types were produced, particularly when energy was low, and duration long. Usually, when attempting to increase duration at a low energy, for example by increasing matching resistance, or decreasing energy for a given duration, by decreasing line voltage, a limit was reached at which it became clear that further changes were not possible. This manifested itself in the form of changes in spark voltage and current, which were often abrupt. An example is shown in Figures I-51 - I-52. These figures show the effect of increasing the matching resistance, keeping other circuit parameters constant, in an attempt to increase spark duration for a 7 mm gap. Figure I-51 shows a 1 μ s 'overmatched' spark, where gap voltage is \sim 400 V and spark current reaches \sim 4 A, using a 1K5 matching resistor. This gave a spark energy of 0.6 mJ. When the resistor was replaced by 50 k Ω , the spark increased in duration to \sim 20 μ s, and energy remained practically constant (0.7 mJ), but voltage and current values changed abruptly, as is shown in Figure I-52. This change was also accompanied by a more diffuse appearance of the discharge. It thus appeared that a different discharge form had been produced from the first.

Similar results were obtained using a single section PFN and increasing gap series resistance, as a number of other workers have done, in order to increase spark duration. Some results, showing gap voltage measurements for a 2 mm gap, are shown in Figures I-53 - I-57. These show the intermediate steps where the form of the voltage curve, and of the discharge, begin to change. The first curve shows a \sim 6 μ s oscillating spark using a 1.7 k Ω resistor. When this resistance was increased to 33 k Ω the spark duration increased to \sim 70 μ s, but a step was seen in the voltage curve, implying a transition, probably to the glow stage. Further increases in resistance, as shown in Figures I-55 - I-57 show a complete transition to a glow discharge voltage.

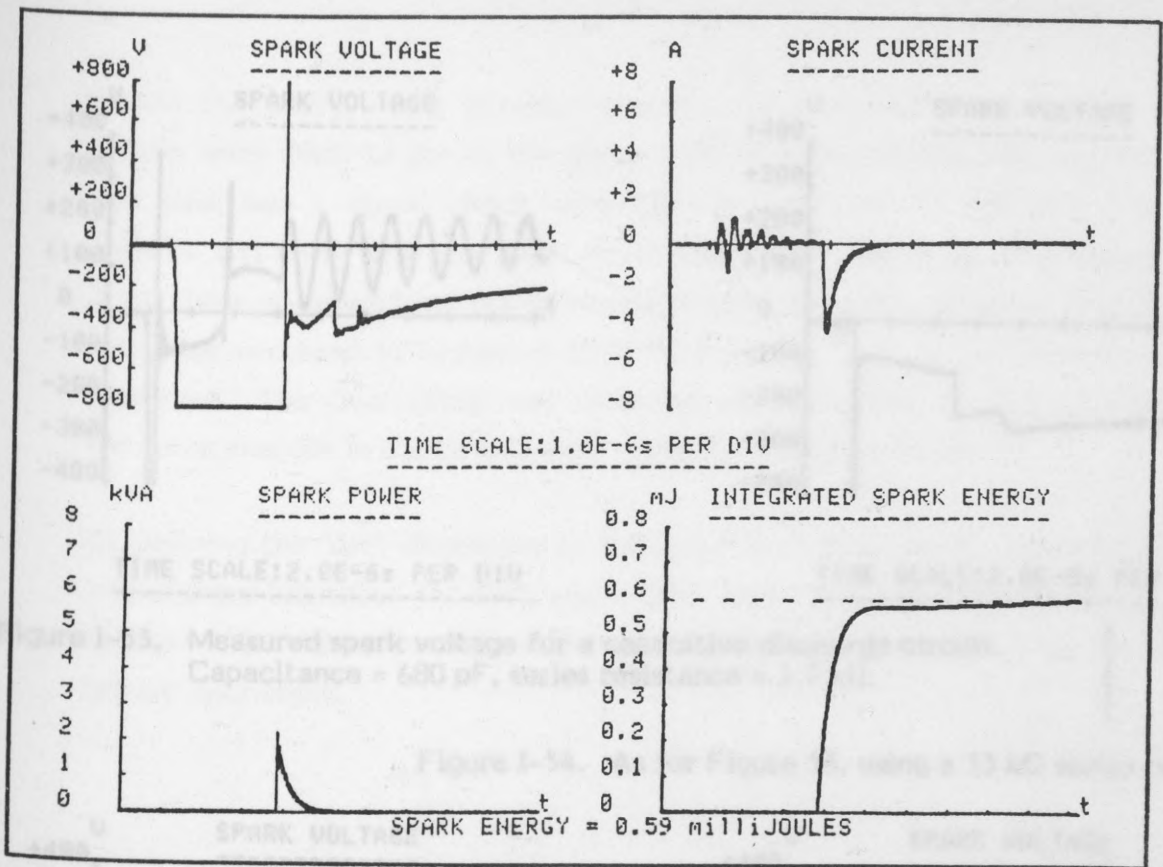


Figure I-51. Spark measurements showing an 'overmatched' spark for a chosen PFN and a 1K5 matching resistor.

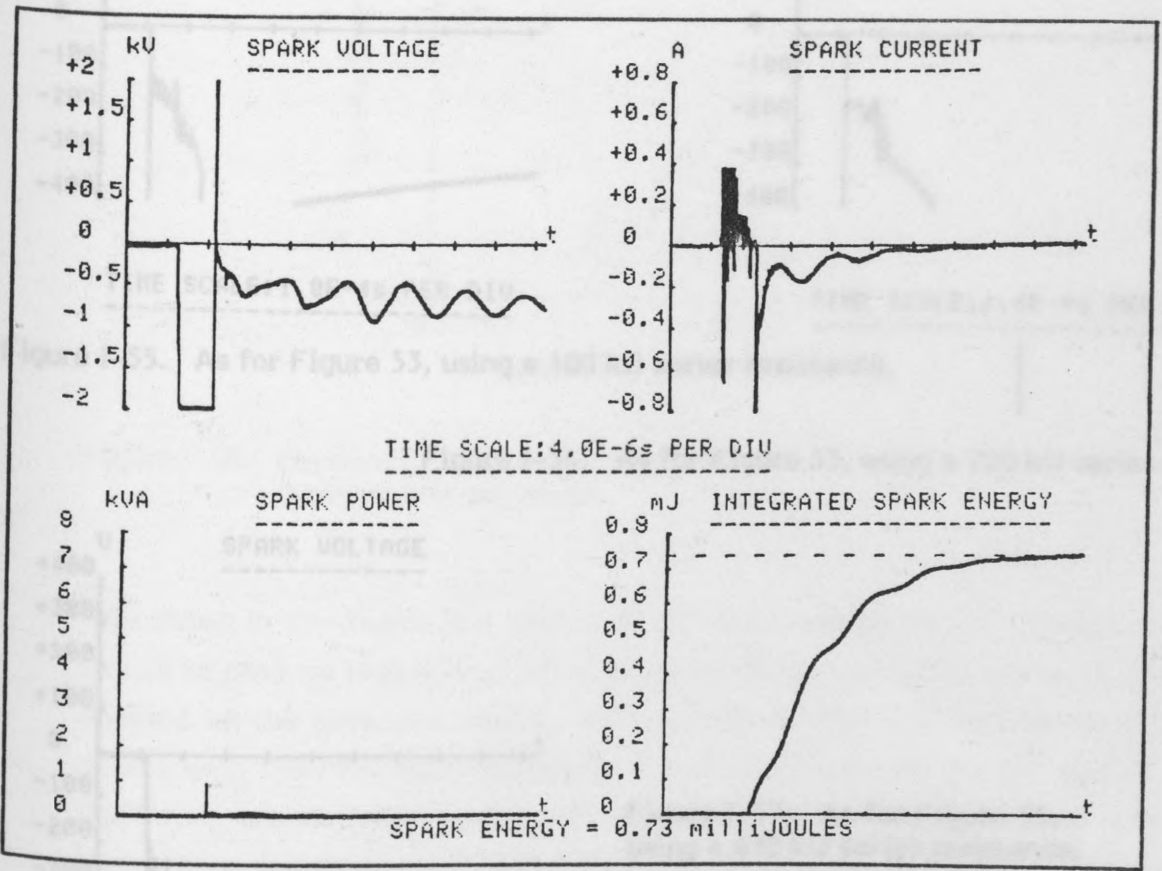
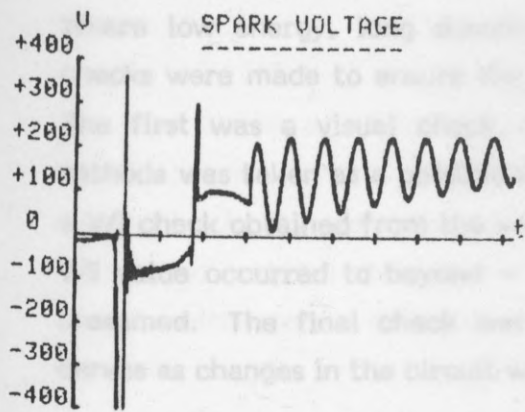
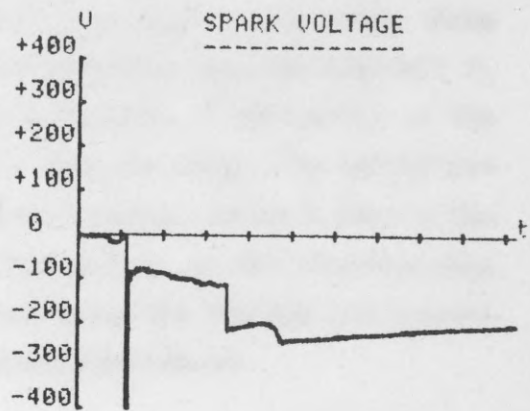


Figure I-52. Spark measurements as above, for similar circuit conditions, using a 50 kΩ matching resistor.



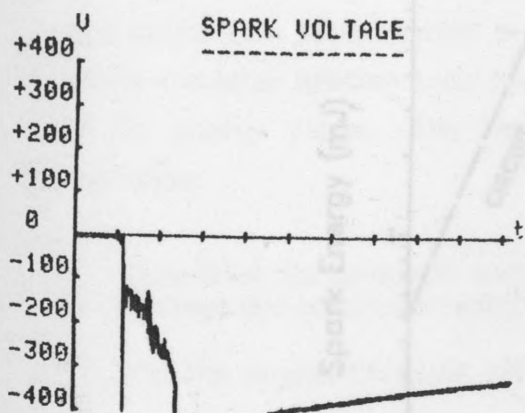
TIME SCALE: $2.0E-6s$ PER DIV



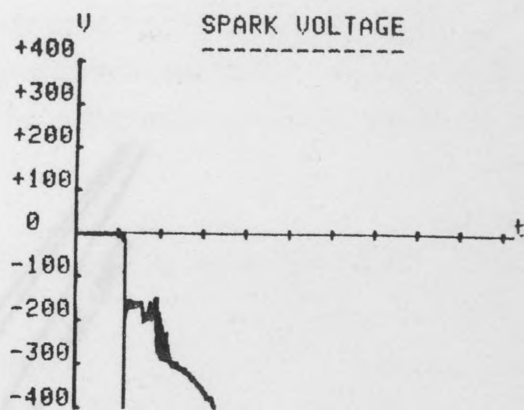
TIME SCALE: $2.0E-5s$ PER DIV

Figure I-53. Measured spark voltage for a capacitive discharge circuit. Capacitance = 680 pF, series resistance = 1.7 kΩ.

Figure I-54. As for Figure 53, using a 33 kΩ series resistance.



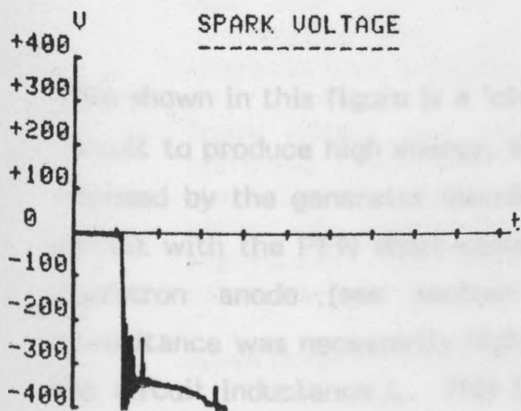
TIME SCALE: $1.0E-4s$ PER DIV



TIME SCALE: $1.0E-4s$ PER DIV

Figure I-55. As for Figure 53, using a 100 kΩ series resistance.

Figure I-56. As for Figure 53, using a 220 kΩ series resistance.



TIME SCALE: $1.0E-4s$ PER DIV

Figure I-57. As for Figure 53, using a 470 kΩ series resistance.

Where low energy, long duration sparks were produced in this work, three checks were made to ensure the same mode of discharge (see also Appendix 3). The first was a visual check, whereby any indication of diffusivity at the cathode was taken as a possible indication of a glow discharge. The second was a V/I check obtained from the voltage and current curves. Where a jump in the V/I value occurred to beyond $\sim 1000 \Omega$, a change from an arc discharge was presumed. The final check was made by examining the voltage and current curves as changes in the circuit were made, as described above.

By defining the 'arc' discharges in this way, the circuit limits, called the 'arc limits' were identified for each gap width. These are shown in Figure I-58 and represent the highest possible values of spark duration, for given spark energies, for arc discharges.

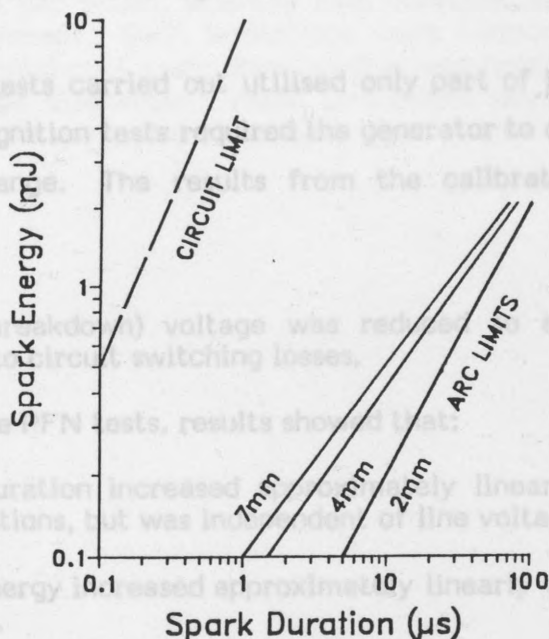


Figure I-58. Physical limitations on spark energy as a function of spark duration and gap width.

Also shown in this figure is a 'circuit limit' which represents a limitation of the circuit to produce high energy, short duration discharges. This was a limitation imposed by the generator circuit, and was due to the total inductance of the circuit with the PFN short-circuited. The bulk of this inductance was at the thyatron anode (see section 3.1.1). At such energies, where circuit capacitance was necessarily high, the time-constant product (LC) was bound by the circuit inductance L. This limitation showed a similar trend for all three gap widths.

7. CONCLUSIONS

The construction of an electric spark generator based on a PFN modulator type circuit, proved successful in producing controlled spark discharges at energies below 10 mJ. The generator was shown to produce discharges where both spark energy and duration could be varied independently, and on a reproducible basis. This has often been a difficult, if not impossible task using many other previous generator designs.

Spark energies and durations, measured using an accurate probing system and a dual-channel digitiser, compared favourably with the trends predicted by simplified circuit theory. These trends were observed in calibration tests, using selected pulse-forming networks that represented typical operating conditions of the generator when used in ignition tests.

The calibration tests carried out utilised only part of the complete circuit, as use in the later ignition tests required the generator to operate at the lower end of its energy range. The results from the calibration tests revealed the following:

1. Operation (breakdown) voltage was reduced to a value below the line voltage due to circuit switching losses.
2. For the single PFN tests, results showed that:
 - a) Spark duration increased approximately linearly with the number of PFN sections, but was independent of line voltage.
 - b) Spark energy increased approximately linearly with the number of PFN sections.
 - c) Spark energy increased approximately linearly with the line voltage.
 - d) Sparks oscillated and duration increased when the matching resistance was less than the PFN's characteristic impedance and were overdamped when the matching resistance was greater than the characteristic impedance.
 - e) Spark energy and duration were both at a minimum when the matching resistance was approximately equal to the PFN's characteristic impedance. Discharge duration increased about this value of matching resistance, whilst energy only increased significantly below this value of matching resistance. Above this value, the energy stayed almost constant.
 - f) Spark duration was most easily defined under conditions of matching.

All of these observations corresponded well to the results predicted by circuit theory (see section 2). As a result, the theoretical model was used as a guide to predicting values of spark energies and durations, when varying circuit parameters for a given PFN configuration. Exact energies were measured in the gap, however, as the strict laws of circuit theory, based on a resistive load, were not obeyed exactly using a spark-gap load.

3. Varying gap width from 2 mm to 7 mm, for a particular PFN/matching-resistor combination, caused an approximately linear increase in discharge energy. This was due to a proportional increase in gap voltage, whilst gap current stayed constant, indicating a constant current mode of operation. Discharge duration was also independent of gap width. Increasing the number of PFN sections caused a more marked increase in discharge energy with gap width. This held for both unidirectional and oscillatory discharges.
4. The production of low duration discharges was found to be limited for a particular spark energy, due to thyatron anode inductance that limited the current rate of rise in the circuit. Further limitations existed according to gap width, whereby long duration discharges were limited by circuit current. Such limitations were termed 'arc limits' as they marked the maximum spark duration that was possible for a given energy using arc-type discharges. These limitations were associated with the gap, and not the generator circuit.

CONTENTS

1. INTRODUCTION	1
1.1 Background	1
1.2 The present work	1
PART 2: GAS IGNITION STUDIES	
2. EXPERIMENTAL	10
2.1 Description of tests	10
2.2 The explosion vessel	10
2.3 Gas mixing and ignition procedure	10
2.4 The flash-schlieren apparatus	10
3. RESULTS OF IGNITION TESTS	109
3.1 Results for the 2 mm gap	109
3.2 Results for the 4 mm gap	110
3.3 Results for the 7 mm gap	110
4. SCHLIEREN PHOTOGRAPHS: RESULTS	112
4.1 Results for the 2 mm gap	112
4.2 Results for the 4 mm and 7 mm gaps	114
5. DISCUSSION OF RESULTS	122
6. CONCLUSIONS	126

I. INTRODUCTION

1.1 Background

CONTENTS

4,5,6,11,12,50,32,48,49. The collected work of Lewis and van E. Page

1. INTRODUCTION	97
1.1 Background	97
1.2 The present work	100
2. EXPERIMENTAL	101
2.1 Description of tests	101
2.2 The explosion vessel	103
2.3 Gas mixing and ignition procedure	103
2.4 The flash-schlieren apparatus	107
3. RESULTS OF IGNITION TESTS	109
3.1 Results for the 2 mm gap	109
3.2 Results for the 4 mm gap	110
3.3 Results for the 7 mm gap	110
4. SCHLIEREN PHOTOGRAPHS: RESULTS	112
4.1 Results for the 2 mm gap	112
4.2 Results for the 4 mm and 7 mm gaps	114
5. DISCUSSION OF RESULTS	122
6. CONCLUSIONS	128

Unfortunately, many of the above-mentioned aspects of a spark discharge have not been studied independently, meaning that it is very difficult to establish exactly how important they are regarding the ignition process. Furthermore, where they have been investigated, they have generally only been related qualitatively to the process of ignition of a given gas mixture.

1. INTRODUCTION

1.1 Background

The 'minimum ignition energy' (MIE) of gas mixtures has been studied in considerable depth by a number of workers using electric sparks^{4,5,6,11,12,30,32,48,49}. The collected work of Lewis and von Elbe¹⁰ is particularly noteworthy because of their in-depth study of MIE using hydrocarbons. In their and other ignition models, certain simplifications were made in order to arrive at a minimum ignition energy term. The most significant of these is the assumption that spark energy is introduced to an ignitable gas mixture within an infinitesimally short time. A consideration of the manner in which this energy is converted to heat energy required for ignition has not been included in such models, although recent work by Maly²⁸ and Hill²⁹ has begun to address this problem.

Since Lewis and von Elbe's work, a number of workers have reported apparent effects of spark discharge duration on MIE values using gas mixtures^{30,31,32}. Observations have usually been made using a capacitive discharge circuit where spark duration was increased by incorporating a series resistor. The general result has been that the measured increase in discharge duration is accompanied by a decrease in MIE to a minimum value, despite an energy loss in the resistor. In such cases, 'MIE' is usually defined in terms of the stored circuit energy. A complete explanation of this result has not yet been forthcoming.

Besides studies of discharge duration, a great deal of evidence (see for example (11) and (33)) has been amassed that would suggest that thermal ignition theory should be modified by considering various electrical phenomena associated with the spark discharge. Breakdown voltage, rate of rise of current in the gap, and form of discharge, are just some of the many variables that have been suggested as influencing the ignition process when using electric sparks.

Unfortunately, many of the above-mentioned aspects of a spark discharge have not been studied independently, meaning that it is very difficult to establish exactly how important they are regarding the ignition process. Furthermore, where they have been investigated, they have generally only been related qualitatively to the success of ignition of a given gas mixture.

This applies in particular to discharge duration. This has rarely been isolated as an independent variable^{5,34} when studying MIE, and has not been related to the physical mechanisms governing the transfer of electrical (spark) energy in the gas to heat energy (thermalisation). 'Spark energy' has also been defined as both a stored circuit energy, and a dissipated energy, under these circumstances, which has made it difficult to compare data from different workers. It is of no surprise, therefore, that evidence concerning effects of duration on MIE are conflicting and have not yet led to a unified theory of spark ignition of gas mixtures.

A careful analysis of the wide variation in circuit types used to produce electric sparks, and the methods used to vary spark duration, shows that other aspects of the spark discharge have been varied as a result of increasing discharge duration. A typical case of this is the previously-mentioned technique of inserting series resistance in a capacitive circuit. As resistance is increased, increasing discharge duration, so the rate of energy release in the gap varies also, in an undetermined manner. Furthermore, the mode of the discharge (see Appendix 3) may also change under such conditions.

It is clear that a full understanding of the role of 'discharge duration' on MIE must be related to the resultant effect on the thermalisation of energy in the spark gap. Such a study must therefore include either more or equally important aspects of the discharge. Of these, the rate of discharge of energy would appear to be the most important aspect, because it will directly affect the process of heat transfer to the gas mixture. It would appear, therefore, that since duration is related to the rate of discharge of energy, according to how the spark is produced, the most pertinent study of discharge duration must also include and quantify both of these variables. Such a study is not possible using conventional capacitive discharge circuits, and results with these only reflect the circuit's operation, without identifying the importance of independent variables associated with the spark discharges that they produce.

Thus, apparent effects of discharge duration were noticed as early as the 1920's when systematic work first began using electric sparks to ignite gas mixtures³⁵. This led to alternative theories of ignition, notably electrical (ionisation) theories^{25,36,37} that could explain electric-spark ignition

phenomena. Furthermore, various terms were introduced to describe the 'type of spark' being used. Morgan²⁴ spoke of 'capacitive' and 'inductive' sparks according to the type of circuit that was used to create the discharge. He, like many others to follow, spoke of a spark's igniting power in terms of the circuit producing the spark, and not the spark itself. It is precisely this approach that has hindered a proper interpretation of spark ignition.

Interestingly, Patterson and Campbell³⁸ remarked, at an earlier date, upon the difficulty in comparing the results of other workers using various spark generating circuits. One may almost be tempted to say that their insight, as far back as 1919, was before its time, as it astutely commented on the failure of other workers to define ignition success in terms of the spark itself. Until that time, and indeed until long after, only empirical relationships could relate the different 'minimum igniting intensities' measured by different workers. Thus they wrote:

"In other words, the result of all these experiments are stated in terms of the properties of the instrument used for producing the spark; they are not stated in terms of the properties of the spark itself, and it is doubtless the properties of the spark itself which determine its igniting power. That power must depend in some way on such characteristics of the spark as the average or maximum current through it, the time that it lasts, the potential between the terminals, the variation of that potential with the time, and so on. It is only if the igniting properties of the spark can be defined in terms of such characteristics that a result will be reached which is really general and permits a prediction of the igniting power of any spark produced by any experimental arrangement or a consideration of the best arrangement to produce a spark of given igniting power."

Much of the earlier work before 1947, some of it contradictory, became invalidated by Blanc et al.³⁹ who for the first time reported flame-quenching effects due to the spark electrodes. This phenomenon was investigated in detail using capacitive discharges. Blanc found that below a certain electrode spacing (the quenching distance for the gas mixture) values of MIE rose abruptly due to loss of heat from the flame kernel to the electrodes. Differences in MIE values below and above the quenching distance were often of orders of magnitude.

Interpretations of measured decreases in MIE with increasing 'duration', (i.e. when using capacitive-resistive circuits) have since been put forward. Rose and Priede⁴⁰ explained such results in terms of increased ionisation in the

gap, over a longer discharge period, and a reduction in the discharge channel volume, which would imply that energy is discharged into a smaller volume of gas, which is consistent with thermal ignition theory. Later, Eckhoff³ interpreted the effect of increased duration in terms of a reduction of radiative and conductive losses from the spark, as well as reduced losses due to shock waves and expansion work prior to ignition. At present, the aspect of losses, be they radiative, conductive or shock-related, is still not fully understood, and serves only as an hypothesis to explain 'duration effects'. Some evidence does exist, however, that shows the presence of such losses^{41,42,43,44,45}, but an exact quantification of these for a given spark discharge has not been forthcoming.

1.2 The present work

In the present work a single gas mixture (2.7 % propane-air) was used to study the effects of discharge duration on minimum ignition energy, as a function of gap width. The use of a pulse-generating discharge circuit allowed duration to be studied independently of spark energy. The principle idea of these tests was to attempt to relate observed duration dependencies on MIE to the manner in which the spark kernel grew following discharge. This was facilitated using a flash-schlieren system.

No attempt was made in the work to derive an ignition theory based on the observations made, which would have required an in-depth study using a wider range of gas mixtures, together with a complete examination of the thermalisation of the spark discharge. The work was originally intended as a preliminary study to the dust-ignition work, described in Part 3. In particular, schlieren photographs of the expanding spark kernels in air lay the ground-work for the interpretation of the dust-ignition results.

2. EXPERIMENTAL

2.1 Description of tests

For these tests, a single lean-mixture of propane-air was chosen, for the following reasons:

- a) It enabled spark energy and duration to be varied independently over a wide range, for gap widths from 2 mm to 7 mm. A richer mixture, with a lower MIE, would have limited the range of spark energy/duration combinations using this spark generator.
- b) Reported quenching distances for a lean mixture are higher than for a stoichiometric mixture¹⁰, meaning that effects of gap width both above and below the reported values could be easily studied.
- c) It led to complete combustion when ignition was observed.

In the tests using the electric spark generator, the spark energy and duration were altered independently of one another, covering the duration range $0.2 \mu\text{s}$ to $\sim 100 \mu\text{s}$. This was repeated using three gap widths, 2 mm, 4 mm and 7 mm. For a fixed duration, energy was varied and the frequency of ignition from ten ignition trials was recorded. Energy was increased or decreased accordingly, until the boundary between ignition and no-ignition was located. Ignition probabilities were then plotted on a graph of spark energy versus spark duration.

When varying spark duration, the form of the spark power versus time curve, as measured by the probing circuit, was kept of a unidirectional form as shown in Figure II-1. When duration was increased, the 'rectangular' form of this relationship was usually kept constant. Where it proved difficult to produce an arc discharge of constant power when increasing duration, a curve of the form shown in Figure II-2 was produced.

Following these ignition tests, combinations of spark energies, durations and gap widths were chosen and a series of schlieren photographs was taken for the spark, both in air, and in the presence of the gas mixture.

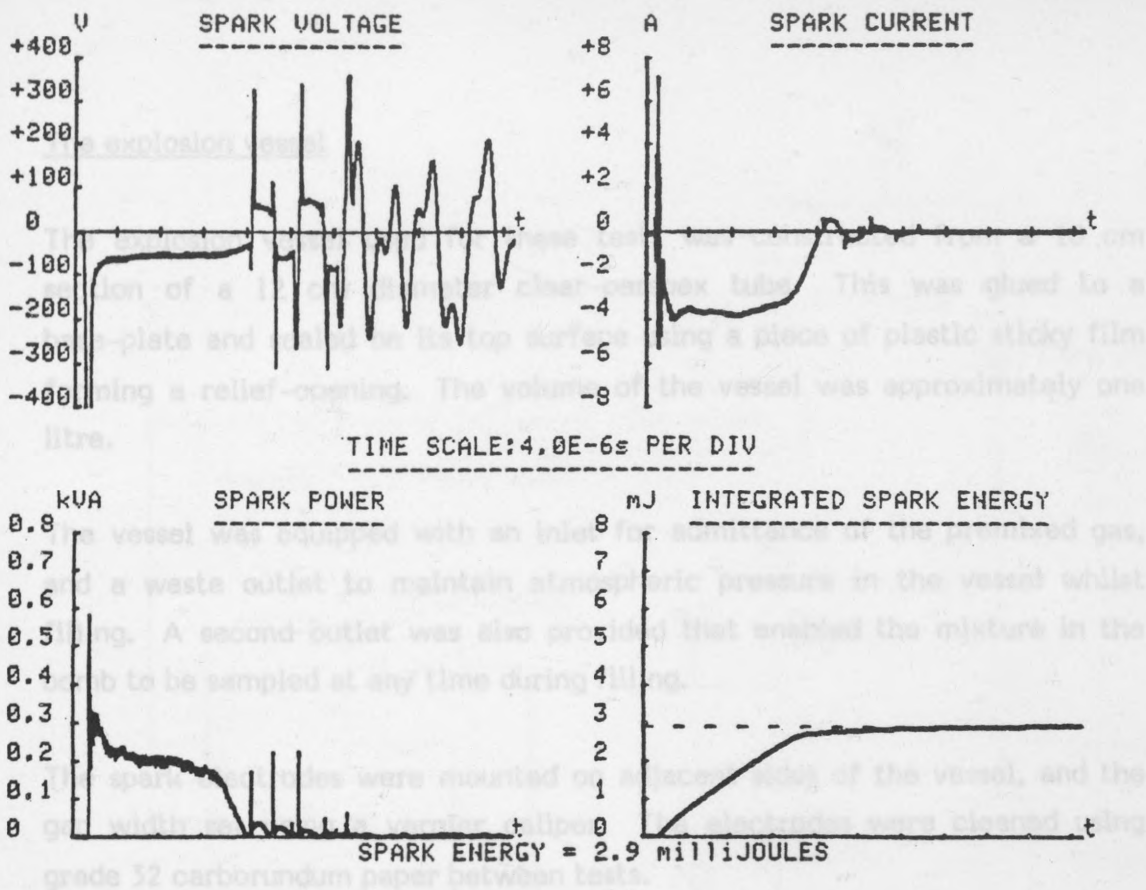


Figure II-1. A typical spark-data acquisition showing a nearly 'square' power \rightarrow time relationship.

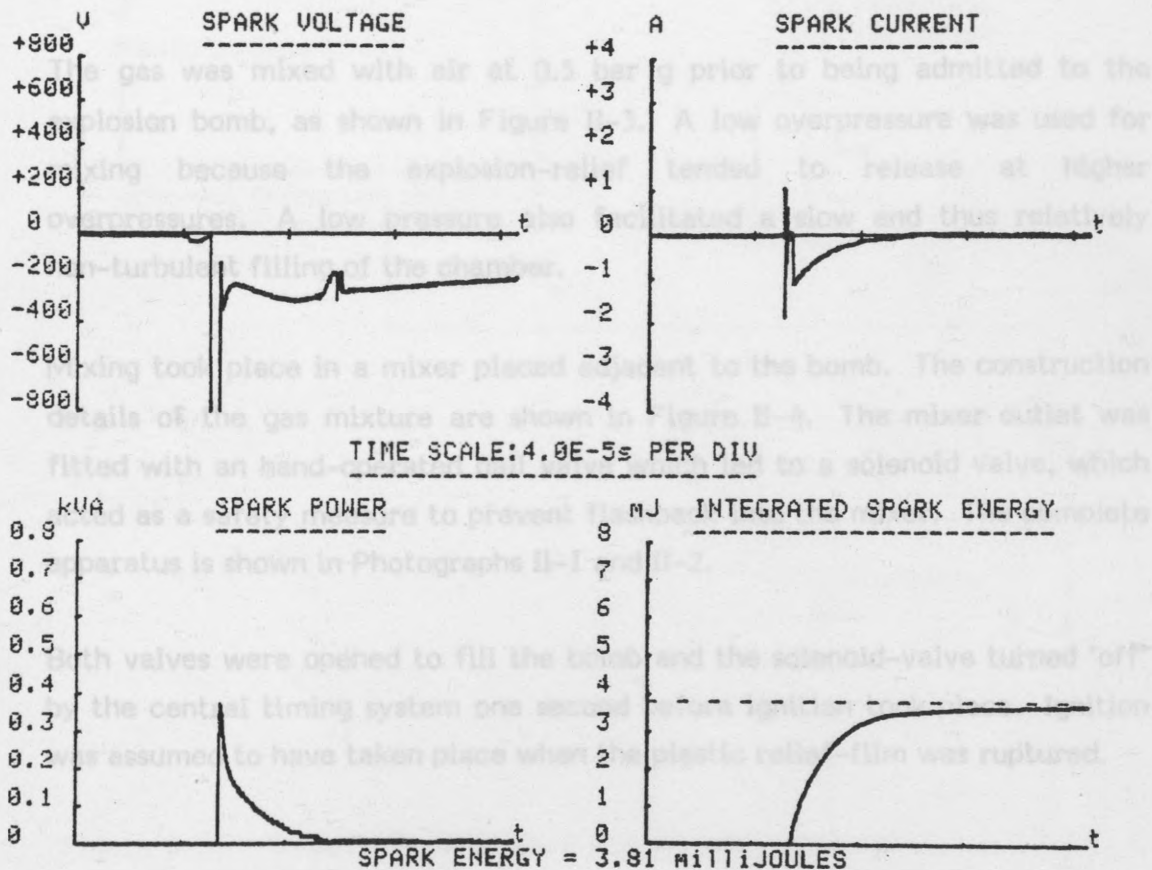


Figure II-2. A typical spark-data acquisition showing a 'decaying' power \rightarrow time relationship.

2.2 The explosion vessel

The explosion vessel used for these tests was constructed from a 10 cm section of a 12 cm diameter clear-perspex tube. This was glued to a base-plate and sealed on its top surface using a piece of plastic sticky film forming a relief-opening. The volume of the vessel was approximately one litre.

The vessel was equipped with an inlet for admittance of the premixed gas, and a waste outlet to maintain atmospheric pressure in the vessel whilst filling. A second outlet was also provided that enabled the mixture in the bomb to be sampled at any time during filling.

The spark electrodes were mounted on adjacent sides of the vessel, and the gap width set using a vernier caliper. The electrodes were cleaned using grade 32 carborundum paper between tests.

2.3 Gas mixing and ignition procedure

The gas was mixed with air at 0.5 bar g prior to being admitted to the explosion bomb, as shown in Figure II-3. A low overpressure was used for mixing because the explosion-relief tended to release at higher overpressures. A low pressure also facilitated a slow and thus relatively non-turbulent filling of the chamber.

Mixing took place in a mixer placed adjacent to the bomb. The construction details of the gas mixture are shown in Figure II-4. The mixer outlet was fitted with an hand-operated ball valve which led to a solenoid valve, which acted as a safety measure to prevent flashback into the mixer. The complete apparatus is shown in Photographs II-1 and II-2.

Both valves were opened to fill the bomb and the solenoid-valve turned 'off' by the central timing system one second before ignition took place. Ignition was assumed to have taken place when the plastic relief-film was ruptured.

Figure II-3. Schematic diagram of the gas mixing system.

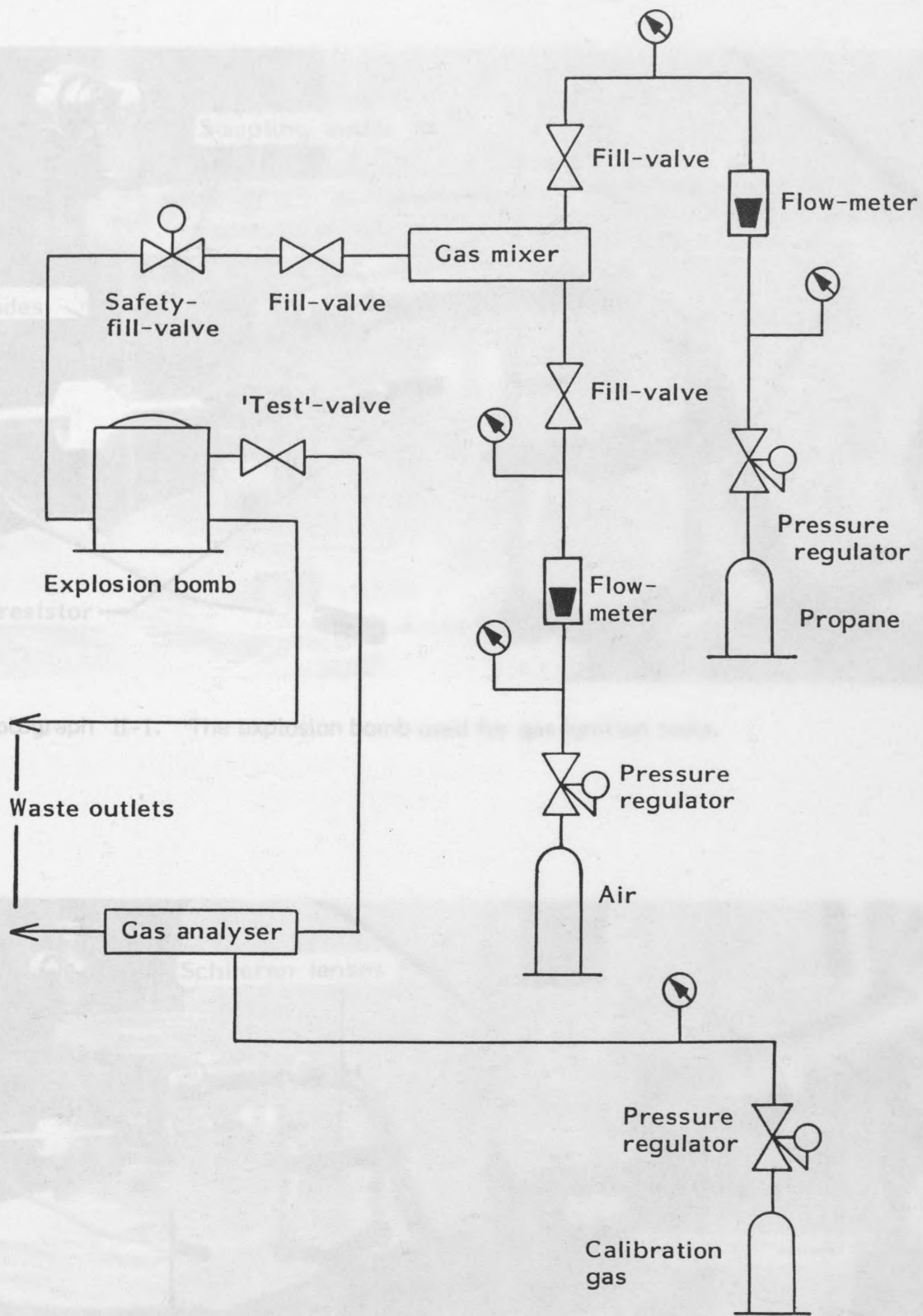
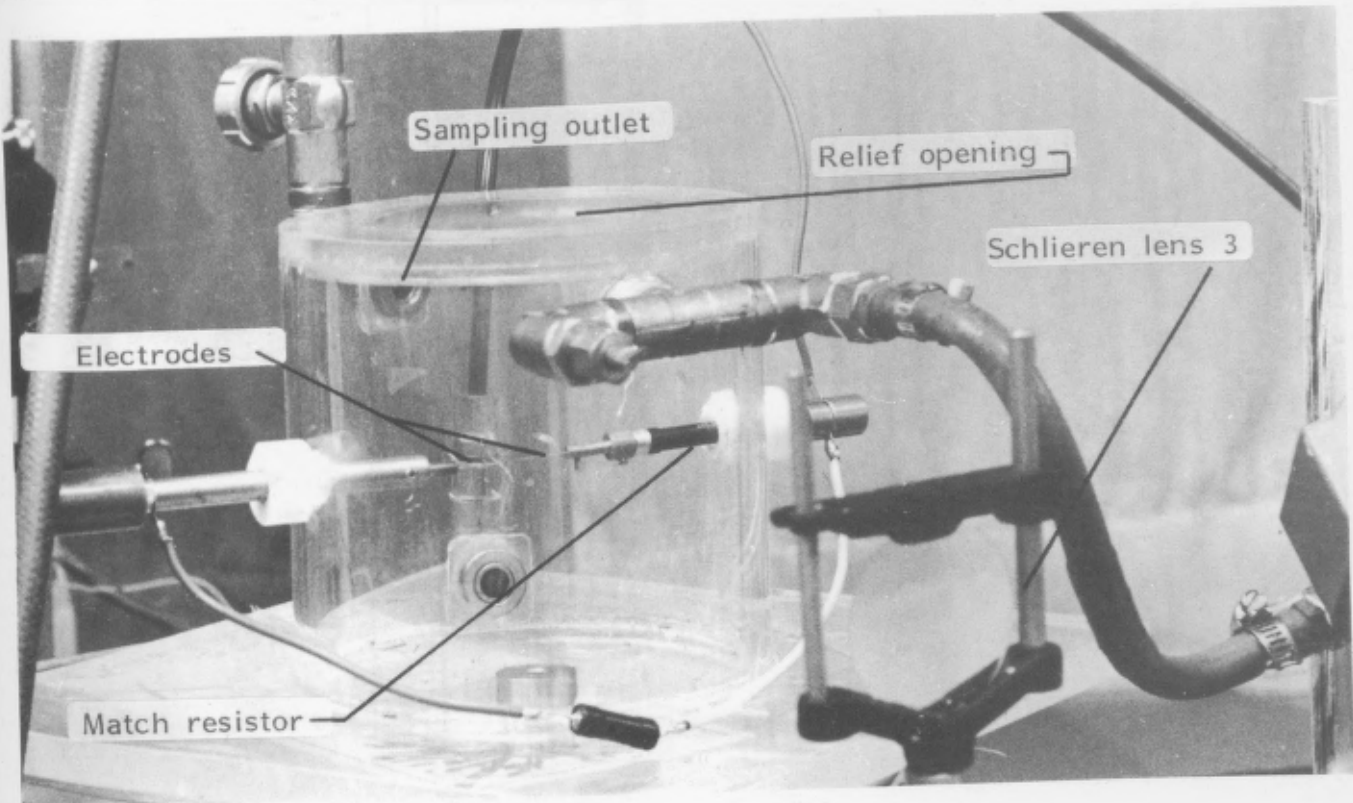
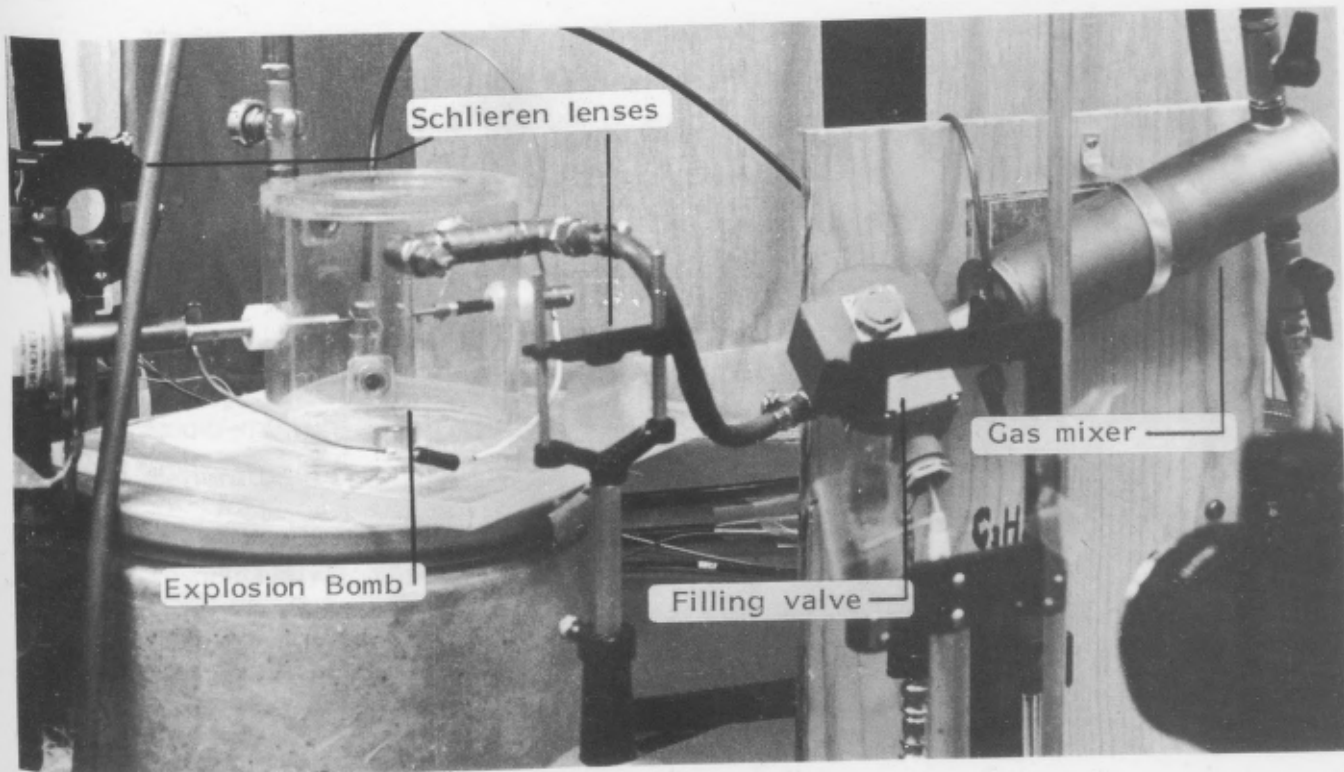


Figure II-3. Schematic diagram of the gas mixing system.



Photograph II-1. The explosion bomb used for gas ignition tests.



Photograph II-2. The explosion bomb and gas mixer.

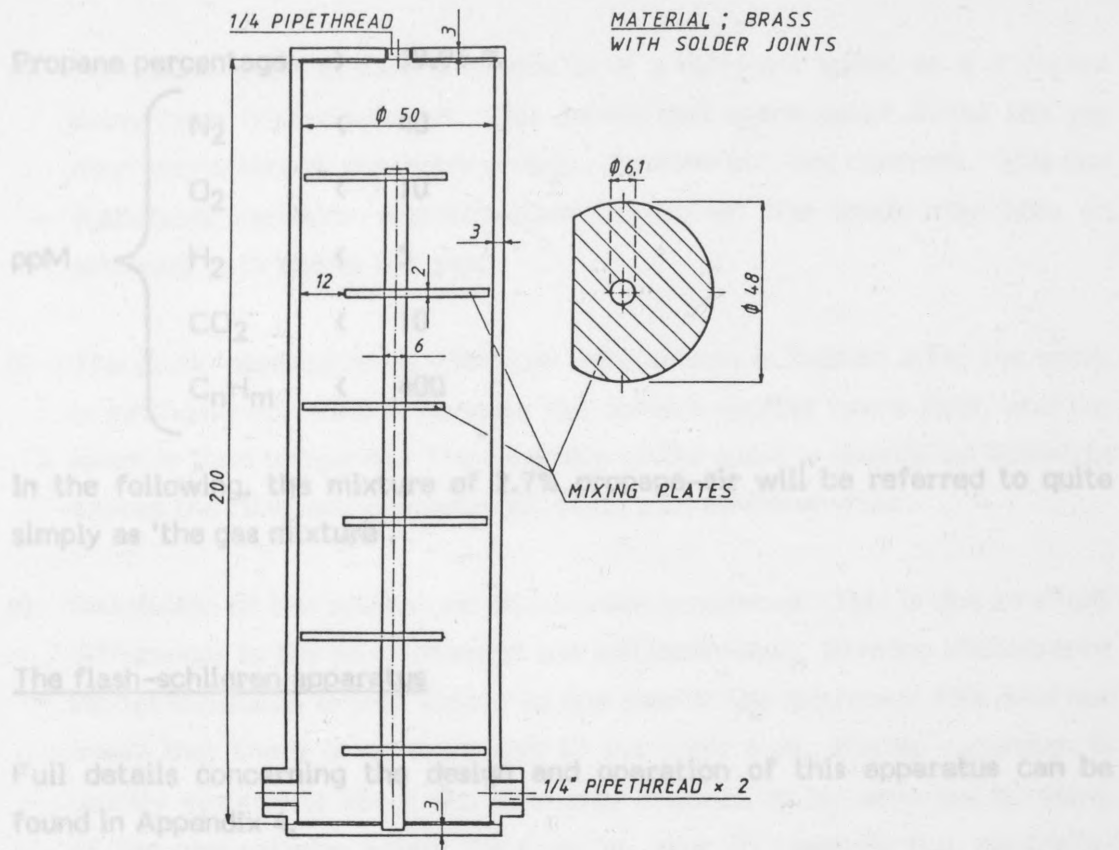


Figure II-4. Cross-section of the gas mixer.
Dimensions in millimeters.

Under continuous operation a new admixture of gas was used regardless of whether or not a previous ignition had been obtained. This procedure was ensured by removing the relief-film after each ignition attempt, which enabled unburned gas/combustion products to escape to the atmosphere. A new film was then placed over the relief to seal the bomb, which was subsequently refilled for 60 seconds.

During filling a LEYBOLD-HERAEUS BINOS 1 gas analyser sampled the bomb-mixture which was varied to yield 2.7 % propane-air. The analyser was calibrated twice daily using a standard 4.92 % propane-nitrogen mixture. Ambient temperature and relative humidity were $21 \pm 2^\circ\text{C}$ and $42 \pm 8\%$, respectively.

The propane was obtained from Norsk Hydro and was analysed by them as follows:

Propane percentage	>	99.95 %
ppM	}	N ₂ < 40
		O ₂ < 10
		H ₂ < 5
		CO ₂ < 10
		C _n H _m < 400

In the following, the mixture of 2.7% propane-air will be referred to quite simply as 'the gas mixture'.

2.4 The flash-schlieren apparatus

Full details concerning the design and operation of this apparatus can be found in Appendix 4.

The timing sequence when using the schlieren system first opened the camera shutter, then triggered a spark 1/4 second later (to allow for shutter opening time) and finally triggered the light-flash after a pre-chosen time interval. The camera motor-drive automatically advanced the film-frame after each 1/2 second exposure. The timing system also controlled filling and valve closure of the explosion bomb, together with high voltage and explosion warning signals.

The quality of the schlieren photographs was theoretically dependant upon L3 (see Figure A1) and the camera lens but was limited in practice by the optical properties of the perspex explosion chamber. In the photographs that follow, this manifests itself as a series of weak horizontal streaks across the upper and lower edges of the images. These effects did not generally create any problems in the interpretation of the schlieren photographs.

It is important, however, to note the method used for obtaining the schlieren photographs as this greatly influenced the quality of the results. Thus:

- a) Each photograph in each sequence is of a different spark, at a different delay-time from discharge. This means that spark-paths across the gap may vary although the spark energy, duration etc. are constant. This is a statistical variation whereby upon breakdown the spark may take an arbitrary path across the gap.
- b) The spark 'persists' even when the light-source is flashed after the spark is extinguished. This is because the camera shutter opens first, and the spark is then triggered. The intensity of the spark is usually sufficient to expose the film, and can even act as its own schlieren-flash.
- c) Resolution of the system varies between sequences. This is due to slight differences in the positioning of the schlieren-stop. In many photographs kernel expansion is only visible to one side of the discharge; this does not imply that there is no expansion to the other side. Kernel expansion is usually symmetric about the discharge channel, as is borne out by many of the photographs, where the stop has been successfully (i.e. centrally) positioned.
- d) Definition of the kernel varies between sequences. Once again this is due to the positioning of the schlieren-stop but also depends upon the combination of camera lens/film used, and the brightness of the schlieren-flash. These were often varied to find the optimum conditions for each spark. In addition, better quality results were obtained with time, i.e. as more experience was gained using the system.

The printed times on each photograph refer to the delay from spark-triggering (breakdown) to the schlieren flash. Physical distances and dimensions are implied from the electrode gap-width assuming a linear cross-section and spherical symmetry around the gap. The cathode is on the left of each photograph.

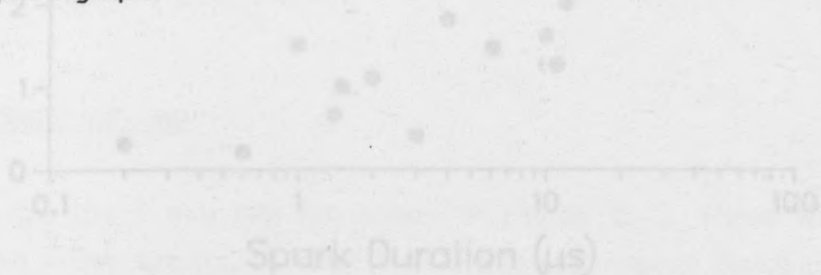


Figure II-5. Ignition results using a 2 mm gap showing the region of ignition uncertainty.

3. RESULTS OF IGNITION TESTS

The ignition-test results are shown in Figures II-5 to II-7. These figures show the ignition probabilities for combinations of spark energy and duration for gap widths 2 mm, 4mm and 7 mm.

3.1 Results for the 2 mm gap

The results for the 2 mm gap width (see Figure II-5) show that the lowest spark energy yielding ignition lay at 3.1 mJ, at durations of 1.5 μs and 45 μs . Over the range 1 μs to $\sim 100 \mu\text{s}$, the energy required for ignition lay at approximately 3 - 4 mJ and did not show any obvious dependence on discharge duration. This is apparent from the region of 'ignition uncertainty' which is plotted in the figure. This region corresponds to combined values of spark energy and duration that yielded a probability of ignition between zero and unity. Below the shaded region no ignition was observed; above the region ignition occurred with a probability of $0.1 \leq P \leq 1$. This region represents the dependence of MIE on spark duration.

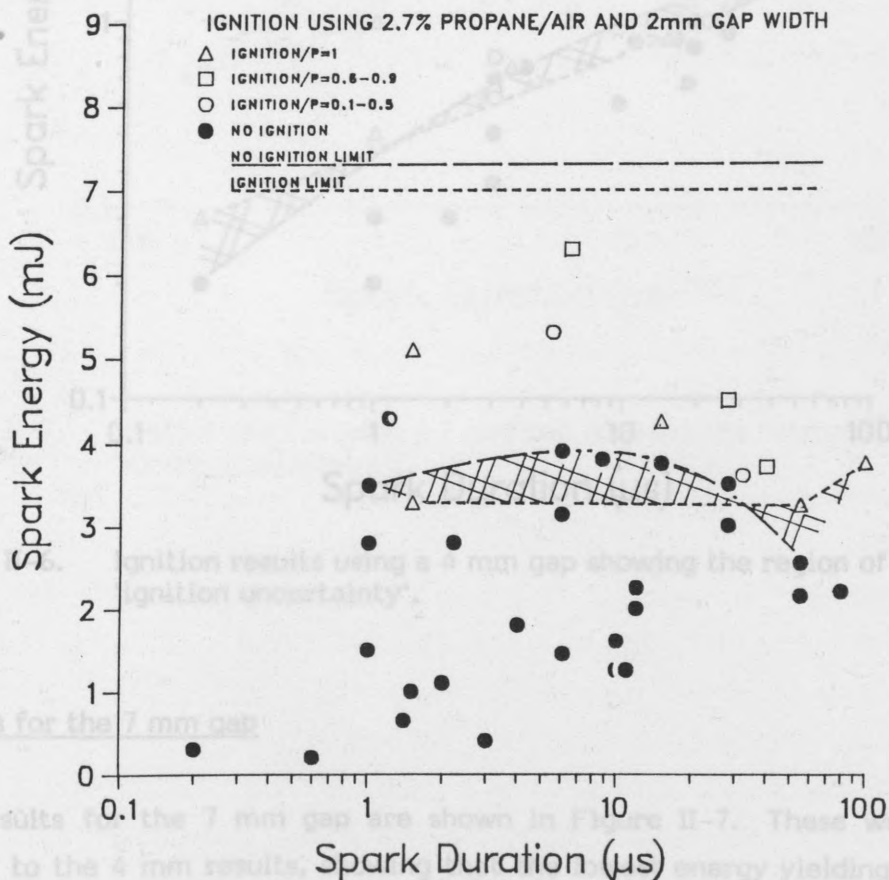


Figure II-5. Ignition results using a 2 mm gap showing the region of 'ignition uncertainty'.

3.2 Results for the 4 mm gap

The results using the 4 mm gap are shown in Figure II-6. These results show that the lowest spark energy yielding ignition was 0.3 mJ at a duration of 0.2 μs . Ignition energy was then found to rise as duration was increased, so that at 80 μs the lowest energy yielding ignition was 1.7 mJ.

The region of 'ignition uncertainty' shows the boundary between ignition and no-ignition. This clearly shows an increase in minimum ignition energy as a function of spark duration.

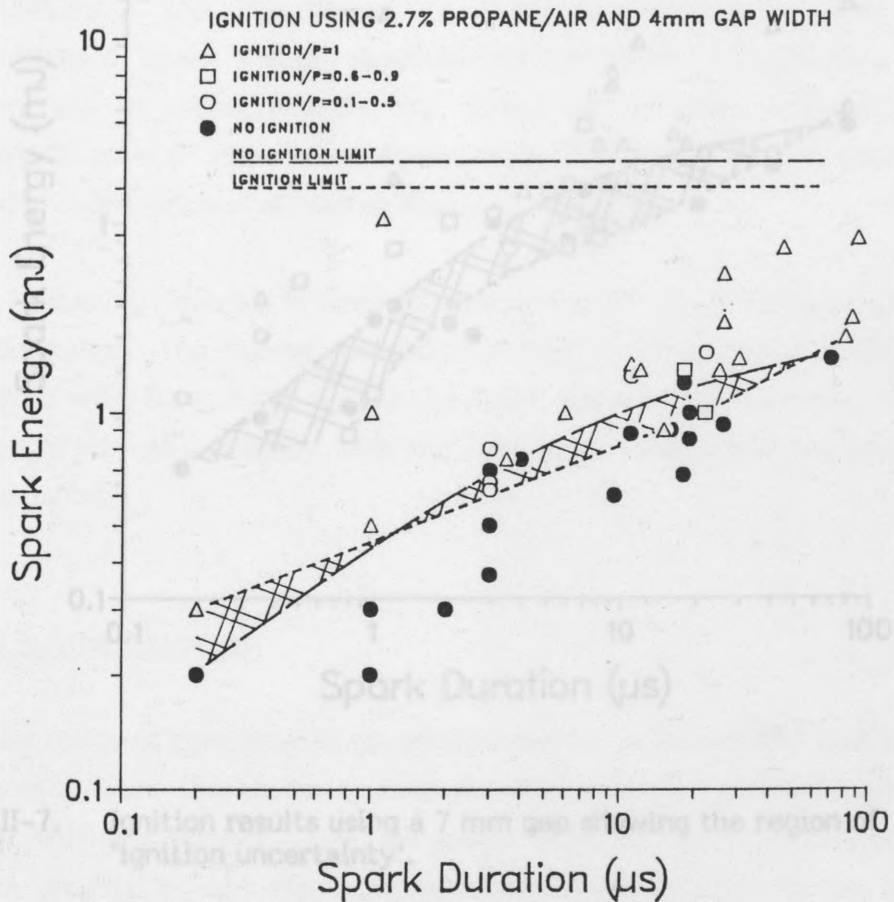


Figure II-6. Ignition results using a 4 mm gap showing the region of 'ignition uncertainty'.

3.3 Results for the 7 mm gap

The results for the 7 mm gap are shown in Figure II-7. These were very similar to the 4 mm results, showing that the lowest energy yielding ignition was 0.27 mJ at a duration of 0.8 μs . Ignition energy rose with an increase in spark duration, so that at 80 μs an energy of 2 mJ was required. The region

of 'ignition uncertainty' shows that the minimum ignition energy increased with duration, in much the same way as was observed using the 4 mm gap, although the boundary between the limits of ignition and no-ignition was broader for the 7 mm results.

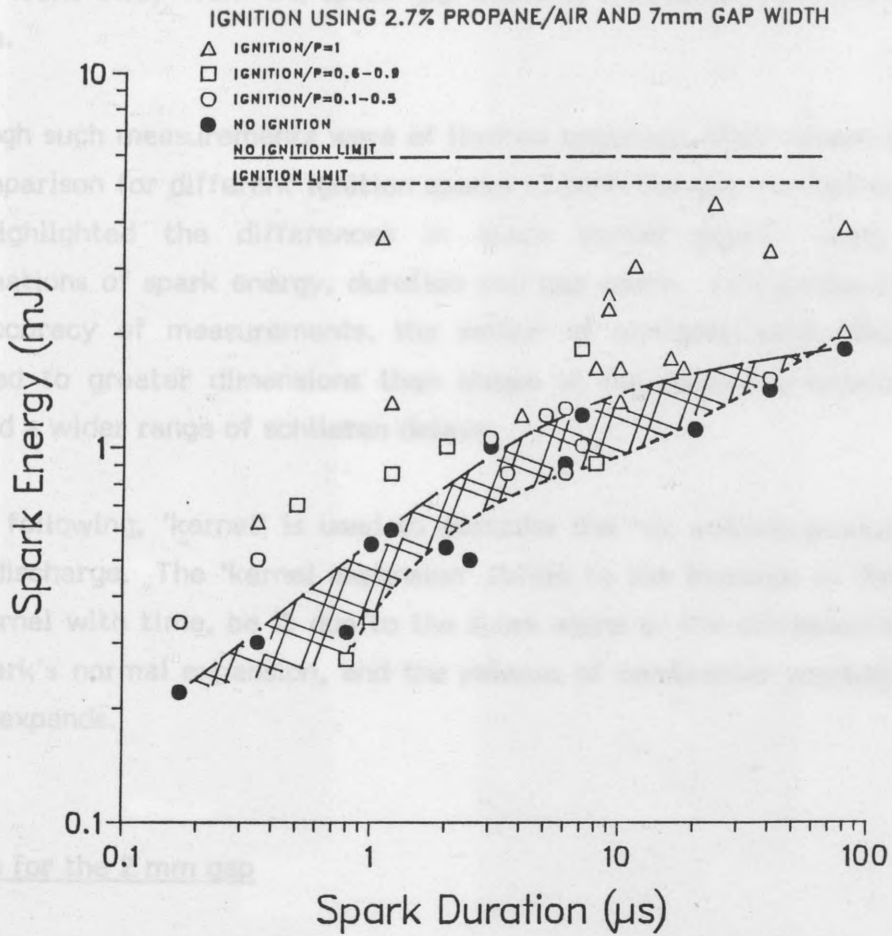


Figure II-7. Ignition results using a 7 mm gap showing the region of 'ignition uncertainty'.

4. SCHLIEREN PHOTOGRAPHS: RESULTS

The schlieren photographs, showing spark kernel expansion for the three gap widths, offer a range of comparisons that could hopefully help to explain the trends observed in the ignition tests. In particular, the expansion of the kernel front away from the spark gap could be measured from the schlieren images.

Although such measurements were of limited accuracy, they served as a basis of comparison for different ignition sparks in both the gas mixture and in air, and highlighted the differences in spark kernel growth using various combinations of spark energy, duration and gap width. To improve the range and accuracy of measurements, the series' of schlieren photographs were enlarged to greater dimensions than shown in the following examples, and covered a wider range of schlieren delays.

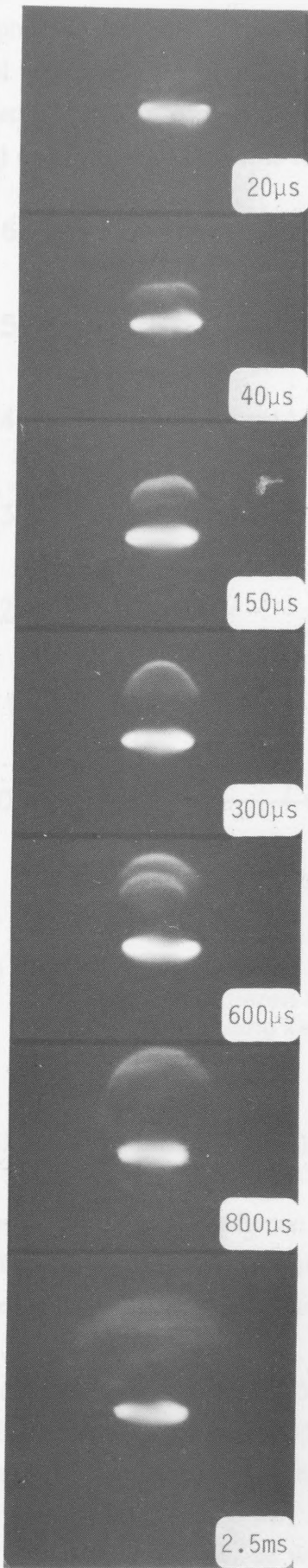
In the following, 'kernel' is used to describe the hot volume produced by a spark discharge. The 'kernel expansion' refers to the increase in the size of this kernel with time, be it due to the spark alone or the combined effect of the spark's normal expansion, and the release of combustion products as the kernel expands.

4.1 Results for the 2 mm gap

From the range of ignition and no-ignition points in Figure II-5 two values of spark energy were chosen for a given duration, one that yielded ignition, and one that only just did not. The two sparks were 3.6 mJ/30 μ s and 4.5 mJ/30 μ s. The growths of the flame kernels using these two sparks are shown in Photographs II-3 and II-4. From the photographs alone it is difficult to discern any visual differences in kernel growth until the final picture in each sequence, i.e. at 2.5 ms following discharge. A comparison of kernel sizes, however, in terms of the equivalent radial distance of the kernel front from the spark gap centre, shows that a difference in kernel growths occurs after about 0.8 ms. This is shown in Figure II-8. This time corresponds to that at which a self-propagating flame develops in the mixture, independent of the ignition source, and is a measure of the so-called 'induction time' of the mixture. This value is of the same order of magnitude as values measured by other workers using hydrocarbon-air mixtures^{44,45,46}.

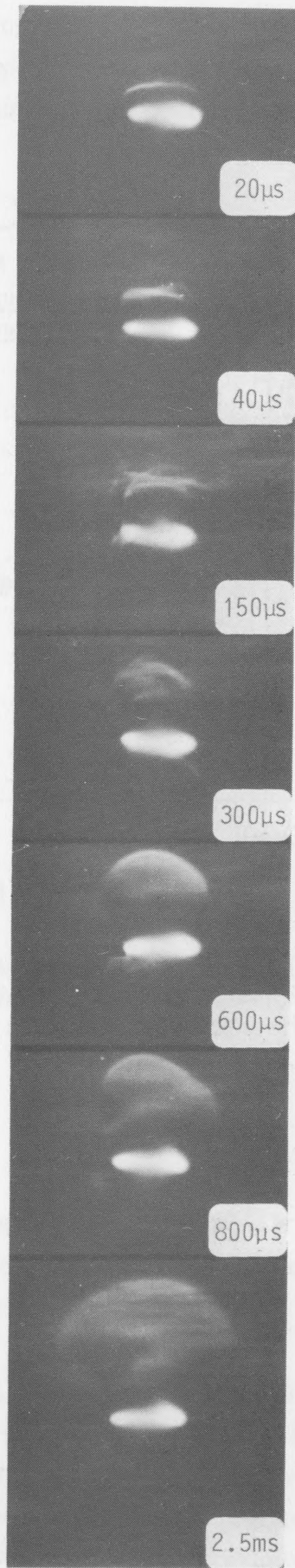
Schlieren photograph series' II-3 and II-4.

(kernel size (mm))



Photograph series II-3.

3.6 mJ/30 μ s spark in
gas mixture (2 mm gap).



Photograph series II-4.

4.5 mJ/30 μ s spark in
gas mixture (2 mm gap).

The photographs shown here show a cylindrical development of the flame kernel front, up to about 40 μs , whereupon the kernel becomes more spherical in shape. This is probably due to increased conducted heat losses at the kernel extremes up until this time.

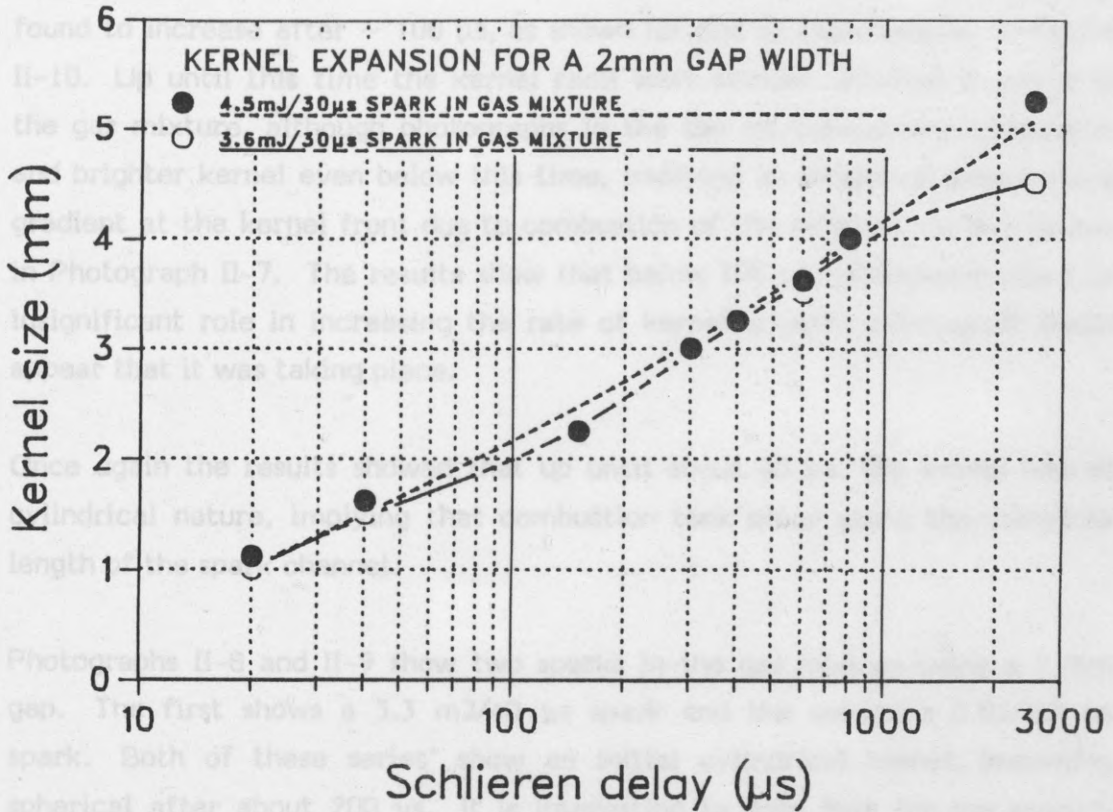


Figure II-8. Kernel sizes for two sparks in the gas mixture using a 2 mm gap. 'Schlieren delay' refers to the time at which an image of the expanding kernel was recorded following spark discharge.

4.2 Results for the 4 mm and 7 mm gaps

For these gap widths schlieren photographs were taken using a wide range of spark energies/durations, in both air and in the presence of the gas mixture. Some of the results are shown in Photographs II-5 to II-9.

The first two photographs, II-5 and II-6, show two sparks in air with similar durations (1 mJ/22 μs and 2.35 mJ/26 μs) for a 4 mm gap. These show the increase in spark kernel expansion that resulted from an increase in spark energy (at similar durations). As can be seen in the photographs, the initial kernel is cylindrical, but, as was also observed in the previous photographs, became more spherical beyond about 40 μs . Results from these series' and

from a third series using a 4.3 mJ/25 μ s spark, are shown in Figure II-9. This figure shows an increase, both in kernel size, and in expansion rate, as a function of time following discharge, as spark energy was increased.

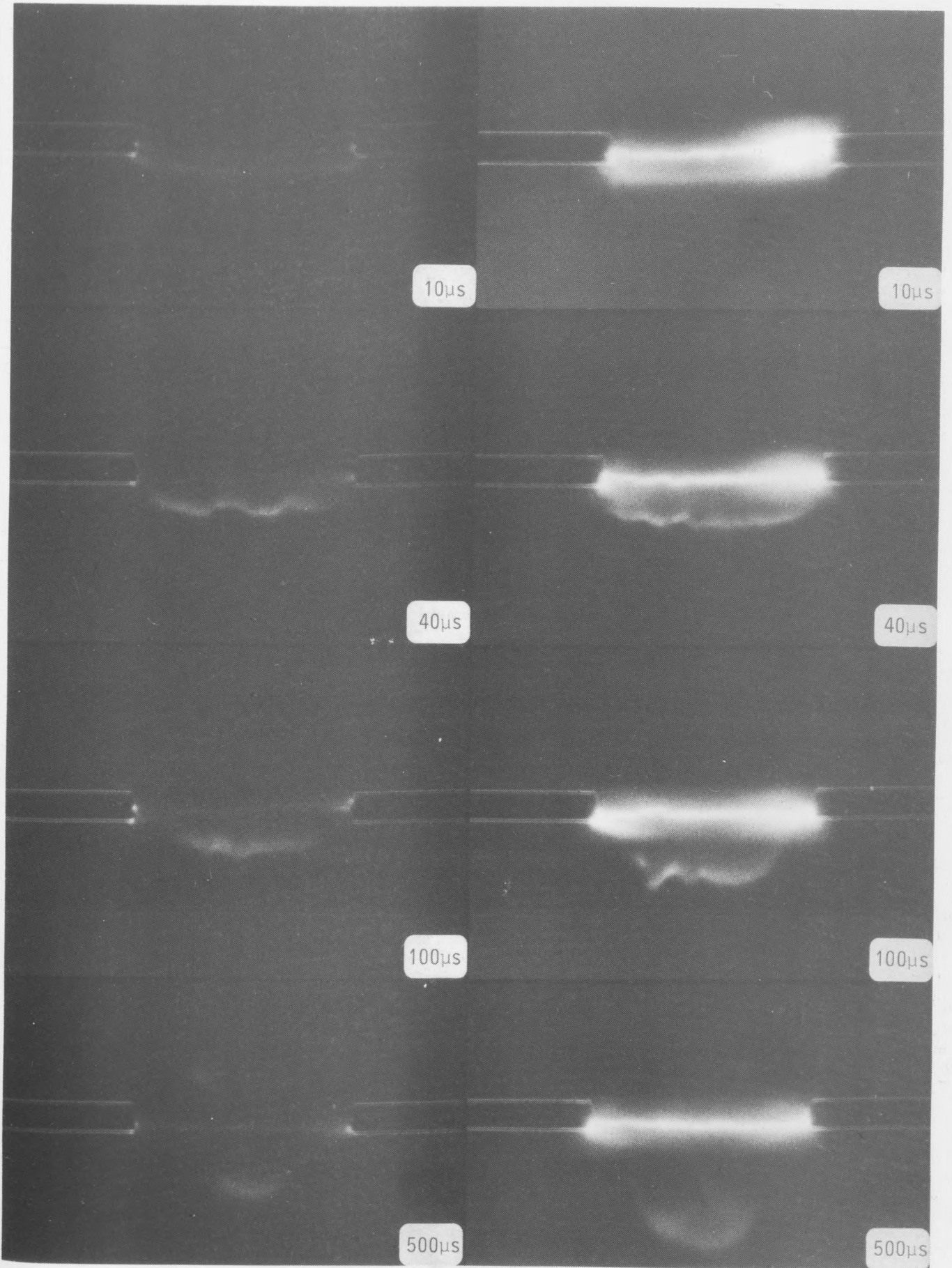
When these tests were repeated in the gas mixture, kernel volumes were found to increase after $\sim 100 \mu$ s, as shown for one of these sparks, in Figure II-10. Up until this time the kernel radii were similar, whether in air or in the gas mixture, although photographs in the gas mixture showed a broader and brighter kernel even below this time, implying an increased temperature gradient at the kernel front due to combustion of the mixture. This is shown in Photograph II-7. The results show that below 100 μ s, combustion plays an insignificant role in increasing the rate of kernel growth, although it would appear that it was taking place.

Once again the results showed that up until about 40 μ s, the kernel was of cylindrical nature, implying that combustion took place along the complete length of the spark channel.

Photographs II-8 and II-9 show two sparks in the gas mixture using a 7 mm gap. The first shows a 3.3 mJ/40 μ s spark and the second a 0.85/1.2 μ s spark. Both of these series' show an initial cylindrical kernel, becoming spherical after about 200 μ s. It is interesting to note that for the second, lower energy spark, the kernel is seen to 'shrink' towards the channel centre at this time, whereas the first spark takes some milliseconds before assuming a fully spherical shape. The reason for this could be due to the lower energy density of the expanding kernel in the second case, due to a lower spark energy. Conductive losses to the electrodes and surroundings at the kernel ends would therefore be expected to increase in this case.

Plots of kernel size, based on the growth of the kernel edge, are shown in Figure II-11. This figure also shows the kernel expansions for one other spark in the gas mixture. This was picked out to yield 2 fundamental comparisons; one where spark energy was increased for a given duration, and one where spark duration was increased for a given spark energy.

When varying energy, spark duration was held constant at about 1.1 μ s, and energy increased from 0.85 to 3.6 mJ. When varying duration, energy was held constant at about 3.6 mJ, and duration increased from 1.1 μ s, to 40 μ s. These changes are shown by the arrows in Figure II-12.



Photograph series II-5.

1 mJ/22 μ s spark in air
(4 mm gap).

Photograph series II-6.

2.35 mJ/26 μ s spark in air
(4 mm gap).

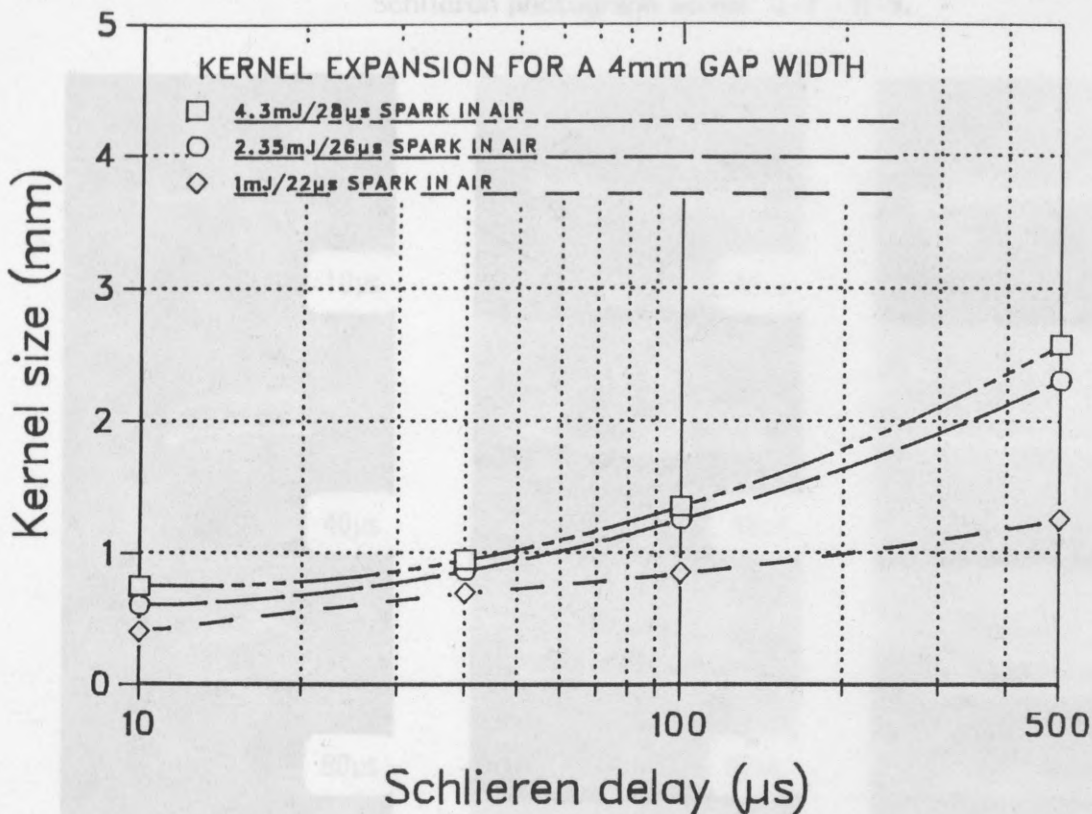


Figure II-9. Kernel sizes for three sparks in air using a 4 mm gap. 'Schlieren delay' refers to the time at which an image of the expanding kernel was recorded following spark discharge.

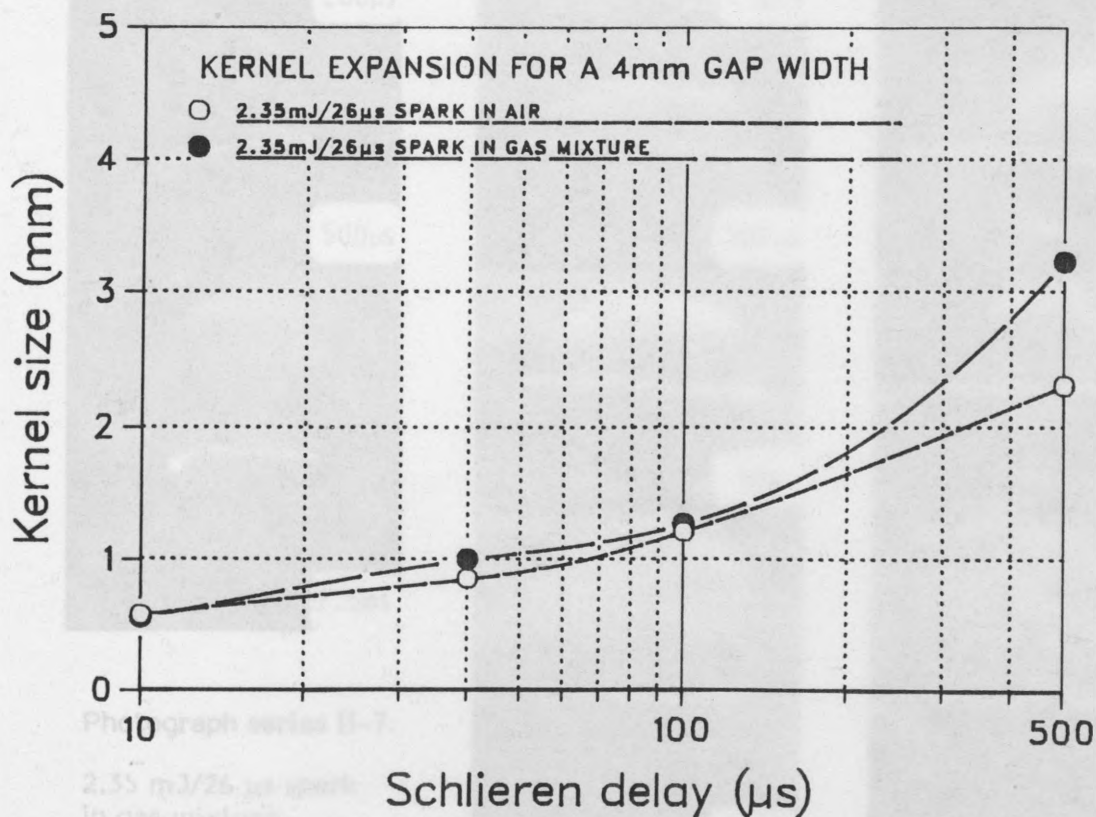
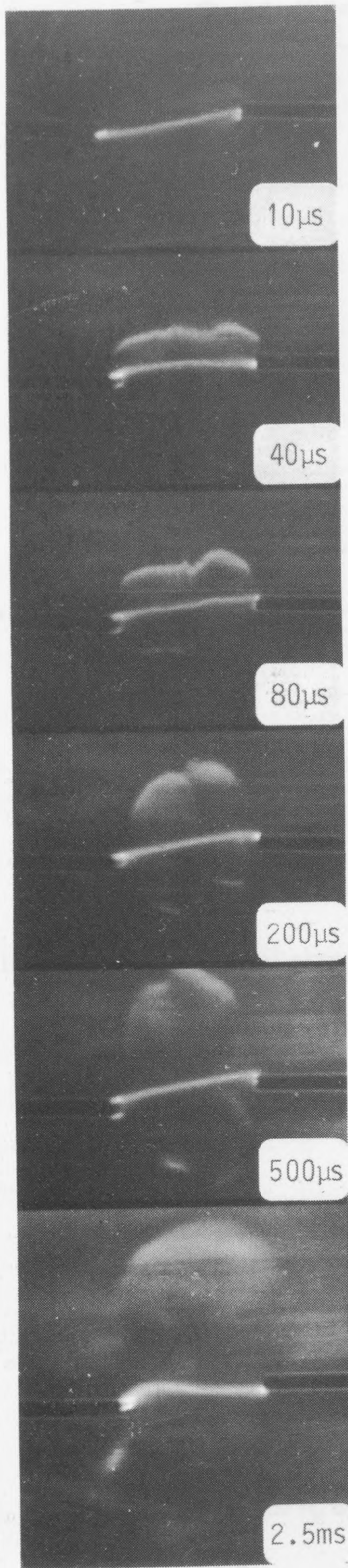


Figure II-10. Kernel sizes for a 2.35 mJ spark both in air and in the gas mixture.



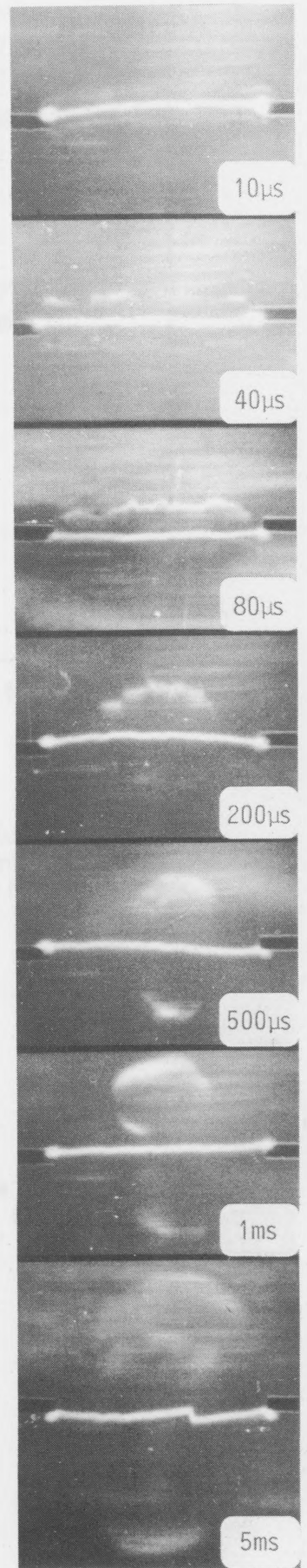
Photograph series II-7.

2.35 mJ/26 μs spark
in gas mixture
(4 mm gap).



Photograph series II-8.

3.3 mJ/40 μs spark
in gas mixture
(7 mm gap).



Photograph series II-9.

0.85 mJ/1.2 μs spark
in gas mixture
(7 mm gap).

KERNEL EXPANSION FOR A 7mm GAP WIDTH

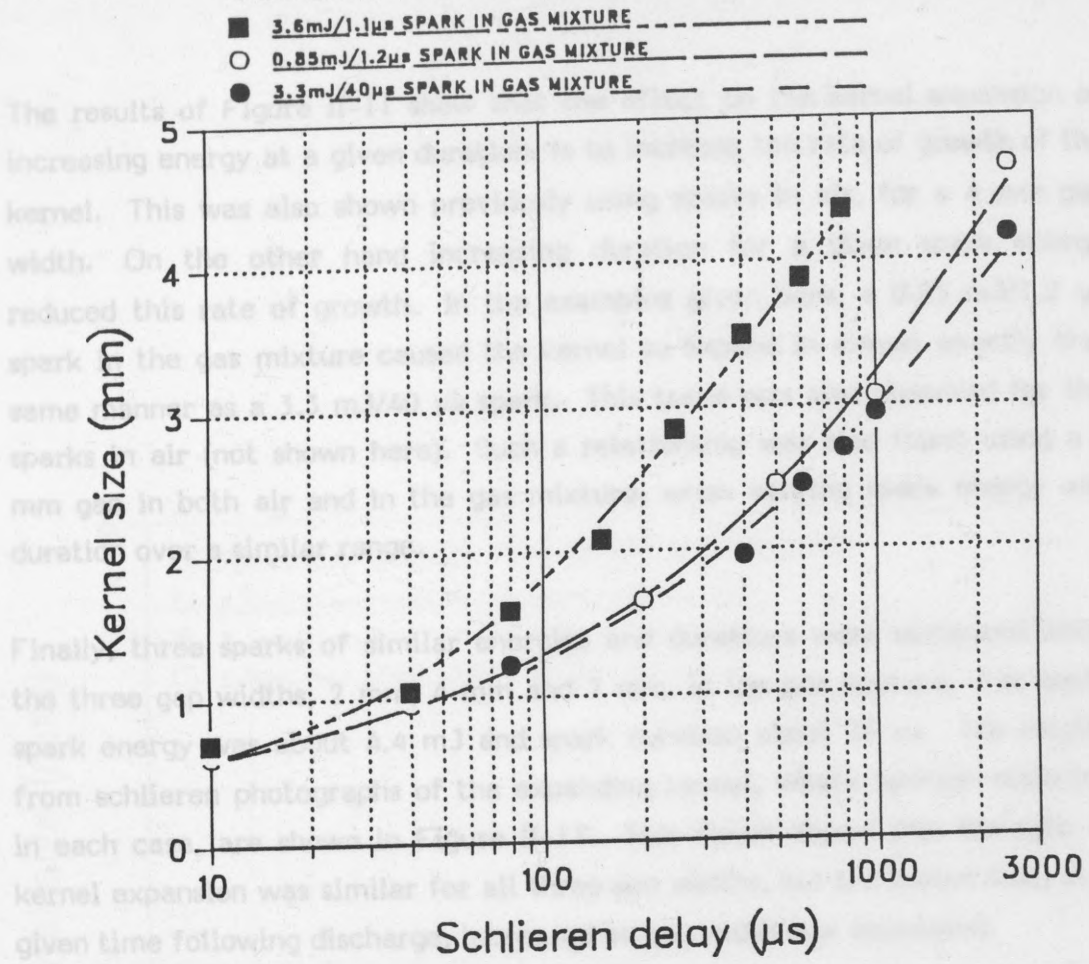


Figure II-11. Kernel sizes for three sparks in the gas mixture using a 7 mm gap. 'Schlieren delay' refers to the time at which an image of the expanding kernel was recorded following spark discharge.

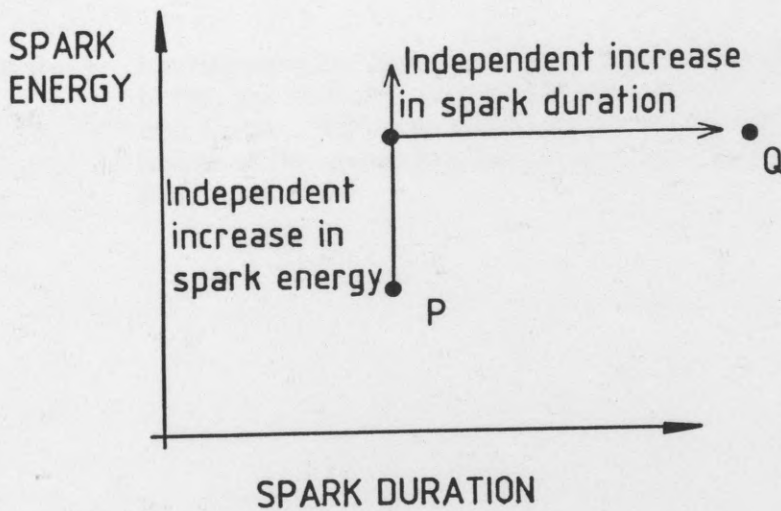


Figure II-12. Figure showing basis of comparison of kernel sizes keeping spark energy or duration constant, for a given gap width.

The results of Figure II-11 show that the effect on the kernel expansion of increasing energy at a given duration, is to increase the rate of growth of the kernel. This was also shown previously using sparks in air, for a 4 mm gap width. On the other hand increasing duration for a given spark energy reduced this rate of growth. In the examples given here, a 0.85 mJ/1.2 μ s spark in the gas mixture caused the kernel to expand in almost exactly the same manner as a 3.3 mJ/40 μ s spark. This trend was also observed for the sparks in air (not shown here). Such a relationship was also found using a 4 mm gap in both air and in the gas mixture, when varying spark energy and duration over a similar range.

Finally, three sparks of similar energies and durations were compared using the three gap widths, 2 mm, 4 mm and 7 mm, in the gas mixture. For each, spark energy was about 4.4 mJ and spark duration about 25 μ s. The results from schlieren photographs of the expanding kernel, where ignition occurred in each case, are shown in Figure II-13. This figure shows that the rate of kernel expansion was similar for all three gap widths, but the kernel size, at a given time following discharge, increased as gap width was decreased.

The increase in kernel size at lower gap widths is probably due to an increase in energy per unit length of the spark gap. If one assumes that expansion and ignition take place due to the positive column of the discharge⁴⁴, then the spark may be treated as a line source. In this case one would expect that decreasing the length of the line, or column, maintaining total energy, would increase the resultant size of the kernel, as was observed.

Figure II-13. Kernel sizes for three sparks of similar energies and durations in the gas mixture. Gap width took values of 2 mm, 4 mm and 7 mm. "Schlieren delay" refers to the time at which an image of the expanding kernel was recorded following spark discharge.

DISCUSSION OF RESULTS

The most striking feature of the kernel expansion in the gas mixture could be ignited with spark durations below 1 μ s. The kernel size increased by an order of magnitude when the gap width was increased to 2 mm. At the lower gap width the kernel size was approximately constant at about 1 mm for spark durations from 10 μ s to 50 μ s.

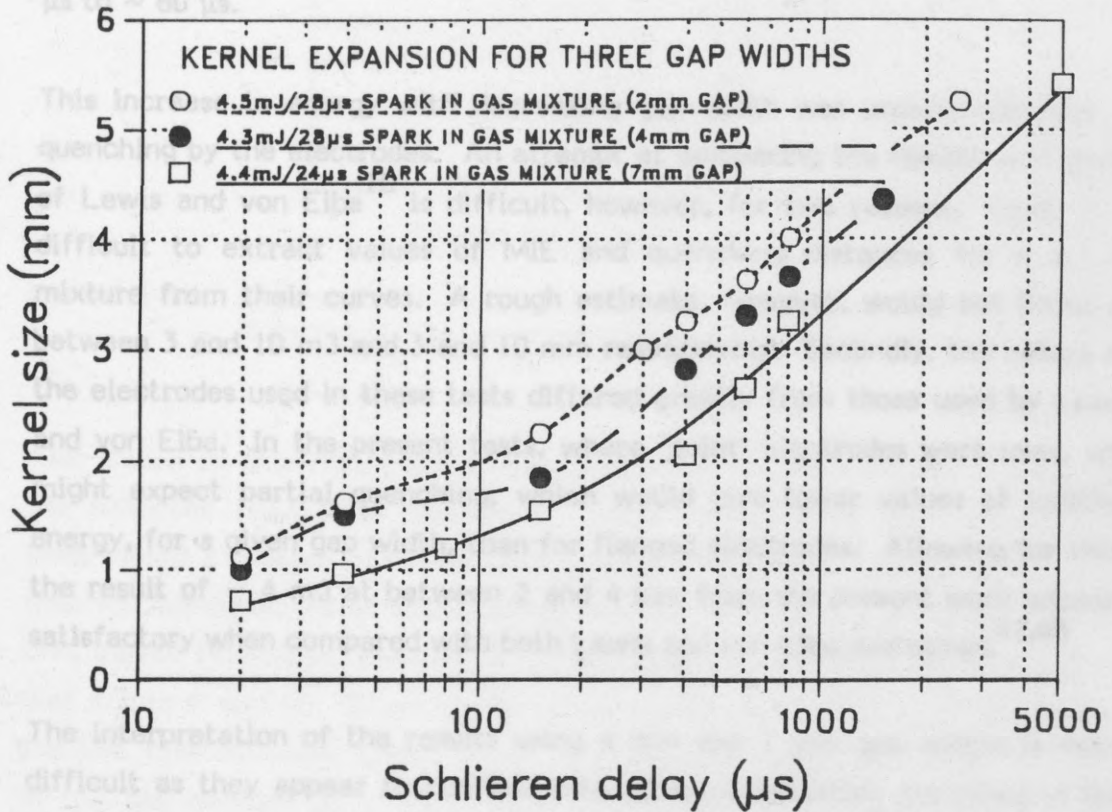


Figure II-13. Kernel sizes for three sparks of similar energies and durations in the gas mixture. Gap width took values of 2 mm, 4 mm and 7 mm. 'Schlieren delay' refers to the time at which an image of the expanding kernel was recorded following spark discharge.

One may begin by suspecting a measurement error for such short durations. From the present data it is very unlikely that measurement error is the cause of the trend. An explanation may be found in the data from the schlieren photographs. In the present case, pulse circuit and a typical capacitor circuit

5. DISCUSSION OF RESULTS

The most striking feature of the ignition results is the fact that this gas mixture could be ignited using spark energies as low as 0.3 mJ for spark durations below 1 μ s. The results also showed that minimum ignition energy increased by an order of magnitude when gap width was decreased from 4 mm to 2 mm. At the lower gap width, the energy required for ignition was approximately constant at about 4 mJ as spark duration was varied from ~ 1 μ s to ~ 80 μ s.

This increase in energy with decreasing gap width was undoubtedly due to quenching by the electrodes. An attempt at comparing the results with those of Lewis and von Elbe¹⁰ is difficult, however, for two reasons. First, it is difficult to extract values of MIE and quenching distances for a 2.7 % mixture from their curves. A rough estimate, however, would put these at between 3 and 10 mJ and 3 and 10 mm respectively. Secondly, the nature of the electrodes used in these tests differed greatly from those used by Lewis and von Elbe. In the present tests, where 'point' electrodes were used, one might expect partial quenching, which would give lower values of ignition energy, for a given gap width, than for flanged electrodes. Allowing for this, the result of ~ 4 mJ at between 2 and 4 mm from the present work appears satisfactory when compared with both Lewis and von Elbe and others^{47,48}.

The interpretation of the results using 4 mm and 7 mm gap widths is more difficult as they appear to conflict with other observations described in the literature. First of all, minimum values of ignition energy for a 2.7 % propane-air mixture, as measured by Lewis and von Elbe¹⁰ and Calcote⁴⁸, were an order of magnitude higher. Secondly, the effect of an increase in discharge duration, using capacitive circuits with other gas mixtures, has apparently been to reduce the spark energy required for ignition¹¹.

One may begin by suspecting a measurement error of the spark energies, at such short durations. From the calibration results in Part 1, it would seem very unlikely that measurement errors could account for such a pronounced trend. An explanation may be sought, however, by considering the results from the schlieren photographs, together with the operation of both the present, pulse circuit and a typical capacitive circuit.

First, one may approximate the 'region of ignition uncertainty', found for the 4 mm and 7 mm gaps, as monotonic relationships, defining the MIE of the mixture. This is shown below, for the 7 mm gap, in Figure II-14.

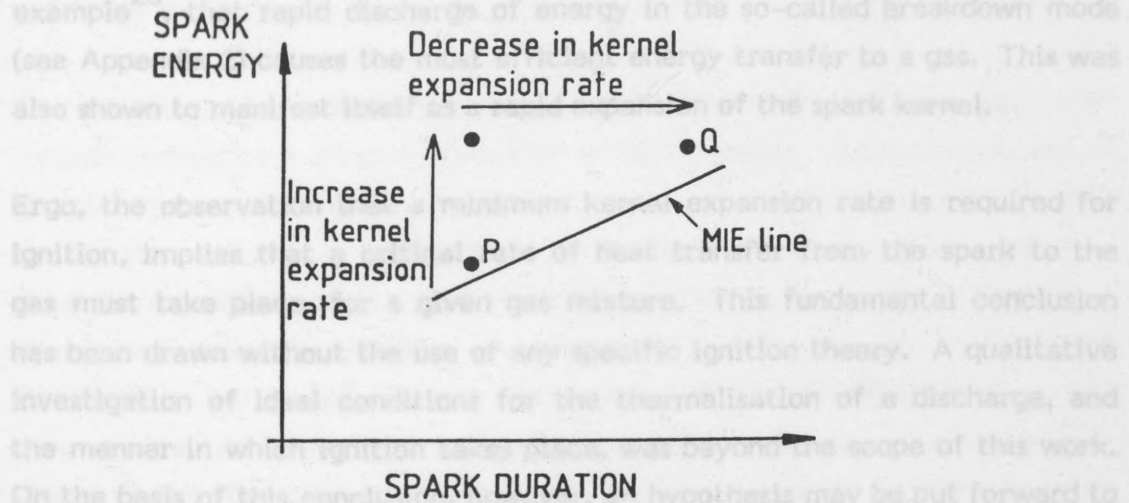


Figure II-14. Figure showing the effect of altering spark energy and duration on the kernel expansion, for a 7 mm gap width.

Also shown on this figure are arrows, indicating the comparisons made using the schlieren results, in Section 4. These arrows show the influences of independent increases in either spark energy or duration. The results showed that for combinations of spark energy and duration lying just above the MIE line, kernel expansion, whether in air or in the gas mixture, was very similar (see points P and Q). It would therefore appear that points at or just above the MIE line represent sparks whose kernels expand at similar rates, whether in the gas mixture or in air. Since kernel expansion increases for points above this line, one may conclude that the MIE line also represents a minimum kernel expansion rate required for ignition. This rate is a measure of the induction time of the succeeding layer of the gas mixture ahead of the flame kernel.

The rate of expansion of the spark kernel is related to the manner in which energy is delivered to the spark channel. This refers to the distribution of the energy in time and space. Assuming ignition to be a thermal phenomenon, it is reasonable to assume that the rate of thermalisation of a spark, i.e. the rate of transfer of heat energy to the gas mixture, is a critical factor in determining ignition. A change in this rate will manifest itself as a change in the expansion of the hot plasma (or kernel) following the thermalisation process. It follows, therefore, that without direct recourse to the thermalisation process, the efficiency of a spark as an ignition source in a

gas mixture may be related to the expansion of the spark kernel. Inefficient, or slow transfer of electrical energy to heat energy will lead to a slow expansion of the kernel, and vice versa. It has recently been shown, for example²⁸, that rapid discharge of energy in the so-called breakdown mode (see Appendix 2) causes the most efficient energy transfer to a gas. This was also shown to manifest itself as a rapid expansion of the spark kernel.

Ergo, the observation that a minimum kernel expansion rate is required for ignition, implies that a critical rate of heat transfer from the spark to the gas must take place, for a given gas mixture. This fundamental conclusion has been drawn without the use of any specific ignition theory. A qualitative investigation of ideal conditions for the thermalisation of a discharge, and the manner in which ignition takes place, was beyond the scope of this work. On the basis of this conclusion, however, an hypothesis may be put forward to explain why these results appear to conflict with those of other workers.

One reason for the apparent conflict is the method in which spark duration was varied in the current tests. This was varied independently of spark energy, and while maintaining the rate of energy release in the gap. This contrasts with the conventional method of including a circuit resistance in a capacitive discharge circuit to increase discharge time. Such a method will necessarily alter the rate of energy release to the spark gap as resistance is increased. This rate will tend to decrease with increase in resistance, in an undetermined manner. This will mean that, for a specific combination of spark energy and duration, the rate of energy release in the gap will be markedly different for capacitive-resistive (C-R) circuits than for a pulse circuit.

In view of the above observations relating MIE to a minimum rate of kernel growth, it would appear that using resistance to increase discharge duration, leading to an arbitrary rate of energy release, in turn leads to an unknown rate of expansion of the spark kernel, which may not be above the minimum required for ignition. Clearly, however, because ignition energy decreases as resistance is first introduced in the circuit, and this reduces the rate of energy release in the gap, other factors appear to influence the success of ignition using pure capacitive discharges. These may include an increase in

shock and expansion work losses for discharges below $0.1 \mu\text{s}$, as has been suggested by other workers^{3,10,43}. This being the case, one would expect ignition energy to rise below about $0.1 \mu\text{s}$ for the 4 mm and 7 mm results presented in this work.

The present results, therefore, may reflect the ability of this generator circuit to produce a given combination of spark energy, duration and rate of energy release, which causes an optimum thermalisation of the spark, leading to ignition. Such a combination is unlikely to be possible using a capacitor-resistor circuit. This is probably because, in order to achieve a given spark energy/duration as was used here, resistance must be increased significantly, particularly for gap widths above a few millimeters. This would mean a slow transfer of energy to the gas mixture, particularly in the initial stages of the discharge, meaning a slow kernel expansion. Furthermore, for such high values of resistance (typically $> 100 \text{ k}\Omega$) the form of the discharge may change (for example to a glow type) so that conditions may be far from optimum for ignition. On the other hand, using a pulse circuit, thermalisation and expansion are more rapid due to the fast rise of current in the gap, and because circuit impedances are very much lower than for a resistive circuit. Thus the results imply that the initial rate of energy release in the gap is a critical factor in determining ignition. This was also observed by Riddlestone¹². Unfortunately, the nature of this work did not allow a quantitative study of this parameter to be made, although the results would indicate that the energy release within a time shorter than $0.2 \mu\text{s}$ following discharge, was critical. ($0.2 \mu\text{s}$ was the shortest spark duration used in this work).

It has also been suggested by Bartels⁶, when using methane-air mixtures, that 'the rate of energy dissipation in the early stages of the discharge most likely governs the ignition process and determines at which energy level ignition will take place'. This being the case, this initial rate will clearly be higher, for a given spark energy and duration, for a pulse discharge, than for a discharge produced from an high impedance circuit. This is made possible by the mode of operation of the spark generator, where operating voltages were up to 50% lower than those using a conventional static-breakdown, capacitive circuit (see Part 1). This in turn meant that lower energies could be produced for a given duration, whilst maintaining the rate of energy release in the gap, over the discharge duration. It appears, therefore, that this last term is a critical factor influencing the thermalisation process in the spark channel.

The ignition results do not, therefore, necessarily conflict with the results of other workers. Instead they verify that where the effects of duration on MIE are being studied, it is very important to maintain other aspects of the discharge constant. For a simple capacitive circuit this is not possible, not least because breakdown voltage is fixed for a given gap width and cannot be either reduced or exceeded. This means that maintaining the rate of energy feed to the spark gap cannot be achieved using such a circuit when varying discharge duration.

The conclusions from this hypothesis are depicted in Figure II-15. This figure shows the results from the present ignition tests and those from an hypothetical C-R circuit. Also shown for the results for the pulse circuit is an upward trend in the MIE curve below $0.2 \mu\text{s}$ (the lowest value used in the tests). The exact form of this curve is unknown, but knowing that pure capacitive discharges of 0.3 mJ could not ignite the gas mixture^{10,48}, the curve would be expected to rise.

As is shown in the figure, the effect of increasing series resistance for a capacitive circuit is typically to reduce the MIE to a minimum value. The values shown on the figure would be typical for a 7 mm gap, where a (capacitive) MIE of 3 mJ may be measured. Reducing the capacitance would decrease the discharge duration, and any attempt to increase the duration using series resistance would result in combined energies/durations that lay below the capacitive MIE curve. On the other hand the pulse circuit is shown to yield lower MIE values, as transfer of spark energy to the gas mixture occurs under more ideal conditions. Discharges from the capacitive circuit, yielding similar energies/durations as the pulse circuit are seen not to yield ignition due to a less efficient transfer of spark energy to the gas mixture.

This study has not answered the question as to why pure capacitive discharges are less efficient than those produced using a series resistance in the circuit. In the light of the above arguments, this could be due to increased losses in channel expansion for such rapid energy dissipation. Clearly, a thorough investigation of the heat transfer processes using such rapid discharges in inflammable, quiescent gas mixtures is needed to explain this common observation. Also needed is a study relating the rate of energy release in a spark discharge to the thermalisation process in the spark channel.

CONCLUSIONS

The results from the ignition tests using a 2.7 % propane-air mixture showed that:

1. Using controlled spark durations, higher voltages than for a conventional spark discharge could be maintained constant while varying spark energy and rate of energy release in the spark gap. The large difference in measured energies was explained in terms of the different modes of operation of the pulse circuit compared with capacitive circuit.

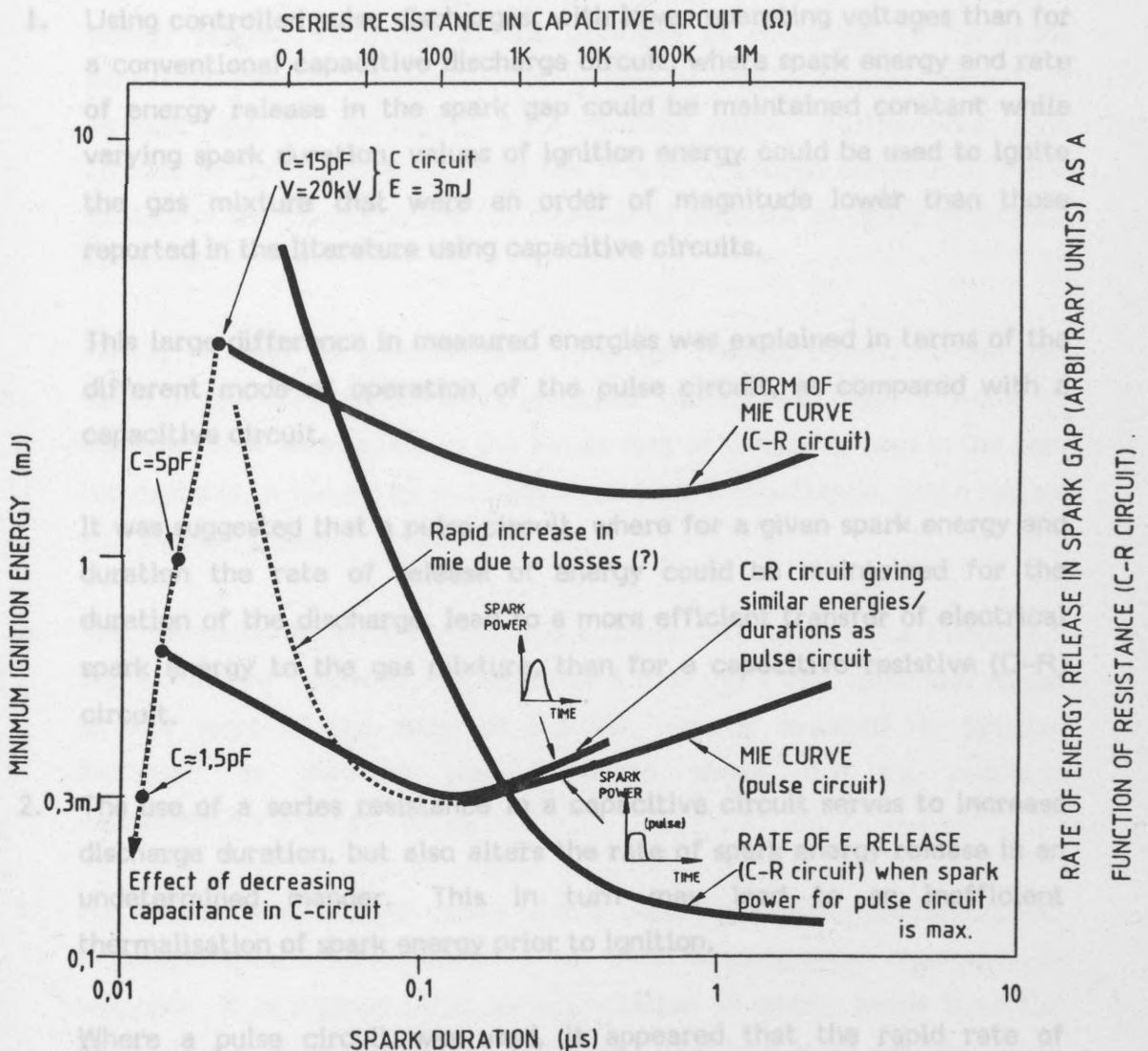


Figure II-15. A comparison of MIE curves for the pulse circuit and a capacitive-resistive circuit using a quiescent 2.7 % propane-air mixture. In the latter case, values are hypothetical, and measured in the spark gap. Also shown are values of capacitance and voltage for a capacitive circuit using a 7 mm gap and flanged electrodes.

6. CONCLUSIONS

The results from the ignition tests using a 2.7 % propane-air mixture showed that:

1. Using controlled pulse discharges, with lower operating voltages than for a conventional capacitive discharge circuit, where spark energy and rate of energy release in the spark gap could be maintained constant while varying spark duration, values of ignition energy could be used to ignite the gas mixture that were an order of magnitude lower than those reported in the literature using capacitive circuits.

This large difference in measured energies was explained in terms of the different mode of operation of the pulse circuit, as compared with a capacitive circuit.

It was suggested that a pulse circuit, where for a given spark energy and duration the rate of release of energy could be maintained for the duration of the discharge, lead to a more efficient transfer of electrical spark energy to the gas mixture, than for a capacitive-resistive (C-R) circuit.

2. The use of a series resistance in a capacitive circuit serves to increase discharge duration, but also alters the rate of spark energy release in an undetermined manner. This in turn may lead to an inefficient thermalisation of spark energy prior to ignition.

Where a pulse circuit was used, it appeared that the rapid rate of discharge of spark energy, in particular within a time shorter than $0.2 \mu\text{s}$ following breakdown, served to increase the efficiency of energy transfer to the spark plasma (kernel). This was made possible by the mode of operation of the spark generator, where energy could be rapidly dissipated in the spark gap, regardless of duration, due to the 'rectangular' form of energy release using low impedance PFN's matched to the spark gap.

This manifested itself in an indirect manner, in the rate of expansion of the spark kernel following discharge. Results indicated that minimum ignition energy values at given durations caused the kernel to expand at a minimum rate, whether in air or the gas mixture. This, it is thought, was instrumental in leading to successful ignition.

3. The results of an independent variation of discharge duration above the quenching distance for the gas mixture, showed a strong dependence of MIE on the manner in which energy was dissipated in the gap with time. It was argued that this aspect of the discharge process was more important than the duration itself, which only reflected the rate of energy release according to the principle of operation of the spark generator circuit. Thus minimum values of MIE measured using C-R circuits have not necessarily been absolute values. Furthermore, such circuits do not directly establish the role of discharge duration as other aspects of the discharge are not maintained constant as series resistance in varied.
Finally, it may be assumed that even the present results reflect the mode of operation of the spark generator circuit used here. It would be expected that an increase in the initial rate of energy release in the gap, for example, achieved by reducing stray circuit inductance, could reduce MIE values further.
4. The quenching distance for this gas mixture was found to lie between 2 and 4 mm. At values of gap width of 4 mm and 7 mm, minimum values of MIE were of the order of 0.3 mJ. Energy required for ignition increased as duration was increased above 0.2 μ s, reaching approximately 2 mJ at 100 μ s.
5. The reason for the higher values of MIE using pure capacitive discharges, as compared to those measured in this work, or using series resistance, is unknown. It is proposed that an examination of energy losses from the spark plasma, using such rapid discharges, may lead to an explanation of this phenomenon. Further work is necessary in this area.
6. The present results indicate that the classic 'thermal' theory of ignition, based on the concept of a 'minimal flame', as originally proposed by Lewis and von Elbe, should be modified to incorporate the thermalisation process of a given spark discharge, produced under given conditions. Until this is done, results using different spark-circuit configurations will appear to conflict with one another.
7. Schlieren studies of the expanding spark kernel in the gas mixture showed that:

- a) The induction time, i.e. the time at which a self-propagating flame was observed, as opposed to the observation of a decaying flame kernel, was approximately 0.8 ms.
- b) In the case of ignition, significantly different kernel development, as compared with that in air, could not be observed below 100 μ s following discharge.
- c) An increase in discharge energy for a given duration, maintaining the shape of the spark power versus time curve, led to an increase in the kernel expansion rate, whether in air or in the gas mixture.

Likewise, an increase in discharge duration for a given spark energy, tended to decrease the kernel expansion rate.

- d) At constant spark energy and duration, kernel expansion rate was approximately constant as gap width was varied, but the distance of the kernel edge from the spark gap centre was larger, at any given time following discharge, for shorter gap widths. This indicated that the spark energy per unit length of the gap was related to the kernel size, as defined in this work.

8. The low values of MIE measured here were obtained using a spark-generation technique that is exclusive to the laboratory. Such a circuit configuration is unlikely to arise in a plant, where accidental spark discharges are usually of a capacitive nature. For safety purposes, therefore, it is suggested that MIE values using the classical C-R circuit are maintained as guidelines.

The results from this work would suggest that an inflammable gas mixture be designated two values of minimum ignition energy. The first would be the sensitivity to ignition by capacitive sparks, and represent the potential hazard of the gas mixture. The second would be an absolute value obtained by laboratory means, as described in this work.

9. Further work is required to study spark thermalisation using capacitive discharge circuits, and to relate these investigations to a unified spark-ignition theory, that would account for observed changes in spark kernel expansion rate as spark energy and duration are varied. Work is also required to study the times involved, during which energy release in the gap is critical in leading to ignition.

CONTENTS

	Page
1. INTRODUCTION AND REVIEW	134
2. OUTLINE OF WORK	138
2.1 Description of tests	138
2.2 Ignition tests using the stabiliser powder	139
2.3 Ignition tests using the three further powders	140
3. ESTABLISHING THE CHOICE OF EQUIPMENT AND TECHNIQUE	141
PART 3: DUST IGNITION STUDIES	
3.1 Choice of test apparatus	141
3.2 Experimental procedure	145
3.3 High-speed camera tests	148
3.4 Optimising dust dispersion and concentration	149
3.4.1 The first dispersion method	149
3.4.2 The second dispersion method	155
3.4.3 Comparing the two dispersion systems	158
3.5 Measurement checks of spark energies	162
3.5.1 Test method	162
3.5.2 Results of tests	163
4. RESULTS OF IGNITION TESTS USING THE STABILISER POWDER	171
4.1 Interpreting the results	171
4.2 Results for the 2 mm gap	171
4.3 Results for the 4 mm gap	175
4.4 Results for the 7 mm gap	175
4.5 Comparing the results for the three gap widths	175
5. SCHLIEREN PHOTOGRAPHS USING THE STABILISER POWDER; TESTS AND RESULTS	178
5.1 Outline of tests	178
5.2 Interpreting the schlieren photographs	181
5.3 Results of the tests	185
5.3.1 Results for the first schlieren series (a)	185
5.3.2 Results for the second and third schlieren series (b) and (c)	187
5.3.3 Results for the fourth schlieren series (d)	191
5.3.4 Results for the fifth schlieren series (e)	194
5.3.5 Results for the sixth schlieren series (f)	196

CONTENTS cont.

CONTENTS	<u>Page</u>
1. INTRODUCTION AND REVIEW	134
2. OUTLINE OF WORK	138
2.1 Description of tests	138
2.2 Ignition tests using the stabiliser powder	139
2.3 Ignition tests using the three further powders	140
3. ESTABLISHING THE CHOICE OF EQUIPMENT AND TECHNIQUES USED IN THE EXPERIMENTS	141
3.1 Choice of test apparatus	141
3.2 Experimental procedure	145
3.3 High-speed camera tests	148
3.4 Optimising dust dispersion and concentration	149
3.4.1 The first dispersion method	149
3.4.2 The second dispersion method	155
3.4.3 Comparing the two dispersion systems	158
3.5 Measurement checks of spark energies	162
3.5.1 Test method	162
3.5.2 Results of tests	163
4. RESULTS OF IGNITION TESTS USING THE STABILISER POWDER	171
4.1 Interpreting the results	171
4.2 Results for the 2 mm gap	171
4.3 Results for the 4 mm gap	173
4.4 Results for the 7 mm gap	175
4.5 Comparing the results for the three gap widths	175
5. SCHLIEREN PHOTOGRAPHS USING THE STABILISER POWDER; TESTS AND RESULTS	178
5.1 Outline of tests	178
5.2 Interpreting the schlieren photographs	181
5.3 Results of the tests	183
5.3.1 Results for the first schlieren series (a)	183
5.3.2 Results for the second and third schlieren series' (b) and (c)	187
5.3.3 Results for the fourth schlieren series (d)	191
5.3.4 Results for the fifth schlieren series (e)	194
5.3.5 Results for the sixth schlieren series (f)	196

CONTENTS cont.

	<u>Page</u>
6. A SIMPLIFIED SPARK IGNITION MODEL FOR DUST CLOUDS	199
6.1 Introduction	199
6.2 The model	199
7. DISCUSSION OF THE SCHLIENEN RESULTS FOR THE STABILISER POWDER BASED ON THE IGNITION MODEL	204
7.1 Discussion of the results of schlieren series a)	204
7.2 Discussion of the results of schlieren series' b) and c)	205
7.3 Discussion of the results of schlieren series d)	211
7.4 Discussion of the results of schlieren series e)	214
7.5 Discussion of the results of schlieren series f)	214
8. RESULTS AND DISCUSSION OF IGNITION TESTS USING THE THREE FURTHER POWDERS	217
8.1 Results for 'Benzanthron'	217
8.2 Results for 'Lycopodium spores'	217
8.3 Results for 'PAN'	219
8.4 Results and discussion of schlieren photographs for the three powders	219
9. INTERPRETATION AND DISCUSSION	225
9.1 Obtaining general relationships between spark energy and duration	225
9.2 A representation of the ignition process	232
9.3 Definition of minimum ignition energy	234
10. FURTHER APPLICATION OF THIS WORK	236
10.1 Why are 'long' sparks more effective ignition sources than 'short' ones?	236
10.2 Suggestions for a laboratory test method	239
11. SUMMARY OF RESULTS AND CONCLUSIONS	242

1. INTRODUCTION AND REVIEW

The observation that minimum spark ignition energy (MIE) for dust clouds is dependent on spark duration dates back to Boyle and Llewellyn⁸ and Line⁹ who observed dependancies as early as the 1950's. More recently, other workers^{3,34,50} have also confirmed effects of duration on MIE. These effects were usually expressed in terms of the reduction in the stored energy in a capacitive test circuit, required to yield ignition, due to the inclusion of a series resistance or inductance. Such effects have also been observed using dust layers⁵¹.

This reduction in stored energy has further implied that the energy discharged in the gap has also been reduced as a consequence. This is because using series resistance, a significant quantity of the stored energy may be lost in this part of the circuit; for series inductance such a loss is not necessarily incurred. This has led to the widespread use of series inductance instead of resistance, as in this case the gap discharge energy is assumed to equal the stored, capacitive circuit energy, as for a 'pure' capacitive discharge^{52,53}. Most workers, at the present time, measure discharged energies to avoid confusion and to enable direct comparisons to be made with other circuits, where discharges may be generated by other means. In either case, however, whether stored, circuit energies are used, or measured, discharged energies, the general observation regarding a decrease in MIE with increase in discharge duration, has been the same. This has meant that pure capacitive discharges of short durations have been found to be the least effective ignition sources.

Most of the interpretations put forward for this have assumed that a significant energy is lost from a 'fast' spark as it forms, as opposed to a 'slow' spark. Eckhoff and Enstad⁴², for example, interpreted this influence in terms of the degree of removal of dust particles by the spark channel expansion wave. Others^{10,40} have simply assumed that shock and radiation losses increase significantly as one approaches very short durations for a given spark energy. The most general interpretation has been made in terms of thermal losses from the spark, both at very short and very long durations. At short durations, one has assumed that a rapid loss of energy occurs to the dust cloud itself, whereas at long durations a certain quantity of the energy may be wasted as ignition takes place. An 'optimum duration' is, therefore,

said to exist, where these losses are minimised. In this case the rate of discharge of spark energy is assumed to match the 'induction times' of single particles in the dust cloud. As processes of volatilisation, carbonisation, and other reaction processes of the dust particles require finite times, so the optimum spark duration has been assumed to directly reflect these times.

Ballal⁵⁴ proposed a theory of spark ignition of dust clouds based upon The exact reasons for 'duration dependences' have not, however, been fully understood and quantified. In addition, some scepticism is still abounding concerning the true implication and value of MIE measurements based upon laboratory tests, where duration has been increased. In particular, it is often argued that where an electrostatic hazard is to be evaluated for a given dust cloud, the reason for observing lower values of (stored) MIE at increased durations, where additional circuit elements have been used, are irrelevant⁵⁴. Other workers^{3,50} feel that a comparative scale of 'ignition sensitivities' may gauge the possible hazard that a dust may present in cloud form. Such sensitivities are based on an optimum spark duration at which the measured MIE (in the discharge) is at a minimum.

The picture is made even more confusing by the wide variation in test circuits used for the evaluation of MIE. Furthermore, it is not always clear whether energies are stored values or those discharged in the spark gap. This has led to values of MIE in the literature varying by orders of magnitude. The U.S. Bureau of Mines⁵⁵, for example, uses a test circuit that is neither 'purely' capacitive, nor optimum for obtaining absolute minimum ignition energies. Other test stations, such as ICI in Great Britain⁵⁴ use a simple capacitive circuit, where MIE is defined in terms of stored circuit energy. A recently-formed German-based working party 'minderzüntenergie', has chosen to standardise the test circuit to include a fixed inductor, so that values of stored circuit energy required to ignite a given dust are typically 1-2 orders of magnitude lower than that from a simple capacitive circuit¹⁴. These values also assume a complete transfer of circuit energy to the spark gap.

Coupled with the various conditions under which MIE is measured and defined, are the further complications of dust dispersion, and the electrode arrangement used to pass the spark. As a result, an integrated and certain discharges, be they 'long', 'short', 'capacitive', 'inductive' etc., yield ignition, while others do not. A study such as this could relate the success of

comprehensive picture of the interaction of an electric spark with a dust cloud is still lacking. Most important, the reasons for observing widely different ignition energies for similar dusts have not been brought together in a unifying theory.

Ballal³⁴ proposed a theory of spark ignition of dust clouds based upon vapour-cloud ignition, and developed terms for predicting MIE and quenching distances, as for a gas mixture. It is unfortunate, however, that a spark discharge was, in this theory, only stated in terms of its energy and duration. It is quite fundamental that following spark breakdown, the ensuing discharge is a measure of the spark's influence on the external circuit. It is therefore quite reasonable to assume that the discharge characteristics, not least the release of energy with time, are of utmost importance in leading to ignition. The influences of these characteristics have not yet been completely investigated for the ignition of dust clouds. Indeed, even the use of the term 'duration' has been replaced, in certain current guidelines¹⁴ by the magnitude of circuit impedance causing the duration increase. Clearly, in order to understand how and why 'duration' influences MIE, one must study the manner in which dust is ignited by a spark when duration is varied. The results of such a study can then be correlated with the observed, or measured, changes in the spark discharge itself.

An underlying conclusion, that quantitatively brings the complete field of observations together, without itself being based on solid experimental evidence, is that the manner in which spark energy is discharged in time and space is vitally important⁵⁶. This is the fundamental starting point for relating the incendivities of various electrostatic discharges, such as brush and corona discharges, to the simple capacitive spark used as a laboratory tool. The basic knowledge that is still lacking, concerns the manner in which such discharges 'thermalise' as functions of their characteristics, and how the hot spark kernel leads to ignition. If this information were available, it would be easier to explain the apparent effects of spark duration on MIE.

Despite various attempts at quantifying discharge characteristics, in terms of the success of ignition, the transition from spark to flame kernel in dust-air mixtures has not been studied. Such observations could help to explain why certain discharges, be they 'long', 'short', 'capacitive', 'inductive' etc., yield ignition, while others do not. A study such as this could relate the success of

ignition to the spark that caused it, and to the initial development of a flame kernel in a given dust-air mixture.

This was the approach used in the present work. Four powders were chosen, one of which was studied in detail, using various configurations of spark gap-width, spark energy and duration. A high-speed schlieren system was also used that produced images of the expanding spark kernel as it developed into a self-propagating flame. Based on the results from these studies, a simple model of the ignition process was proposed, where the effects of spark duration were explained. The three further powders were used to confirm the trends predicted by the model. Finally, some suggestions were made as to why previous effects of duration were observed, and how a laboratory test for MIE could be improved, following the results found in this work.

2. OUTLINE OF WORK

2.1 Description of tests

To initiate investigations on the ignitability of dust clouds, a range of six powders was chosen. This range consisted of the following:

- a) 'Stabiliser powder' (a dye additive)
- b) Aluminium flakes
- c) Sulphur
- d) Benzanthron (a polymer stabiliser)
- e) Lycopodium spores
- f) Polyacrylonitrile

These were chosen as they were all found to ignite using spark energies below 5 mJ. From this range, the first dust was tested comprehensively. This was for two reasons. First and foremost, it was found to disperse easily using the system developed for these tests (see Section 3.1). Secondly, it could be ignited using energies below 1 mJ. This meant that spark energies and durations, used to ignite this dust, were of a similar magnitude as those used to ignite the propane/air mixture (see Part 2). The other advantages of this dust were that it was easy to handle in the laboratory once burnt (i.e. the apparatus was easily cleaned) and was safe and easy to use.

The first group of tests using the stabiliser powder studied the effect of spark duration on minimum spark ignition energy using three gap widths, 2 mm, 4mm and 7 mm. For these tests two dispersion mechanisms were used, as described in Section 3.4. From the results of this first test series, a range of spark energy/duration combinations were picked out, and a series of high-speed schlieren photographs taken for each. These were then analysed in the form of 6 comparisons, in order to show how the initial stages of ignition changed as spark energy and duration and gap width were varied. Comparisons were then made on the basis of a simplified model of spark ignition, presented in Section 6.

From the remaining five powders, three were chosen for a further group of tests. These were Benzanthron, Lycopodium and Polyacrylonitrile (PAN). Aluminium flakes and sulphur were not used, as difficulties were encountered

when dispersing them using the system designed for these tests. In addition, initial schlieren tests were unsuccessful and showed, particularly for aluminium, that a new test method and apparatus would have had to be constructed for meaningful tests to be run.

For the three remaining powders, minimum spark ignition energies were studied, varying spark duration, using one gap width only (4 mm). For these tests the first of the two dispersion systems was used, and fewer ignition points were taken than for the stabiliser powder. These tests served to yield a range of results using the spark generator, that could be directly compared with those for the stabiliser powder. Finally, a series of schlieren photographs was taken using one spark energy/duration combination for each dust. These were then compared with the stabiliser powder using the same ignition spark.

The majority of the work that is described in the following sections deals with the stabiliser powder, which was investigated in more depth than the other three. This was in order to show that

- a) a commercially produced powder could be ignited using electric sparks with energies below 1 mJ
- b) the manner in which the spark was produced could significantly influence the success of ignition, and furthermore, the mechanisms leading to ignition

For these tests, the apparatus and conditions of dispersion were chosen and optimised carefully. This was a tedious process and was not repeated for the remaining three dusts. The results for these dusts, therefore, serve primarily to indicate the effects of varying spark duration on the magnitude of the minimum ignition energies. A comprehensive test run for each dust would have demanded more time than was available for this work.

The descriptions of the four powders are given in Appendix 5.

2.2 Ignition tests using the stabiliser powder

Ignition energy tests using this dust were modelled on the previous gas-ignition tests, except that preliminary measurements were necessary to

establish optimum conditions for dispersion. Two dispersion methods were chosen in order to compare ignition data using two states of dust-cloud movement at the moment of ignition. These were termed the 'single' and 'double' dispersion methods. Exhaustive tests were first carried out using both methods to establish optimum values of ignition delay(s), mass of dispersed dust and dispersion pressure (see Section 3.4). Ten random "check-point" combinations of spark energy and duration were then chosen for each of three gap widths, 2mm, 4mm and 7mm, and ignition probabilities compared using both methods of dispersion. As will be shown, these methods yielded similar results. It was important to establish this before comprehensive tests were run, so that the analysis of the schlieren photographs, taken using the single dispersion method, could be related to both sets of tests.

The remaining tests were split up into two experimental runs (i.e., using each dispersion method) consisting of three series' of tests, where electrode gap width took values of 2mm, 4mm and 7mm. At each gap width spark energy was varied over durations from 0.1 μ s to \sim 100 μ s.

According to the observed trends in the ignition tests, various combinations of spark duration and energy and gap width were chosen and schlieren sequences recorded for the first 80ms following spark discharge. Most of these photographs were taken using the single dispersion method. The schlieren system used is presented in Appendix 4.

2.3

Ignition tests using the three further powders

These tests utilised just one method of dust dispersion (the so-called 'single' dispersion method) and followed the same experimental procedure as was used for the stabiliser powder. The number of test points was reduced, and a single gap width of 4 mm used.

Settings of dispersion pressure and ignition delay were fixed, and the mass of each dust varied until the energy required for ignition was at a minimum at a given spark duration. Spark energy was then varied over durations from 0.1 μ s to \sim 100 μ s for each dust, using a 4 mm gap width.

3. ESTABLISHING THE CHOICE OF EQUIPMENT AND TECHNIQUES USED IN THE EXPERIMENTS

3.1 Choice of test apparatus

Preliminary tests began in a standard Hartmann-type apparatus, whereby dust was dispersed in an upward direction towards the spark gap. Despite the relative ease with which the dust could be dispersed, high speed photographs of the gap cross-section (the 5 cm² area used for schlieren studies in subsequent tests) revealed a wide variation in the distribution of dust around the gap at fixed points in time. This variation was observed regardless of dispersion pressure and quantity of dispersed dust. This phenomenon was thought to be primarily related to the large distance between dispersion cup and electrodes (~ 15 cm), but was observed even when a new tube was constructed and distance varied from 5 to 25 cm. Clearly a new, improved method was necessarily for dispersing the dust into the gap area. For this reason, the standard Hartmann-type dispersion system was abandoned, and an alternative system constructed.

As it was important to reproduce the conditions existing around the ignition area, and indeed through the burnable cloud, as closely as possible between shots, a new dispersion system was designed. This dispersed powder from above and consisted of a curved dispersion tube similar in principle to that found on a Godbert-Greenwald furnace. This is shown in Figure III-1. The dispersion nozzle was positioned some 25 mm above the spark gap by fastening the tube to the explosion vessel as depicted in Figure III-2. The vessel was derived from the standard Hartmann tube, having the same diameter but being reduced in length from 40 cm to 27 cm. The complete dispersion/ignition arrangement is shown in Figure III-3.

The vessel was mounted at its base by a sliding ferrule, that was clamped fast into a fixed cup, shown in Figure III-2. The vessel was held to the ferrule using two O-rings, and this complete assembly mounted in the cup. Its exact height in the cup was adjustable using a securing screw passing through the cup wall. The cup itself was mounted on a steel base, which closed the vessel end at its base and which was clamped to a floor-standing optical bench. All components of the schlieren system used in the tests, including the camera, laser source and schlieren lenses (see Appendix 4) were mounted on the bench

Figure III-1. Dispersion tube assembly for dust-cloud ignition experiments.

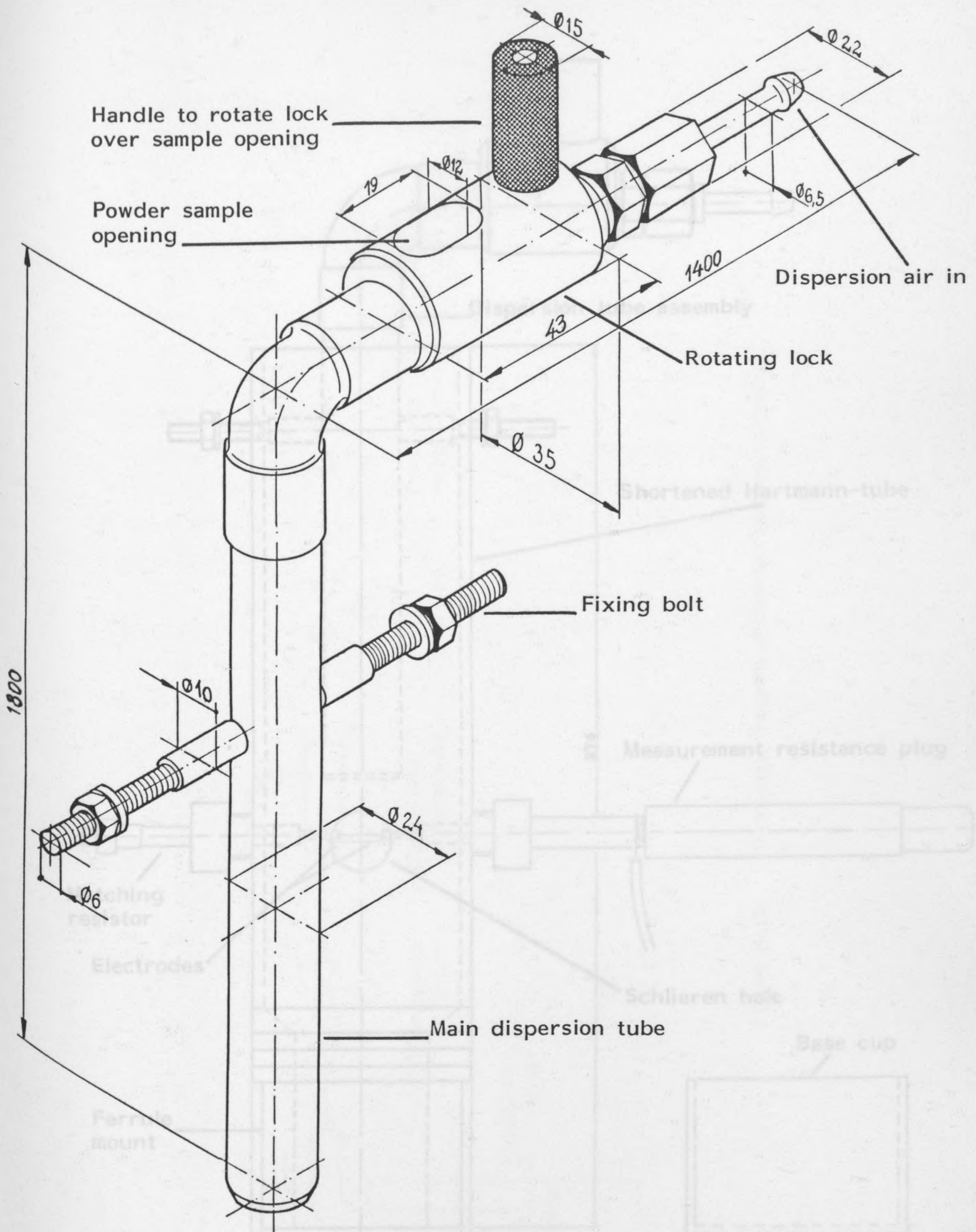


Figure III-1. Dispersion tube assembly for dust-cloud ignition experiments.

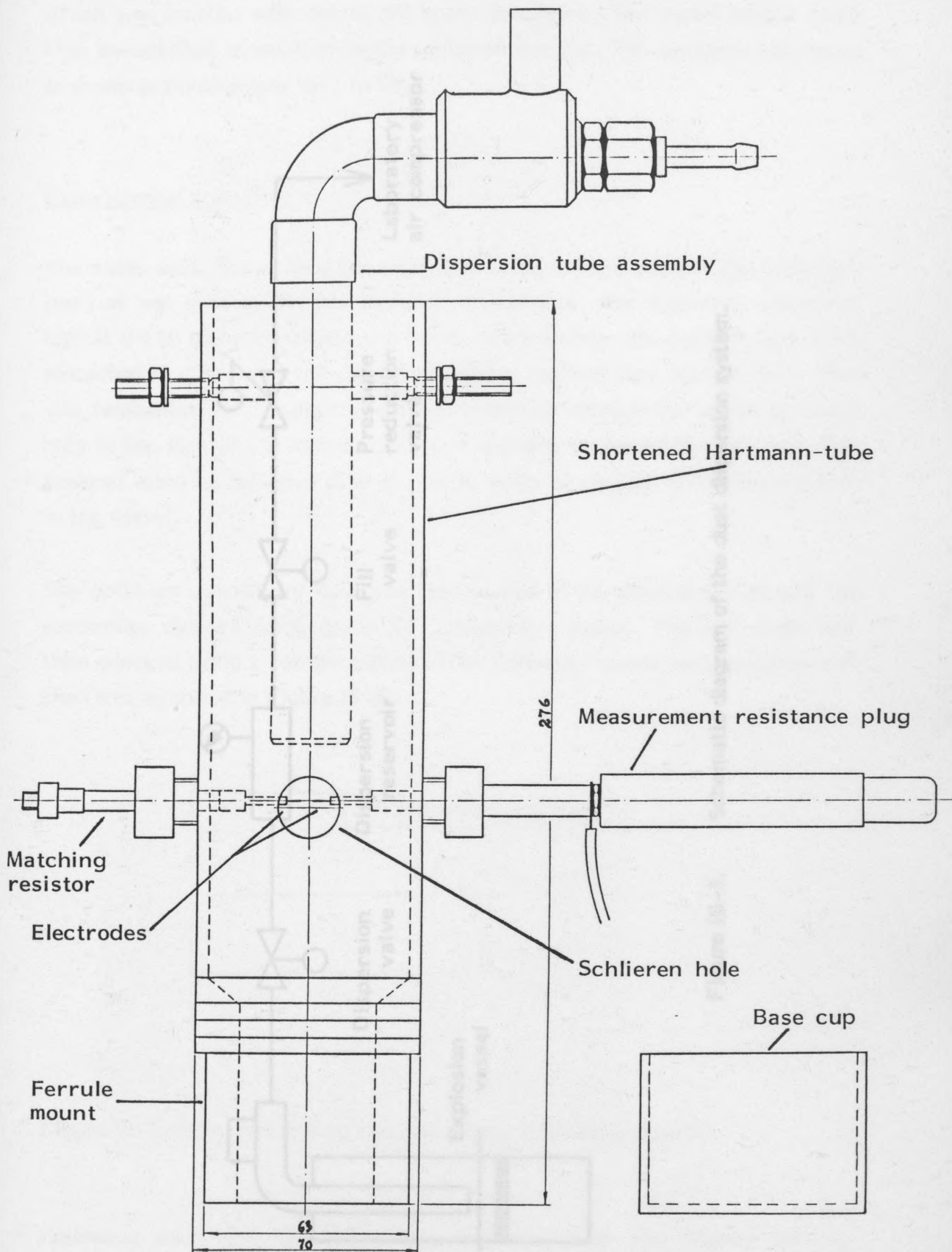


Figure III-2. Cross-section of dust cloud ignition apparatus.

which was located adjacent to the spark generator. The vessel height could thus be adjusted in relation to the schlieren system. The complete apparatus is shown in Photographs III-1 to III-3.

Experimental procedure

The tests using dusts were tried on the wire electrode pair (the 'standard gap') as was used in the gas-ignition experiments. For a spark circuit (PFN) components and gap width, spark energy and duration were first measured in situ using the standard dispersion method (see Section 3.3). This was facilitated by using the probe-tip through the 1/8 in. diameter hole in the side of the ignition vessel. Following measurement the hole was covered using an adhesive plastic film in order to contain the dust in the vessel.

The optimum quantity of dust was then placed in the dispersion reservoir, the electrodes cleaned using grade 32 carborundum paper. The gap width was then checked using a feeler caliper. The following timing-test sequence was then run, as shown in Figure III-4.

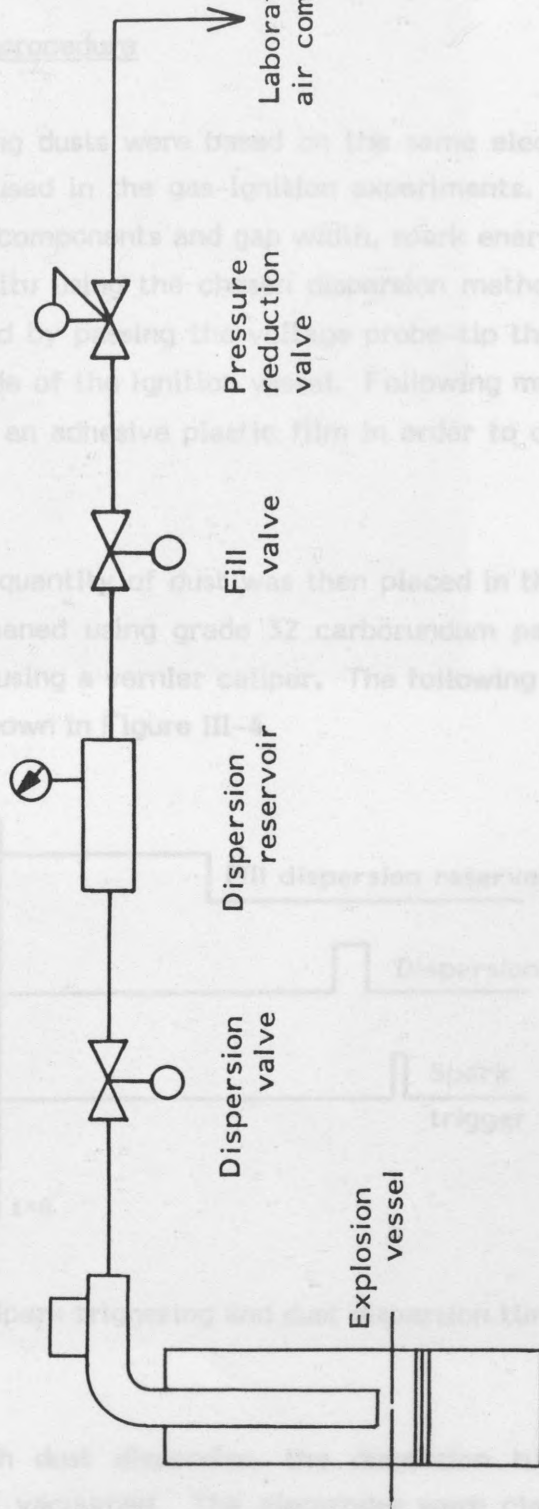


Figure III-3. Schematic diagram of the dust dispersion system.

Figure III-4. Spark timing and dispersion timing diagram.

Following each dust dispersion test the vessel was flushed and the ignition vessel evacuated. The electrodes were cleaned once again and the gap-width checked. Two spark tests were made using each spark energy/duration combination.

which was located adjacent to the spark generator. The vessel height could thus be adjusted in relation to the schlieren system. The complete apparatus is shown in Photographs III-1 to III-4.

3.2 Experimental procedure

The tests using dusts were based on the same electrode pair (the 'standard gap') as was used in the gas-ignition experiments. For a specific choice of circuit (PFN) components and gap width, spark energy and duration were first measured in situ using the chosen dispersion method (see Section 3.5). This was facilitated by passing the voltage probe-tip through the schlieren-beam hole in the side of the ignition vessel. Following measurement, this hole was covered using an adhesive plastic film in order to contain the dispersed dust in the vessel.

The optimum quantity of dust was then placed in the dispersion tube and the electrodes cleaned using grade 32 carborundum paper. The gap width was then checked using a vernier caliper. The following timing-test sequence was then run, as shown in Figure III-4.

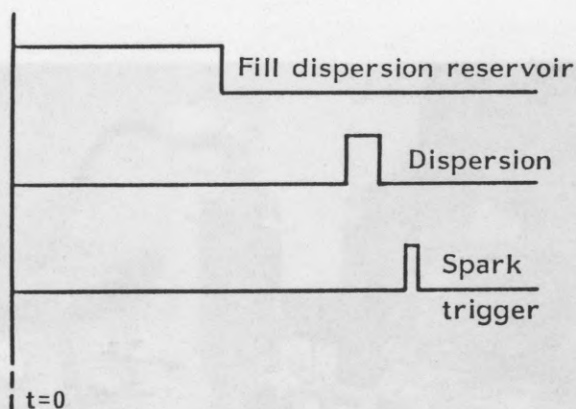
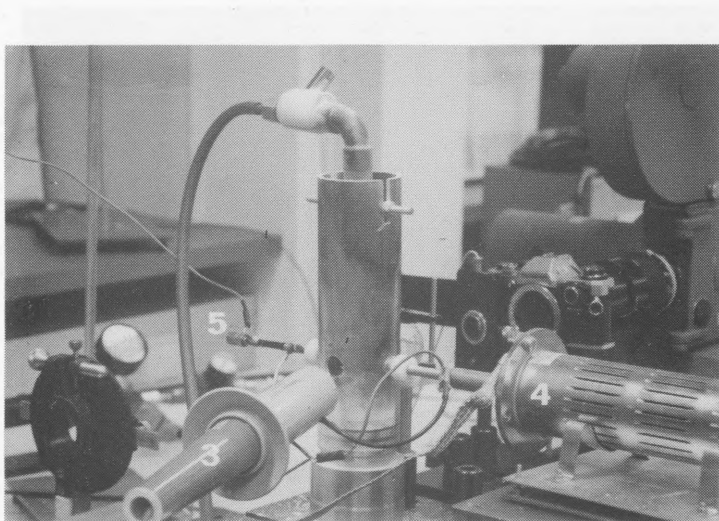


Figure III-4. Spark triggering and dust dispersion timing diagram.

Following each dust dispersion, the dispersion tube was flushed and the ignition vessel vacuumed. The electrodes were cleaned once again and the gap-width checked. Ten ignition tests were made using each spark energy/duration combination.



Photograph III-1.

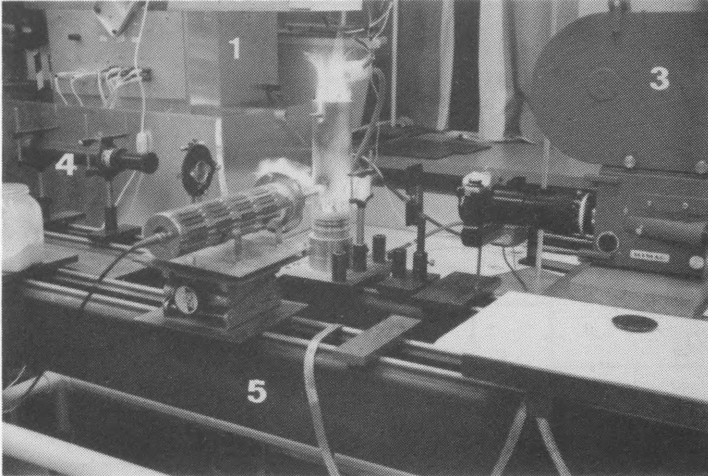


Photograph III-2.

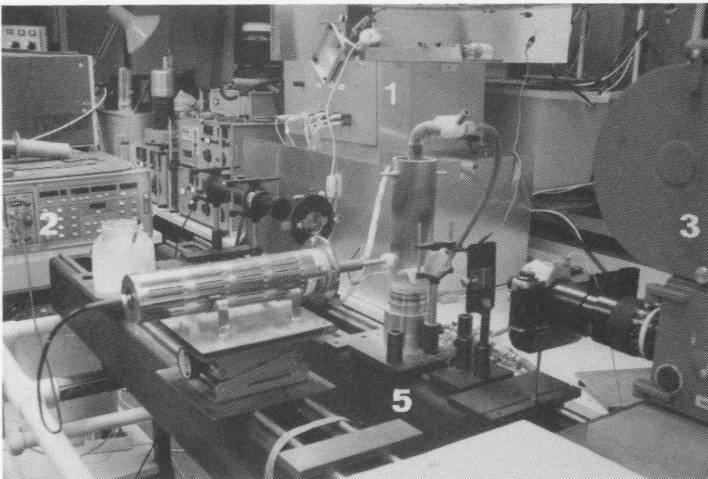
Photographs III-1 and III-2.

Two views of the dust cloud ignition apparatus (1) and dust dispersion tube (2). Also shown is (3) the high voltage measurement probe, (4) the current measuring resistor, and (5) the high voltage resistor connection.

For high-speed photography, the schlieren apparatus has been assembled in a special extensive fitting arrangement as seen. This included the high speed camera and electronic system in addition to the laser and spark triggering. The complete fitting arrangement is as shown below in Figure III-3.



Photograph III-3.



Photograph III-4.

Photographs III-3 and III-4.

Layout of experimental apparatus, showing (1) the thyatron housing, (2) the digitiser, (3) the high-speed camera, (4) the laser source, and (5) the optical bench and remaining schlieren components.

For ignition tests using the schlieren apparatus (see Appendix 4) a more extensive timing programme was run. This switched the high speed camera and electronic shutter in addition to dispersion and spark triggering. The complete timing sequence is as shown below in Figure III-5.

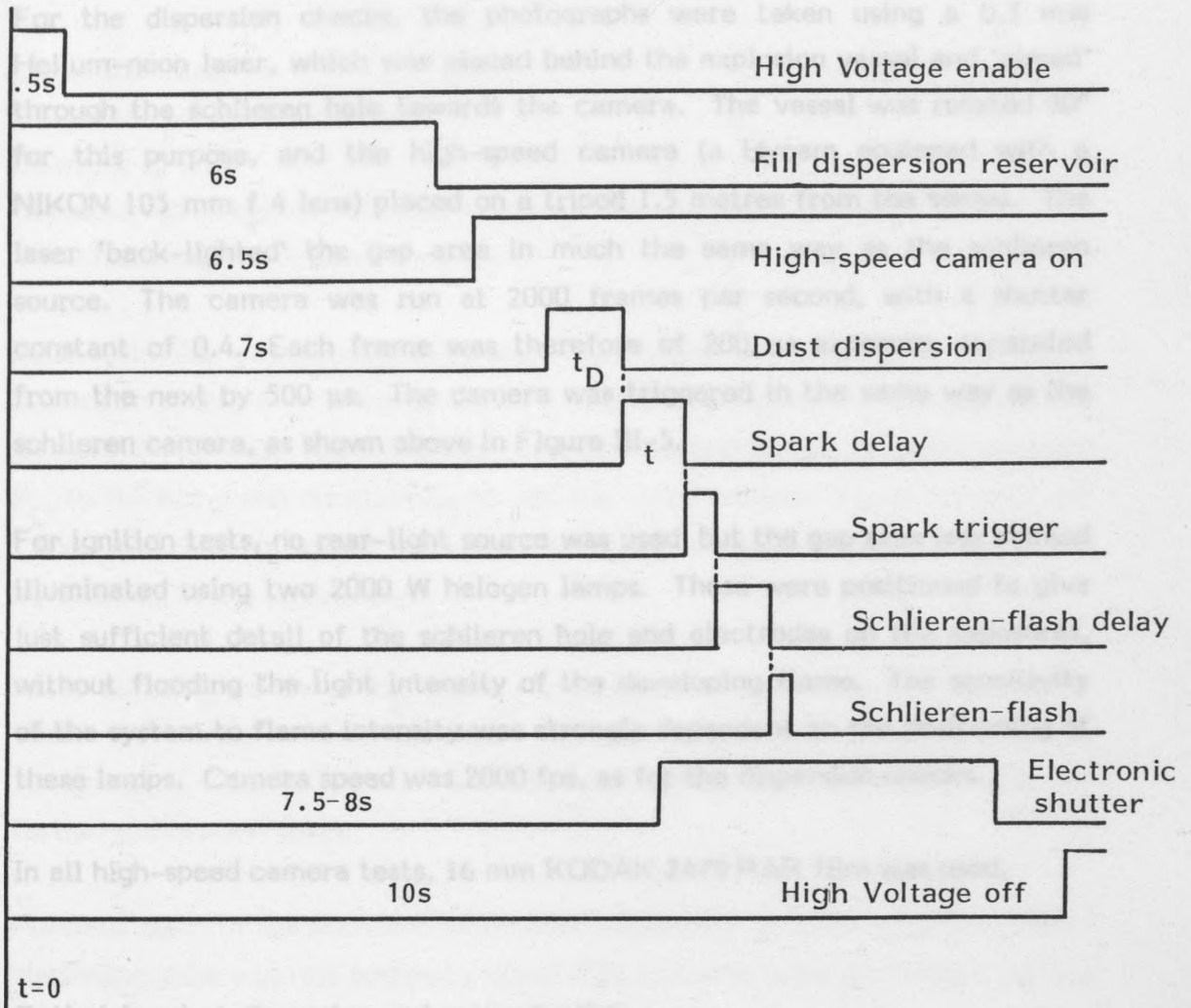


Figure III-5. Complete timing diagram showing schlieren camera triggering.

3.3 High-speed camera tests

In addition to the high-speed schlieren apparatus, described in Appendix 4, a second high-speed camera was used for filming dust dispersion and ignition. Its primary use was to aid the selection of a suitable moment of ignition, by identifying the time at which dust was present in the gap area. It also showed the distribution of dust particle agglomerates using the two dispersion

methods. Furthermore, it served as a means of verifying the point of ignition relative to the spark gap. This was particularly useful for the second dispersion method, where ignition was observed downstream of the electrodes (see Section 6).

The following variables were then optimised in order to reproduce the dust distribution as well as possible:
For the dispersion checks, the photographs were taken using a 0.3 mW Helium-neon laser, which was placed behind the explosion vessel and 'aimed' through the schlieren hole towards the camera. The vessel was rotated 90° for this purpose, and the high-speed camera (a Hycam equipped with a NIKON 105 mm f 4 lens) placed on a tripod 1.5 metres from the vessel. The laser 'back-lighted' the gap area in much the same way as the schlieren source. The camera was run at 2000 frames per second, with a shutter constant of 0.4. Each frame was therefore of 200 μ s exposure, separated from the next by 500 μ s. The camera was triggered in the same way as the schlieren camera, as shown above in Figure III-5.

By reducing pressure P_D to 0.4 bar g and duration t_D to 100 ms, more uniform dispersion resulted. For ignition tests, no rear-light source was used, but the gap area was instead illuminated using two 2000 W halogen lamps. These were positioned to give just sufficient detail of the schlieren hole and electrodes on the exposures, without flooding the light intensity of the developing flame. The sensitivity of the system to flame intensity was strongly dependent on the positioning of these lamps. Camera speed was 2000 fps, as for the dispersion checks.

In all high-speed camera tests, 16 mm KODAK 2479 RAR film was used.

3.4 Optimising dust dispersion and concentration

Previous tests in the standard minimum ignition test at CMI using a modified Hartmann tube and this powder showed that ignitions were obtainable using a as the lower limit of the test equipment. This was obtained using concentrations in the range
For each of the dispersion methods, a comprehensive series of tests was run in order to establish optimum conditions for ignition. These tests were for the stabiliser powder only, for which an in-depth analysis of spark ignition was made. Tests using the three other powders utilised the same conditions of dispersion as for the stabiliser, except that the powder mass was optimised in each case.

3.4.1 The first dispersion method

As a flame reaching the vessel walls, as this was the limited extent of the dust cloud.
To disperse the dust, a known quantity was first placed in the tube opening which was then sealed off. A pulse of compressed air at known overpressure

was then applied to the dispersion tube inlet which raised the powder into the vertical section. Dust was then allowed to fall along the tube length down to the gap area. A very localised cloud was formed around the gap area using this method. The following variables were then optimised in order to reproduce the dust distribution as well as possible:

Dispersion pressure	P_D	(bar g)
Dispersion pressure duration	t_D	(ms)
Quantity of dust	m	(mg)
Distance from dispersion nozzle to electrodes	d	(mm)
Time from dispersion pulse to spark	t	(ms)

First estimates of reproducibility were made using the naked eye. Too high a dispersion pressure (~ 1 bar g) led to a visible eddying around the gap area as was previously observed using the Hartmann apparatus. By reducing pressure P_D to 0.4 bar g and duration t_D to 100 ms, more uniform dispersion resulted. Care was taken to isolate the vessel as well as possible from ventilation and air streams in the laboratory.

After locating values of P_D and t_D in this way, d was adjusted. Very little visible difference in cloud formation was noticed when varying d from 15 to 30 mm so a value of 25 mm was arbitrarily chosen as an initial value for further calibration tests.

Previous tests in the standard minimum ignition test at CMI using a modified Hartmann tube and this powder showed that ignitions were obtainable using a spark energy as low as 4.5 mJ, which was the lower limit of the test equipment. This was obtained using concentrations in the range 200–800 g.m.⁻³. Using a 4.5 mJ spark-ignition source, tests were repeated in this vessel using various quantities of dust to find a suitable mass value m . Values that gave high ignition probabilities tended to be higher than those in the Hartmann apparatus, probably due to a large quantity of dust remaining in the vertical dispersion tube. The concept of 'concentration' i.e. mass per unit volume could not be accurately used here because of the tendency of the dispersed dust to remain in the bottom half of the vessel, around the gap area. 'Ignition' was defined as a flame reaching the vessel walls, as this was the limited extent of the dust cloud.

Starting values of the above variables were fixed as follows:

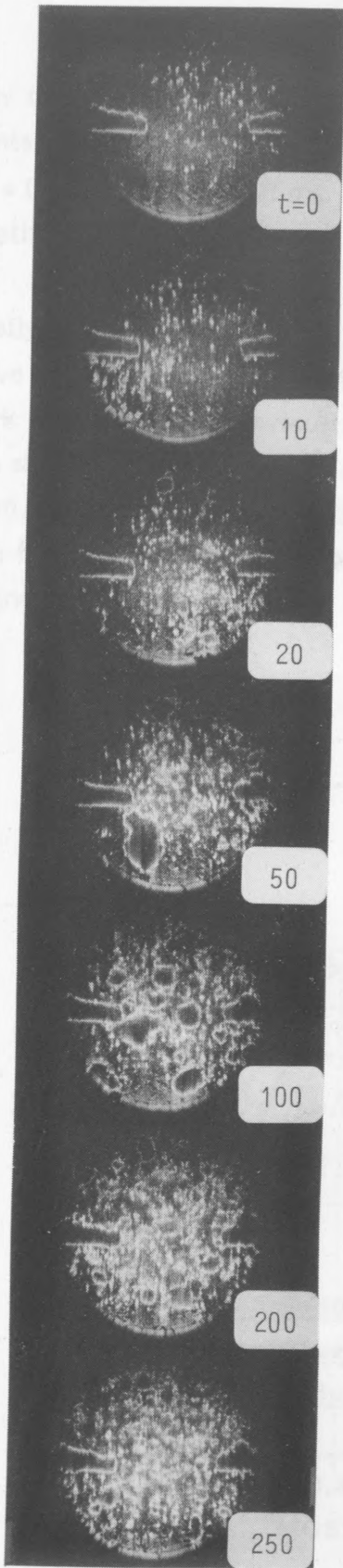
P_D	=	0.4 bar g
t_D	=	100 ms
d	=	25 mm
t	=	250 ms
Electrode gap spacing	=	4 mm

't' was chosen as being the time after dispersion when dust was clearly visible and well distributed in the gap area, as indicated by high-speed photographs of the dispersion. These are shown in series' III-5 and III-6. The first series shows the distribution of dust in the gap area with time, using the above variables. The diameter of each circular image is ~ 8 mm, the spark gap being set at 4 mm. These results show agglomerated particles falling into the gap area. After ~ 50 ms large agglomerates (of ~ 2 mm diameter) appeared, and at 250 ms particles and agglomerates were well distributed in the gap area. This time was therefore chosen for the initial value of t.

The second series follows the movement of one large agglomerate 20 ms after dispersion, in order to establish a rough estimate of particle velocity. From the scale of the photographs this was estimated to lie at $\sim 1 \text{ ms}^{-1}$. The last seven photographs in this series show how this agglomerate is broken up following impact with one of the electrodes.

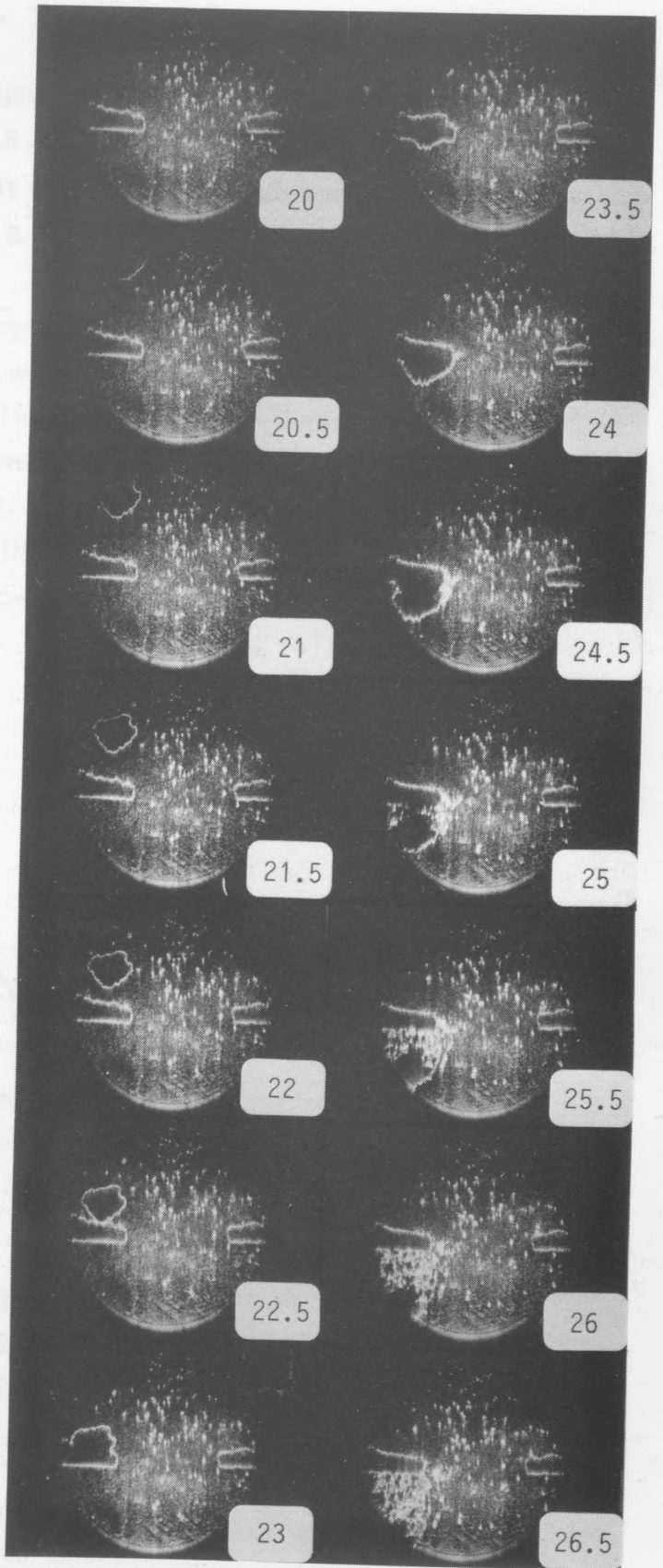
A comprehensive test series was then run using five mass values and reducing spark energies to 2 mJ and 1.1 mJ. Ignition probability was measured from 10 tests for each mass value. These tests resulted in the curves shown in Figure III-6.

This figure shows that a reduction in spark energy tended to reduce the ignition probability over the range 0.2 g to 1 g. By taking highest ignition probabilities for each spark energy in the figure, an optimum mass value was obtained. This was equal to 0.4 g. Tests were then repeated using the second spark (2 mJ/16 μ s), i.e. where a probability of 1 of ignition was obtained at one mass value only (0.4 g). For this spark, combinations of dispersion pressure and duration were varied using the mass value above and two other values, one at 0.5 g, one at 0.3 g. Then tests using each mass value were carried out. This gave the curves in Figures III-7 - III-10.



Photograph series III-5.

High-speed photographs of dust-distribution in the spark gap. Times are in milliseconds, following dispersion.



Photographs series III-6.

High-speed photographs showing the movement of an agglomerate in the gap, 20 ms after dispersion.

Only one curve in these figures gave an ignition probability of 1 at two mass points, with a probability of 0.8 at the third. This was the combination $P_D = 0.4 \text{ bar g}$, $t_D = 200 \text{ ms}$. This combination was chosen for further tests, together with a mass value of 0.4 g.

Finally, a test series was run to optimise ignition delay time, t . Keeping the above variables fixed, delay time was varied from 100 ms to 750 ms for the 3 spark energies used previously. This resulted in the curves in Figure III-11. This showed the highest ignition probability of 1 for the two sparks (2 mJ and 4.5 mJ) at a delay time of 500 ms. This was also the value of delay time that gave the highest ignition probability for the weaker 1.1 mJ spark. The final settings were therefore set as follows:

$P_D = 0.4 \text{ bar g}$
 $t_D = 200 \text{ ms}$
 $m = 0.4 \text{ g}$
 $t = 500 \text{ ms}$

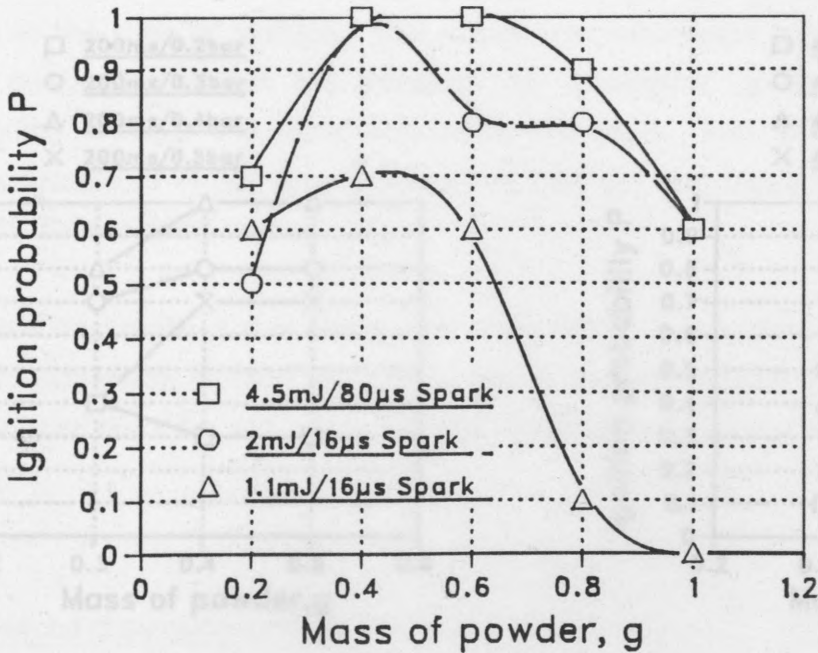


Figure III-6. Ignition probabilities using three sparks as a function of mass of dispersed powder.

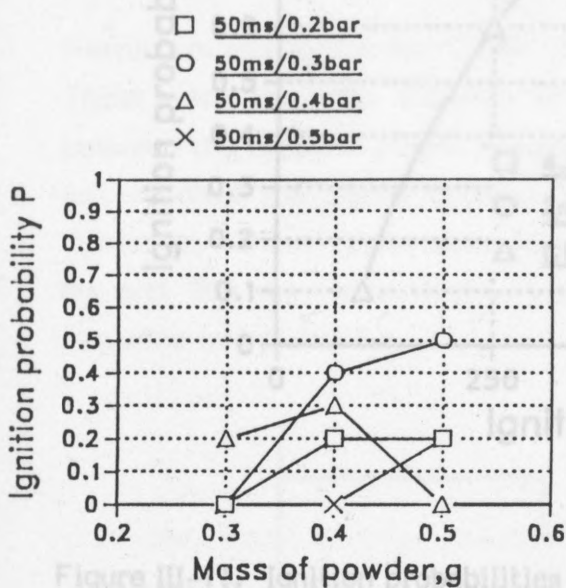


Figure III-7.

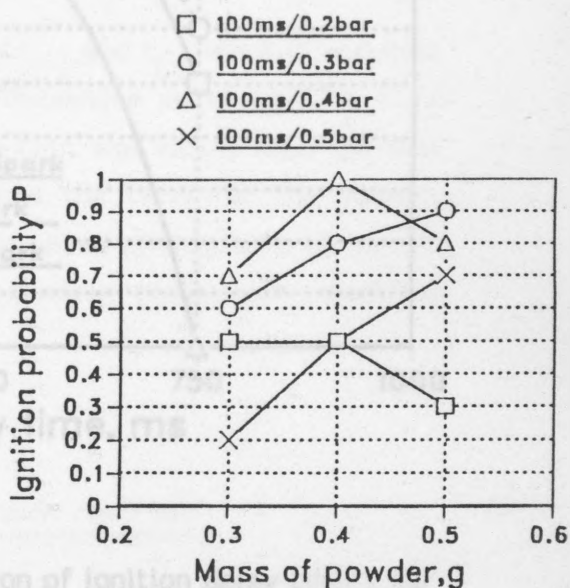


Figure III-8.

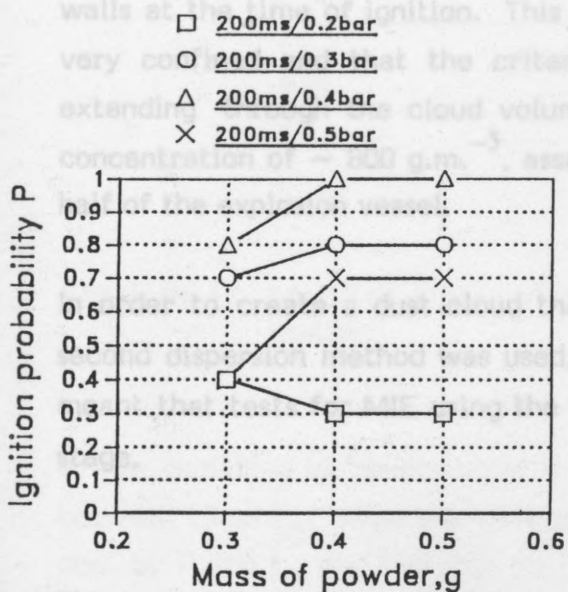


Figure III-9.

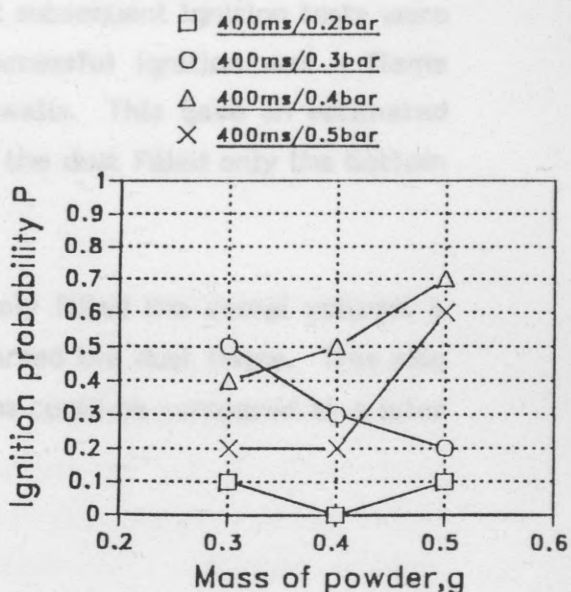


Figure III-10.

Figures III-7-III-10.

Ignition probabilities as a function of three values of mass of dispersed powder, for one spark (2 mJ/16 μ s). Each figure shows four combinations of dispersion time t_D and dispersion pressure P_D .

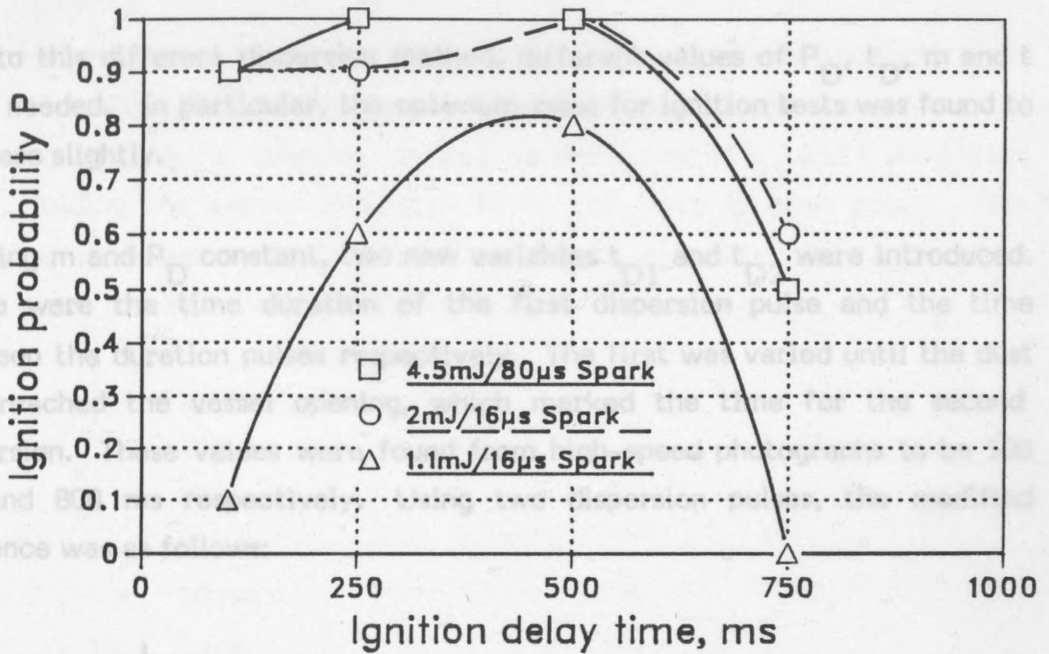


Figure III-11. Ignition probabilities as a function of ignition delay time t for three sparks.

This method of dispersion created a cloud that barely extended to the vessel walls at the time of ignition. This meant that subsequent ignition tests were very confined and that the criterion for successful ignition was a flame extending through the cloud volume to the walls. This gave an estimated concentration of $\sim 800 \text{ g.m.}^{-3}$, assuming that the dust filled only the bottom half of the explosion vessel.

In order to create a dust cloud that completely filled the vessel volume, a second dispersion method was used, that dispersed the dust twice. This also meant that tests for MIE using the two systems could be compared at a later stage.

3.4.2 The second dispersion method

The second method, used a second, short dispersion pulse just prior to ignition, which served to a) re-disperse the 'lost' dust in the vertical dispersion tube and b) cause particles to move through the gap in a fixed (downward) direction at the moment of ignition. The first pulse was longer than that used previously in order to completely fill the vessel volume with dispersed dust.

Due to this different dispersion method, different values of P_D , t_D , m and t were needed. In particular, the optimum mass for ignition tests was found to increase slightly. Keeping m and P_D constant, two new variables t_{D1} and t_{D2} were introduced. These were the time duration of the first dispersion pulse and the time between the duration pulses respectively. The first was varied until the dust just reached the vessel opening, which marked the time for the second dispersion. These values were found from high-speed photographs to be 500 ms and 800 ms respectively. Using two dispersion pulses, the modified sequence was as follows:

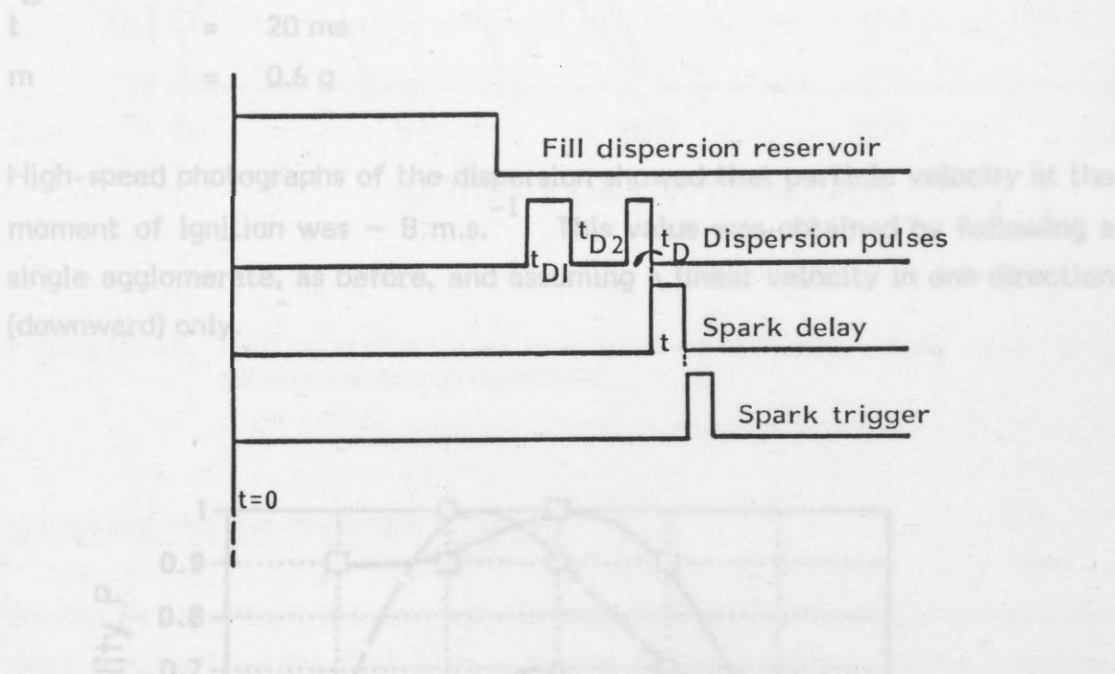


Figure III-12. Modified timing diagram for the second (double) dispersion method.

It now remained to 're-optimize' m , the mass of powder, and the relationship between t and t_D . Mass was optimized using a similar method to the previous one, by fixing t_D and t at 100 ms and 50 ms respectively and taking 20 tests at each spark energy of 1 mJ, 2 mJ and 4.5 mJ for 5 mass points. Figure III-13 shows the curves that resulted. Taking the peak values of probability as before, a mass of 0.4-0.6 g was obtained. Three further points at 0.5 g were therefore taken, which gave probabilities of 0.9, 0.9 and 0.6 for each of the three spark energies 4.5 mJ, 2 mJ and 1.1 mJ. A value of 0.6 g

Figure III-13. Ignition probability using three sparks as a function of mass of dispersed powder.

was therefore chosen for further tests. This gave an estimated concentration value of $\sim 600 \text{ g.m.}^{-3}$, assuming the whole tube was filled. Using the 2 mJ spark and keeping P_D constant, various combinations of t_D and t were then tried, yielding the curves in Figure III-14 (10 tests at each point). This showed an optimum combination of 80 ms for t_D and 20 ms for t . The final values were, therefore, set as follows:

- P_D = 0.3 bar g
- t_{D1} = 500 ms
- t_{D2} = 800 ms
- t_D = 80 ms
- t = 20 ms
- m = 0.6 g

High-speed photographs of the dispersion showed that particle velocity at the moment of ignition was $\sim 8 \text{ m.s.}^{-1}$. This value was obtained by following a single agglomerate, as before, and assuming a linear velocity in one direction (downward) only.

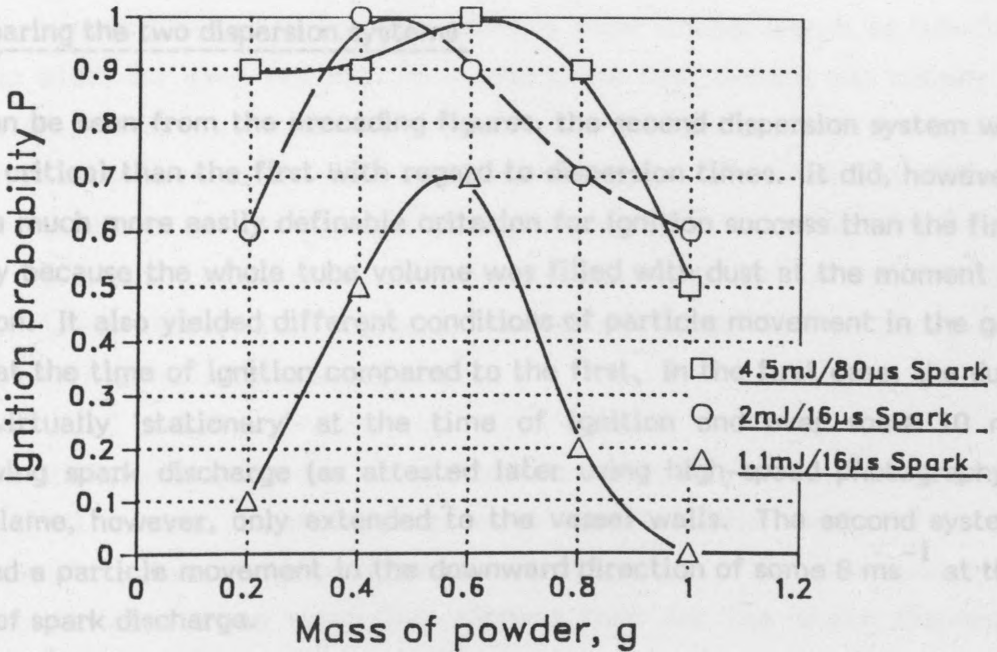


Figure III-13. Ignition probabilities using three sparks as a function of mass of dispersed powder.

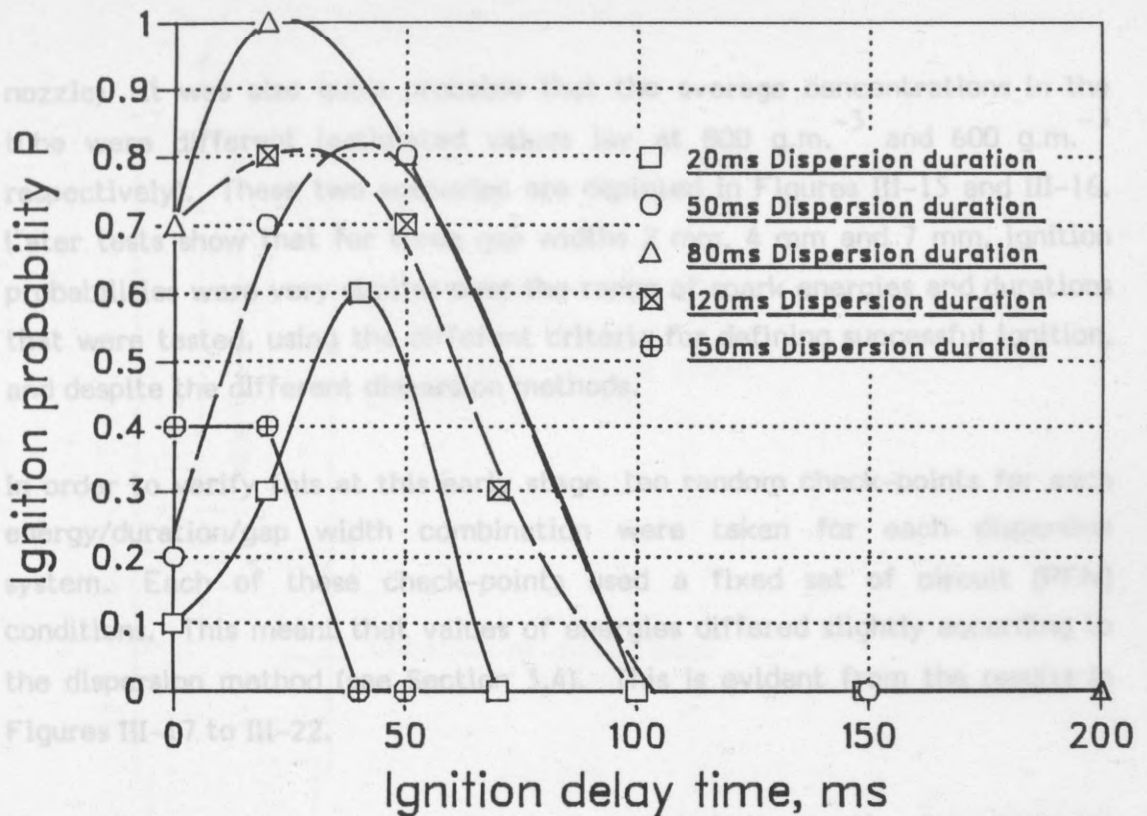


Figure III-14. Ignition probabilities as a function of ignition delay time t and second dispersion duration t_D .

3.4.3 Comparing the two dispersion systems

As can be seen from the preceding figures, the second dispersion system was more critical than the first with regard to dispersion times. It did, however, give a much more easily definable criterion for ignition success than the first simply because the whole tube volume was filled with dust at the moment of ignition. It also yielded different conditions of particle movement in the gap area at the time of ignition compared to the first. In the first case, the dust was virtually 'stationary' at the time of ignition and over some 10 ms following spark discharge (as attested later using high-speed photography). The flame, however, only extended to the vessel walls. The second system yielded a particle movement in the downward direction of some 8 ms^{-1} at the time of spark discharge.

The two discharge systems provided a means of comparison between measured ignition energies in a virtually 'steady-state' cloud (in the gap area) and a cloud where ignition was initiated in a moving dust/air stream at a fixed velocity (determined by P_D and the diameter of the dispersion

nozzle). It was also quite probable that the average concentrations in the tube were different (estimated values lay at 800 g.m.^{-3} and 600 g.m.^{-3} respectively). These two scenarios are depicted in Figures III-15 and III-16. Later tests show that for three gap widths 2 mm, 4 mm and 7 mm, ignition probabilities were very similar over the range of spark energies and durations that were tested, using the different criteria for defining successful ignition, and despite the different dispersion methods.

In order to verify this at this early stage, ten random check-points for each energy/duration/gap width combination were taken for each dispersion system. Each of these check-points used a fixed set of circuit (PFN) conditions. This meant that values of energies differed slightly according to the dispersion method (see Section 3.4). This is evident from the results in Figures III-17 to III-22.

These figures show a very close agreement between the two systems, allowing for the slightly higher measured energies using the double-dispersion system. The lower ignition probabilities that were observed using the second system might be expected on the grounds of conductive heat loss from the spark kernel as it is blown downstream with the particles. This is discussed in Sections 4 and 5, where tests for each system are compared. In absolute terms, however, values of ignition energies show similar trends as functions of gap width for each system. As a result, the first system was chosen for schlieren studies where the spark kernel resided in the gap area and ignition occurred at a fixed point relative to the electrodes. This made the schlieren studies easier, as preliminary schlieren tests using the second system showed slight variations in the point of ignition. This often led to the schlieren source (laser) having to be moved along the tube length to find the ignition point, which could be a laborious process.

On the other hand, where the cloud filled the vessel volume, (using the second system), it became faster and easier to repeat ignition tests. This was because of the ease of defining the success of ignition. For this reason, more test-points were taken using this method than for the single dispersion method.

Figure III-16. Distribution of dust particles using the second dispersion method.

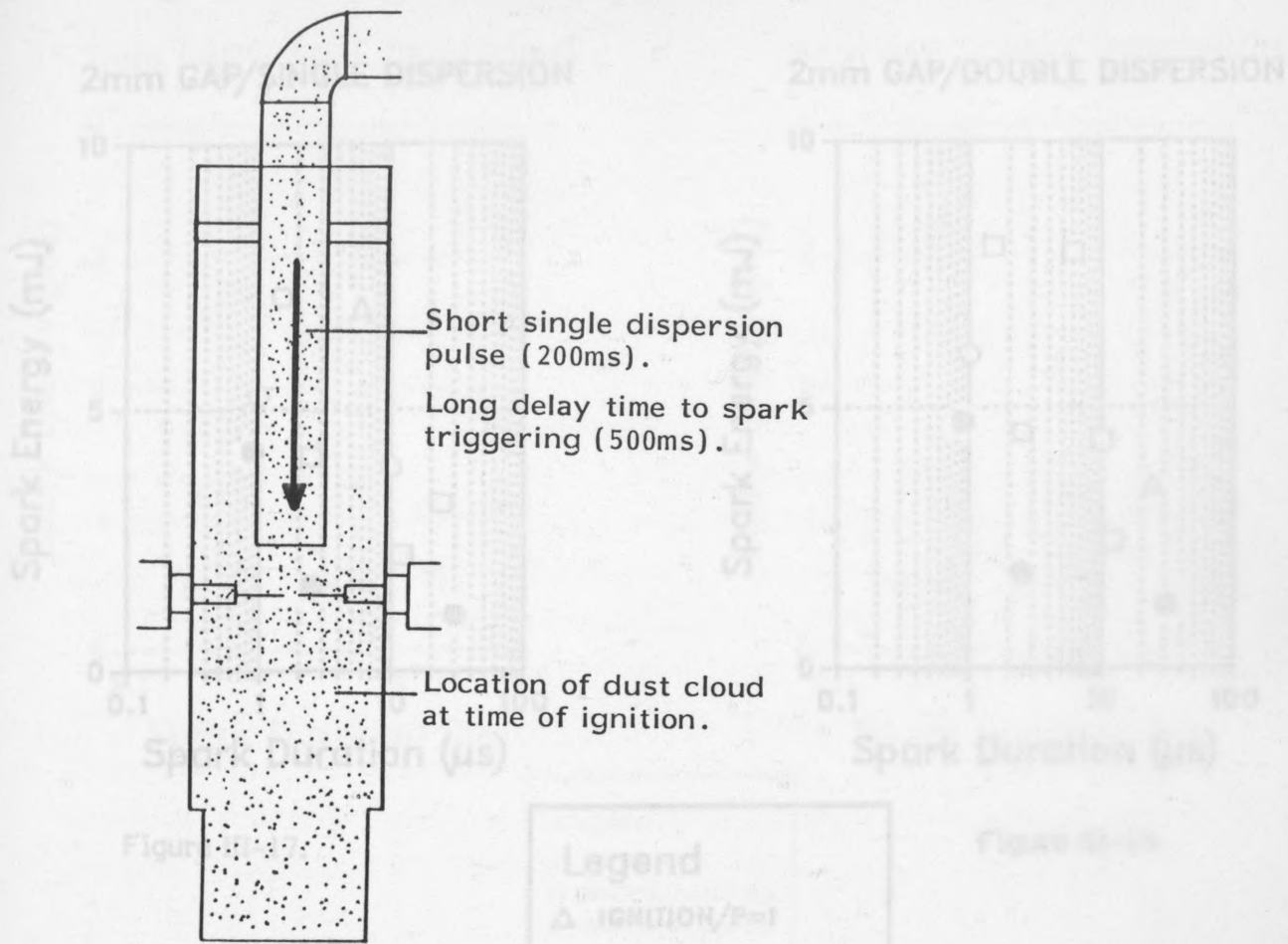


Figure III-15. Distribution of dust particles using the first dispersion method.

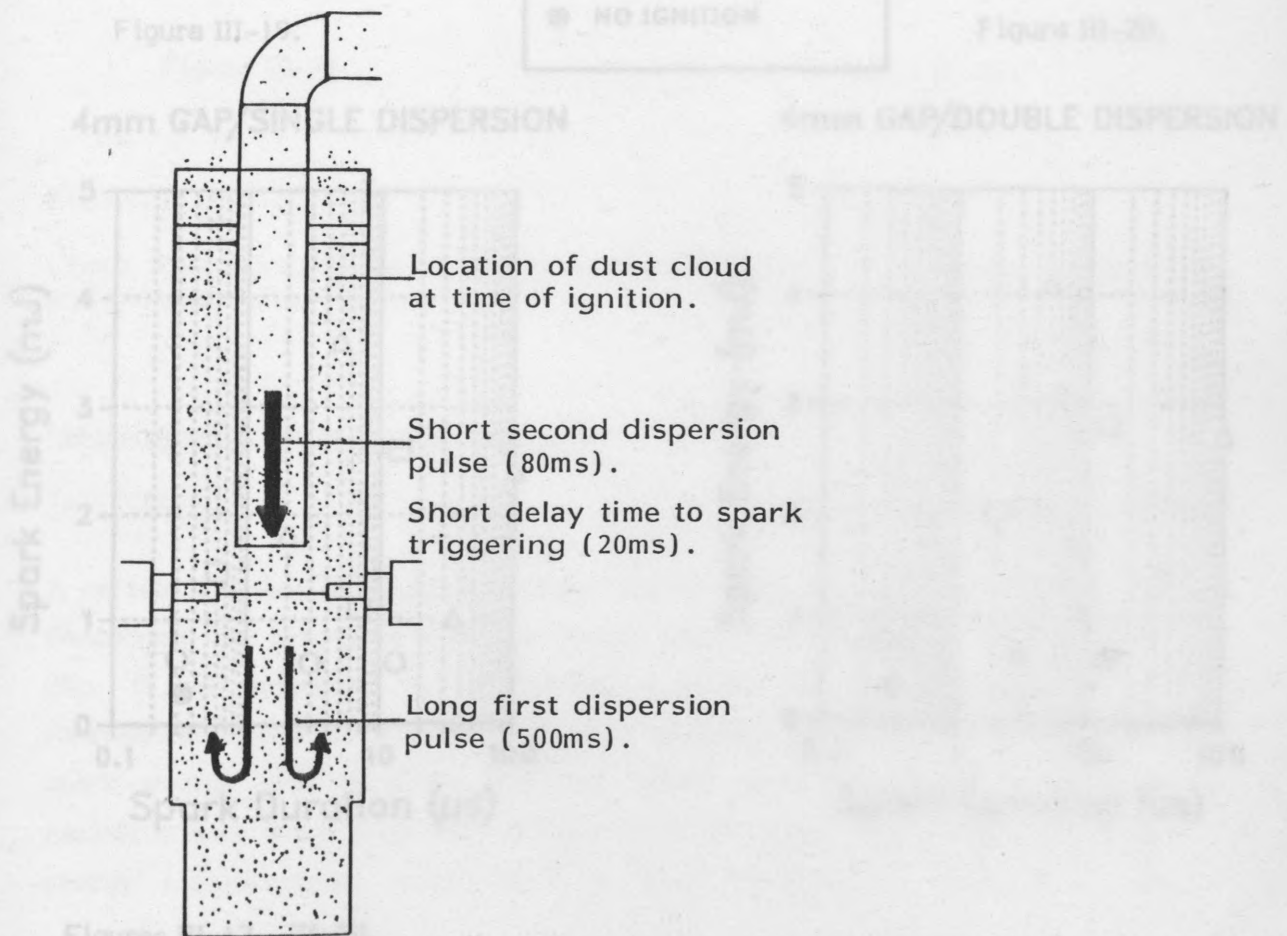


Figure III-16. Distribution of dust particles using the second dispersion method.

2mm GAP/SINGLE DISPERSION

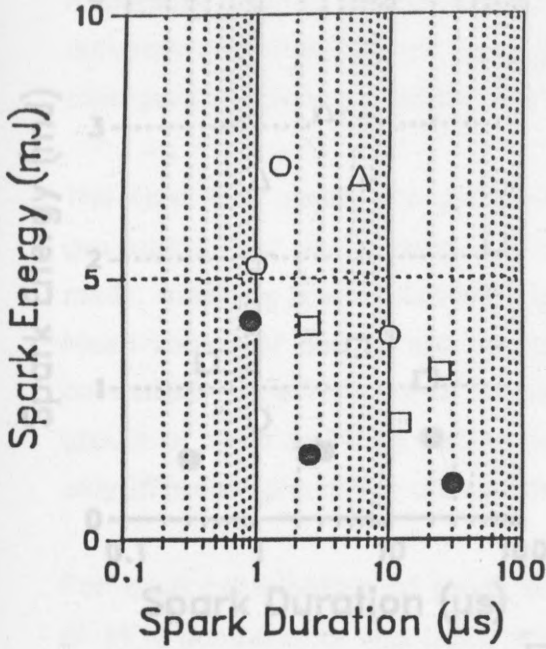


Figure III-17.

2mm GAP/DOUBLE DISPERSION

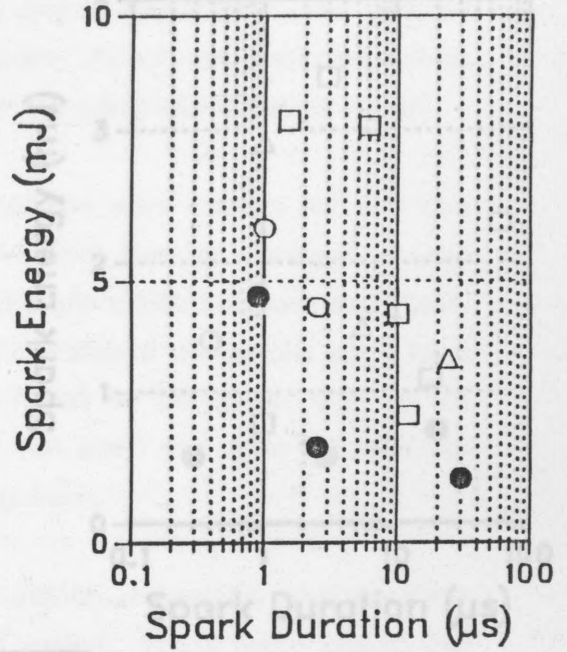


Figure III-18.

Figure III-19.

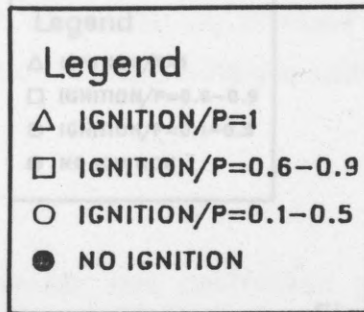
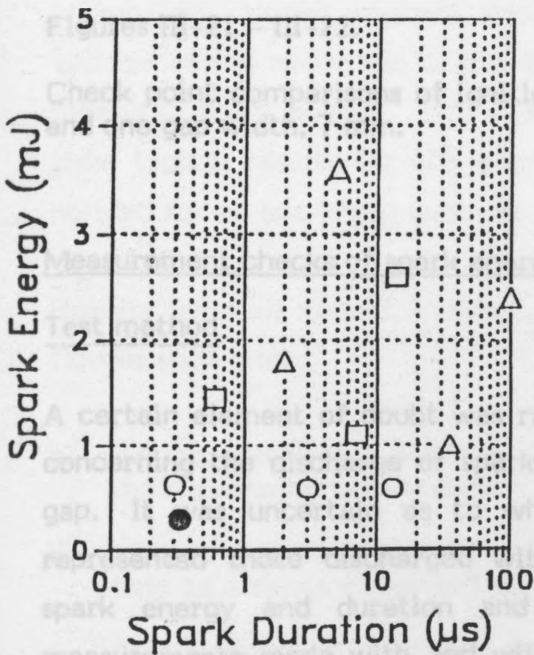
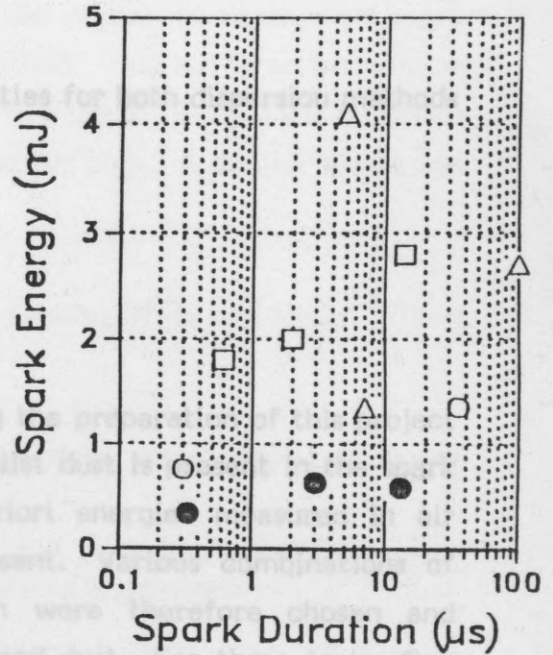


Figure III-20.

4mm GAP/SINGLE DISPERSION



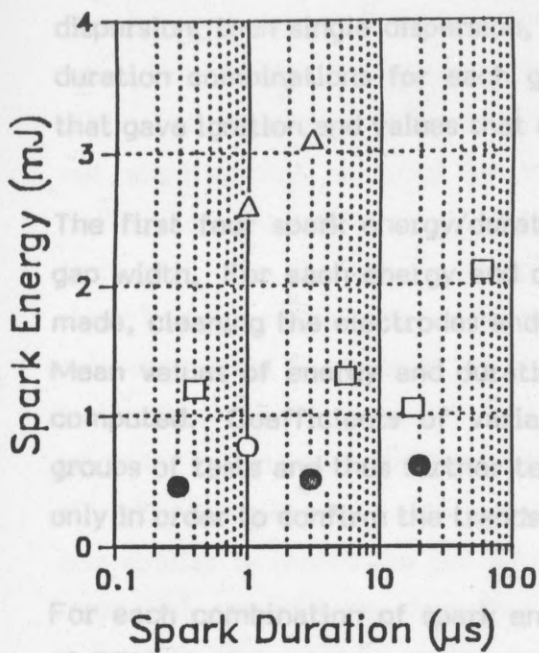
4mm GAP/DOUBLE DISPERSION



Figures III-17 - III-20.

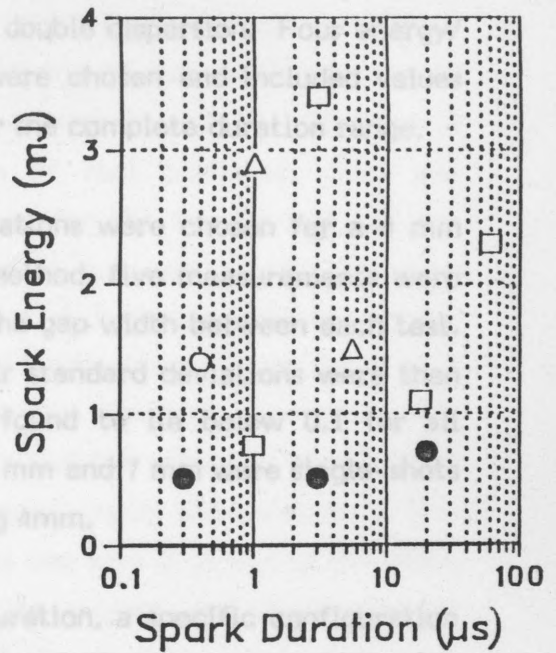
Check-point comparisons of ignition probabilities for both dispersion methods and two gap widths, 2 mm and 4 mm.

7mm GAP/SINGLE DISPERSION

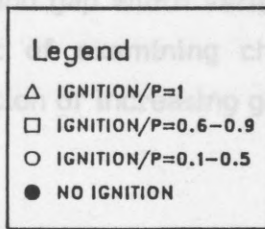


Spark Duration (μs)

7mm GAP/DOUBLE DISPERSION



Spark Duration (μs)



3.5.2 Results of tests

Results showed that spark duration was unaffected by either dispersion method and was constant in all measurements. Spark energy remained unaltered, as would be expected from the principle of operation of the circuit.

Figure III-21.

Figure III-22.

Figures III-21 - III-22.

Check point comparisons of ignition probabilities for both dispersion methods and one gap width, 7 mm.

show typical results for one spark and gap width only. A similar trend was noticed for all spark/gap width combinations.

3.5 Measurement checks of spark energies

3.5.1 Test method

A certain element of doubt was raised during the preparation of this project concerning the discharge of spark energy whilst dust is present in the spark gap. It was uncertain as to whether a priori energies measured in air represented those discharged with dust present. Various combinations of spark energy and duration and gap width were therefore chosen and measurements made with and without dispersed dust. For these tests, five energy measurements were made at each combination using first, no

dispersion, then single dispersion, and finally double dispersion. Four energy/duration combinations for each gap width were chosen and included values that gave ignition and values that did not over the complete duration range.

The first four spark energy/duration combinations were chosen for a 4 mm gap width. For each energy and dispersion method, five measurements were made, cleaning the electrodes and checking the gap width between each test. Mean values of energy and duration and their standard deviations were then computed. Coefficients of variation were found to lie below 0.1 for all groups of tests and thus further tests using 2 mm and 7 mm were single-shots only in order to confirm the trends found using 4mm.

For each combination of spark energy and duration, a specific configuration of PFN components was used, and gap width varied. These tests, therefore, served a second purpose, that of examining changes of measured spark energies and durations as a function of increasing gap width.

3.5.2 Results of tests

Results showed that spark duration was unaffected by either dispersion method and was constant in all measurements. Spark current also remained unaltered, as would be expected from the principle of operation of the circuit (a constant current source). Measurements did reveal, however, that spark voltage varied according to the dispersion method. This led to an increase in measured spark energy. This is exemplified in Figures III-23 - III-25, which show typical results for one spark and gap width only. A similar trend was noticed for all spark/gap width combinations.

Results from all measurements are shown in Figures III-26 and III-27. These figures show that:

- a) An increase in gap width increased the discharge energy whilst discharge duration remained constant.
- b) Discharge energy tended to increase as dust particles were introduced, first as a single dispersion and then as a double dispersion.
- c) This increase in discharge energy was observed whether or not ignition ensued (see ignition successes (IG) marked on the figures).

The increase in spark energy for each test point became most significant when the double dispersion method was used and at one point approached 40%. This was found to be due to the air movement through the gap and was not significantly affected by the presence of dust particles. This was confirmed by (double) dispersing using no dust for the four sparks and the 4mm gap. No changes in energy/duration were apparent. It thus became clear that air movement in the gap at the time of discharge influenced spark measurements. In physical terms, this energy increase manifested itself as a gap-voltage increase, quite possibly due to the localised increase in air pressure in the spark-discharge channel. This had the effect of 'bending' or elongating the spark channel, as was also found by Ballal and Lefebvre⁵. This was similar to increasing gap width, which, as was also observed in the tests, increased gap-voltage, and thus energy. Gap current remained constant regardless of gap width or dispersion. This is already apparent from Figures III-23 - III-25 and is also shown in Figures III-28 - III-30 where gap width is varied for one set of circuit conditions. Similar results were shown in Figures I-48 - I-50 in Part 1.

Changes in discharged energy using a single dispersion were seen to be small in comparison to those observed using a double dispersion. This was undoubtedly due to the long delay time (~ 0.5 s) between dispersion and spark-triggering in the single dispersion case, meaning that air velocity in the gap was slow (well below 1 m.s.^{-1}). On the other hand, previous observations had shown that air velocity at the time of spark triggering using double dispersion was $\sim 8 \text{ m.s.}^{-1}$. This was clearly enough to increase pressure in the gap by a significant factor to cause a large increase in gap voltage.

It is also interesting to note that even using the longest spark ($\sim 100 \mu\text{s}$) no effect of the ensuing explosion on the discharge was noticeable. The reason for this becomes apparent when studying schlieren photographs of the ignition process (see Section 6).

The observed increase in discharged spark energy as the dispersion method was altered, meant that the experimental procedure had to include an in situ spark energy measurement, using each of the dispersion methods. This is described in Section 3.2.

Above spark
measured using
double dispersion
method (spark
energy = 1.37 mJ).

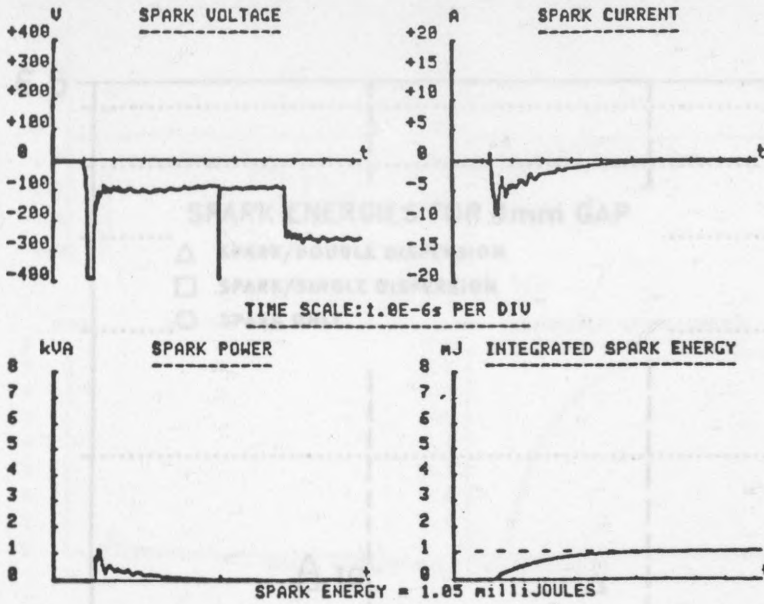


Figure III-23.
1.05 mJ spark
measured in air.

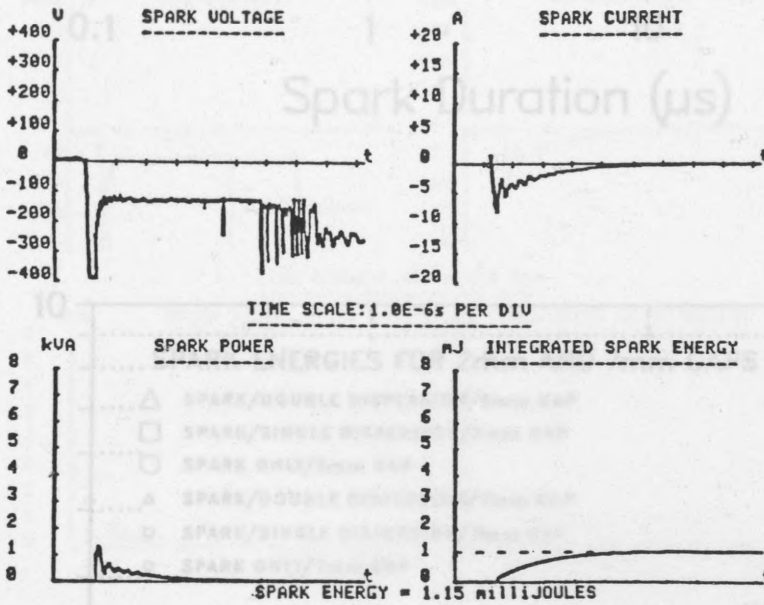


Figure III-24.
Above spark
measured using
single dispersion
method (spark
energy = 1.15 mJ).

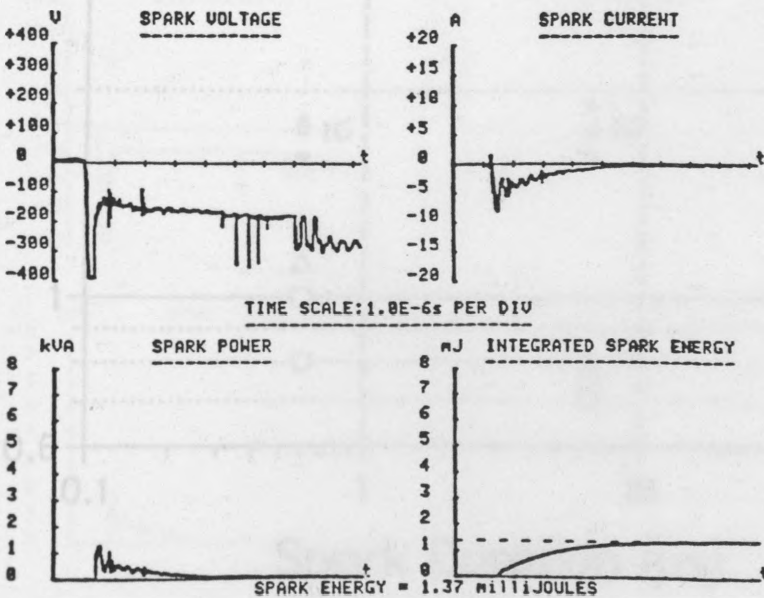


Figure III-25.
Above spark
measured using
double dispersion
method (spark
energy = 1.37 mJ).

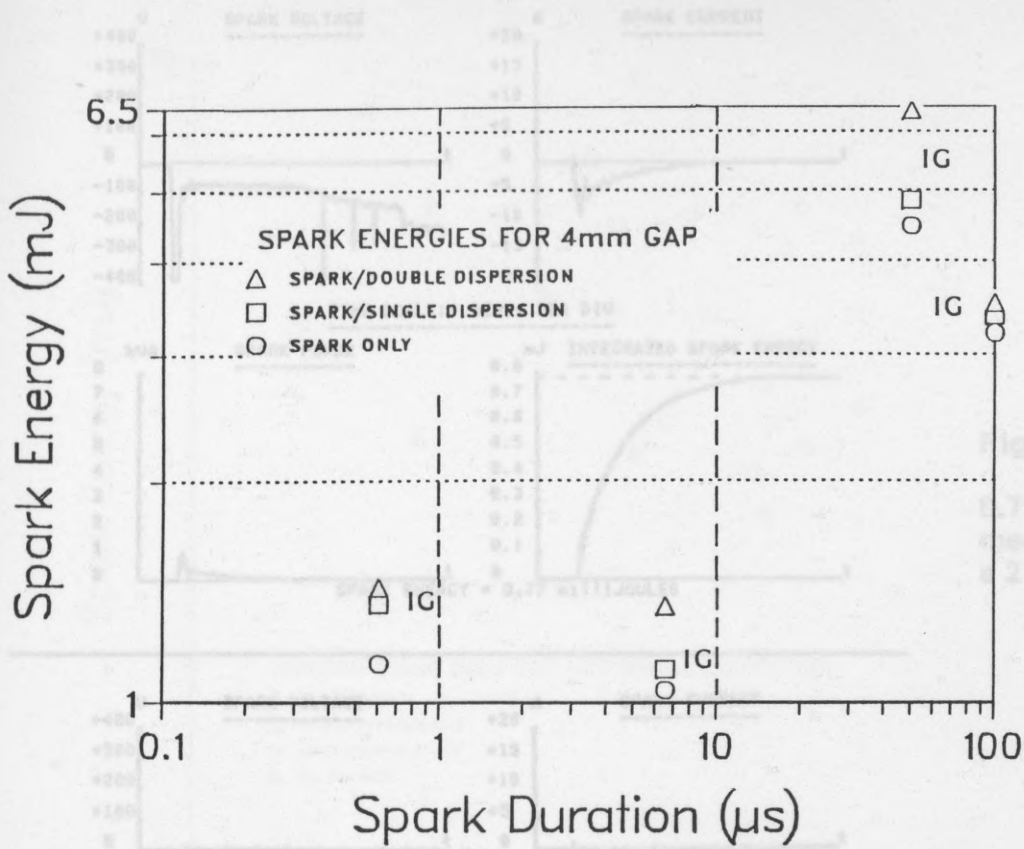


Figure III-26.

Measured spark energies and durations as a function of dispersion for a 4 mm gap.

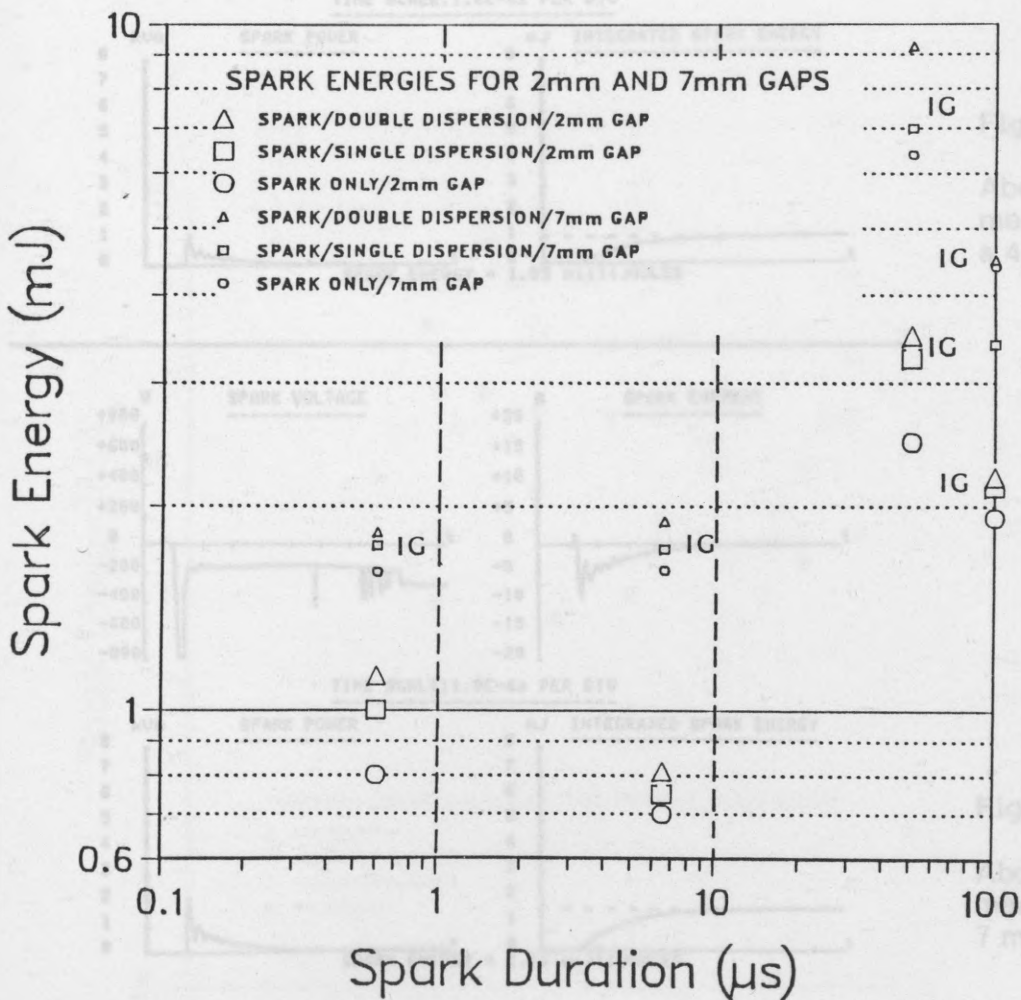


Figure III-27.

Measured spark energies and durations as a function of dispersion for 2 mm and 7 mm gaps.

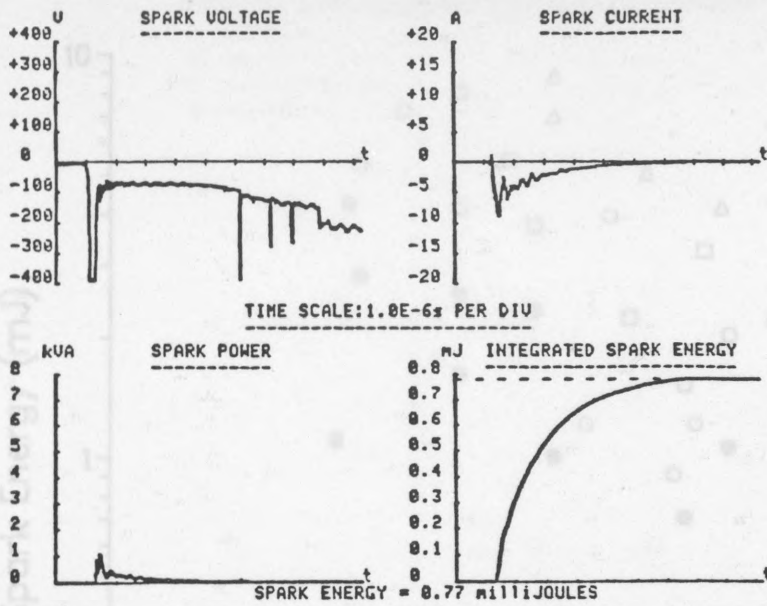


Figure III-28.

0.77 mJ spark measured for a 2 mm gap.

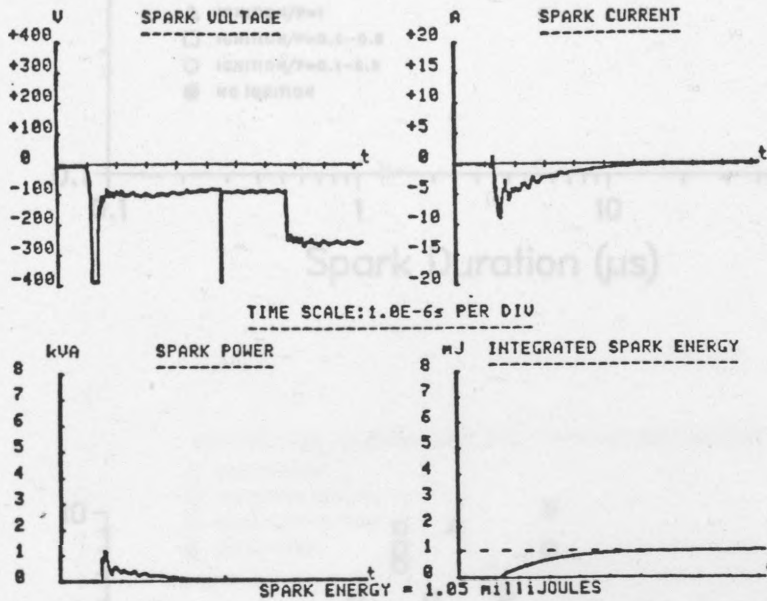


Figure III-29.

Above spark measured for a 4 mm gap.

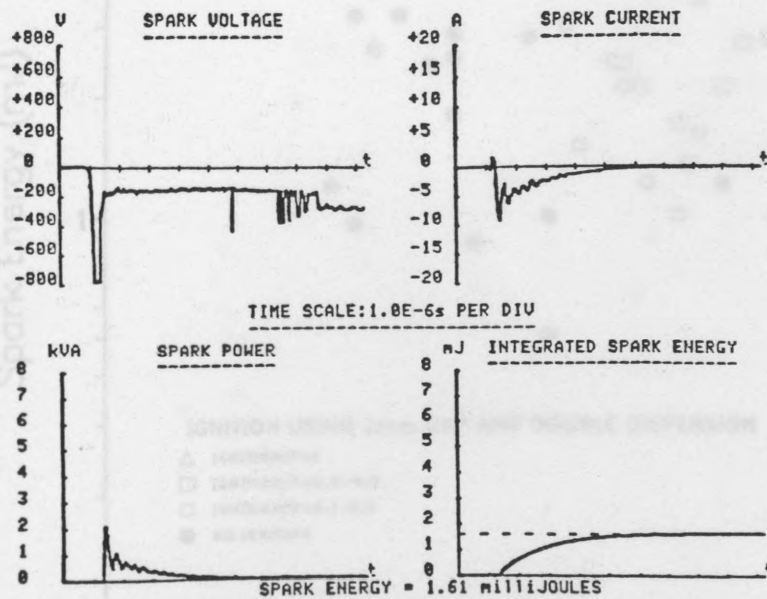


Figure III-30.

Above spark measured for a 7 mm gap.

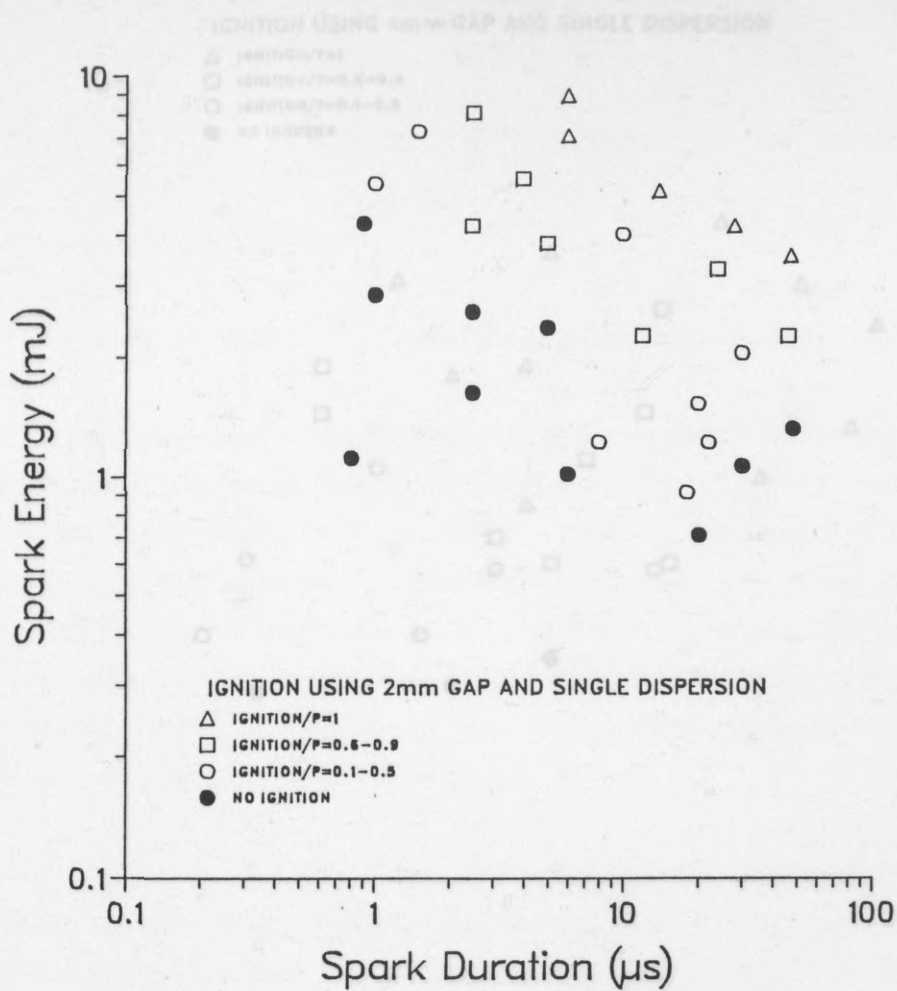


Figure III-31.

Results of ignition tests for the stabiliser powder, for a 2 mm gap and single dispersion.

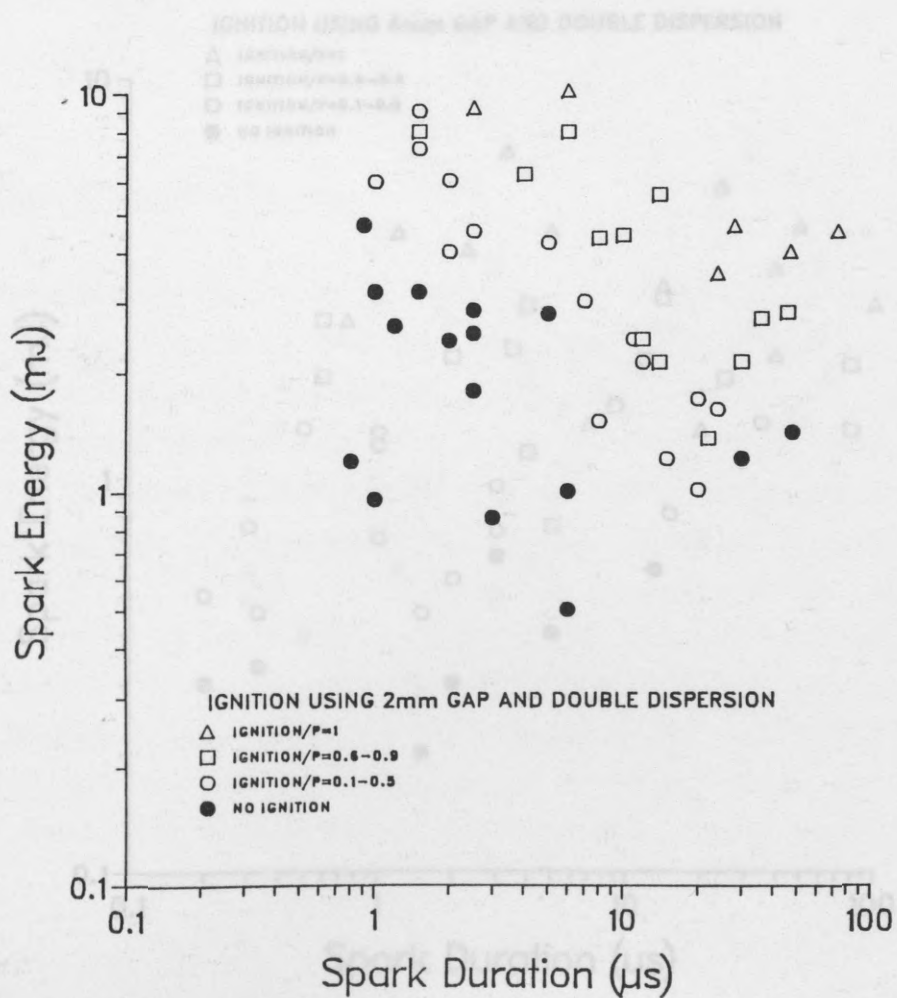


Figure III-32.

Results of ignition tests for the stabiliser powder, for a 2 mm gap and double dispersion.

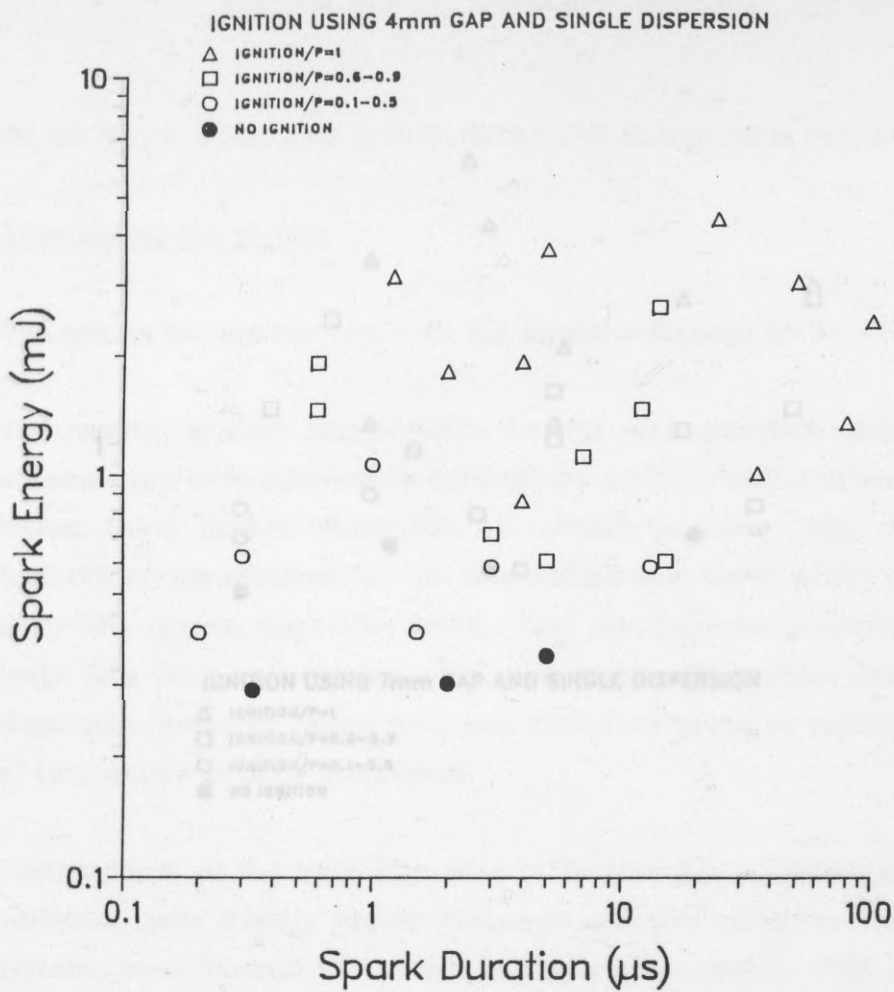


Figure III-33.

Results of ignition tests for the stabiliser powder, for a 4 mm gap and single dispersion.

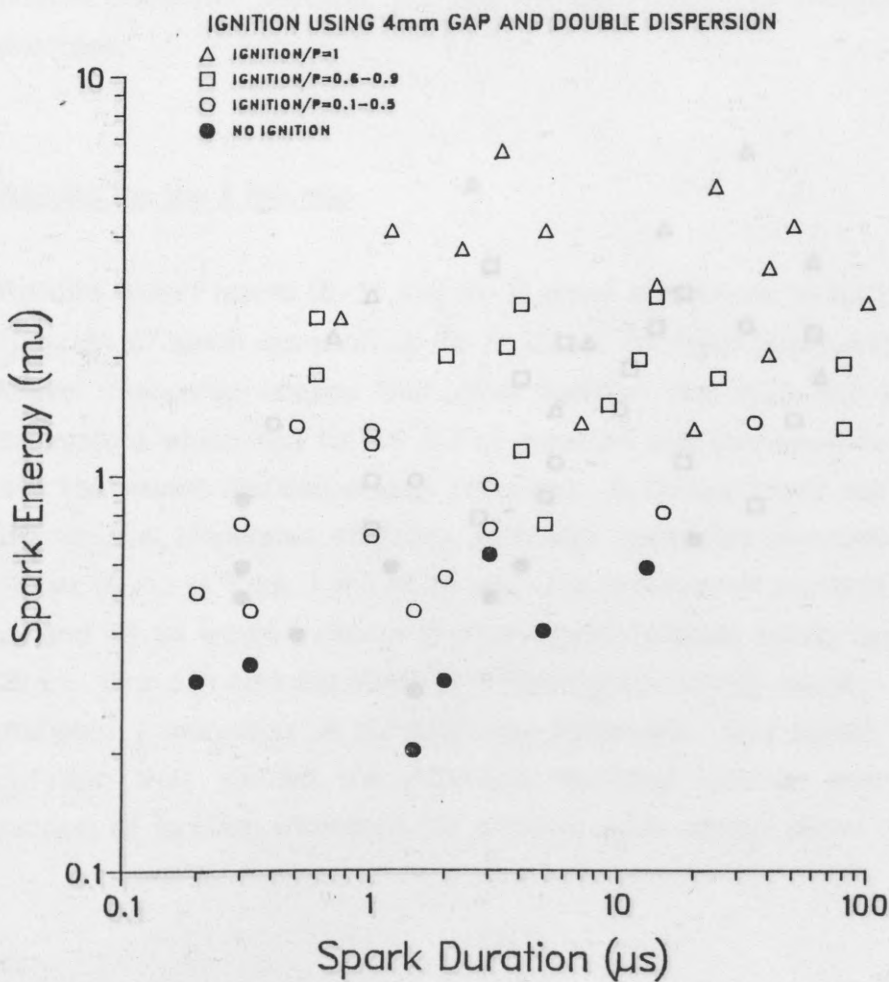


Figure III-34.

Results of ignition tests for the stabiliser powder, for a 4 mm gap and double dispersion.

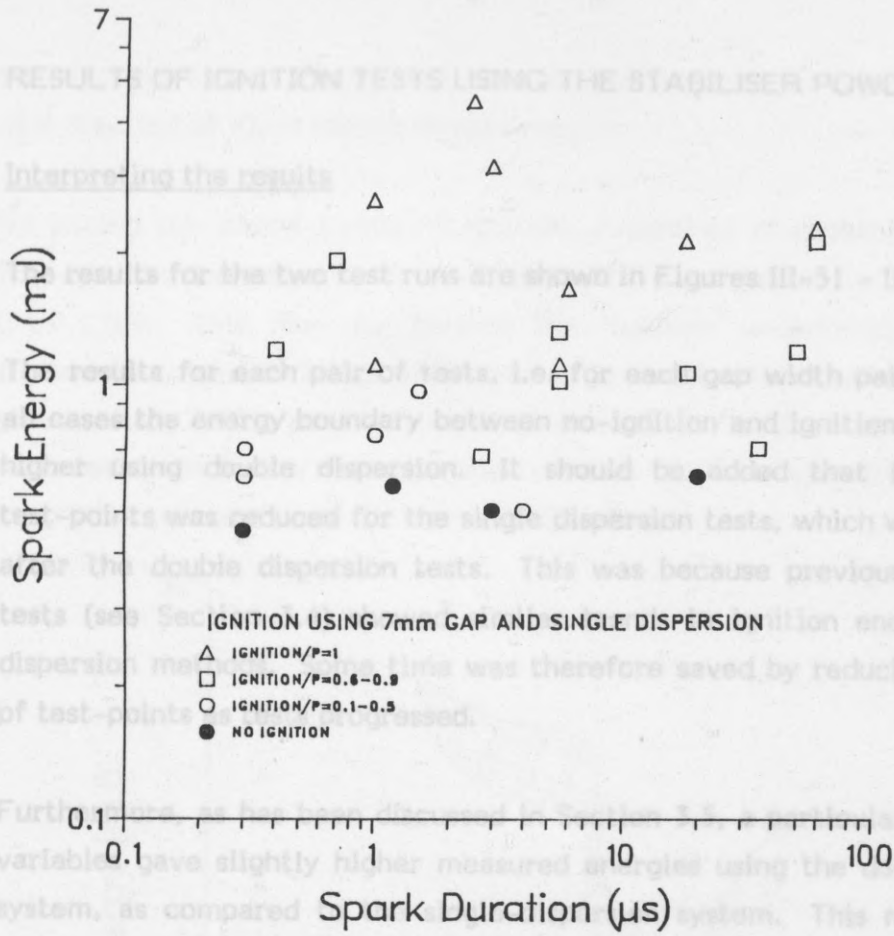


Figure III-35.

Results of ignition tests for the stabiliser powder, for a 7 mm gap and single dispersion.

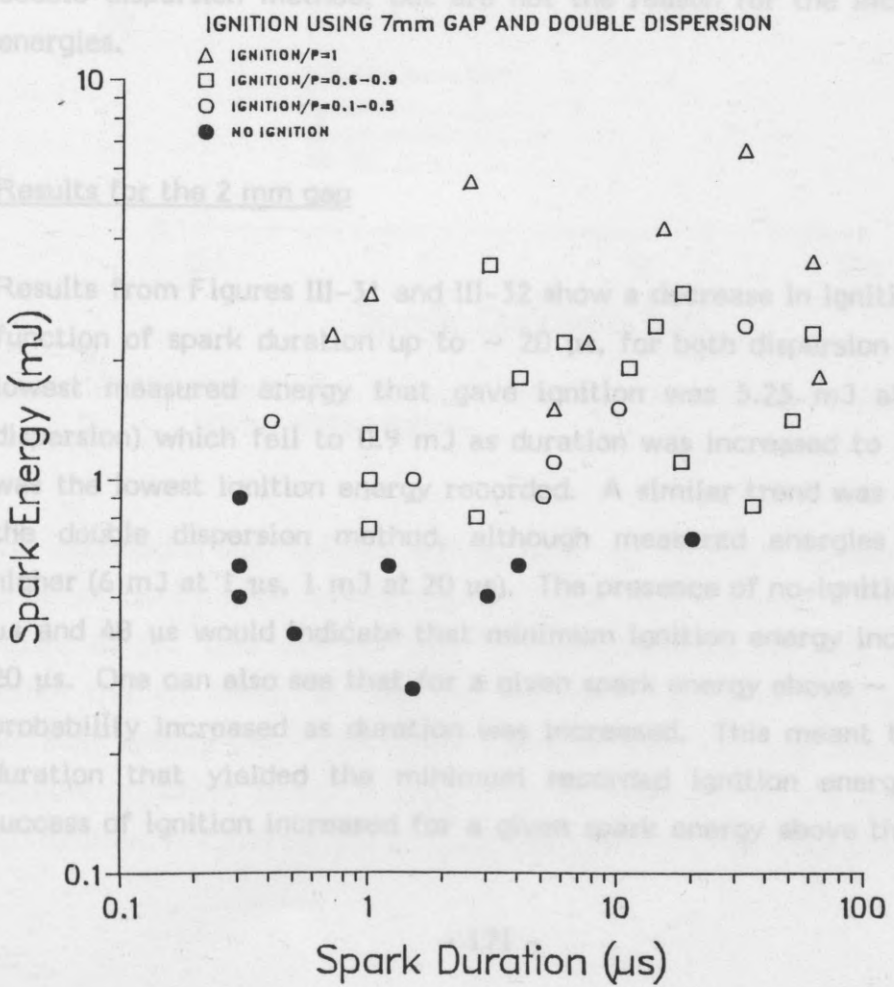


Figure III-36.

Results of ignition tests for the stabiliser powder, for a 7 mm gap and double dispersion.

4. RESULTS OF IGNITION TESTS USING THE STABILISER POWDER

4.1 Interpreting the results

The results for the two test runs are shown in Figures III-31 - III-36.

The results for each pair of tests, i.e. for each gap width pair, show that in all cases the energy boundary between no-ignition and ignition ($0 < P \leq 1$) was higher using double dispersion. It should be added that the number of test-points was reduced for the single dispersion tests, which were performed after the double dispersion tests. This was because previous 'check-point' tests (see Section 3.4) showed similar trends in ignition energies for both dispersion methods. Some time was therefore saved by reducing the number of test-points as tests progressed.

Furthermore, as has been discussed in Section 3.5, a particular set of circuit variables gave slightly higher measured energies using the double dispersion system, as compared to the single-dispersion system. This means that the range of spark energies in the figures is different from one dispersion method to the other. These reflect the increase in discharged energies due to the double dispersion method, but are not the reason for the increased ignition energies.

4.2 Results for the 2 mm gap

Results from Figures III-31 and III-32 show a decrease in ignition energy as a function of spark duration up to $\sim 20 \mu\text{s}$, for both dispersion methods. The lowest measured energy that gave ignition was 5.25 mJ at $1 \mu\text{s}$ (single dispersion) which fell to 0.9 mJ as duration was increased to $\sim 20 \mu\text{s}$. This was the lowest ignition energy recorded. A similar trend was observed using the double dispersion method, although measured energies were slightly higher (6 mJ at $1 \mu\text{s}$, 1 mJ at $20 \mu\text{s}$). The presence of no-ignition points at $30 \mu\text{s}$ and $48 \mu\text{s}$ would indicate that minimum ignition energy increased beyond $20 \mu\text{s}$. One can also see that for a given spark energy above $\sim 20 \mu\text{s}$, ignition probability increased as duration was increased. This meant that above the duration that yielded the minimum recorded ignition energy ($\sim 20 \mu\text{s}$), success of ignition increased for a given spark energy above the minimum of

0.9 mJ. The lowest energy that gave an ignition probability of 1 was 3.45 mJ at a duration of 47 μs (single dispersion).

By joining the lowest points of ignition, regardless of probability, and those for non-ignition, as shown in Figure III-37, a region is created where $0 < P < 0.9$. This may be termed the 'ignition uncertainty region', and represents combined values of spark energy and duration that may or may not give ignition. The 'minimum ignition energy' for a given spark duration is expected to lie in this region, which is shown for the single dispersion results, as ignition energies were the lowest in this case.

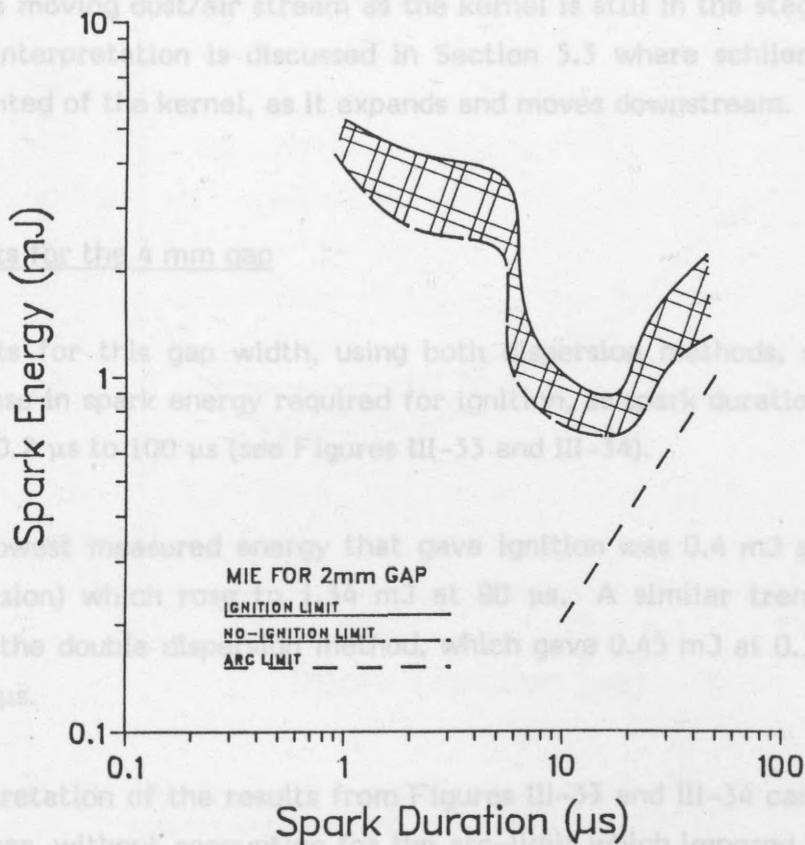


Figure III-37. Results for the stabiliser using a 2 mm gap, showing 'ignition uncertainty region'.

The assumption that ignition energy does not decrease further beyond $\sim 20 \mu\text{s}$ is validated when taking the arc limit into account. This is shown in Figure III-37. One can see that all ignition points for this gap width fall within the arc limit, so that the minimum measured here represents the minimum energy that could ignite this dust using this gap arrangement. The absolute minimum energy is seen to lie between 0.7 mJ (no ignition) and 0.9 mJ (ignition, $P = 0.3$) for the single dispersion tests, for a duration of 20 μs .

Despite the fact that more ignition trials were made using double dispersion, the scatter in ignition probability points in the two sets of results was similar. Recorded energies that gave ignition tended to be slightly lower for the single dispersion results, but otherwise the tendency for each group of probabilities to fall across the duration range was similar in both cases.

The reason for the slight difference in lower ignition energies for the two dispersion methods could well lie in the loss of thermal energy in the spark kernel, as it is forced downstream by the second dispersion pulse (which occurs just prior to spark triggering). This loss of energy is a conductive loss to the moving dust/air stream as the kernel is still in the stage of expanding. This interpretation is discussed in Section 5.3 where schlieren pictures are presented of the kernel, as it expands and moves downstream.

4.3 Results for the 4 mm gap

Results for this gap width, using both dispersion methods, showed a slight increase in spark energy required for ignition, as spark duration was increased from 0.2 μs to 100 μs (see Figures III-33 and III-34).

The lowest measured energy that gave ignition was 0.4 mJ at 0.2 μs (single dispersion) which rose to 1.34 mJ at 80 μs . A similar trend was observed using the double dispersion method, which gave 0.45 mJ at 0.3 μs and 1.3 mJ at 80 μs .

Interpretation of the results from Figures III-33 and III-34 can be misleading, however, without accounting for the arc-limit which imposed a lower limit on spark energy as a function of duration. This meant that the lower trial-points beyond $\sim 10 \mu\text{s}$ were the lowest arc-energy values obtainable in the spark gap. Thus the apparent increase in energy required for ignition beyond 10 μs was caused by a physical restraint to produce low energy, long duration (arc) discharges. Between $\sim 1 \mu\text{s}$ and 10 μs , ignition energy rose for both sets of results, although more significantly using double dispersion. Assuming the arc limit to continue its trend beyond 100 μs (see Section 6.6 in Part I), one would expect ignition energy to increase as a function of duration beyond this value.

By drawing the ignition uncertainty region for the single dispersion results, which, as was also noticed for the 2 mm results, gave the lowest ignition energy values, the minimum ignition energy band is obtained as a function of duration. This is shown in Figure III-38. Also shown is the arc limit as found by experimentation, for the 4 mm gap. This figure shows that minimum ignition energy lay between 0.3 mJ and 0.4 mJ at durations from 0.2 μs to 2 μs .

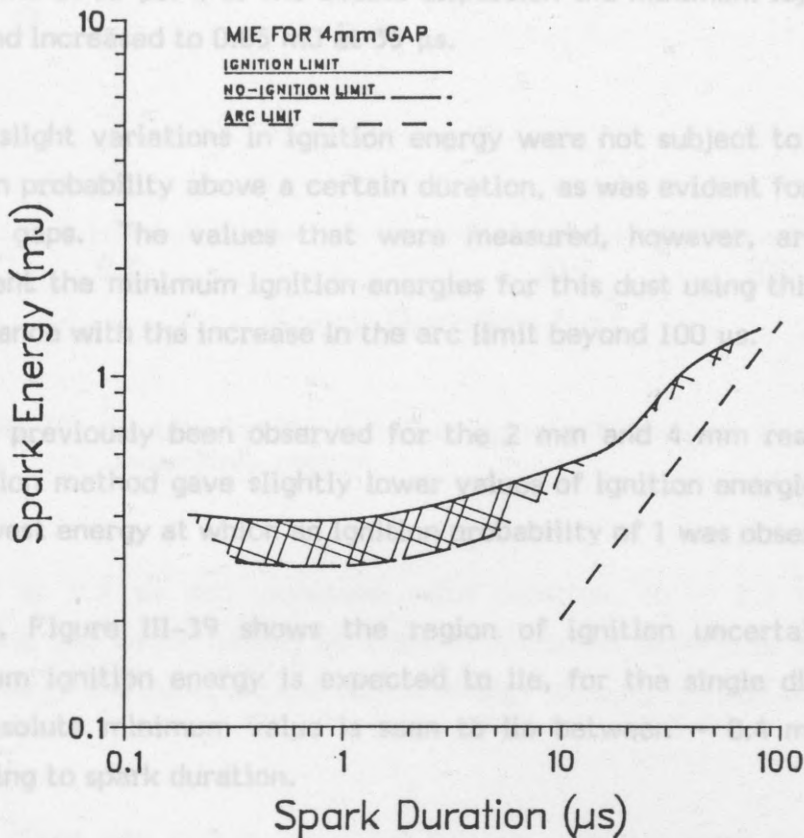


Figure III-38. Results for the stabiliser using a 4 mm gap, showing 'ignition uncertainty region'.

From the results of Figures III-33 and III-34 one can see that the scatter in ignition probabilities was greatest at low durations, (below $\sim 15 \mu\text{s}$), and extended over an order of magnitude of spark energy. Above $\sim 15 \mu\text{s}$ the scatter was reduced, and although ignition energy increased, the probability of ignition also tended to increase as the arc limit was approached. This is particularly clear from the single dispersion results. Assuming that this trend continues beyond 100 μs , one would expect scatter to diminish and ignition probability to increase for energies lying above the minimum.

4.4 Results for the 7 mm gap

Results using a 7 mm gap and the two methods of dispersion did not show any clear relationship between ignition probability and spark duration. For both dispersion methods the lowest energies that gave ignition were almost constant over the range of durations that was tested. For the single dispersion the lowest value lay at 0.5 mJ at a duration of 4 μ s and increased to 0.7 mJ at 35 μ s. For the double dispersion the minimum lay at 0.75 mJ at 1 μ s and increased to 0.85 mJ at 35 μ s.

These slight variations in ignition energy were not subject to an increase in ignition probability above a certain duration, as was evident for the 2 mm and 4 mm gaps. The values that were measured, however, are expected to represent the minimum ignition energies for this dust using this gap width, in accordance with the increase in the arc limit beyond 100 μ s.

As has previously been observed for the 2 mm and 4 mm results the single dispersion method gave slightly lower values of ignition energies, and showed the lowest energy at which an ignition probability of 1 was observed.

Finally, Figure III-39 shows the region of ignition uncertainty, in which minimum ignition energy is expected to lie, for the single dispersion tests. The absolute minimum value is seen to lie between \sim 0.4 mJ and 0.7 mJ, according to spark duration.

4.5 Comparison of the results for the three gap widths

Each of the three gap widths showed a different relationship between spark energy required for ignition and spark duration. For each gap width, this relationship was similar using either single or double dispersion, although the single dispersion method tended to yield slightly lower values of ignition energy.

For a 2 mm gap width, a significant decrease in ignition energy was apparent when duration was increased from 1 μ s to 20 μ s. Ignition energy in this range fell from 5.25 mJ to 0.9 mJ and increased again beyond 20 μ s. This trend disappeared when gap width was increased to 4 mm. Ignition energy fell to

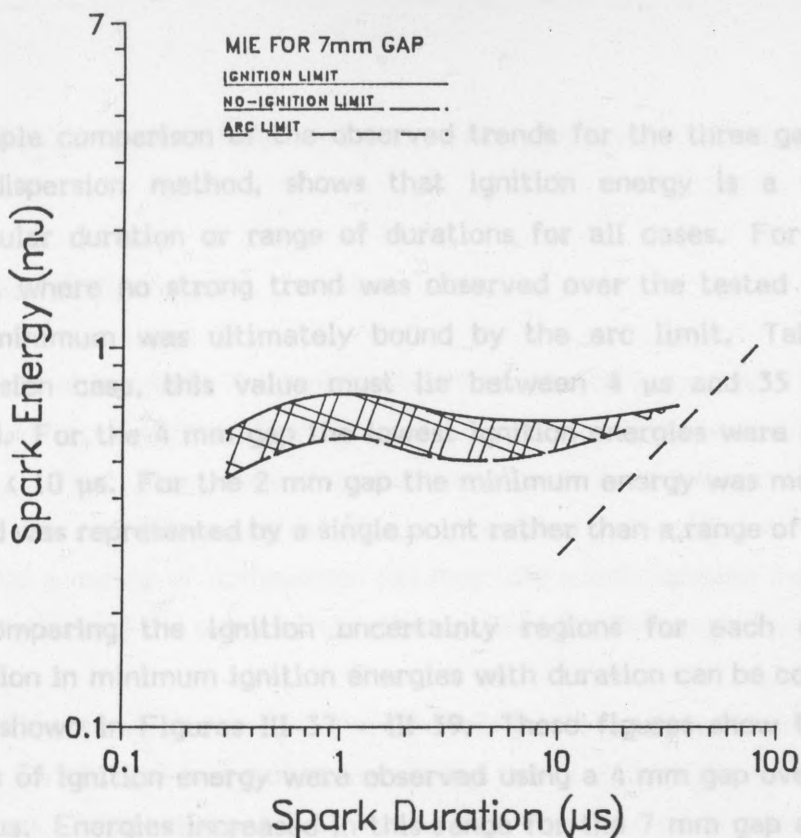


Figure III-39. Results for the stabiliser using a 7 mm gap, showing 'ignition uncertainty region'.

0.4 mJ at 0.2 μs and increased, with duration, to ~ 1.3 mJ at 80 μs . Increasing gap width further to 7 mm revealed no significant trend between spark energy and duration; the lowest energy yielding ignition was 0.5 mJ at 4 μs .

For all three gap widths, recorded ignition energies were bounded by the practical arc-limits found previously (see Section 6.6 in Part I). For the 4 mm and 7 mm results this meant that ignition energy necessarily increased beyond a particular duration. In other words the arc limit governed the ignition energy required to ignite the dust as duration was increased. For the 2 mm results this effect was not apparent until duration increased beyond 20 μs , when ignition energy also increased. The presence of no-ignition points at 30 μs and 48 μs (see Figure III-31 and III-32) tends to support the fact that ignition energy increased independent of the arc limit. Because increases of duration at such low energies were not physically possible, however, any hypothetical increase in duration would automatically require an increase in energy. It would thus appear that like the 4 mm and 7 mm results, ignition energy may ultimately be bound by the arc-limit.

A simple comparison of the observed trends for the three gap widths, using one dispersion method, shows that ignition energy is a minimum at a particular duration or range of durations for all cases. For the 7 mm gap width, where no strong trend was observed over the tested duration range, this minimum was ultimately bound by the arc limit. Taking the single dispersion case, this value must lie between 4 μs and 35 μs (see Figure III-36). For the 4 mm gap the lowest ignition energies were observed in the range $< 10 \mu\text{s}$. For the 2 mm gap the minimum energy was measured at $\sim 20 \mu\text{s}$ and was represented by a single point rather than a range of points.

By comparing the ignition uncertainty regions for each gap width, the variation in minimum ignition energies with duration can be compared. These were shown in Figures III-37 - III-39. These figures show that the lowest values of ignition energy were observed using a 4 mm gap over the range 0.2 - 35 μs . Energies increased in this range for the 7 mm gap and further still for the 2 mm gap.

Three questions arise from the results of Figures III-37 - III-39. First of all, is the mechanism of ignition the same, for the 4 mm and 7 mm widths, in the range where ignition energy is apparently independent of spark duration? Secondly, why were ignition energies higher for a 2 mm gap, and why was such a duration dependence observed in this case? Lastly, was the mechanism of ignition the same, regardless of gap width or spark duration, assuming sufficient spark energy for ignition?

To help answer these questions, a number of comparisons were made, based on schlieren photographs of the expanding spark kernel, as described in the following section.

A range of combinations of spark energy and duration was chosen for the study. In each case the position of ignition in the vessel varied. For these tests the spark generator was adjusted to give spark energy measurements of 4 mJ/1 μs in both cases. These tests were run in order to show the different locations of ignition for each dispersion method, and to help explain why the single dispersion method gave lower ignition energy values than the double dispersion method.

An explanation of this effect was put forward in the preceding section. It was suggested that the double dispersion method caused the spark

5. SCHLIEREN PHOTOGRAPHS USING THE STABILISER POWDER; TESTS AND RESULTS

5.1 Outline of tests

The plots obtained in the ignition tests for the three gap widths were used as the basis for a series of schlieren tests. These tests were included for two reasons. First, they were important as a means of interpreting the ignition results for the three gap widths as described in Section 4. Secondly, they provided a means of comparison between the spark-ignition mechanisms using this powder and the propane/air mixture used in previous tests.

For each gap width a range of spark energies/durations was chosen according to the trends that were observed in the previous ignition tests. Most of the schlieren studies were for 2 mm and 4 mm gap widths where significant differences in minimum ignition energies were observed. Comprehensive studies using the 7 mm gap width were not made because of the similarity of the ignition results using this gap with the 4 mm gap results.

The details of the high-speed schlieren apparatus used for these tests, are given in Appendix 4. The switching of all operations, including the high speed camera and dust dispersion, was controlled by the central timing system, as was described in Section 3.2.

A range of combinations of spark energy and duration was chosen for the schlieren comparisons, which are described by the following tests:

- a) One spark energy/duration was studied, that gave an ignition probability of 1 for the 4 mm gap using both dispersion methods. In each case the position of ignition in the vessel varied. For these tests the spark generator was adjusted to give spark energy measurements of 4 mJ/1 μ s in both cases. These tests were run in order to show the different locations of ignition for each dispersion method, and to help explain why the single dispersion method gave lower ignition energy values than the double dispersion method.

An explanation of this effect was put forward in the preceding section. It was suggested that the double dispersion method caused the spark

kernel to lose heat by conduction to the air/dust mixture that was blowing it downstream. To help verify this explanation, the schlieren photographs of ignition using the double dispersion method, were taken at various positions downstream of the spark gap. For these series' a new explosion vessel was constructed. This was similar in dimensions to the previous one, but incorporated rectangular windows in place of the round 'schlieren holes' found on the first vessel. These windows extended some 7.5 cm below the spark gap as is shown below in Figure III-40.

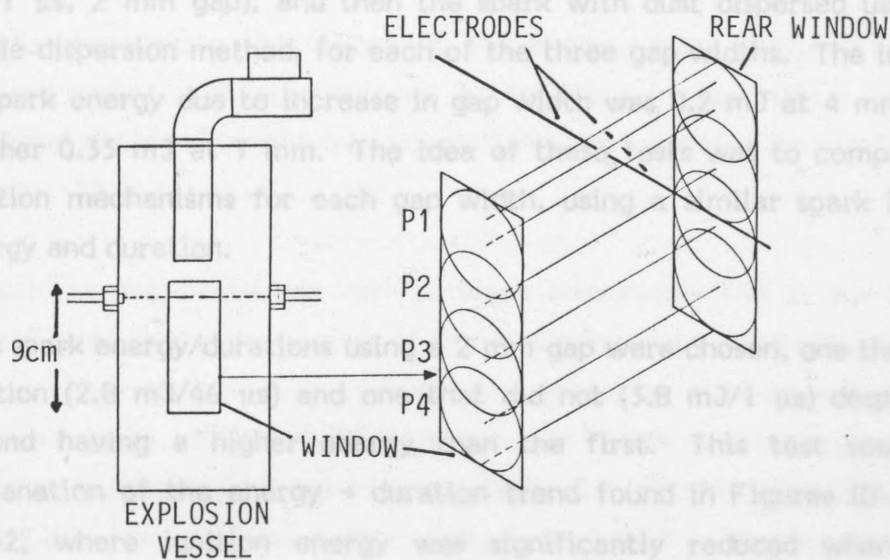


Figure III-40. Second explosion vessel for studying downstream ignition, showing the enlarged schlieren window and four schlieren fields P1 - P4.

Using this new vessel, four schlieren series' were run, each one corresponding to the four schlieren fields marked P1 - P4 in Figure III-40. Each field was chosen by adjusting the vessel height relative to the fixed positions of the laser source and camera. Running each series over a period of 80 ms made it possible to identify the position of ignition relative to the spark gap, and the times involved before flame propagation became apparent.

For the 'normal' schlieren runs, using the first dispersion method or no dispersion whatsoever, the original explosion vessel was used. In this

case the position of the schlieren field was fixed, and corresponded to position P1 in the above figure.

High-speed photographs were also taken of the flame development using both the new vessel, and the original vessel, and these compared with the schlieren results.

- b) One spark energy/duration was chosen that gave an ignition probability of 0 for the 2 mm gap, but a value of 1 for the 4 mm and 7 mm gaps. For these tests six schlieren series' were run: first the spark in air (3.8 mJ/1 μ s, 2 mm gap), and then the spark with dust dispersed using the single dispersion method, for each of the three gap widths. The increase in spark energy due to increase in gap width was 0.2 mJ at 4 mm and a further 0.35 mJ at 7 mm. The idea of these tests was to compare the ignition mechanisms for each gap width, using a similar spark ignition energy and duration.
- c) Two spark energy/durations using a 2 mm gap were chosen, one that gave ignition (2.8 mJ/46 μ s) and one that did not (3.8 mJ/1 μ s) despite the second having a higher energy than the first. This test sought an explanation of the energy \rightarrow duration trend found in Figures III-31 and III-32, where ignition energy was significantly reduced when spark duration was increased to an optimum value.
- d) Three spark durations using one gap width (4 mm) and similar spark energies were chosen, that all gave ignition probabilities of 1. The sparks investigated were 4 mJ/1 μ s, 4.2 mJ/50 μ s and 2.7 mJ/100 μ s. These tests were performed in order to show any differences that might exist in the spark ignition process as a function of spark duration, for a fixed gap width.
- e) Two sparks were chosen that had a similar duration, one using a 2 mm gap and one a 4 mm gap. Both sparks gave ignition of the dust/air mixture, giving ignition probabilities of 1. The sparks were 2.8 mJ/46 μ s for the 2 mm gap, and 4.2 mJ/50 μ s for the 4 mm gap. Initial spark powers for the two sparks were similar in magnitude. This test was performed in order to see if there was any effect of gap width on the ignition process, where the spark expanded at a fixed rate.

- f) One spark energy/duration combination was chosen that gave an ignition probability of $0 < P < 1$ using one gap width. For these tests four schlieren series' were run: first the spark in air (1.33 mJ/0.5 μ s), and then the spark using dust, where one series showed successful ignition ($P = 0.4$) and the other two showed unsuccessful ignitions ($P = 0.6$). The idea of these tests was to help to define the criterion governing the success of ignition when ignition probability was less than unity.

5.2 Interpretation of the schlieren photographs

All of the photographs that follow in this analysis were obtained using the 'high-speed camera schlieren system' as described in Appendix 4. Some of the obtained photographs require explanation before conclusions can be drawn from them. Thus:

- 1) Resolution and brightness vary between sequences. This is due to small differences in the positioning of the schlieren knife-edge between tests. In practice all elements (lenses etc.) must be cleaned and replaced between tests, so that slight differences in image quality may result due to a re-positioning of one of these elements. Usually this difference is negligible, and the most important factor that influences the image quality is the state of the surface of L3 (the schlieren lens). This inevitably becomes partially covered with dispersed dust just prior to ignition. This alone may cause strong variations in the image quality. In addition, quality of the photographs tended to increase as time went on and more experience with the system was obtained.
- 2) Some photographs show what appear to be layers of burning dust. In Appendix 4 it is shown that these are in fact interference patterns caused by lens (L3) aberrations. Often these patterns appear more pronounced towards the image boundaries, which is a function of the knife edge positioning relative to L3 (see Appendix 4). Sometimes, however, they are visible across the whole image plane.
- 3) The image (the flame kernel) often appears to propagate in one direction only. This is not always the case, but it is a function of the knife-edge positioning, as is shown in Appendix 4. Simple tests showed that this

effect was a direct result of the axial positioning of the knife edge, and the degree to which the image field was darkened to obtain the schlieren effect. Thus for dark image fields, where sparks in air were recorded, the knife-edge position gives a more symmetrical image, which is also free of interference lines. For light image fields (where dust is present) the knife-edge introduces interference lines depending on its positioning, and tends to exclude one half of the L3 image from the image plane. In most of the experiments the knife-edge was positioned vertically so that for light image fields (i.e. for ignition tests) an image was apparent in one half of the image plane only. Additional tests where the knife-edge position was reversed, showed that the image was in fact symmetrical and not asymmetrical as in many of the photographs.

- 4) The delay time marked on each schlieren photograph refers to the time the photograph was taken following the moment of spark discharge, in milliseconds. Each exposure time, however, must also be taken into account, particularly for delay times within the first millisecond. The exposure time is constant for each picture and is a function of the camera speed and 'shutter constant'. In the present tests, using a film speed of 8000-9000 fps, the exposure time is approximately 20 μ s. This means that a time uncertainty exists of approximately 90 μ s, so that comparing two film series' in time is subject to this uncertainty divided by two (\sim 45 μ s). This represents a small error above 1 ms (\sim 5%) but may be significant, particularly for the first pictures in each series.
- 5) Due to the shutter constant time of the high-speed camera, the definition of the schlieren images is theoretically limited. In practice, however, this effect is almost negligible, because spark and flame expansion velocities were relatively slow compared to the velocity of the shutter. As an example, on the scale of these photographs, assuming a flame expansion velocity of 5 ms^{-1} , an image 'blur' of 0.25 mm results. This may usually be neglected as it does not severely detract from the image clarity.
- 6) Some of the photographs show a series of bright spots on the image field. This was found to be due to settled dust on the schlieren lens L3, and was not an ignition phenomenon.

- 7) Interpretation of the photographs, as for any schlieren images, is purely qualitative and no temperatures are available from them. For the most sensitive settings, for example for the sparks in air, the sensitivity of the system was very high and temperature changes as low as 20°C were estimated to be measurable. In all cases a brightening of the schlieren field is due to a reduction in medium density, i.e. a reduction in refractive index due to an increase in temperature, and vice versa. Thus an expanding spark or flame kernel is made visible by the presence of areas of increased brightness over the background field. Solid objects (for example the electrodes) appear opaque, i.e. black. The cathode is on the left in the photographs.

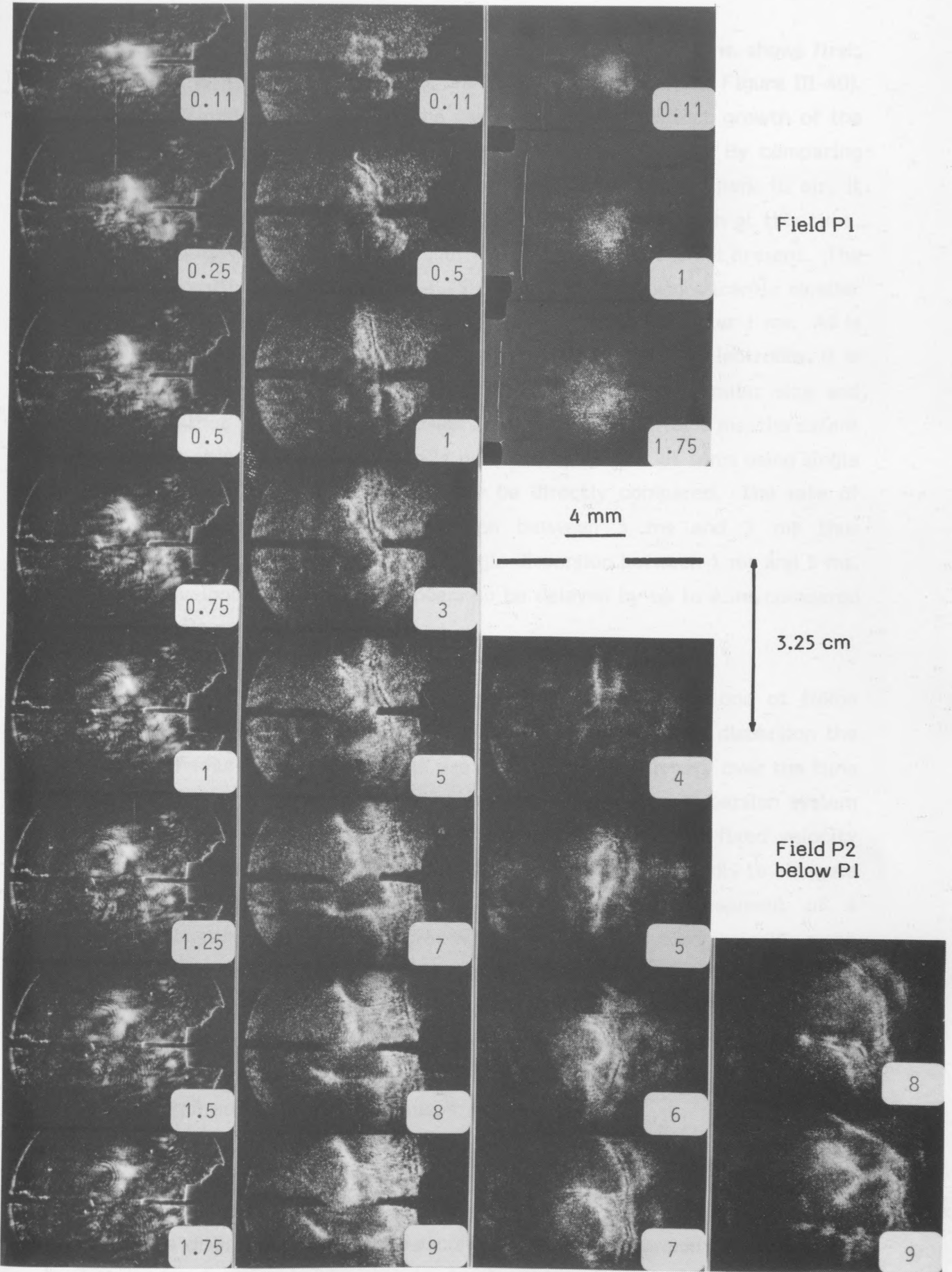
As for the single shot (gas ignition) schlieren studies, physical distances and dimensions are obtained from the electrode size and spacing, assuming a linear cross-section and spherical symmetry around the gap.

5.3 Results and discussion of the tests

5.3.1 Results and discussion for the first schlieren series (a)

The results of the three test runs are condensed into four sequences, as shown in Photographs III-7 - III-9. This shows first the development of the 4 mJ/1 μ s spark in air, then of the spark/flame kernel using the first dispersion method, and finally two sequences showing ignition using the second dispersion method. The spark energies were the same in all three cases.

In each of the sequences, the time scales for spark or flame kernel growth are different, as each covers a different timespan. The first sequence, showing spark kernel development, shows that a hot kernel is present in the electrode space up to 1.75 ms following spark discharge. No information is available concerning the temperature at this time, but this time gives an estimate of the spark kernel's lifetime. The second series shows that already at 1 ms, a burning front is formed, with a similar profile to that of the spark at this time. After 3 ms this front has broadened and appears independent of any activity in the spark gap. The remaining photographs in this series show a subsequent broadening of this flame front, implying that ignition is complete.



Photograph series III-7.
4 mJ/1 μ s spark in air.

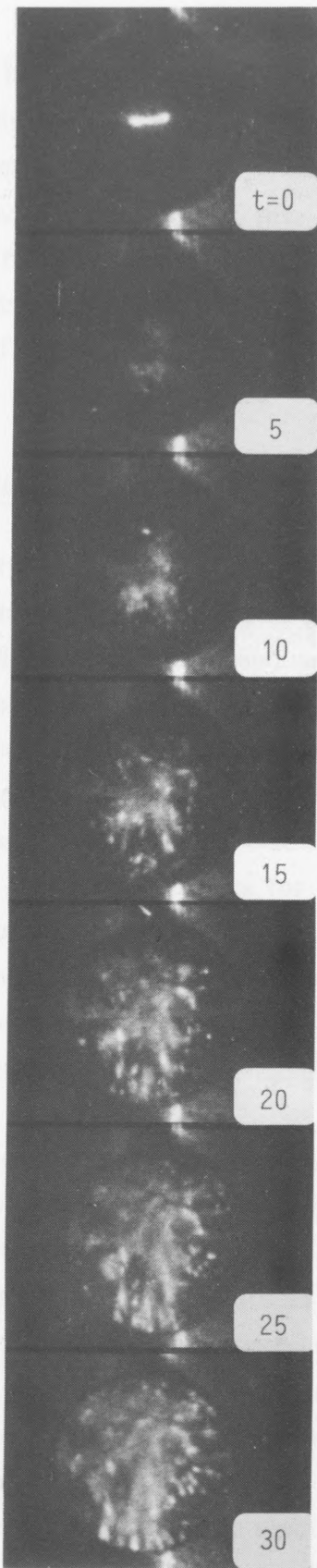
Photograph series III-8.
4 mJ/1 μ s spark in stabiliser cloud using 1st dispersion method.

Photograph series III-9.
4 mJ/1 μ s spark in stabiliser cloud using 2nd dispersion method.

The third series of photographs, which consists of two test runs, shows first, the schlieren field P1, and second, the field P2 below P1 (see Figure III-40). The first three photographs, in the gap area, show a distinct growth of the spark kernel within 1.75 ms, and its movement downstream. By comparing the photograph at 1.75 ms with that in the series for the spark in air, it appears that dust has begun to contribute to the kernel growth at this time, which is otherwise seen to decay over this time when dust is not present. The size and profile of the kernel at 1.75 ms are, however, significantly smaller than those of the kernel using the single dispersion method after 1 ms. As is shown by the remaining four photographs downstream of the electrodes, it is not until some 5 ms that the kernel front approaches a similar size and profile to that seen using single dispersion after 1 ms. After 7 ms, the extent of burning using double dispersion is comparable to that at 5 ms using single dispersion. At 9 ms both images may be directly compared. The rate of flame expansion for double dispersion between 5 ms and 7 ms thus corresponds to a similar growth for single dispersion between 1 ms and 5 ms. Flame development therefore appears to be delayed by up to 4 ms compared to the single dispersion case.

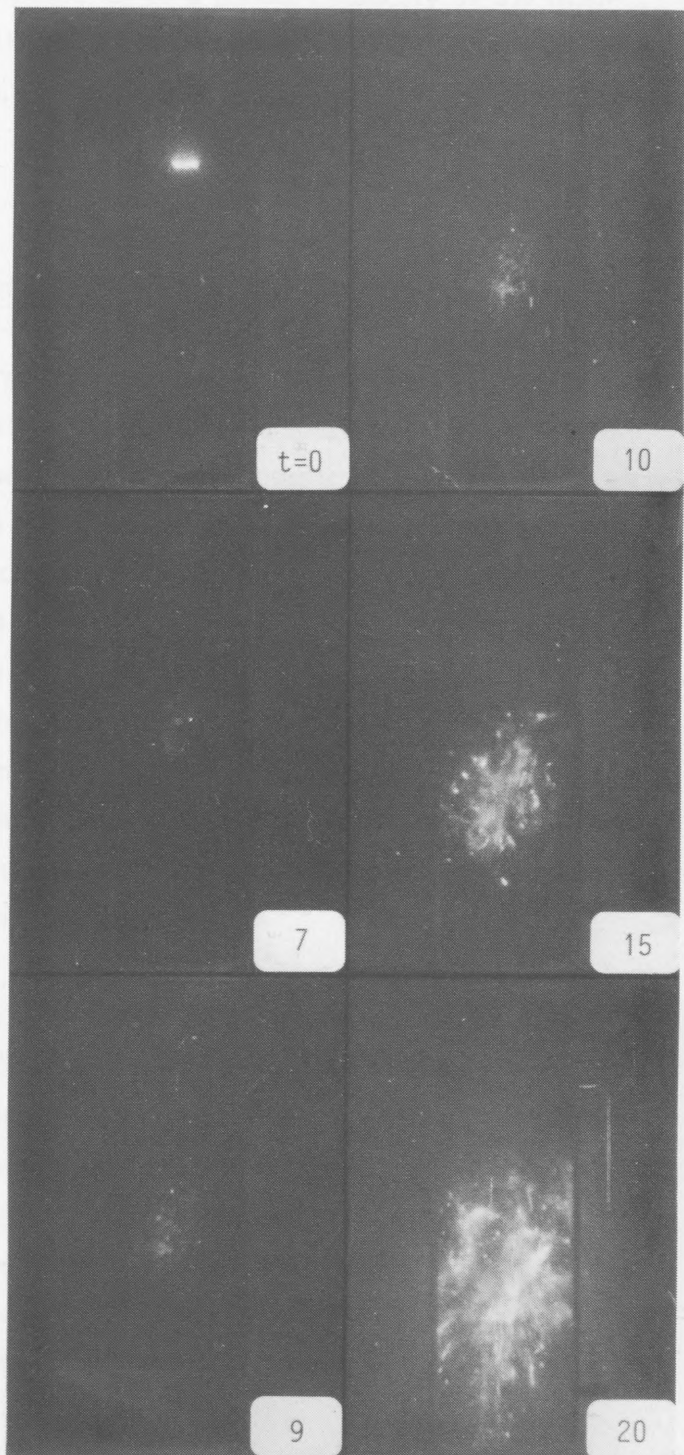
The comparison between the two dispersion mechanisms is one of flame growth under 'static' and 'dynamic' conditions. Using single dispersion the dust/air medium in and around the gap is essentially stationary over the time required for a propagating flame to develop. The double dispersion system represents a case where the dust/air medium moves with a fixed velocity during this time. The net effect of this movement is undoubtedly to elongate the kernel and increase the time to the initial development of a self-propagating flame. The increase in this time will automatically mean that a higher loss of heat to the surrounding medium will take place, so that effective energy for ignition will be decreased. In addition, energy loss is increased over the static case, because of the flow of dust/air past the spark kernel. This could explain the reason for the higher values of spark ignition energy required using the double dispersion method.

The phenomenon of downstream ignition may be seen again in the 'normal' high-speed photographs shown in series' III-10 and III-11. These show, first the single dispersion results, and second the double dispersion results. In the latter case, ignition can be seen to develop approximately 3 cm downstream of the electrodes, as was also found in the schlieren tests.



Photograph series III-10.

High-speed photographs of ignition using a 4 mJ/1 μ s spark and the 1st dispersion method. Ignition develops around gap area. Times in milliseconds.



Photograph series III-11.

High-speed photographs of ignition using a 4 mJ/1 μ s spark and the 2nd dispersion method. Ignition develops \sim 3 cm downstream of gap area.

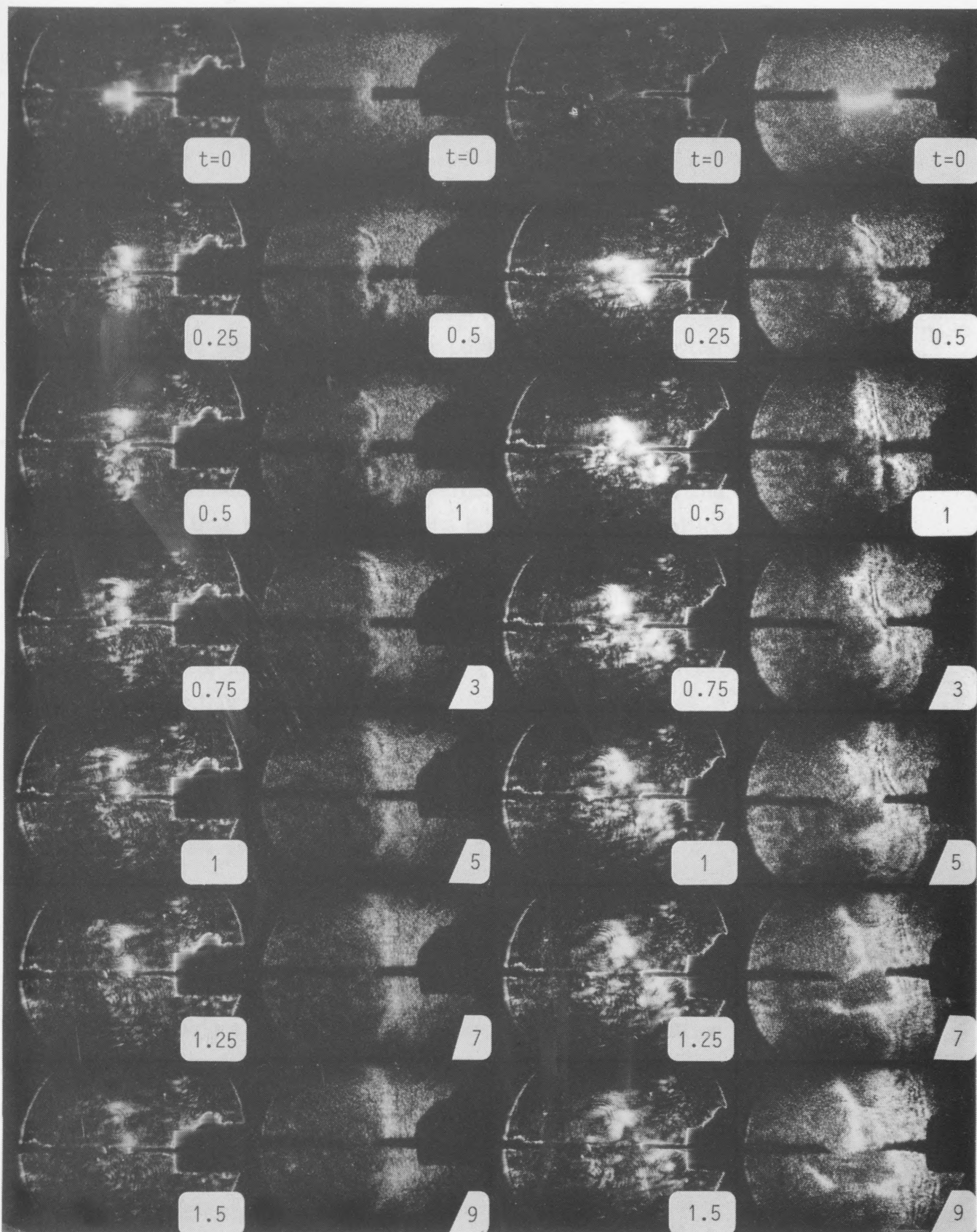
Finally, a rough confirmation of air velocity may be made for the double dispersion case from the third and fourth photographs of the final schlieren series. These show a downward movement of ~ 20 mm of the kernel front over a time of 2.25 ms. This corresponds to a (linear) velocity of 8.9 m.s.^{-1} . This value compares well with the previous estimate of 8 m.s.^{-1} which was obtained with dust alone. The 0.9 m.s.^{-1} error corresponds to the expansion of the kernel during this time.

5.3.2 Results and discussion for the second and third schlieren series' b) and c)

The results for the first series of tests b) are shown in the four series' in Photograph III-12. This shows first the $3.8 \text{ mJ}/1 \mu\text{s}$ spark in air for the 2 mm gap, and of the subsequent expansion with dust present, then the spark in air using a 4 mm gap, and then with dust present. The spark was produced using the same circuit conditions in each case. An increase in spark energy to 4 mJ was therefore observed for the 4 mm gap (see Section 3.5). The photographs show a quenched ignition for the 2 mm case and a successful ignition for the 4 mm case. Results for the 7 mm gap were very similar to those for the 4 mm gap and are not reproduced here. The small increases in dissipated energy due to an increase in gap width were, according the ignition results shown in Figures III-31 - III-36, considered too small to be solely responsible for the dramatic change in ignition success.

The first series for the 2 mm gap shows a rapid expansion of the spark kernel up to 0.5 ms, which then starts to decay, becoming extinct within 1.5 ms. On the other hand the spark kernel in the 4 mm gap grows at a slower rate and starts to decay as late as 1 ms, and at a slower rate than for the 2 mm case. This agrees well with the results found previously in the gas ignition experiments where similar energies and durations (expressed in terms of spark power) caused a faster expansion of the spark kernel as gap width was reduced. This expansion is measured in terms of axial displacement of the kernel edge from the electrodes.

The ignition results for the 2 mm gap show a similarly rapid expansion of the spark kernel, but events following 1 ms show unsuccessful ignition. The flame front begins to decay and heat diffusion to the dust/air mixture causes a complete extinction within some 20 ms (not shown here).



3.8 mJ/1 μ s spark in air
(2 mm gap).

3.8 mJ/1 μ s spark in
stabiliser cloud
(2 mm gap).

4 mJ/1 μ s spark in air
(4 mm gap).

4 mJ/1 μ s spark in
stabiliser cloud
(4 mm gap).

The 4 mm gap results show a more intense kernel front at 0.5 ms and 1 ms which is also broader than for the 2 mm case at these times. The front expands beyond 1 ms and broadens as it does so, eventually leading to an ignition of the complete dust cloud within the confines of the vessel walls.

The fact that the spark gave ignition using the 4 mm gap, and no ignition using the 2 mm gap, would indicate that quenching losses to the spark kernel, as it begun expanding, reduced the effective energy for ignition. This is borne out in the second series in Photograph III-12, where the expanding kernel was seen to distort at its point of contact with the right electrode. This was not apparent from the 4 mm results.

Evidence of lower losses from the spark kernel to the electrodes, is available from a comparison of the spark kernel growths in air for the two gap widths. The fact that the longevity of the buoyant spark kernel in the spark gap is greater for the 4 mm gap than for the 2 mm gap, implies a lower loss of heat energy to the electrodes. Assuming that loss of heat to the surroundings is the same in both cases, this further implies that a greater kernel energy is available for ignition using the 4 mm gap. This is confirmed by the success of ignition in this case.

The results for the second test (c) using a 2 mm gap are shown in Photograph III-13. This compares a 2.8 mJ/46 μ s spark in air and with dust present, and the 3.8 mJ/1 μ s spark under similar conditions.

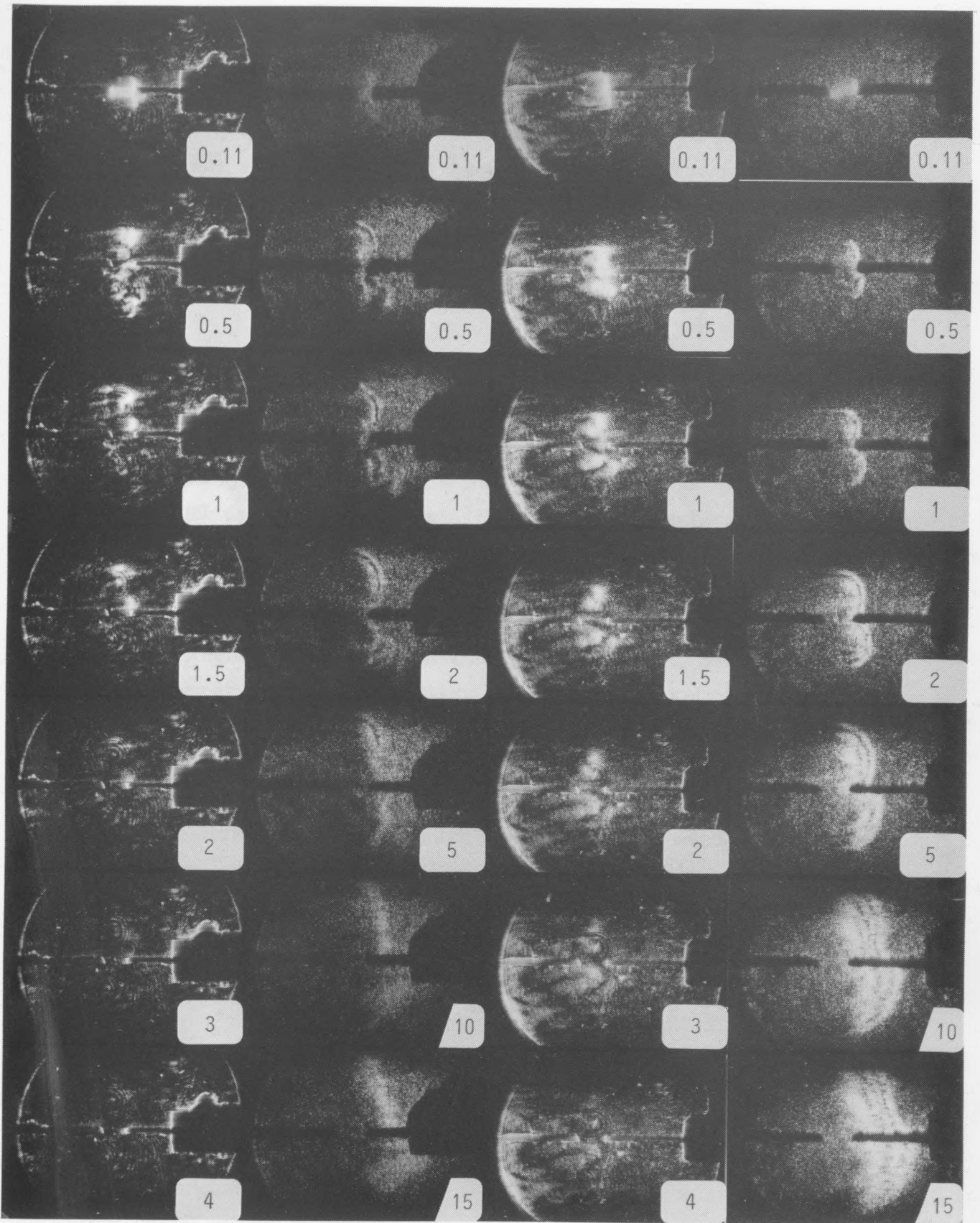
The first spark sequence shows a rapid expansion and decay of the spark kernel, which extinguished within 1.5 ms. On the other hand, the lower energy, longer duration spark shown in the third series, decays less rapidly, extinguishing at around 2 ms. A comparison of the ignition series' shows a lower expansion rate for the higher duration spark, up to 2 ms, but like the previous photograph using the 4 mm gap, the kernel is broader and more intense. Beyond 2 ms, the kernel front expands across the viewing field for the second spark, whereas it decays for the first spark, leading to eventual extinction.

3.8 mJ/1 μ s spark in
air (2 mm gap).

3.8 mJ/1 μ s spark in
stabiliser cloud
(2 mm gap).

2.8 mJ/46 μ s spark in
air (2 mm gap).

2.8 mJ/46 μ s spark in
stabiliser cloud
(2 mm gap).



3.8 mJ/1 μ s spark in air (2 mm gap).

3.8 mJ/1 μ s spark in stabiliser cloud (2 mm gap).

2.8 mJ/46 μ s spark in air (2 mm gap).

2.8 mJ/46 μ s spark in stabiliser cloud (2 mm gap).

It would appear from these results, that where the spark kernel longevity was short, due to an high spark power and thus rapid expansion, ignition is unsuccessful. This was in spite of the energy being greater than for the second case, where spark duration was longer, and thus spark power was lower. In this latter case, the spark kernel longevity was increased and ignition occurred, despite visible effects of quenching. The longevity and rate of expansion of the spark kernel, therefore, as determined by the initial spark power, were decisive in leading to successful ignition.

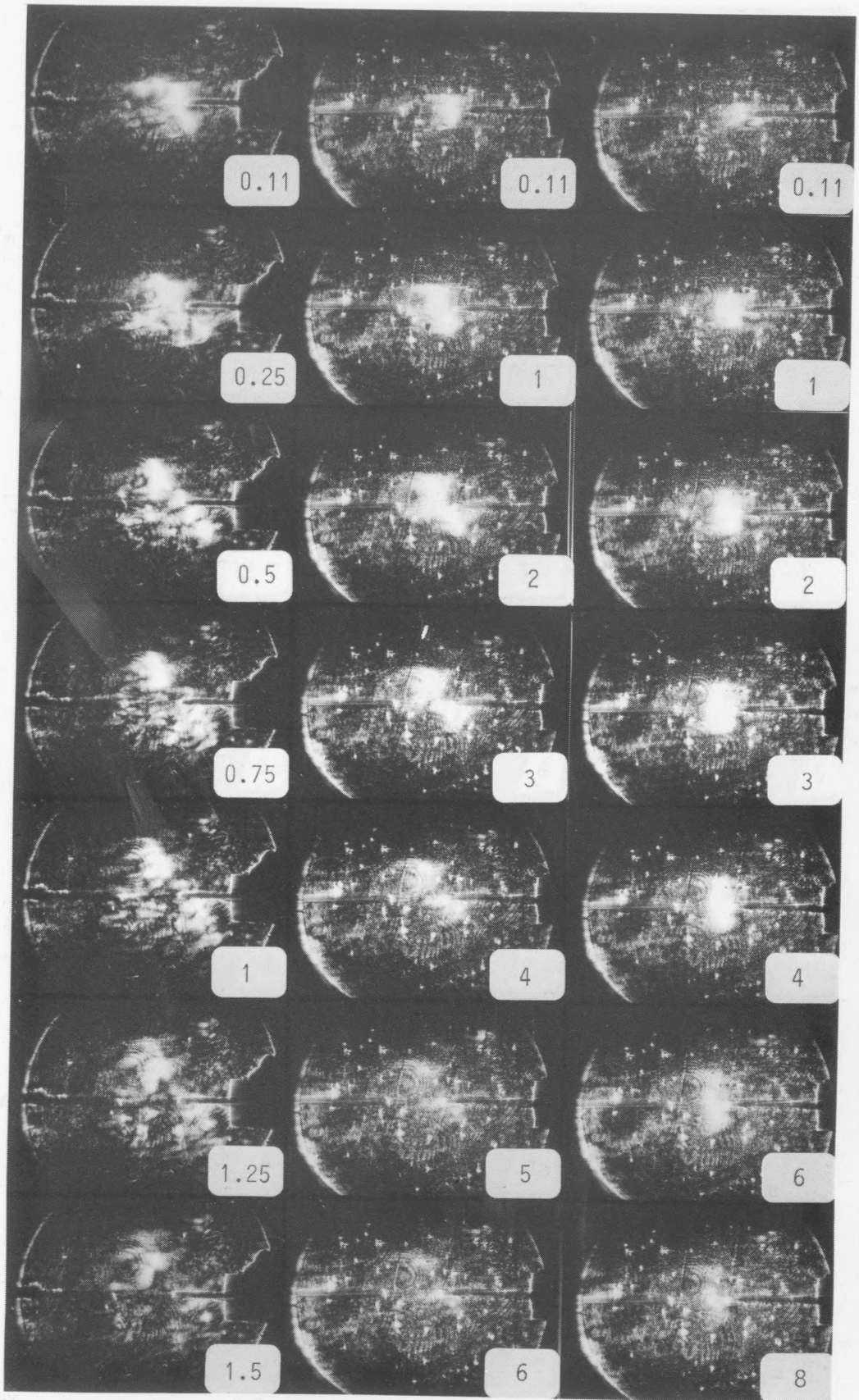
5.3.3 Results and discussion for the fourth schlieren series (d)

The results from this series of tests are shown in Photographs III-14 and III-15. Photograph III-14 shows the three sparks 4 mJ/1 μ s, 4.2 mJ/50 μ s and 2.7 mJ/100 μ s in air at different times following discharge. Photograph III-15 shows the same sparks in the dust/air mixture for the first 20 ms following discharge.

From Photograph III-14 one can compare the spark kernel expansion and delay times as a function of duration. The first, short duration spark, shows a rapid expansion to a large kernel size within 1 ms. Following this time, heat is rapidly lost from the kernel due to its large surface area. The second spark series shows a slower expansion than the first and a smaller maximum kernel size. The kernel size being smaller, losses by diffusion and conduction are also lower, and the lifetime of the kernel is increased to ~ 4 ms. It is increased further still in the third spark series, where, despite a lower energy, a decrease in spark power, manifested by an increase in duration, leads to a smaller kernel which lasts some 6 ms.

The fact that the spark kernel's longevity is increased for similar spark energies as duration is increased, is undoubtedly related to the initial power in the spark discharge. As was shown in the gas ignition work, and in the previous comparison, the spark expansion rate decreased dramatically as initial spark power decreased. The result of a decrease in expansion rate is that kernel volume is reduced at any given instant so that thermal energy losses to the surrounding medium are also reduced. This results in a kernel with a longer lifetime.

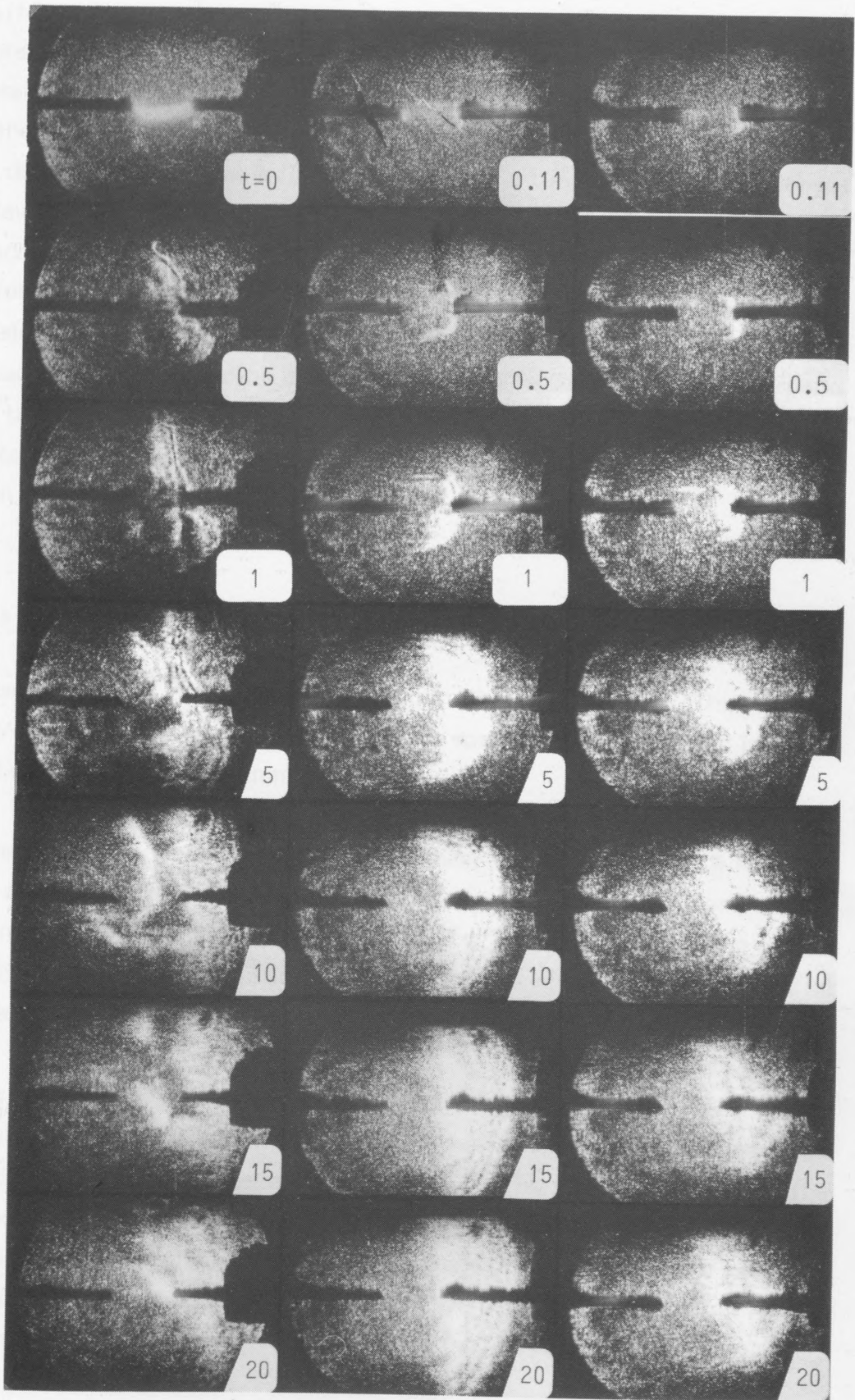
Schlieren photograph series III-14.



4 mJ/1 μ s spark in air
(4 mm gap).

4.2 mJ/50 μ s spark in
air (4 mm gap).

2.7 mJ/100 μ s spark in
air (4 mm gap).



4 mJ/1 μ s spark in
stabiliser cloud
(4 mm gap).

4.2 mJ/50 μ s spark in
stabiliser cloud
(4 mm gap).

2.7 mJ/100 μ s spark in
stabiliser cloud
(4 mm gap).

The effect of such a reduction in spark power on the ignition of the dust/air mixture can be seen from the sequences in Photograph III-15. These show successful ignitions using the three sparks above. It is immediately apparent that the kernel/flame front size is reduced dramatically with an increase in spark duration (a decrease in spark power). At a time when the front leaves the viewing field in the first series (between 5 and 10 ms) the kernel sizes for the second and third sparks are still very much smaller. It may be concluded, therefore, that judgement of the 'success of ignition' on the kernel size can be misleading. The expansion rate of the kernel, due to the initial power in the spark, was also different in each case, being faster for the shorter spark. From the photographs alone, however, it was not possible to relate these rates to the ignition mechanism. A more complete interpretation is given in Section 6.

5.3.4 Results and discussion for the fifth schlieren series e)

The results for this comparison are shown in Photograph III-16. This shows a 2.8 mJ/46 μ s spark for a 2 mm gap and the spark already presented in series d), (4.2 mJ/50 μ s), for the 4 mm gap.

The results for the sparks in air show a slower expansion for the 4 mm gap. This is despite the fact that a greater spark energy is being used compared to the 2 mm case. The shorter lifetime of the kernel for the 2 mm gap is probably due to the significant electrode quenching during its initial expansion.

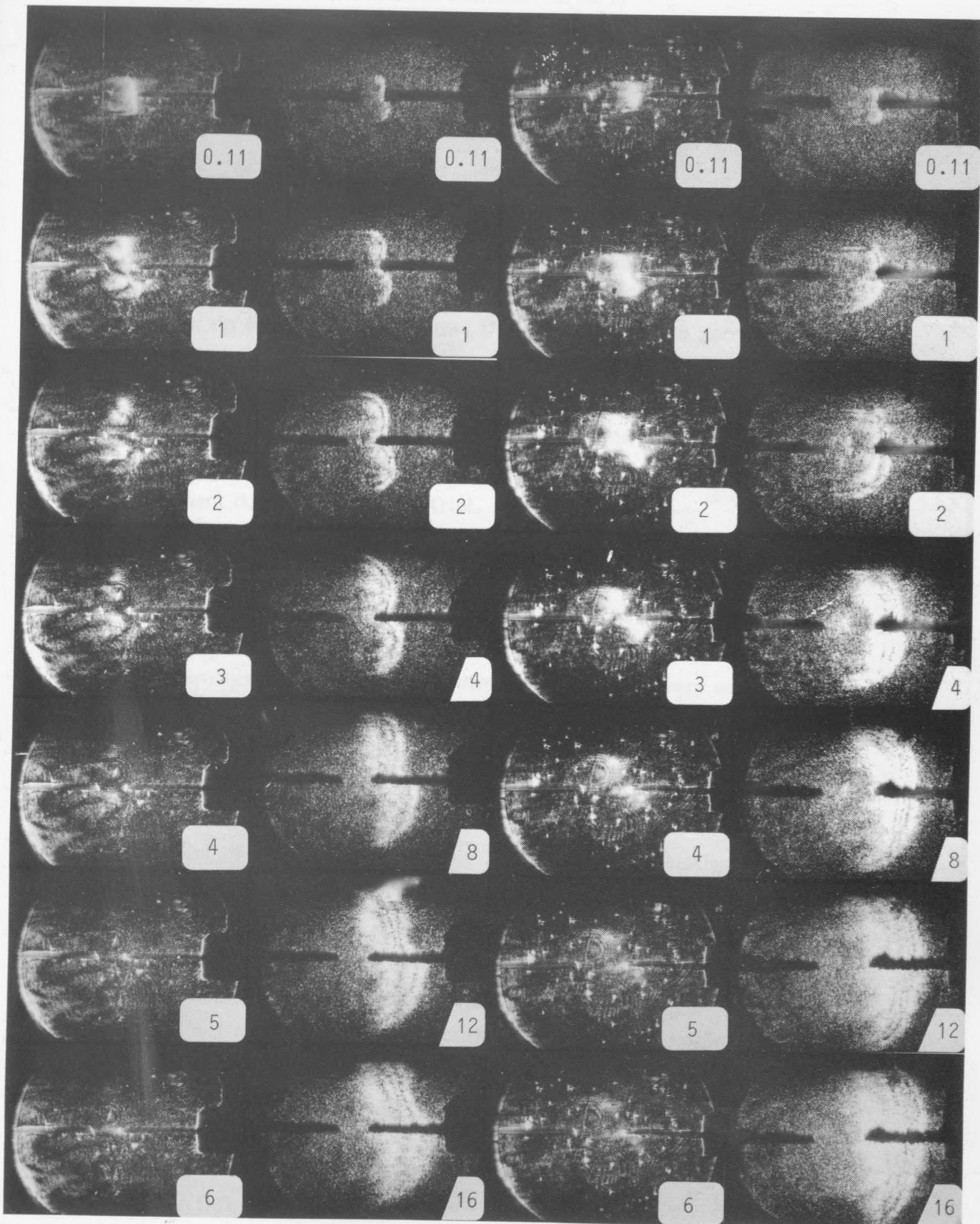
Ignition occurred in both cases, although for the 2 mm gap, the flame kernel was distorted at its point of contact with the electrode (one supposes that this occurred at both electrodes) as it expanded. The rates of a growth of the flame kernels were otherwise similar. This is expected because the initial spark powers were also similar in magnitude. The photographs confirm, therefore, that where ignition occurred, a given spark power led to a similar growth of the flame kernel in the first 16 ms for both 2 mm and 4 mm gaps.

2.8 mJ/46 μ s spark in
air (2 mm gap).

2.8 mJ/46 μ s spark in
stabiliser cloud
(2 mm gap).

4.2 mJ/50 μ s spark in
air (4 mm gap).

4.2 mJ/50 μ s spark in
stabiliser cloud
(4 mm gap).



2.8 mJ/46 μ s spark in air (2 mm gap).

2.8 mJ/46 μ s spark in stabiliser cloud (2 mm gap).

4.2 mJ/50 μ s spark in air (4 mm gap).

4.2 mJ/50 μ s spark in stabiliser cloud (4 mm gap).

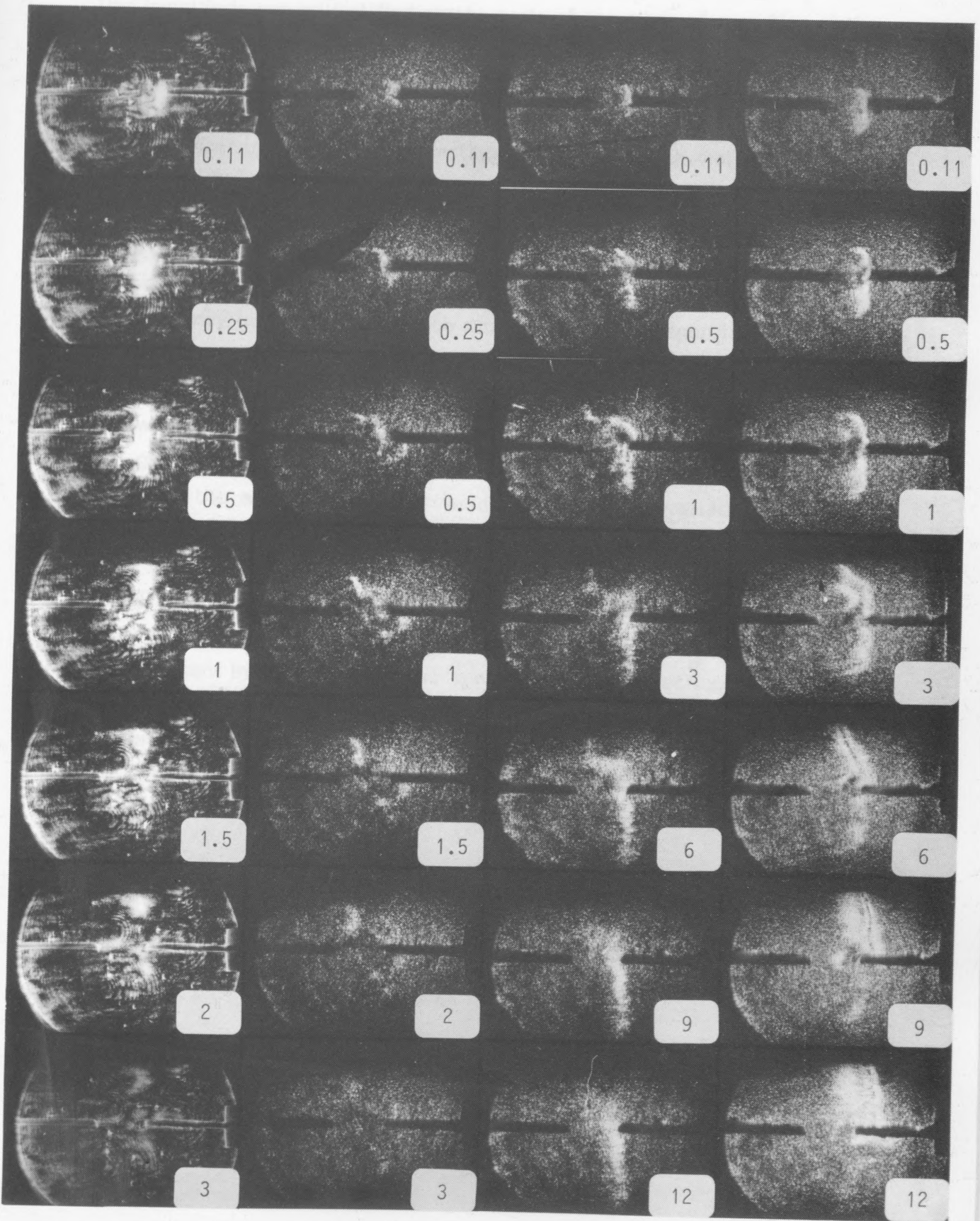
5.3.5 Results and discussion for the sixth schlieren series f)

The results for this series show three attempts at ignition of the dust/air mixture using the same spark where ignition probability was equal to 0.4. The results are shown in Photograph III-17.

The first series shows the development with time of a 1.33 mJ/0.5 μ s spark in air, using a 4 mm gap. This shows a kernel lifetime in the gap area of about 3 ms. The second series shows an unsuccessful ignition. Here it appears that very little dust has been ignited over the lifetime of the spark kernel. The third series, on the other hand, shows the start of a flame kernel expanding beyond 3 ms, but again, ignition is unsuccessful as indicated by the dying of the front after 6 ms. Finally, the fourth series shows a successful ignition where after some 6 ms the flame propagates upwards. The reason for this is unknown but may have been due to a local air current in the explosion vessel at this moment during this ignition trial.

The last series in Photograph III-17, for successful ignition, shows a similar growth of the spark/flame kernel within 12 ms, as was observed in the previous photographs for other sparks, where ignition was successful. It appears, therefore, that successful ignition is determined very early on in the growth of the flame. The last three series' shown here, would indicate, by a straightforward comparison of the kernel sizes in the first two rows of pictures, that this time is within 110 μ s.

Assuming first of all, that spark energy is identical in all trials, the question remains as to the reason why ignition is observed in one trial and not in others. This could be due to small variations in the concentration of dust in the gap volume at the moment of spark discharge from one shot to the next. This effect could also be combined with the effect of agglomerates in the spark gap, acting as heat sinks during initial spark kernel expansion. Furthermore, variations in the distribution of constituent particle sizes and shapes could add to the problem. For a low spark energy (compared to an energy of the same duration that gives an ignition probability of 1), small variations in the amount and distribution of dust in the spark gap may significantly influence the initial stages of spark kernel development. As spark energy is increased these variations may become less important and only affect the success of ignition if they deviate strongly from the 'normal' value. This could explain the scatter in results in Figures III-31 - III-36, and be why ignition probabilities were found to range from 0 to 1 according to spark duration for a wide range of spark energies.



1.33 mJ/0.5 μ s spark in air (4 mm gap).

1.33 mJ/0.5 μ s spark in stabiliser cloud (4 mm gap).
No ignition.

1.33 mJ/0.5 μ s spark in stabiliser cloud (4 mm gap).
No ignition.

1.33 mJ/0.5 μ s in stabiliser cloud (4 mm gap).
Ignition.

This hypothesis can be justified on the basis of the mode of operation of the dispersion system used in these tests. It would be unnatural to assume that dust distribution in the gap was identical between shots using either dispersion method. In particular, the variations in ignition success when varying dispersion pressure by fractions of a bar, which were observed in optimisation tests (see Section 3.4), revealed the sensitivity of the system. And as stated above, when spark energy lies near the minimum required to ignite an optimum mixture, any slight variations in the mixture will necessarily affect ignition success. Large variations, being statistically less frequent, may influence the ignition success for ignition energies lying above the minimum. This was more marked for the double dispersion results, where scatter for all gap widths was greater than for the single dispersion results. This would indicate that reproducibility of the dust distribution in the gap was greater using single dispersion. One would ultimately expect that increasing the energy sufficiently would overcome any variations, however large. This was in fact observed in the ignition tests.

a) The spark discharge produces a volume of hot air, which rapidly cools. In addition to these possible variations in dust concentration in the gap, there is also an inherent uncertainty in the spark discharge characteristics when dust is present in the gap. Previous 'energy checks' (see Section 3.5) revealed small variations of up to 5% in discharged energy for repeated dispersions. Such energy fluctuations due to variations in dust distribution in the gap, and also small physical changes in the spark generating circuit, could help to account for the observed results in ignition tests and in Photograph III-17.

The model is introduced at this stage in order to form a basis for the interpretation of the ignition and schlieren results. Following this, the results are summarised in the form of a general relationship between spark ignition energy and duration.

6.2 The model

The ignition model is built on the assumption that 'successful' ignition is achieved when a critical volume of the dust/air medium is raised to a given temperature. This temperature is that which enables a self-propagating flame to develop through the medium. The establishment of such a volume depends upon the rate of expansion of the hot kernel produced by the spark, the heat

6. A SIMPLIFIED SPARK IGNITION MODEL FOR DUST CLOUDS

6.1 Introduction

From the schlieren results, a picture began to emerge that could explain the ignition results for the three gap widths, as shown in Figures III-31 - III-36. In particular, the results revealed important roles of the spark power, and the subsequent rate of expansion of the hot spark kernel, and quenching losses to the electrodes as the flame kernel grew. In addition, the ignition success appeared to be governed by events occurring very early on in the growth of the flame, probably within 100 μ s.

These observations suggested a simple model for the ignition process, based on heat gain, by the combustion of dust, as the spark kernel first begins to expand. This assumes that the ignition process follows the following steps.

- a) The spark discharge produces a volume of hot air, which rapidly cools due to expansion (this volume is known as the 'kernel').
- b) Heat is transferred from this volume to the dust particles, causing them to produce hot fuel gas or vapour. This may be produced by volatilisation, carbonisation and the reaction of the dust particles with air.
- c) The hot fuel gas or vapour ignites spontaneously as it mixes with the hot kernel, forming a flame volume, and expanding the kernel further.
- d) The kernel volume and temperature increase, as the direct result of combustion, above the values due to spark kernel expansion alone.

The model is introduced at this stage in order to form a basis for the interpretation of the ignition and schlieren results. Following this, the results are summarised in the form of a general relationship between spark ignition energy and duration.

6.2 The model

The ignition model is built on the assumption that 'successful' ignition is achieved when a critical volume of the dust/air medium is raised to a given temperature. This temperature is that that enables a self-propagating flame to develop through the medium. The establishment of such a volume depends upon the rate of expansion of the hot kernel produced by the spark, the heat

energy produced by combustion of the medium, and the losses incurred to the volume during its growth. Assuming a constant specific heat capacity of the medium, the growth of such a volume required for ignition may be qualitatively expressed in terms of a simplified heat energy density equation, as shown below.

$$\frac{\Delta W}{\Delta t} = \frac{\Delta W_A}{\Delta t} - \frac{\Delta W_B}{\Delta t} - \frac{\Delta W_C}{\Delta t} - \frac{\Delta W_D}{\Delta t} \quad (1)$$

(term A) (term B) (term C) (term D)

where t is time following initial spark kernel formation, and W is heat energy per unit volume of the expanding kernel,

and terms ΔW_A , ΔW_B , ΔW_C and ΔW_D refer to

ΔW_A a change in energy density due to heat energy liberated by combustion of dust at the kernel front (a heat gain term)

ΔW_B a change in energy density due to quenching of the kernel by the dust cloud (a heat loss term)

ΔW_C a change in energy density due to quenching of the kernel by the spark electrodes (a heat loss term)

ΔW_D a loss of heat from the spark kernel to the surroundings as it expands

Alternatively, one may speak of an area of the flame front, associated with which is a critical temperature gradient. In order to produce this area, a certain quantity of dust must be fired.

This simplified equation treats the kernel expansion following spark discharge and the formation of an expanding spark kernel as it develops into a flame kernel. The transition from 'spark' to 'flame' kernel is one where expansion of the kernel becomes predominantly dependent upon heat liberation by combustion (term A) and is not a sudden process. The term 'kernel', used through the ensuing analyses, refers to the expanding hot volume of dust/air,

be it due to the spark alone or the combined effect of the spark and combustion. Thus it is freely used to mean 'spark' or 'flame' kernel up until a propagating flame front is established.

As was also shown in Part 2, the initial rate of discharge of spark energy in the gap governs the initial rate of kernel expansion. For pulse-type discharges, this was expressed in terms of the spark power, i.e. the higher the power the more rapid the expansion. This basic relationship is assumed in the analysis that follows. This model assumes the initial formation of an expanding kernel, but it does not include terms for the dissipation of spark energy in the spark gap, or losses of spark energy in any manner or form. These losses would include conductive, radiative and shock losses from the spark channel to the surroundings. In the analysis that follows, the 'success of ignition' is studied on the basis of the above model, and rather than investigate the physical parameters (and losses) of the discharge channel due to a given spark, that lead to a kernel expanding at a given rate, the kernel is examined in terms of the spark causing it. The energy losses from the discharge channel have been studied by a number of workers^{28,41} and were not investigated in this work.

An additional term, W_{CRIT} , is also used in the analysis, and is defined as the 'critical energy density'. This value marks the stage of kernel expansion at which a self-propagating flame through the dust/air medium is possible. The time at which this occurs following spark ignition is referred to as the 'critical induction time', t_{CRIT} . The speed of kernel expansion following this time is assumed to be ignition source independent and is given by the 'normal' flame speed, 's' through the dust/air medium. The value of 's' is mixture dependent, and depends upon dust concentration in the air medium, but may also be affected by other factors, such as turbulence in the dust/air mixture.

This definition of 'induction time' is not to be confused with the induction time for a single dust particle. This will depend upon the chemical composition of the particles and is a quantity governing the rate of chemical reaction through a particle/air mixture. Such a definition of induction time is based on a hypothetical, single particle, that is stationary in the pre-heat zone. Depending on the flame temperature, a given time will elapse before this particle is ignited at the flame front. As flame temperature increases, this induction time will decrease, and vice versa. If the flame temperature is

constant, which may be assumed for a constant flame speed through a homogeneous mixture, then the induction time will be directly related to the flame speed. Since the ignition of single particles depends upon the temperature of the approaching flame-front, and this is not constant during initial expansion of the spark kernel, the induction times for single particles will vary up until a self-propagating flame is established. For rapidly expanding kernels, where temperature falls rapidly with increasing distance from the spark gap, induction times will increase with distance. The exact time will depend upon the final temperature at the kernel front, as given by equation (1) above, and the velocity of kernel expansion.

This criterion is particularly important as the spark kernel just starts to expand, i.e. when the kernel temperature is much higher than that required to ignite most dusts. This initial value may typically reach $60.000 \text{ K}^{57,58}$. As the kernel begins to expand, the temperature at the kernel core falls dramatically and unless burning particles contribute to the expansion, the energy density at the kernel front will be too low to ensure ignition. The energy density at any instant will therefore be given by the expansion rate of the kernel and the ignition temperature of a single particle, i.e. the induction time of a single particle as a function of the velocity of a temperature wave approaching it. This factor is clearly dependent upon the chemical composition of the particles and will vary with particle size and shape etc. It will also depend upon the state of movement and separation of the particles at the moment of ignition.

For arc-type discharges in air, the initial, maximum temperature of the kernel is approximately constant (see Appendix 3) and limited by the continuous energy losses to the electrodes and surroundings. The effect of increasing discharge energy will be to increase the cooling time of the kernel, as it expands. This will, according to the above model, cause an increase in energy density due to term A.

When analysing the spark kernel development with time, the term gap volume 'V' is also introduced. This term refers to the spherical volume contained by the electrode gap for a specific gap width. It is a hypothetical measure of kernel size assuming a spherical growth of the spark kernel, and is assumed to represent the stage of kernel growth beyond which electrode quenching decreases.

7. No attempt in the current work was made to measure values of energy density over the kernel expansion times. The results and analyses were qualitative, as they were based primarily on schlieren photographs. Measurement of these variables could be the subject of further work. Furthermore, the physical mechanisms of heat transfer and chemical kinetics during kernel development and flame propagation were not dealt with here. The model given here simply assumes heat transfer either to or from the kernel, without attempting to include the manner in which it takes place.

7.1 Discussion of the results of schlieren series a)

The increase in time that was observed, from the transition from a spark kernel to a self-propagating flame front, using the double dispersion system, marks an increase in the critical induction time due primarily to conducted losses from the developing spark kernel as it moves downstream. These are represented by term B in equation 1 (see Section 6.2). Increased heat loss in this case while the kernel is expanding will serve to decrease the total energy density in the kernel at a given instant. This is because the volume of hot air produced by the spark (see a) in Section 6.1) is increased due to forced convection. The time taken to reach the critical density W_{CRIT} is therefore increased. Indeed, should ΔW_D be increased further, then a point will be reached when total heat loss will exceed gain due to chemical energy liberated by reaction. This will be the case when air movement is increased further. Such a result might be expected when using high transport velocities in the pneumatic transport of powders. Results⁶² have suggested that very high spark energies would be required for ignition, even of sensitive powders, at high transport velocities (typically $> 20 \text{ m.s.}^{-1}$).

The time at which W_{CRIT} is reached is marked by the position of initial independent flame propagation, assuming a linear dust/air velocity. In addition, accepting the assumptions made so far, subsequent flame propagation, once the ignition criterion has been satisfied, will depend only on the dust/air mixture. In the cases presented here, one would expect that once a flame had begun to propagate in the more turbulent mixture (the double dispersion case), it would develop faster than in the 'static' case. This is borne out by the rapid flame growth in the last 5 pictures of Photograph III-9. These show that from 5 ms to 9 ms, flame growth is comparable to that in the single dispersion case from 1 ms to 5 ms, due to dust/air movement (turbulence) alone. More rapid flame growth is also seen in the high-speed series in Photographs III-10 and III-11.

7. DISCUSSION OF THE SCHLIEREN RESULTS FOR THE STABILISER POWDER BASED ON THE IGNITION MODEL

The results of the schlieren tests are now discussed separately, on the basis of the ignition model. In this way, a picture is steadily established that describes the processes leading to ignition, using the various configurations of gap width, spark energy and spark duration.

7.1 Discussion of the results of schlieren series a)

The increase in time that was observed, from the transition from a spark kernel to a self-propagating flame front, using the double dispersion system, marks an increase in the critical induction time due primarily to conducted losses from the developing spark kernel as it moves downstream. These are represented by term B in equation 1 (see Section 6.2). Increased heat loss in this case while the kernel is expanding will serve to decrease the total energy density in the kernel at a given instant. This is because the volume of hot air produced by the spark (see a) in Section 6.1) is increased due to forced convection. The time taken to reach the critical density W_{CRIT} is therefore increased. Indeed, should ΔW_B be increased further, then a point will be reached when total heat loss will exceed gain due to chemical energy liberated by reaction. This will be the case when air movement is increased further. Such a result might be expected when using high transport velocities in the pneumatic transport of powders. Results^{6B} have suggested that very high spark energies would be required for ignition, even of sensitive powders, at high transport velocities (typically $> 20 \text{ m.s.}^{-1}$).

The time at which W_{CRIT} is reached is marked by the position of initial independent flame propagation, assuming a linear dust/air velocity. In addition, accepting the assumptions made so far, subsequent flame propagation, once the ignition criterion has been satisfied, will depend only on the dust/air mixture. In the cases presented here, one would expect that once a flame had begun to propagate in the more turbulent mixture (the double dispersion case), it would develop faster than in the 'static' case. This is borne out by the rapid flame growth in the last 5 pictures of Photograph III-9. These show that from 5 ms to 9 ms, flame growth is comparable to that in the single dispersion case from 1 ms to 9 ms, due to dust/air movement (turbulence) alone. More rapid flame growth is also seen in the high-speed series' in Photographs III-10 and III-11.

The net effect of a moving dust/air mixture at the moment of ignition is, therefore, a) to prolong the time to the critical stage at which ignition proper can be said to begin, independent of the ignition source, and b) to increase flame propagation speed once ignition has been initiated, due to a higher rate of heat transfer in the dust/air mixture.

Some checks may now be made, based on the above hypotheses. There it was stated that the position of initial flame propagation using double dispersion (independent of the ignition source), marks the time at which the critical ignition criterion has been satisfied in the static case. From the final sequence of schlieren photographs, this is seen to be reached after ~ 5 ms, where flame propagation for the double dispersion case begins 3.2 cm downstream of the electrodes. This scenario is depicted in Figure III-41.

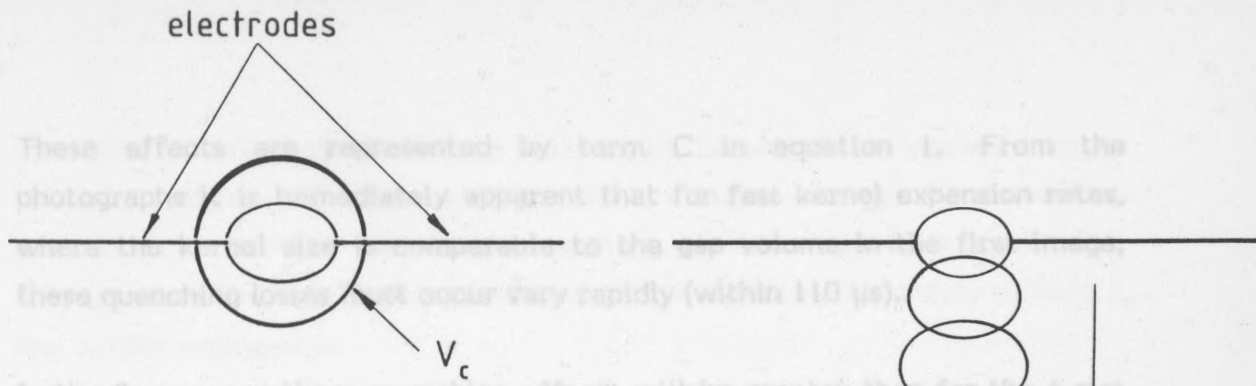
The schlieren image at this point in time, showing initial, independent flame propagation, compares favourably with that for the single dispersion case after 1 ms. This is of course a rough comparison only, made on the basis of the area of activity from the photographs. It confirms, however, an estimate of critical induction times for the two dispersion methods. In the first case this time is approximately 1 ms and in the second case, approximately 5 ms.

7.2 Discussion of the results of schlieren series' b) and c)

The results from the first comparison, b), indicate that electrode quenching plays a decisive role in the establishment of a critical energy density required for ignition. In both the 2 mm and 4 mm cases, the spark electrodes undoubtedly serve to remove heat from the spark kernel as it forms and subsequently expands. The removal of heat, or quenching, takes on two forms,

- a) a quenching of the spark while it is forming, and
- b) a quenching of the spark/flame kernel as it is expanding to a diameter comparable with the gap width

Figure III-41. Simplified model of ignition for both dispersion methods. "Static" refers to an essentially turbulent-free cloud whereas "dynamic" implies that dust particles are moving with a fixed velocity at the moment of ignition.



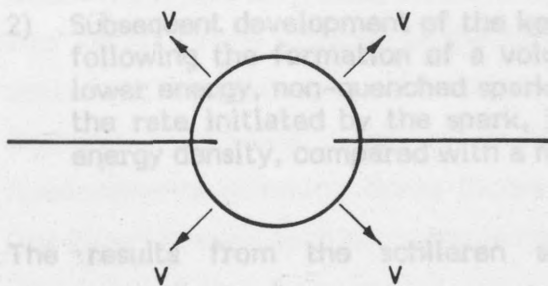
Fast expansion of spark kernel to a volume V_c where energy density is sufficient to ensure further expansion.

Time required ≈ 1 ms.

Slow expansion of kernel to volume V_c due to heat losses to mixture as kernel moves downstream.

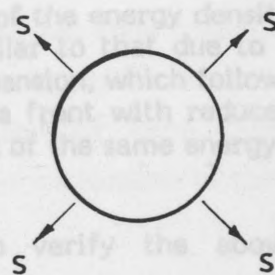
Higher discharge energy required to offset these losses.

Time required ≈ 5 ms.



Subsequent flame velocity (v) mixture dependent and independent of ignition source.

STATIC



Subsequent flame velocity (s) mixture dependent and higher than v due to increased cloud turbulence.

DYNAMIC

Figure III-41. Simplified model of ignition for both dispersion methods. 'Static' refers to an essentially turbulent-free cloud whereas 'dynamic' implies that dust particles are moving with a fixed velocity at the moment of ignition.

These effects are represented by term C in equation 1. From the photographs it is immediately apparent that for fast kernel expansion rates, where the kernel size is comparable to the gap volume in the first image, these quenching losses must occur very rapidly (within 110 μ s).

few simple assumptions.

In the 2 mm case these quenching effects will be greater than for the 4 mm case. This is because the surface area of the (spherical) volume (V) enclosed by the electrodes is eight times smaller and approaches the electrode surface area. Thus at a very early stage, where the spark kernel is expanding to and beyond this volume, a significant quenching effect will take place. At the same time, due to the rapid expansion rate, the heat liberated by chemical reaction will be concentrated at the kernel front. This front is necessarily thin because the energy that has initiated it has been significantly reduced by the aforementioned quenching effects. As a result, the A term in equation 1, which represents the heat gained by combustion, is reduced as the kernel first starts to develop. The overall increase in energy density, ΔW , is therefore also reduced within the time it takes for this volume to form, as compared to the case where quenching had not taken place at this early stage. The whole process may therefore be split into two stages:

- 1) The combustion energy released within the time that the kernel expands to a volume ($\sim V$), is reduced due to the reduction in available ignition energy by quenching terms a) and b).
- 2) Subsequent development of the kernel is a function of the energy density following the formation of a volume V, and is similar to that due to a lower energy, non-quenched spark. In this case, expansion, which follows the rate initiated by the spark, is in the form of a front with reduced energy density, compared with a non-quenched spark of the same energy.

The results from the schlieren sequences help to verify the above hypotheses. For the 2 mm gap, the image intensity is reduced at an early stage (as is seen in the first and second photographs of the second series) due to spark/kernel quenching (see a) and b) above). For the 4 mm gap the quenching effects are very much lower and at a comparable time (e.g. after 0.5 ms) the overall energy density is higher, which is implied by a brighter and broader image. At 1 ms heat losses to the dust air mixture (term B) for the 2 mm gap exceed the heat gain by combustion and the flame front starts to die. On the other hand, a higher energy density at this time for the 4 mm gap, due to more dust burning, ensures a further development of the flame, despite losses due to term B.

The question raised by the second analysis, c), is: why should a lower energy, longer duration spark cause ignition, when a higher energy, short duration spark does not? An answer to this question can be sought by analysing the schlieren results using the simple heat-balance equation (1), and by making a few simple assumptions.

As was postulated in the previous analysis, ignition in the first case, using a short duration spark, is hindered by two factors. The first, and most significant, is the effect of electrode quenching on the spark and spark kernel within the time it takes to develop to a size comparable to the gap width. The second factor is due to the rapid expansion of the kernel, due to the high initial power in the discharge. This rapid growth, in addition to the decrease in available ignition energy due to quenching, means that a limited volume of dust is burning at any given time, and thus contributing to the increase in energy density (given by the A term in equation 1).

This reduction in the volume of burning dust is caused primarily by the difference between the spark kernel expansion rate and the quiescent burning rate of the dust air mixture. For the two sparks used in this test, the kernel sizes and expansion rates are plotted in Figures III-42 and III-43. Also shown is the 4 mJ/1 μ s spark using a 4 mm gap, from the previous analysis. These points were obtained from a more extensive range of photographs than those shown here, and are linear measurements across the schlieren field. 'Kernel size' refers to the distance of the furthest point on the kernel edge from the centre of the spark gap. An estimate of kernel diameter may be made by doubling this value. The rates of expansion are derived from these measurements assuming linear increases for each 125 μ s increment in time (the time between each photographic event).

An important assumption is now made that the expansion of the flame front through the dust/air mixture, at a velocity greater than the normal flame velocity through the mixture, will cause incomplete combustion of the mixture at the flame front. The degree of combustion will depend upon the flame-front temperature, its velocity and the induction time and chemical composition of the particles, as discussed in Section 6. We may further assume that the 'quiescent' flame speed through the dust-air mixture is given by the final points on the figures for the 'successful' ignitions, as an approximate measure only. This value is approximately 0.35 ms^{-1} . One

can see that the first curve in Figure III-42, that for unsuccessful ignition using the 2 mm gap, shows a rapid, initial expansion of the flame front of some 7 ms^{-1} . This large difference in expansion rate, coupled with the quenched conditions in the initial stages of expansion means quite literally that not enough dust is burning to aid flame propagation (i.e. contribution to ΔW in equation (1) by term A is very low). The reason for this, as stated earlier, is due first to a reduction in kernel energy in the gap, and second to the low quantity of burning dust at the stage at which the kernel expands beyond the gap volume.

The curves in Figures III-42 and III-43 showing the kernel size and expansion rate for the second spark in Photograph III-13, show a lower expansion rate than the first. This implies that more dust in the gap volume is contributing to the combustion process at an early stage. Despite high quenching losses (terms B and C) sufficient energy remains in the kernel, which expands at a slow enough rate, to ensure an increase in term A, and thus the overall energy density, eventually leading to ignition.

This is confirmed by the final series in Photograph III-13, which shows the lower expansion rate of the flame front up to $\sim 1 \text{ ms}$ compared with the first spark but the obvious presence of a broader, more intense image, implying a greater energy density (more burning dust per unit volume).

The third curve in Figure III-43 shows the kernel size and expansion rate for the $4 \text{ mJ}/1 \mu\text{s}$ spark using a 4 mm gap. The high expansion rate using this spark still leads to ignition, probably because the quenching losses in the spark gap are very low compared to the heat gain by the (limited) volume of burning dust. Extending the previous argument further, one would expect that even for a 4 mm gap, where quenching losses are low, a lower limit of duration would exist for this energy at which spark kernel expansion is too fast to create a sufficient increase in combustion energy that offsets these losses. This may be the case for high energy, pure capacitive discharges. This is discussed in Sections 9 and 10.

The main conclusion from this analysis is that a rapid spark kernel expansion may be inefficient as an ignition source, because of the low contribution of combustion energy to the expanding kernel. On the other hand very slow expansion velocities would also be inefficient on these grounds, because of excessive quenching losses to the dust/air mixture.

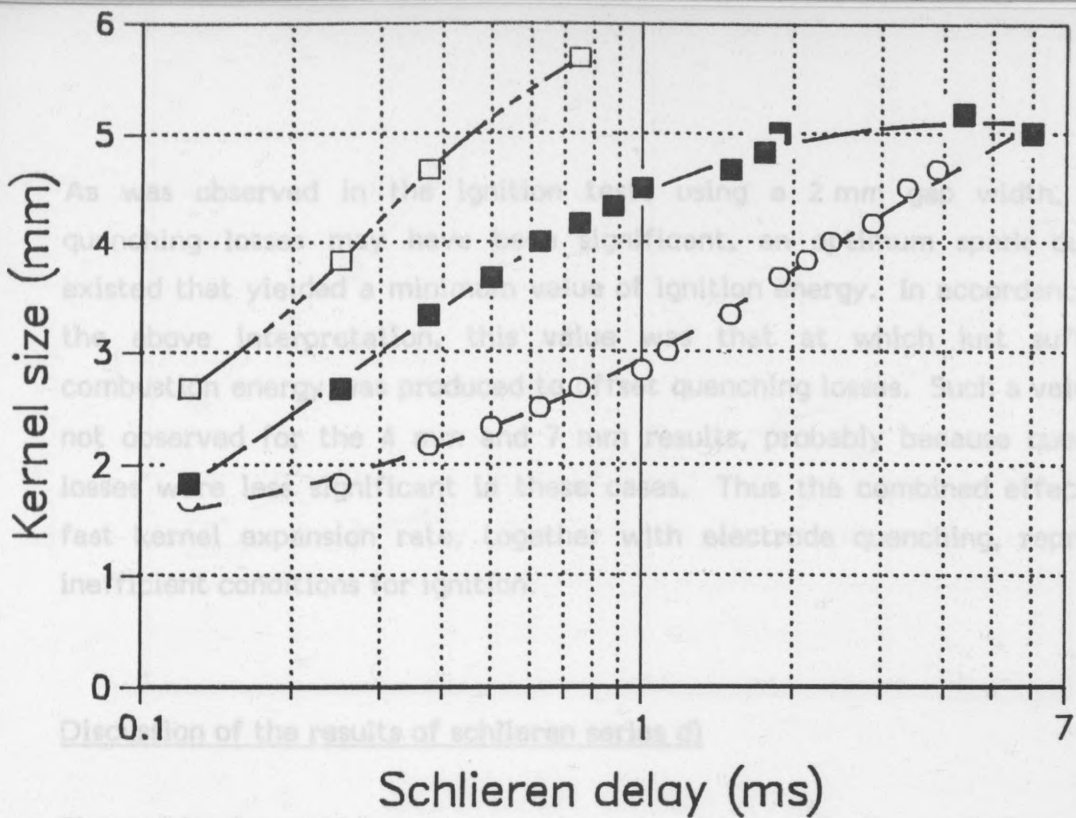


Figure III-42.

KERNEL EXPANSION FOR TWO GAP WIDTHS

- 3.8mJ/1µs SPARK/2mm GAP
- 2.8mJ/46µs SPARK/2mm GAP
- 4mJ/1µs SPARK/4mm GAP

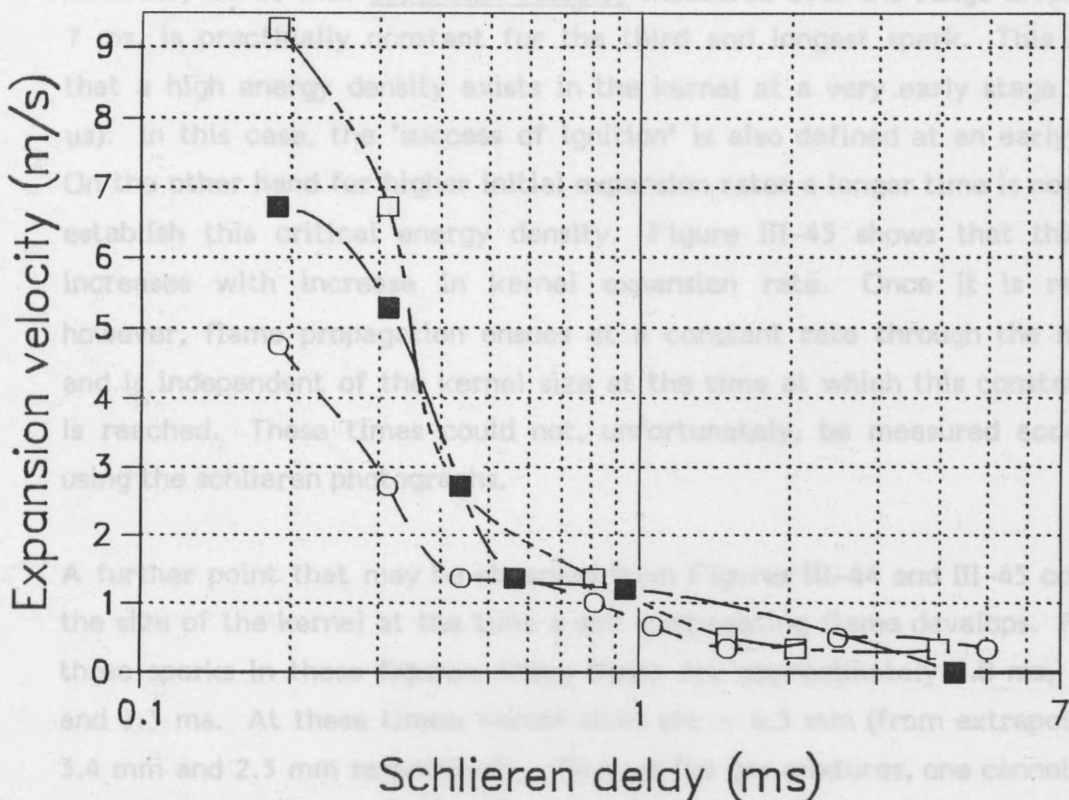
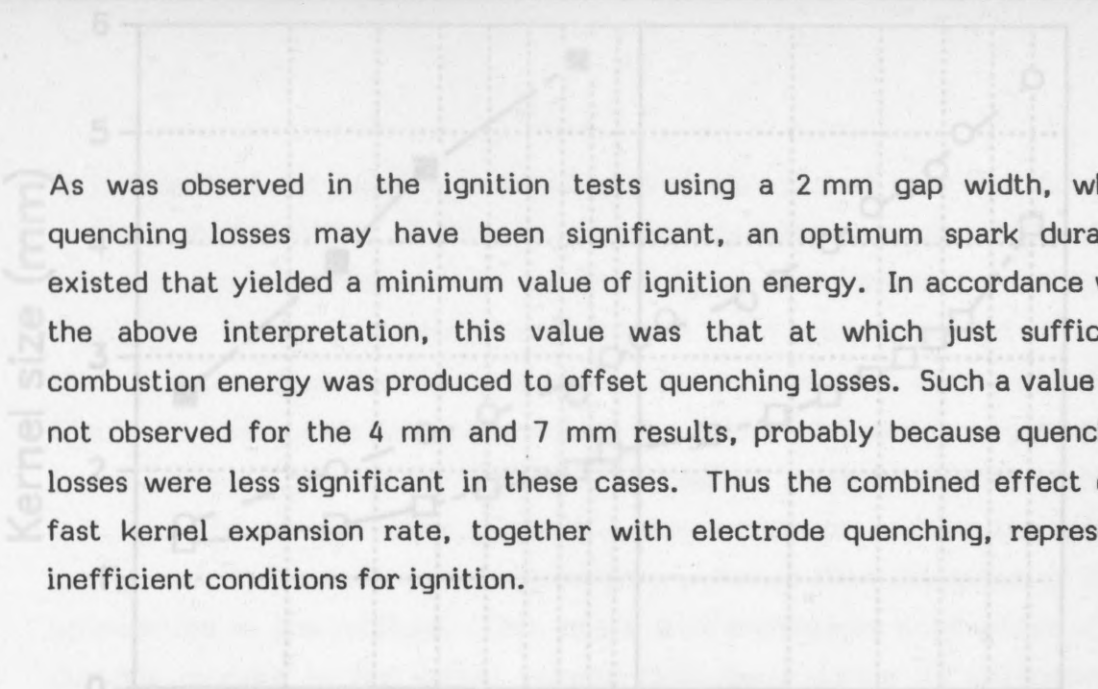


Figure III-43.

Figures III-42 and III-43.

Kernel sizes and expansion velocities for three sparks and two gap widths. 'Schlieren delay' refers to the time at which an image of the expanding kernel was recorded following spark discharge.



As was observed in the ignition tests using a 2 mm gap width, where quenching losses may have been significant, an optimum spark duration existed that yielded a minimum value of ignition energy. In accordance with the above interpretation, this value was that at which just sufficient combustion energy was produced to offset quenching losses. Such a value was not observed for the 4 mm and 7 mm results, probably because quenching losses were less significant in these cases. Thus the combined effect of a fast kernel expansion rate, together with electrode quenching, represents inefficient conditions for ignition.

7.3 Discussion of the results of schlieren series d)

The results from this comparison showed a decrease in the rate of expansion of the kernel as spark power was decreased, using three ignition sparks. Figure III-44 shows the increase in kernel size with time for the three sparks used in this comparison, obtained from a more extensive range of photographs than those shown here. These curves confirm the large differences in kernel size for the three sparks as a function of time. A glance at Figure III-45, however, shows that expansion velocity measured over the range 0.125 ms to 7 ms, is practically constant for the third and longest spark. This implies that a high energy density exists in the kernel at a very early stage ($\sim 125 \mu\text{s}$). In this case, the 'success of ignition' is also defined at an early stage. On the other hand for higher initial expansion rates a longer time is needed to establish this critical energy density. Figure III-45 shows that this time increases with increase in kernel expansion rate. Once it is reached, however, flame propagation ensues at a constant rate through the medium and is independent of the kernel size at the time at which this constant rate is reached. These times could not, unfortunately, be measured accurately using the schlieren photographs.

A further point that may be observed from Figures III-44 and III-45 concerns the size of the kernel at the time a self-propagating flame develops. For the three sparks in these figures, these times are approximately 1.8 ms, 1.5 ms and 1.3 ms. At these times, kernel sizes are ~ 6.5 mm (from extrapolation), 3.4 mm and 2.3 mm respectively. Thus, as for gas mixtures, one cannot speak of a critical kernel size necessary for ignition. Such a kernel size must be stated in terms of the temperature gradient at its front.

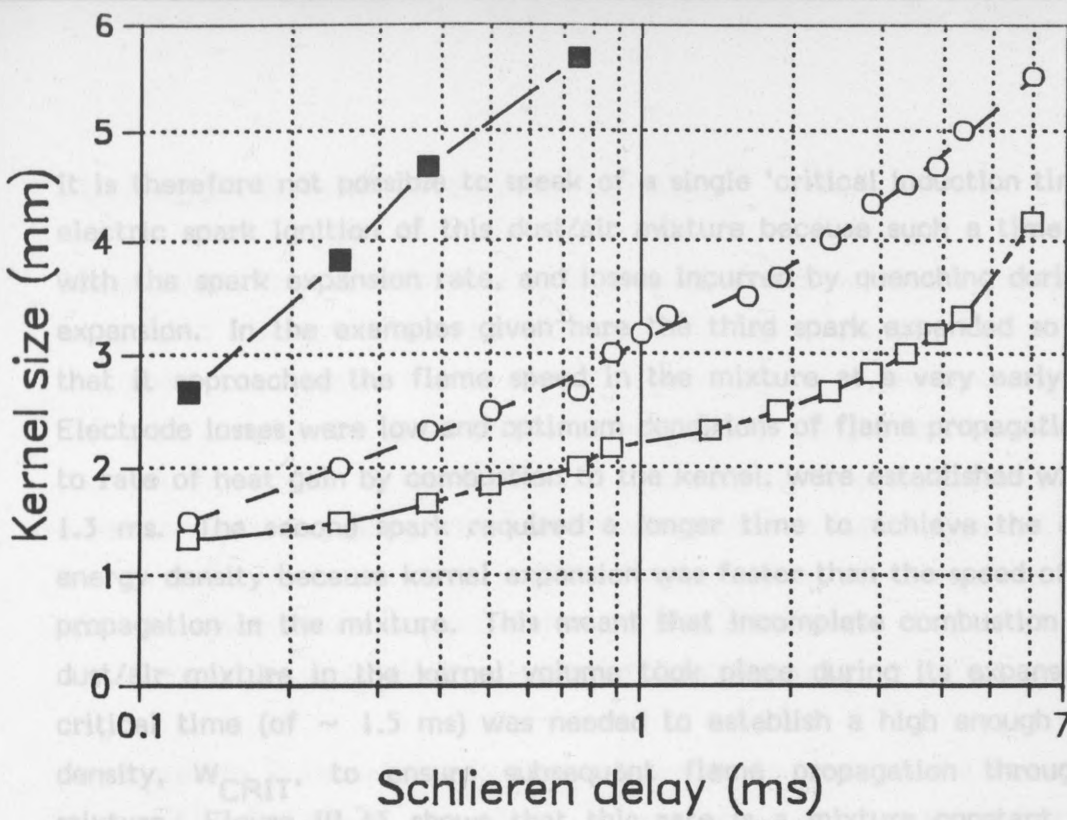


Figure III-44.

KERNEL EXPANSION FOR A 4mm GAP WIDTH

- **4mJ/1µs SPARK** (Solid line)
- **4.2mJ/50µs SPARK** (Dashed line)
- **2.7mJ/100µs SPARK** (Dashed line)

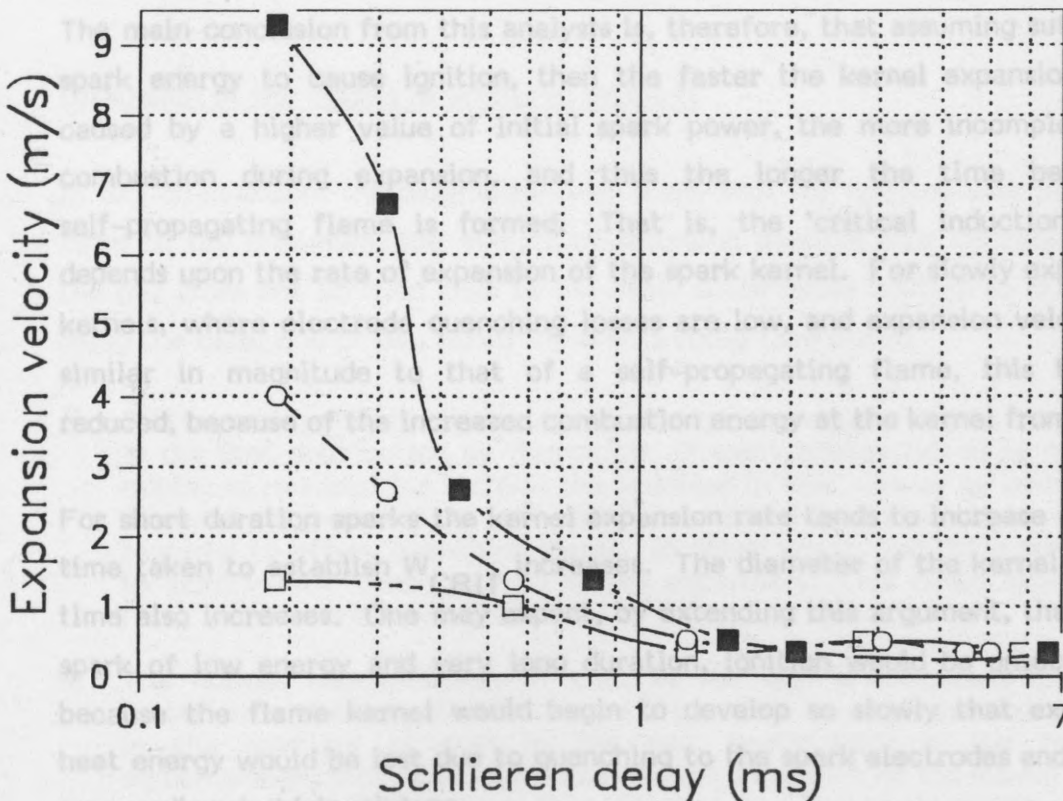


Figure III-45.

Figures III-44 and III-45.

Kernel sizes and expansion velocities for three sparks and a 4 mm gap width. 'Schlieren delay' refers to the time at which an image of the expanding kernel was recorded following spark discharge.

7.4 It is therefore not possible to speak of a single 'critical induction time' for electric spark ignition of this dust/air mixture because such a time varies with the spark expansion rate, and losses incurred by quenching during this expansion. In the examples given here the third spark expanded so slowly that it approached the flame speed in the mixture at a very early stage. Electrode losses were low and optimum conditions of flame propagation, due to rate of heat gain by combustion to the kernel, were established within ~ 1.3 ms. The second spark required a longer time to achieve the critical energy density because kernel expansion was faster than the speed of flame propagation in the mixture. This meant that incomplete combustion of the dust/air mixture in the kernel volume took place during its expansion. A critical time (of ~ 1.5 ms) was needed to establish a high enough energy density, W_{CRIT} , to ensure subsequent flame propagation through the mixture. Figure III-45 shows that this rate is a mixture constant and is independent of the ignition source once W_{CRIT} has been reached. Finally, the first and fastest spark is seen to require the longest time before W_{CRIT} is reached due to its very rapid initial expansion rate. This time is approximately 1.8 ms.

7.5 The main conclusion from this analysis is, therefore, that assuming sufficient spark energy to cause ignition, then the faster the kernel expansion rate, caused by a higher value of initial spark power, the more incomplete the combustion during expansion, and thus the longer the time before a self-propagating flame is formed. That is, the 'critical induction time' depends upon the rate of expansion of the spark kernel. For slowly expanding kernels, where electrode quenching losses are low, and expansion velocity is similar in magnitude to that of a self-propagating flame, this time is reduced, because of the increased combustion energy at the kernel front.

For short duration sparks the kernel expansion rate tends to increase and the time taken to establish W_{CRIT} increases. The diameter of the kernel at this time also increases. One may expect, by extending this argument, that for a spark of low energy and very long duration, ignition would be unsuccessful because the flame kernel would begin to develop so slowly that excessive heat energy would be lost due to quenching to the spark electrodes and to the surrounding dust/air mixture.

7.4 Discussion of the results of schlieren series e)

These results showed successful ignition using both 2 mm and 4 mm gaps and an ignition spark of similar duration and initial spark power. The effects of electrode quenching on kernel expansion were, however, evident using the 2 mm gap. Despite this loss, the increase in energy density due to combustion (term A in equation 1) was sufficient to ensure flame propagation as kernel expansion rate was slow. This quenching effect was not as apparent for the 4 mm results where the density of the flame front at the time of its contact with the electrodes was greater than for the 2 mm case. Relative heat loss due to quenching was therefore lower for the 4 mm gap.

The increases in kernel size and expansion rate for these sparks are shown in the previous Figures III-42 - III-45. A comparison shows very similar trends in expansion rate for both cases and 'critical ignition times', as defined in the previous analysis, are practically identical at ~ 1.5 ms. This result is expected because in both cases spark power is similar, implying a similar initial expansion rate. This is in fact slightly lower for the 2 mm gap because quenching during initial kernel expansion reduces the effective energy for ignition more than it does for the 4 mm gap.

7.5 Discussion of the results of schlieren series f)

In this comparison, the assumption was made that for ignition energies lying close to the minimum, the effects of changing particle size distributions in the gap from one ignition trial to the next, could cause ignition to fail. This being the case, one of two series' of events could take place:

- a) The normal concentration of dust in the gap is reduced due to a variation in the dust distribution by dispersion. If spark energy lies at or near the minimum required for ignition the increase in heat energy by combustion (term A in equation 1) will also be reduced to below the minimum required to offset quenching losses. In other words, too little dust burns to significantly contribute to kernel expansion. This could explain the results shown in the second series in Photograph III-17.
- b) The normal concentration of dust in the gap is increased due to a variation in the dust distribution by dispersion. In this case the increase in the quantity of dust in the gap, particularly in the form of agglomerates, may lead to an increase in quenching of the kernel by the air/dust mixture itself (term B in Equation 1). This could be the case for the third series in Photograph III-17. This series resembles that for the 3.8 mJ spark using a 2 mm gap, where electrode quenching (term C) was predominant.

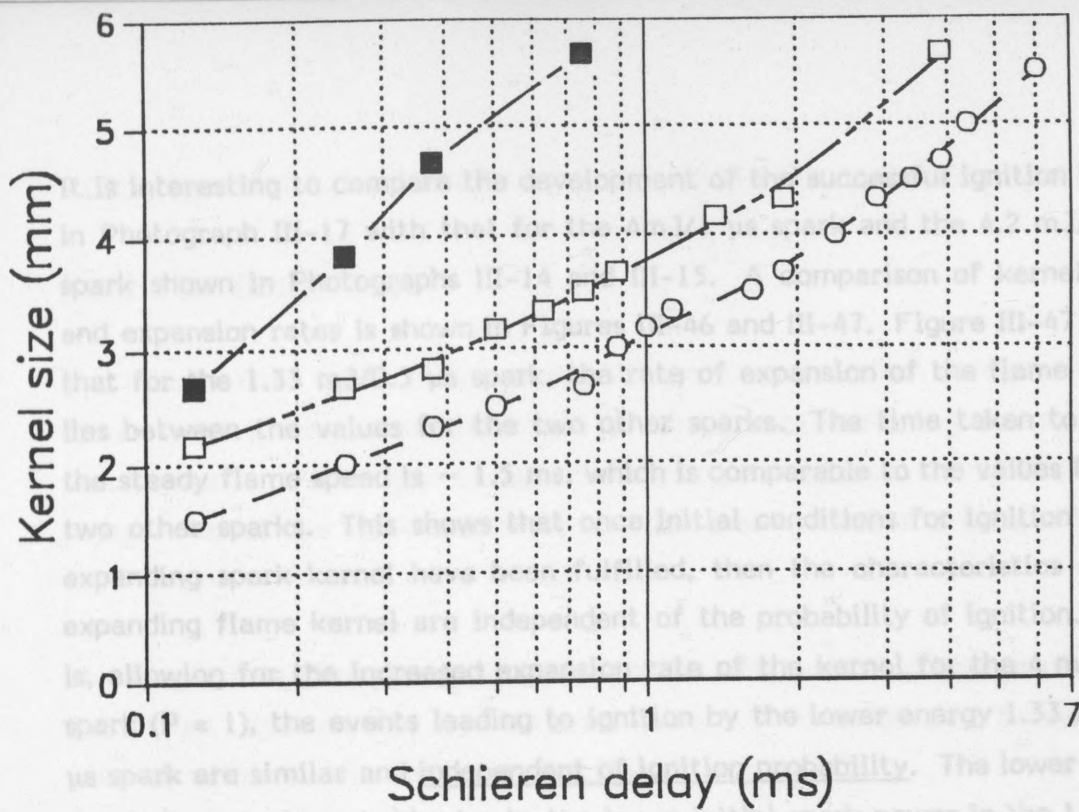


Figure III-46.

KERNEL EXPANSION FOR A 4mm GAP WIDTH

- 1.33mJ/0.5µs SPARK
- 4mJ/1µs SPARK
- 4.2mJ/50µs SPARK

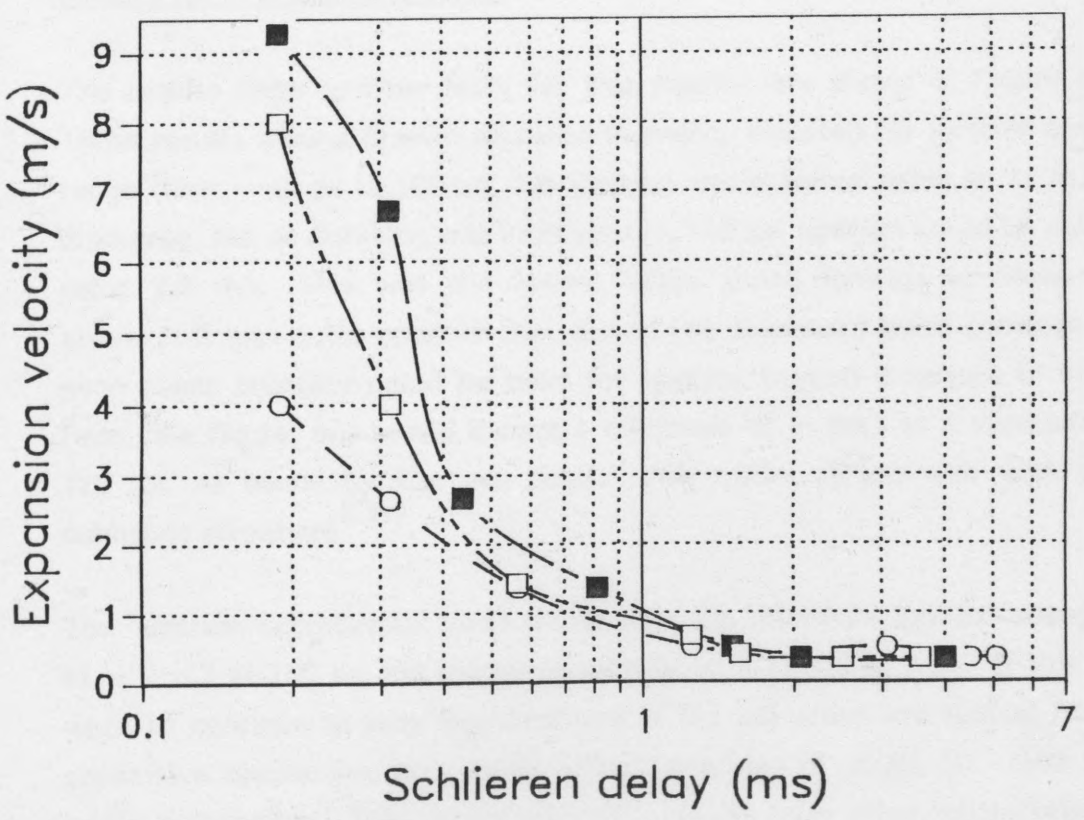


Figure III-47.

Figures III-46 and III-47.

Kernel sizes and expansion velocities for three sparks and a 4 mm gap width. 'Schlieren delay' refers to the time at which an image of the expanding kernel was recorded following spark discharge.

8.1 It is interesting to compare the development of the successful ignition kernel in Photograph III-17 with that for the 4mJ/1 μ s spark and the 4.2 mJ/50 μ s spark shown in Photographs III-14 and III-15. A comparison of kernel sizes and expansion rates is shown in Figures III-46 and III-47. Figure III-47 shows that for the 1.33 mJ/0.5 μ s spark, the rate of expansion of the flame kernel lies between the values for the two other sparks. The time taken to reach the steady flame speed is ~ 1.5 ms, which is comparable to the values for the two other sparks. This shows that once initial conditions for ignition in the expanding spark kernel have been fulfilled, then the characteristics of the expanding flame kernel are independent of the probability of ignition. That is, allowing for the increased expansion rate of the kernel for the 4 mJ/1 μ s spark ($P = 1$), the events leading to ignition by the lower energy 1.33 mJ/0.5 μ s spark are similar and independent of ignition probability. The lower initial expansion rate is probably due to the lower initial spark power in the 1.33 mJ spark. This is confirmed by a shorter lifetime of the spark kernel as shown in Photograph III-17. This reduction in power also leads to a shorter time to constant flame speed ($\sim 0.35 \text{ ms}^{-1}$) which is in accordance with the previous observations (see Figures III-42 - III-47).

8.2 Results for 'Lycopodium spores'

The results from ignition tests for this powder are shown in Figure III-49. These results show a drastic decrease in energy required for ignition over the range from $\sim 10 \mu$ s to 100 μ s. No ignition was obtained using an 11 mJ/5 μ s discharge, but as duration was increased to 100 μ s, ignition could be obtained using 2.7 mJ. This was the lowest value giving ignition in these tests, although it was quite possible that should the downward trend continue, then even lower energies could be used for ignition beyond durations of 100 μ s. From the figure, one would expect a minimum of ~ 2 mJ at a duration of $\sim 120 \mu$ s, as bound by the arc limit. This value agrees well with values published elsewhere^{2,3,7}.

The 'ignition uncertainty' band shows that the minimum ignition energy lies at ~ 2 mJ at 100 μ s and increases sharply to > 11 mJ at 5 μ s. If this curve were to continue to very low durations ($< 0.1 \mu$ s) which are typical for pure capacitive discharges, one would expect energies of about 50 - 100 mJ to ignite lycopodium. This agrees well with results from other laboratories^{1,59}. Because the results tended to resemble those for the stabiliser

8. RESULTS AND DISCUSSION OF IGNITION TESTS USING OTHER POWDERS

8.1 Results for 'Benzanthron'

The results from ignition tests using this powder are shown in Figure III-48. These results show a similar trend to those obtained using the stabiliser powder for a 4 mm gap except that energies required for ignition were higher. As for the stabiliser, these energies were practically independent of spark duration from 0.2 μ s to 100 μ s.

The lowest measured energy yielding ignition was 1 mJ at durations of 0.3 μ s and 35 μ s. Ignition was also obtained using 1.2 mJ at 80 μ s. These points were all within the limitation imposed by the arc limit.

Also shown in this figure is the region of 'ignition uncertainty'. This covers the range 0.7 mJ to 1.2 mJ over the range 0.3 μ s to 80 μ s. The minimum ignition energy is expected to lie in this region.

8.2 Results for 'Lycopodium spores'

The results from ignition tests for this powder are shown in Figure III-49. These results show a drastic decrease in energy required for ignition over the range from \sim 10 μ s to 100 μ s. No ignition was obtained using an 11 mJ/5 μ s discharge, but as duration was increased to 100 μ s, ignition could be obtained using 2.7 mJ. This was the lowest value giving ignition in these tests, although it was quite possible that should the downward trend continue, then even lower energies could be used for ignition beyond durations of 100 μ s. From the figure, one would expect a minimum of \sim 2mJ at a duration of \sim 120 μ s, as bound by the arc limit. This value agrees well with values published elsewhere^{2,3,7}.

The 'ignition uncertainty' band shows that the minimum ignition energy lies at \sim 2 mJ at 100 μ s and increases sharply to $>$ 11 mJ at 5 μ s. If this curve were to continue to very low durations ($<$ 0.1 μ s) which are typical for pure capacitive discharges, one would expect energies of about 50 - 100 mJ to ignite lycopodium. This agrees well with results from other laboratories^{1,59}. Because the results tended to resemble those for the stabiliser

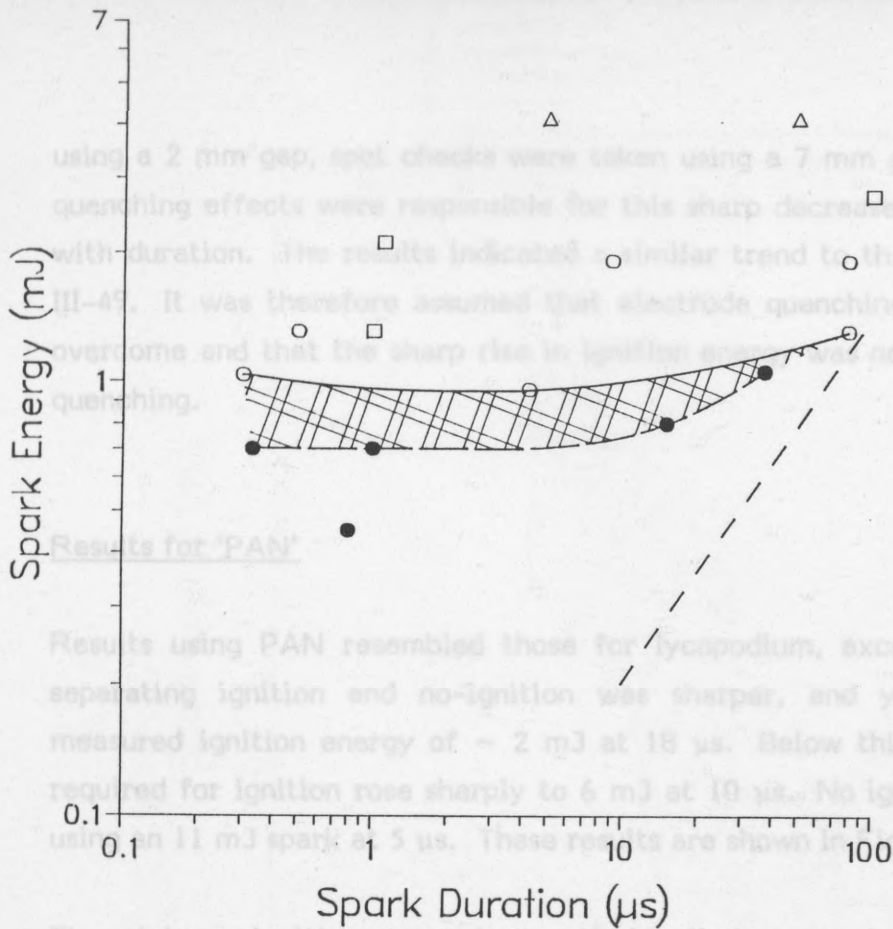


Figure III-48.

Ignition results for Benzanthron, using a 4 mm gap, showing 'region of ignition uncertainty' (MIE band).

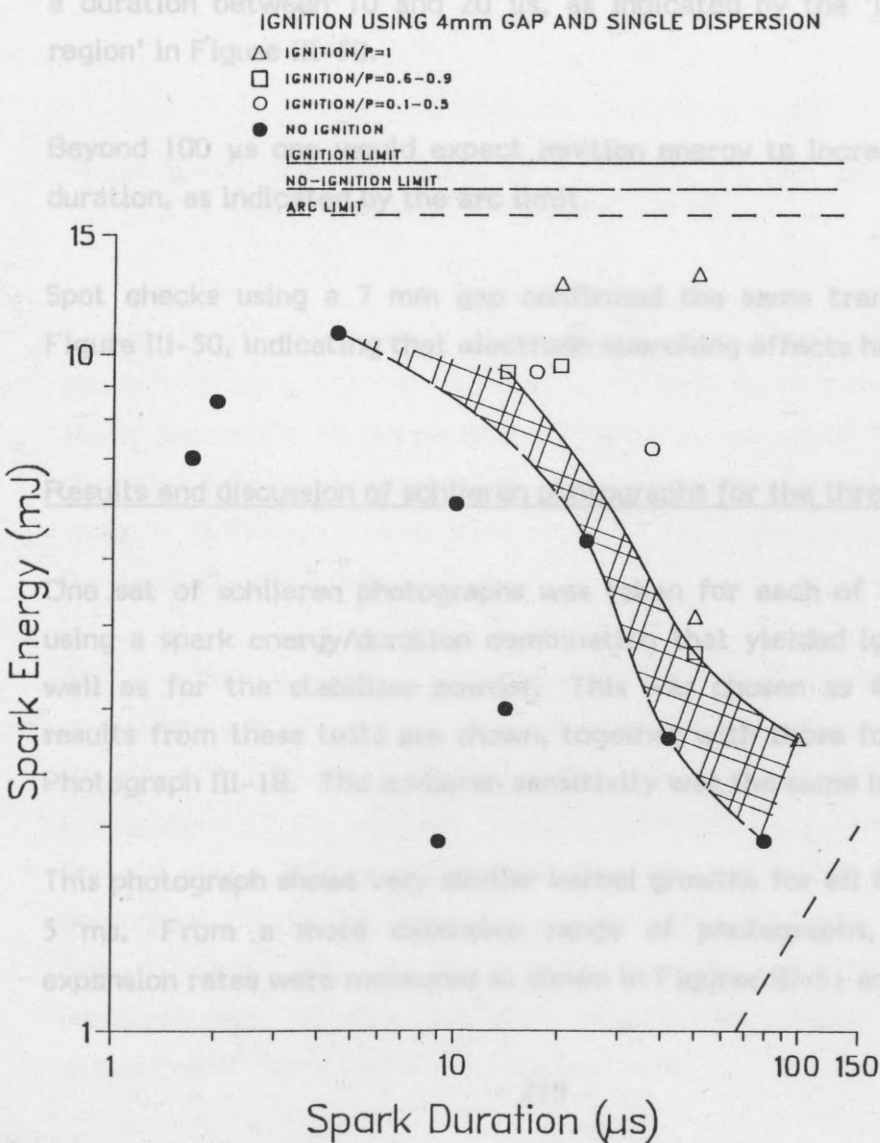


Figure III-49.

Ignition results for Lycopodium, using a 4 mm gap, showing 'region of ignition uncertainty' (MIE band).

using a 2 mm gap, spot checks were taken using a 7 mm gap to see whether quenching effects were responsible for this sharp decrease in ignition energy with duration. The results indicated a similar trend to that shown in Figure III-49. It was therefore assumed that electrode quenching effects had been overcome and that the sharp rise in ignition energy was not due to electrode quenching.

8.3 Results for 'PAN'

Results using PAN resembled those for lycopodium, except that the band separating ignition and no-ignition was sharper, and yielded the lowest measured ignition energy of ~ 2 mJ at $18 \mu\text{s}$. Below this duration, energy required for ignition rose sharply to 6 mJ at $10 \mu\text{s}$. No ignition was possible using an 11 mJ spark at $5 \mu\text{s}$. These results are shown in Figure III-50.

The minimum ignition energy is expected to lie between 1.45 mJ and 2 mJ at a duration between 10 and $20 \mu\text{s}$, as indicated by the 'ignition uncertainty region' in Figure III-50.

Beyond $100 \mu\text{s}$ one would expect ignition energy to increase with increasing duration, as indicated by the arc limit.

Spot checks using a 7 mm gap confirmed the same trend as was found in Figure III-50, indicating that electrode quenching effects had been overcome.

8.4 Results and discussion of schlieren photographs for the three powders

One set of schlieren photographs was taken for each of the three powders, using a spark energy/duration combination that yielded ignition for each, as well as for the stabiliser powder. This was chosen as 4.2 mJ/ $50 \mu\text{s}$. The results from these tests are shown, together with those for the stabiliser, in Photograph III-18. The schlieren sensitivity was the same in all four cases.

This photograph shows very similar kernel growths for all four powders, up to 5 ms. From a more extensive range of photographs, kernel sizes and expansion rates were measured as shown in Figures III-51 and III-52.

IGNITION USING 4mm GAP AND SINGLE DISPERSION

- △ IGNITION/P=1
- IGNITION/P=0.6-0.9
- IGNITION/P=0.1-0.5
- NO IGNITION

IGNITION LIMIT

NO-IGNITION LIMIT

ARC LIMIT

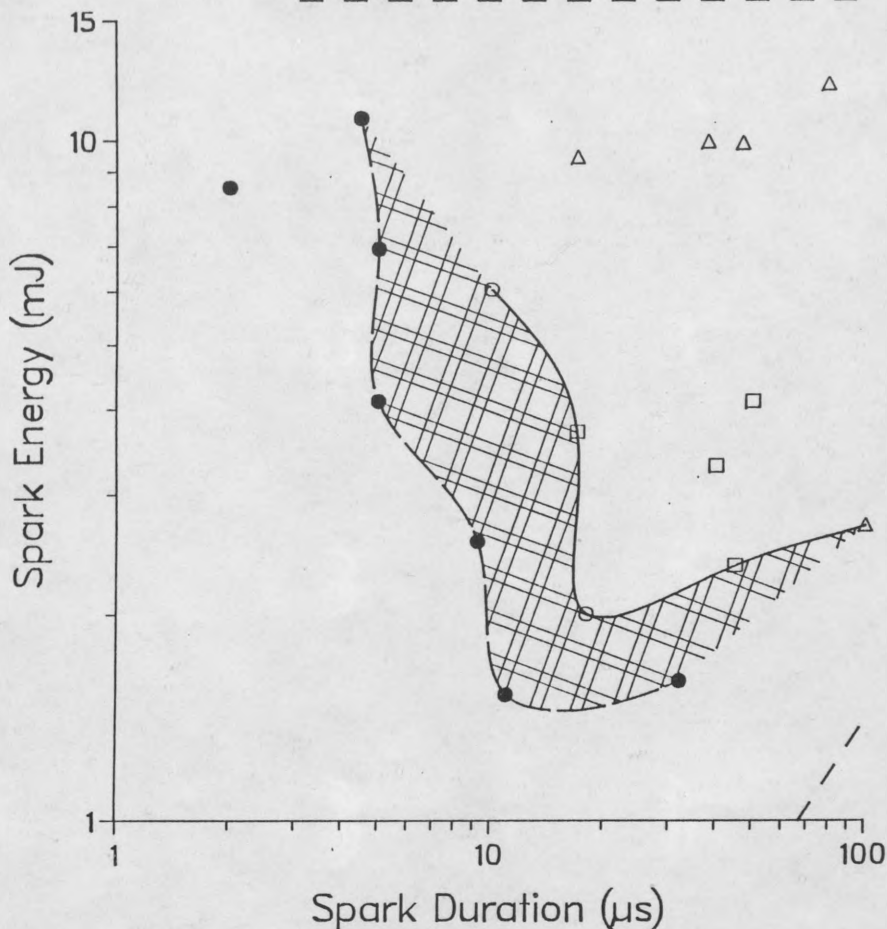
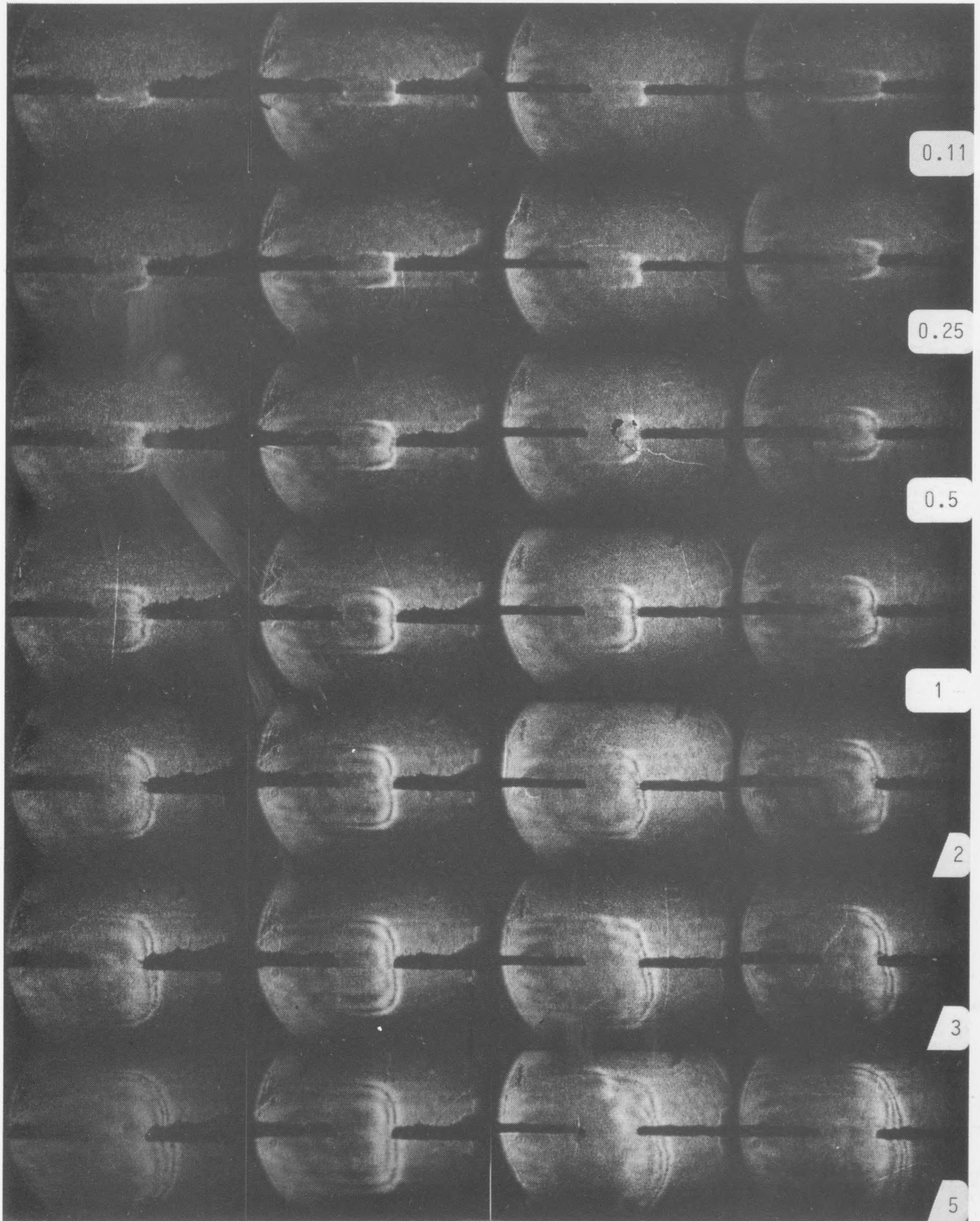


Figure III-50. Ignition results for PAN using a 4 mm gap, showing 'region of ignition uncertainty' (MIE band).

Figure III-51 shows that kernel sizes were practically identical for all powders up until ~ 2 ms, i.e. at a time which marked approximately constant flame speeds for all the powders. This value was about 4 mm, i.e. the kernel diameter was about 8 mm. The 'constant' expansion rates beyond this point were $\sim 0.35 \text{ ms}^{-1}$ (stabiliser), $\sim 0.37 \text{ ms}^{-1}$ (benzanthron), $\sim 0.73 \text{ ms}^{-1}$ (lycopodium) and 0.7 ms^{-1} (PAN).

The consistency of the results shown in Figures III-51 and III-52, is expected on the grounds of the initial kernel expansion rate due to the spark alone. In theory, the expansion of the kernel up until t_{CRIT} should be virtually independent of the dust-air mixture, although t_{CRIT} itself may vary from dust to dust. This is verified by the two curves and is quite clear from photograph III-18. The times t_{CRIT} are also seen to be quite similar for all four powders, and lie at around 1.5 ms. The rough nature of the measurements on the schlieren photographs meant that an accurate evaluation of these times could not be made.



4.2 mJ/50 μ s spark in stabiliser cloud (4 mm gap).

4.2 mJ/50 μ s spark in benzanthron cloud (4 mm gap).

4.2 mJ/50 μ s spark in lycopodium cloud (4 mm gap).

4.2 mJ/50 μ s spark in PAN cloud (4 mm gap).

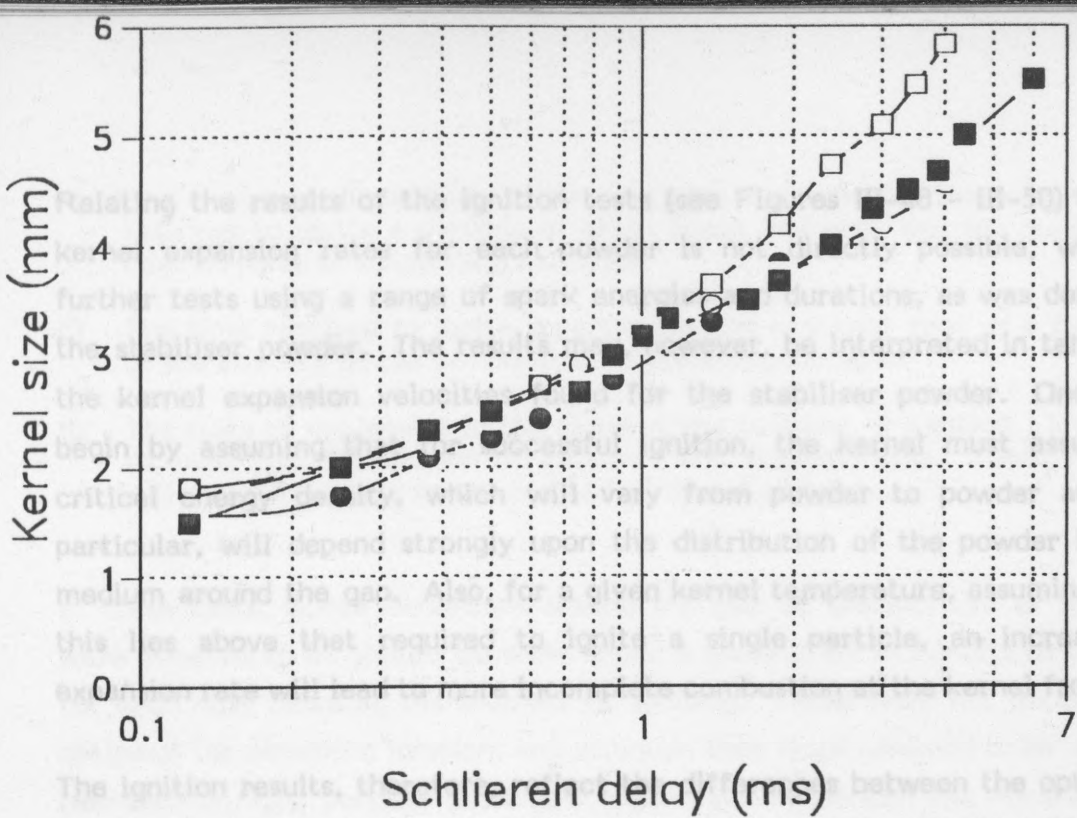


Figure III-51.

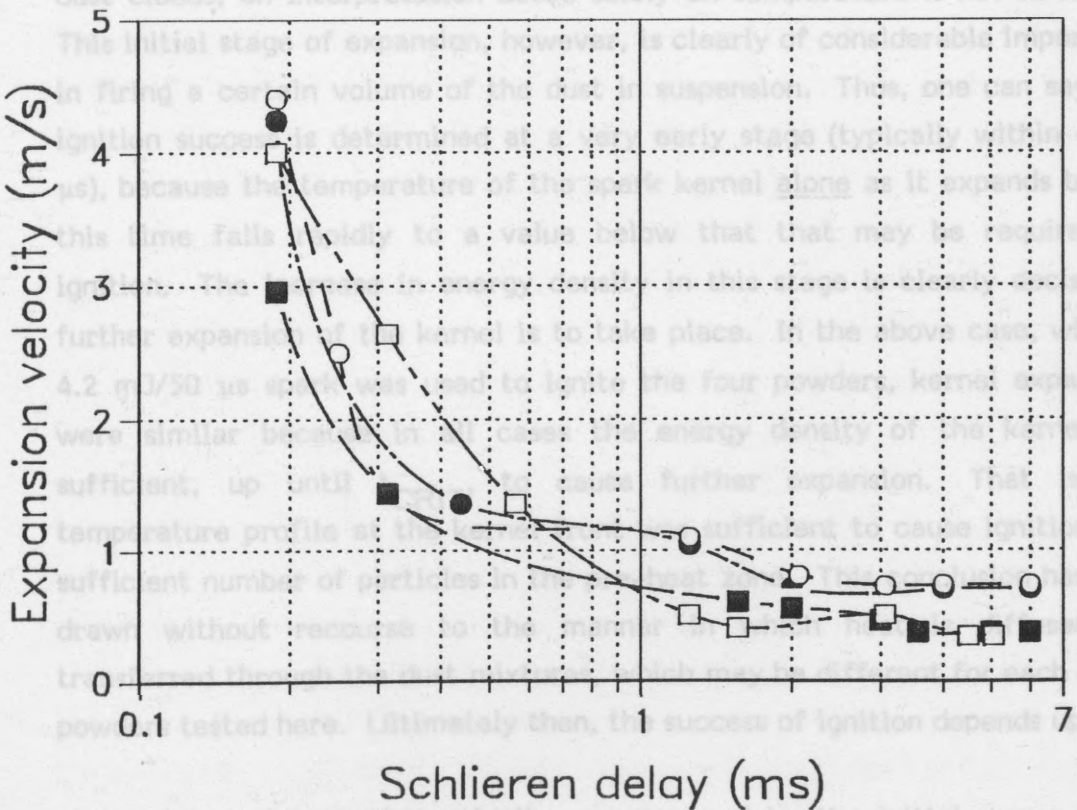


Figure III-52.

Figures III-51 and III-52.

Kernel sizes and expansion velocities for one spark (4.2 mJ/50 μ s), and the four tested powders. 'Schlieren delay' refers to the time at which an image of the expanding kernel was recorded following spark discharge.

Relating the results of the ignition tests (see Figures III-48 - III-50) to the kernel expansion rates for each powder is not directly possible, without further tests using a range of spark energies and durations, as was done for the stabiliser powder. The results may, however, be interpreted in terms of the kernel expansion velocities found for the stabiliser powder. One may begin by assuming that for successful ignition, the kernel must assume a critical energy density, which will vary from powder to powder and, in particular, will depend strongly upon the distribution of the powder in the medium around the gap. Also, for a given kernel temperature, assuming that this lies above that required to ignite a single particle, an increase in expansion rate will lead to more incomplete combustion at the kernel front.

The ignition results, therefore, reflect the differences between the optimum kernel expansion rates for a given spark energy or duration, for the different dust clouds. They cannot be judged on the basis of ignition temperature alone, as it is the combined effect of temperature and expansion rate that governs the success of ignition. Furthermore, in the first few microseconds of expansion, when the kernel temperature is typically some 1 - 2 orders of magnitude higher than measured values of minimum ignition temperature for dust clouds, an interpretation based solely on temperature is not sufficient. This initial stage of expansion, however, is clearly of considerable importance in firing a certain volume of the dust in suspension. Thus, one can say that ignition success is determined at a very early stage (typically within $\sim 100 \mu\text{s}$), because the temperature of the spark kernel alone as it expands beyond this time falls rapidly to a value below that that may be required for ignition. The increase in energy density in this stage is clearly decisive if further expansion of the kernel is to take place. In the above case, where a 4.2 mJ/50 μs spark was used to ignite the four powders, kernel expansions were similar because in all cases the energy density of the kernel was sufficient, up until t_{CRIT} , to cause further expansion. That is, the temperature profile at the kernel front was sufficient to cause ignition of a sufficient number of particles in the pre-heat zone. This conclusion has been drawn without recourse to the manner in which heat is diffused and transferred through the dust mixtures, which may be different for each of the powders tested here. Ultimately then, the success of ignition depends upon

- a) The kernel expansion velocity, as governed by the initial power in the spark (see Part 2).

b) The chemical composition of the particles, in particular the temperature required to ignite a particle of given shape and size, and the method of heat transfer to succeeding particles.

c) The time required to ignite a particle in the pre-heat zone as a function of the velocity of the temperature wave approaching it.

d) The state of movement in the cloud at the moment of ignition. This also includes the distribution of particles and agglomerates. These factors will depend strongly on the method of dust dispersion.

In these tests, where conditions around the gap at the moment of ignition were assumed to be similar between shots, a specific set of conditions existed for each dust cloud at the moment of ignition. These were not necessarily optimum for obtaining ignition, and although they were assumed to be 'static' (see Section 7.1), particle movement must have influenced the results. The results are therefore valid only for this dispersion method and do not necessarily represent absolute minimum ignition energy values.

For a 2 mm gap an increase in spark kernel expansion rate, due to a reduction in spark duration for a given energy, led to an increase in the minimum energy required to ignite the mixture. This was due to a loss of heat energy from the spark kernel at a very early stage of its development, primarily to the spark electrodes (term C). This was shown clearly in Figures III-31 and III-32. This meant that the effective energy in the kernel was reduced, whilst the kernel was contained in the gap volume V. The increase in energy density due to combustion (term A) was therefore reduced. If the effective spark energy under such conditions was reduced to a value lower than that required for ignition, then the total increase with time in ΔW_A was lower than the decrease given by $\Delta W_B + \Delta W_C$, and ignition was unsuccessful. An example of this was given in Figure III-43.

For a 4 mm and 7 mm gap this was not observed because electrode quenching of the spark kernel was reduced to an insignificant level (over the range of durations tested here). In this case, despite a high expansion rate and thus an increase in t_{CRIT} , ignition was obtained even when decreasing spark duration. For low energies and very low durations the increase in energy density with time was necessarily low, i.e. because of the fast expanding kernel front, only a limited number of dust particles at any time contributed to the increase in term A. Thus an increase in the time (t_{CRIT}) needed to reach ΔW_{CRIT} was expected. This was observed in the results for the fourth schlieren series.

9. INTERPRETATION AND DISCUSSION

9.1 Obtaining general relationships between spark energy and duration

The schlieren results presented in Section 5 showed that the rate of spark kernel expansion played a decisive role in determining the success of ignition of the stabiliser powder. If the spark energy was low, and the duration long, then kernel expansion was typically slow. This meant that increase in energy density by combustion of dust particles at the kernel front, was increased, up until t_{CRIT} , as compared with a faster kernel expansion and the same discharge energy. Such a fast expansion occurred for lower duration sparks. In this case the increase in energy density by combustion with time before t_{CRIT} , was reduced, due to the faster expansion of the flame kernel. This in turn led to a higher induction time (t_{CRIT}). In other words, a faster kernel expansion led to a reduction in the rate of increase of energy density of the expanding kernel.

For a 2 mm gap an increase in spark kernel expansion rate, due to a reduction in spark duration for a given energy, led to an increase in the minimum energy required to ignite the mixture. This was due to a loss of heat energy from the spark kernel at a very early stage of its development, primarily to the spark electrodes (term C). This was shown clearly in Figures III-31 and III-32. This meant that the effective energy in the kernel was reduced, whilst the kernel was contained in the gap volume V. The increase in energy density due to combustion (term A) was therefore reduced. If the effective spark energy under such conditions was reduced to a value lower than that required for ignition, then the total increase with time in ΔW_A was lower than the decrease given by $\Delta W_B + \Delta W_C$, and ignition was unsuccessful. An example of this was given in Figure III-43.

For a 4 mm and 7 mm gap this was not observed because electrode quenching of the spark kernel was reduced to an insignificant level (over the range of durations tested here). In this case, despite a high expansion rate and thus an increase in t_{CRIT} , ignition was obtained even when decreasing spark duration. For low energies and very low durations the increase in energy density with time was necessarily low, i.e. because of the fast expanding kernel front, only a limited number of dust particles at any time contributed to the increase in term A. Thus an increase in the time (t_{CRIT}) needed to reach ΔW_{CRIT} was expected. This was observed in the results for the fourth schlieren series.

The loss of kernel energy to the electrodes using a 2 mm gap served to increase the minimum energy required for ignition, from ~ 0.4 mJ using a 4 mm gap, to ~ 1 mJ. This minimum was observed at one duration only ($\sim 20 \mu\text{s}$) as opposed to a wide range of durations for the 4 mm and 7 mm gaps. In accordance with the above hypothesis, this duration, for this spark energy, represented the lowest possible expansion rate whereby an increase in energy density due to combustion just exceeded the loss terms due to quenching (terms B and C). Any further decrease in expansion velocity due to a decrease in energy or an increase in spark duration, would cause an increased loss of kernel energy due to quenching. Any increase in kernel expansion rate, due to a decrease in spark duration, would reduce the energy density due to combustion and thus a higher energy would be required to counteract this reduction.

To test this hypothesis, a final test was performed using the stabilizer and

The loss of heat energy to the electrodes must occur rapidly, however, i.e. before the spark kernel expands beyond the gap volume (V). This result is confirmed by the similarity of the results using a 2 mm gap and both dispersion methods. The same relationship between spark energy and duration was observed in both cases. Since, using double dispersion, the kernel moves downstream at a velocity of $\sim 8 \text{ m.s.}^{-1}$, the time taken to move 0.5 mm (the electrode diameter) is approximately $60 \mu\text{s}$. This represents an estimate of the time needed for quenching losses to occur. This value is in good agreement with that found from two other estimates made in the analyses. The first estimate, based on the evidence in Photograph III-17, was placed at well within $110 \mu\text{s}$, i.e. the time of the first schlieren exposure. The second estimate was made on the basis of the spark kernel decay times when comparing ignition for all four powders (see previous section). For the sparks used in this work, with energies of the order of 1 mJ, these decay times are probably well within $100 \mu\text{s}$. It appears, therefore, that events occurring within this time are decisive for ignition to be successful.

The main gap consists of two point electrodes, which in these tests were

One can also stipulate conditions for the 4 mm and 7 mm gaps where an increase in spark kernel expansion rate due to a decrease in spark duration, would eventually cause a rapid rise in spark energy required for ignition. This would be due to the loss of heat energy to the dust/air mixture itself (term B), and a very low increase in the combustion energy (term A). From the above arguments the time required to establish a self-propagating kernel at flame speed 's' would increase, as would the kernel size at this time. One

can picture a case where, keeping energy at the minimum measured here (~ 0.4 mJ), and decreasing duration below $0.2 \mu\text{s}$ (the shortest used in these tests), spark energy would have to increase to offset loss term B, due to the very fast kernel expansion rate.

Such a relationship would also be expected for the Benzanthron powder, where the energy \rightarrow duration trend was similar to that for the stabiliser. The other two powders, lycopodium and PAN, showed such a relationship in the working range of the tests. The differences observed between the four powders reflected the fact that a determination of a critical expansion rate, for a given spark energy and a given powder, is ultimately dependent upon chemical factors, i.e. the composition of the particles.

To test this hypothesis, a final test was performed using the stabiliser and Benzanthron powders and a pure capacitive discharge circuit as shown in Figure III-53. This figure shows a simplified circuit diagram of the '3-point gap', a standardised system currently in use in various European laboratories¹³. It operates as follows: A high-voltage supply charges up capacitor C to voltage V via a large resistance R. This voltage is slightly lower than that required for static breakdown of the spark gap G. Breakdown of the gap is caused by a pre-ionisation of the main gap by the third electrode which forms gap g. This is triggered at a chosen delay following dust dispersion in the explosion vessel, in which the electrodes are mounted. The trigger pulse for this electrode is obtained from an induction coil, similar to a car-ignition coil.

The spark energy in gap g, when the third electrode is triggered, is assumed to be lower than 0.1 mJ. The discharge in this gap is not visible to the unaided eye. Discharged spark energy is given by $0.5 CV^2$, as it is assumed that all stored capacitive energy appears in the gap G.

The main gap consists of two point electrodes, which in these tests were identical with those used in the previous experiments. All gap components, save the matching resistors, which were replaced by solid brass rods, were identical to those used previously. The third electrode was of the same form as the first two (0.5 mm diameter, stainless steel). The explosion vessel used for these tests was a modified Hartmann tube apparatus. Dust was placed in the base of the vessel in a dispersion cup and a cloud formed by dispersing it upwards. The ignition spark was triggered after a chosen delay time.

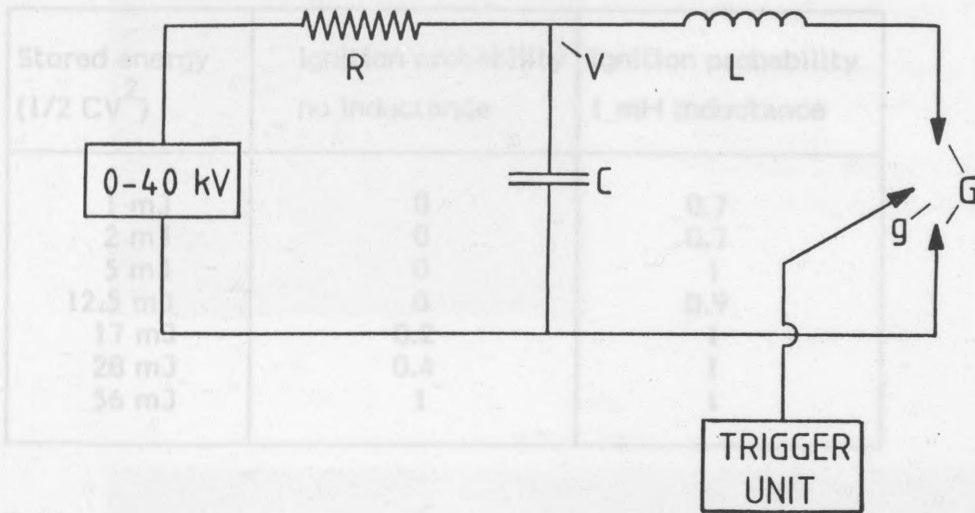


Table III-2. Ignition results using a capacitive discharge circuit and the Benzanthron powder.

Figure III-53. The three electrode capacitive spark discharge circuit.

After optimising the ignition delay time and the mass of dispersed dust in the standard manner, the capacitance C was adjusted for a fixed voltage V . The stored energy was thus increased accordingly. The capacitor was mounted on the electrode contacts on the vessel walls and the charging resistor R connected directly to the capacitor high voltage terminal. This reduced stray capacitance and inductance to a minimum. Using a 4 mm gap width as before, a range of capacitive energies were used, and ignition probabilities recorded for 10 ignition trials. These were as shown below in Tables III-1 and III-2. Also shown are the probabilities of ignition when a 1 mH inductor was placed between the capacitor and high-voltage electrode.

Stored energy ($1/2 CV^2$)	Ignition probability no inductance	Ignition probability 1 mH inductance
1 mJ	0	0.4
2 mJ	0	0.8
5 mJ	0	1
12.5 mJ	0	1
17 mJ	0.5	1
28 mJ	0.9	1
56 mJ	1	1

Table III-1. Ignition results using a capacitive discharge circuit and the stabiliser powder.

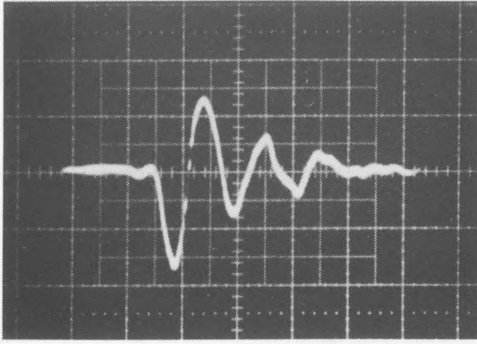
Stored energy (1/2 CV ²)	Ignition probability no inductance	Ignition probability 1 mH inductance
1 mJ	0	0.7
2 mJ	0	0.7
5 mJ	0	1
12.5 mJ	0	0.9
17 mJ	0.2	1
28 mJ	0.4	1
56 mJ	1	1

Table III-2. Ignition results using a capacitive discharge circuit and the Benzanthron powder.

These tables show an increase in spark energy, for capacitive discharges of an order of magnitude required to ignite both the stabiliser and Benzanthron powders. The effect of including an inductance was to reduce the stored energy required for ignition, as has been observed by other workers^{1,2,3,7,9}. Energy values using the inductor were similar to those observed in the previous experiments.

In order to confirm the possible increase in spark kernel expansion velocity for capacitive discharges, as compared with longer discharges, oscillographic recordings of the spark current waveform in the discharge were made. These were obtained by mounting a measurement resistance on the gap-earth terminal as before (see Part I). Measurements were made for three sparks: first a 1 mJ capacitive spark, then the same spark using an inductance whereby ignition was obtained, and finally a 17 mJ capacitive spark where ignition was just obtained. These are shown in Photographs III-19 - III-21.

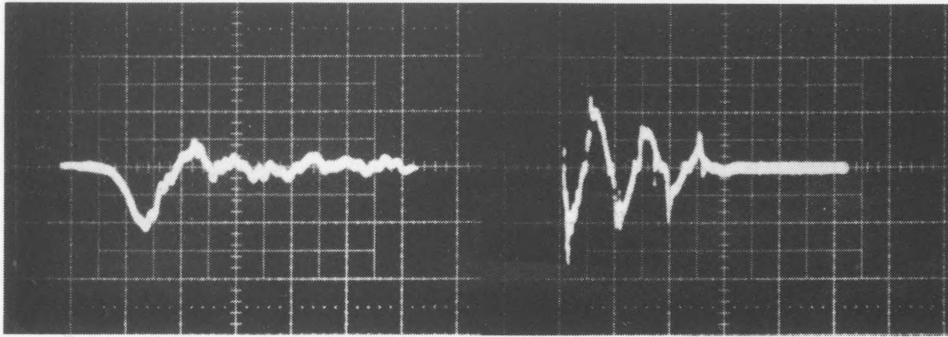
The first photograph (III-19) shows the current trace for the 1 mJ discharge. This lasts ~ 70 ns and shows a peak current of ~ 35 A. Photograph III-20 shows the current waveform, on two time scales, for the above spark, after placing an inductance of 1 mH in the circuit. The first pulse, lasting ~ 25 ns, resulted from a streamer formed in the gap, due to the pointed electrodes. Some few microseconds following this event the capacitive (circuit) energy appeared as a oscillatory waveform lasting ~ 3 μs and showing a peak current



Photograph III-19.

Current trace for a 1 mJ
capacitive discharge in a
4 mm gap.
Vertical scale 20 A/div.
Horizontal scale 20 ns/div.

2 μ s

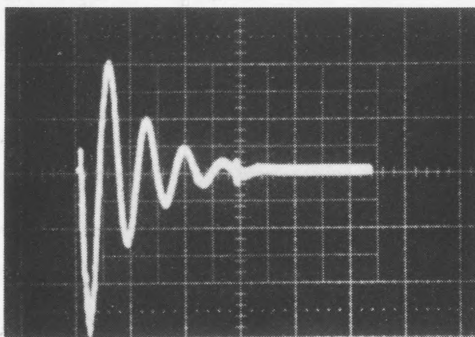


Photographs III-20 a) and b).

Current traces of a 1 mJ
capacitive discharge with a
1 mH series inductance.

a) Shows the pre-breakdown current.
Vertical scale 20 A/div.
Horizontal scale 20 ns/div.

b) Shows the discharge current.
Vertical scale 0.2 A/div.
Horizontal scale 1 μ s/div.



Photograph III-21.

Current trace for a 17 mJ
capacitive discharge in a
4 mm gap.
Vertical scale 40 A/div.
Horizontal scale 0.1 μ s/div.

of ~ 0.35 A. Thus the inclusion of the circuit inductance decreased the current by a factor of 100 and increased duration by a factor of ~ 40 . The final Photograph, III-21, shows the current trace for the 17 mJ capacitive discharge. This shows a peak current of ~ 120 A and a duration of $\sim 0.3 \mu\text{s}$.

These photographs show that in a capacitive circuit, energy is dissipated very rapidly, and that for both 1 mJ and 17 mJ sparks, this dissipation time is of the order of a hundred nanoseconds. The results of the ignition tests using these sparks are therefore in line with the suggested ignition model. That is, for such rapid discharges, stored circuit energy must be increased significantly to increase the energy density at the kernel front due to combustion, which is otherwise limited by the extremely fast kernel expansion rate. The ignition tests confirm this increase, where 12.5 - 17 mJ was needed to ignite the powders, as opposed to just 1 mJ from the slower discharge. In this latter case the circuit inductance undoubtedly served to reduce the kernel expansion rate, and therefore increase the ratio of heat gain to loss (A : B), leading to ignition at 1 mJ.

Other losses, in particular those due to shock wave formation, will of course increase for very fast discharges, i.e. typically below $0.1 \mu\text{s}$. This will be the case for pure capacitive discharges and, together with a rapid increase in kernel expansion rate, will necessitate higher stored (circuit) energies. The hypothesis that the formation of a shock wave could account for the rapid increase in ignition energy observed at such low durations does not appear to be valid, however, despite it accounting for an increase in energy loss. The concept of a 'dust free zone'^{42,43} is undoubtedly relevant for higher energies than were used here, but seems unlikely to apply where energies lay at or below ~ 1 mJ. In particular, for the stabiliser powder, using a 4 mm gap, ignition energy was as low as ~ 0.4 mJ at $0.2 \mu\text{s}$ and appeared to be decreasing further (see Figure III-33). Had energy (E) been kept constant at below $0.1 \mu\text{s}$, then, according to the model (see Figure III-33) proposed by Enstad⁴³, the radial displacement (r) of dust particles, due to a spherical kernel, would be given by

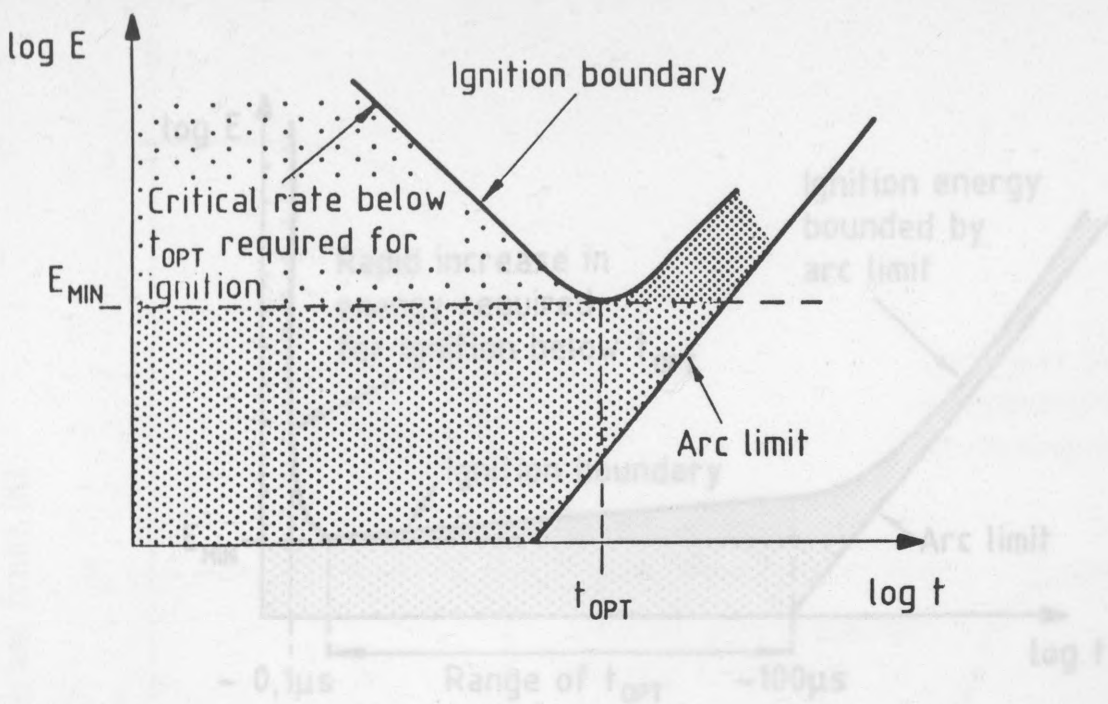
$$r \approx \left(\frac{E}{10p} \right)^{1/3}$$

where p is initial pressure and is typically ~ 200 bar. This gives a maximum displacement of approximately $125 \mu\text{m}$. This effect is therefore small, and is unlikely to cause the rapid increase in required energy to ~ 17 mJ. At durations well below $0.1 \mu\text{s}$, this effect may become more pronounced, however. Furthermore, the results for lycopodium and PAN would indicate that an effect other than that due to shock displacement, is at work. For both of these powders, ignition energy rose dramatically, as it did for the stabiliser, as duration was decreased, but did so at values of duration well above those required to initiate such a shock wave. Thus, although energy losses due to shock formation undoubtedly increase with a decrease in duration, this aspect alone is unlikely to explain the rapid increase in energy that was observed.

The results for all four powders are summarised in Figures III-54 and III-55. The first figure shows the results for the 2 mm gap and the stabiliser powder, where electrode quenching was observed. This figure also represents the general trend in the results, based on the simple ignition model, for both lycopodium and PAN, at a gap width of 4 mm. The second figure is a more specific representation of the results for the stabiliser powder and Benzanthron. The times on the t -axis were those found for these powders. This curve would also be expected to cover any powder, and for any gap width, by a suitable choice of these times. It therefore represents and summarises the interpretation of the spark ignition results obtained in this work. In particular, these figures show that whether effective spark energy is reduced by electrode quenching, or whether kernel expansion is too fast for a given energy, where quenching does not occur, a similar relationship results, albeit on a different time scale. Furthermore, due to increased 'induction times' as particle size is increased for a given powder, one would expect optimum values of MIE and duration to increase accordingly.

9.2 A representation of the ignition process

This representation shown in Figure III-56, was suggested by a number of observations based on the schlieren results, where events leading up to successful ignition were found to be critical in the first $100 \mu\text{s}$. Such a statement also appears valid in view of the spark kernel lifetimes (in air) for the energies used here (\sim mJ). Measurements by Marthinen and Tholl⁵⁷ of temperature decay as a function of spark energy, would suggest that this estimate is conservative for such low energies.



Kernel expansion too fast and / or quenching losses high, particularly to electrodes.
Overall gain in energy density too low for ignition.



Spark energy too low to cause a significant increase in energy density.
No ignition observed.



Kernel expansion too slow and quenching losses high, particularly to surroundings.
Overall gain in energy density too low for ignition.

E_{MIN}

Minimum ignition energy.

t_{OPT}

Spark duration at which ignition energy is at a minimum.

Figure III-54. Generalised results for the stabiliser powder, using a 2 mm gap. The 'ignition boundary' separates the areas of no-ignition and ignition (ignition occurring above the boundary). This curve also applies to the results for Lycopodium and PAN at higher gap widths.

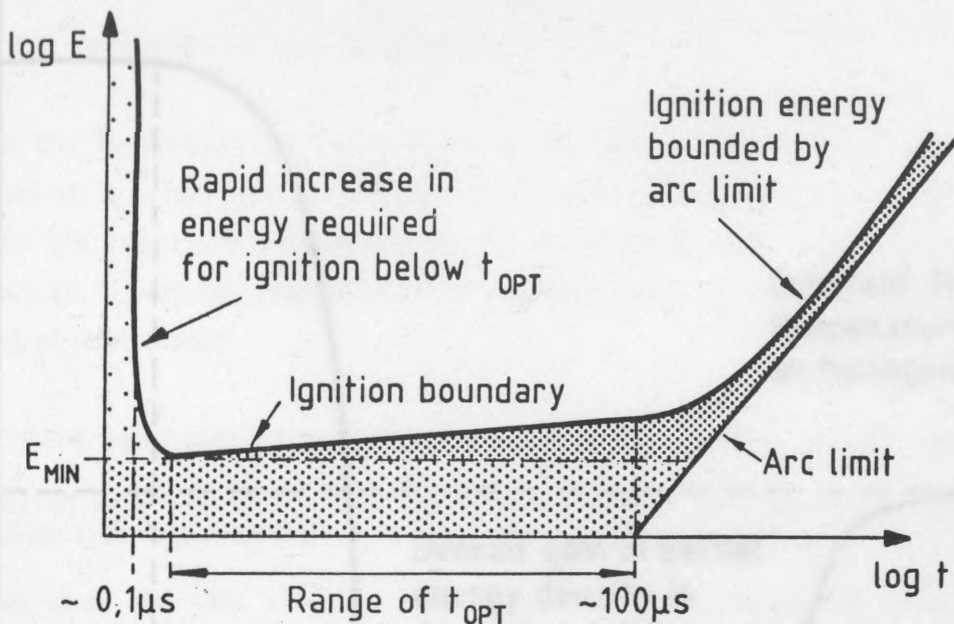


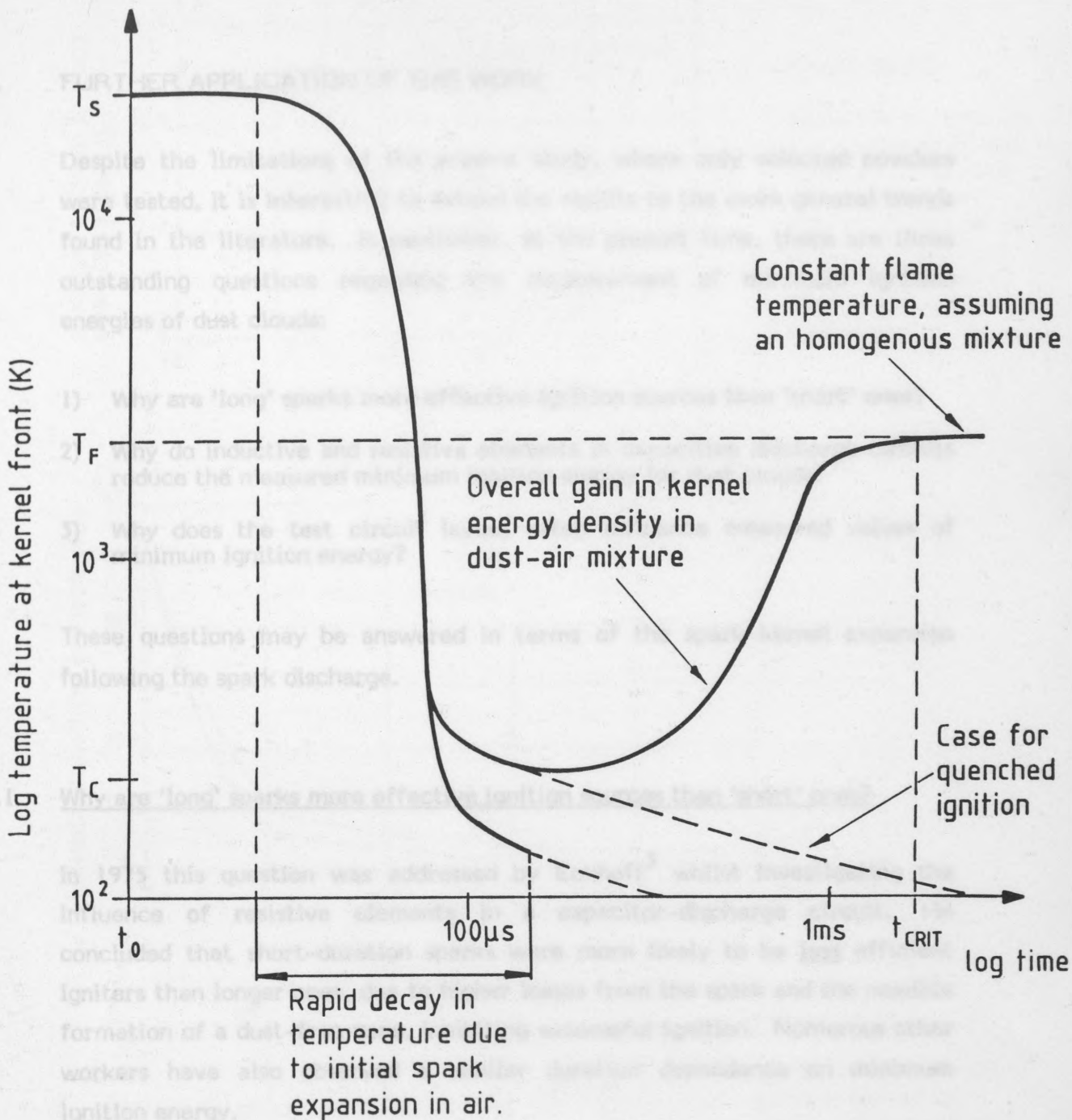
Figure III-55. Generalised results for the stabiliser and Benzanthron, using a 4 mm gap. This curve also represents the general trend in the results for all powders and gap widths, on various time scales. For key see previous page.

Figure III-56 shows a typical temperature decay profile of an electric spark in air, and with dust present. It assumes an homogeneous dust-air mixture, which, like a quiescent gas mixture, will have a constant flame temperature.

9.3 Definition of minimum ignition energy

In accordance with the interpretation of the ignition results for the four powders, the following definition of 'minimum ignition energy' may be put forward.

The 'minimum spark ignition energy' (MIE) for a given dust-air mixture, is defined as the spark energy at which the spark kernel develops at a slow enough rate, so that the rate in increase in energy density, caused by the combustion of dust particles, just exceeds the rate of loss of energy density from the kernel. Such losses are predominantly due to quenching by the electrodes and the dust/air mixture. The rate of expansion of the kernel is dependent upon the spark duration, which is a measure of the initial electrical power of the spark (the initial rate of spark energy dissipation) and thus the MIE is necessarily a spark duration dependent term.



t_0 : Time at which spark kernel forms

T_C : Typical dust-cloud self-ignition temperature

T_F : Flame temperature

T_s : Initial kernel temperature (typically ~60,000 K)

Figure III-56. A generalised model of the spark kernel to flame kernel transition, showing the increase in temperature at the kernel front due to combustion. t_{CRIT} is the time at which a self-propagating flame develops.

10. FURTHER APPLICATION OF THIS WORK

Despite the limitations of the present study, where only selected powders were tested, it is interesting to extend the results to the more general trends found in the literature. In particular, at the present time, there are three outstanding questions regarding the measurement of minimum ignition energies of dust clouds:

- 1) Why are 'long' sparks more effective ignition sources than 'short' ones?
- 2) Why do inductive and resistive elements in capacitive discharge circuits reduce the measured minimum ignition energy for dust clouds?
- 3) Why does the test circuit layout often influence measured values of minimum ignition energy?

These questions may be answered in terms of the spark kernel expansion following the spark discharge.

10.1 Why are 'long' sparks more effective ignition sources than 'short' ones?

In 1975 this question was addressed by Eckhoff³ whilst investigating the influence of resistive elements in a capacitor-discharge circuit. He concluded that short-duration sparks were more likely to be less efficient igniters than longer ones, due to higher losses from the spark and the possible formation of a dust-free zone, inhibiting successful ignition. Numerous other workers have also observed a similar duration dependence on minimum ignition energy.

Traditionally, spark duration using simple capacitive discharge circuits, has been increased by including resistive or inductive circuit elements. For example, Boyle and Llewellyn⁸ obtained the plots shown in Figure III-57 using magnesium and aluminium clouds, and incorporating a series resistance. Stored circuit energy was found to fall as resistance was increased, reaching a minimum when resistance was equal to $10^4 - 10^5$ ohms. Drastic reductions in MIE have also been obtained by recent workers, for example Van Laar¹ and Glarner⁷. These are shown in Figures III-58 and III-59. In both cases the inclusion of a series inductance served to reduce the stored circuit energy required to ignite their samples in much the same way as Boyle and Llewellyn observed.

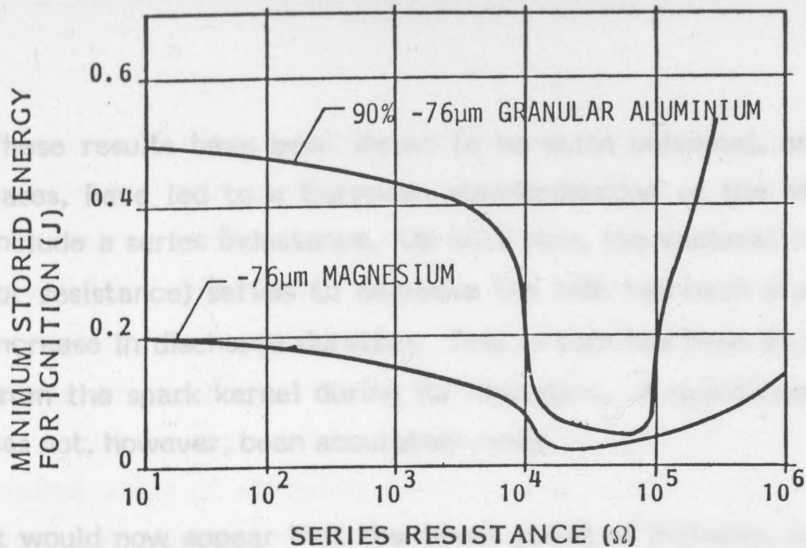


Figure III-57.

Variation in minimum stored circuit energy required for ignition of magnesium and aluminium clouds, as a function of series resistance. Results from Boyle and Llewellyn.

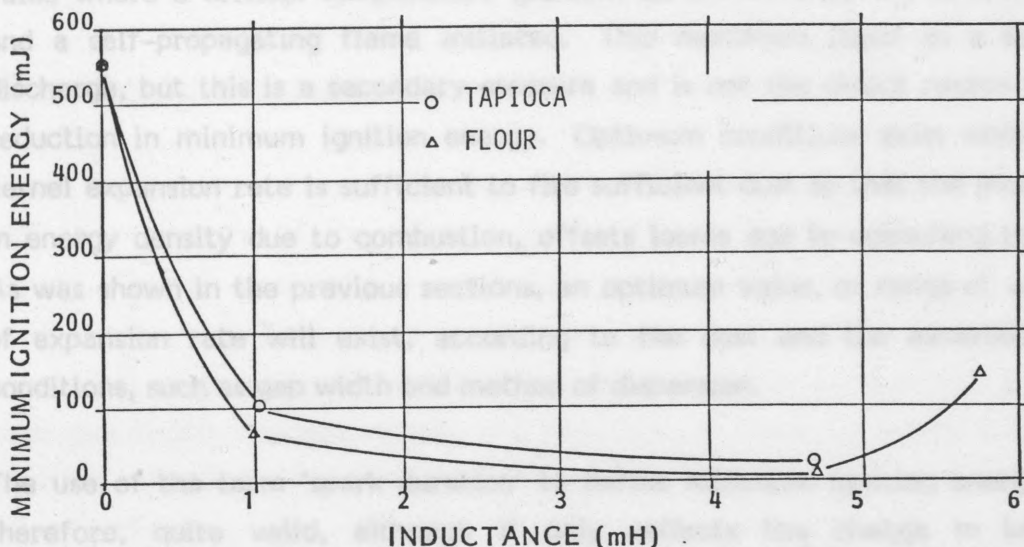


Figure III-58.

Variation in minimum ignition energy for ignition of tapioca and flour clouds, as a function of series inductance. Results from Van Laar.

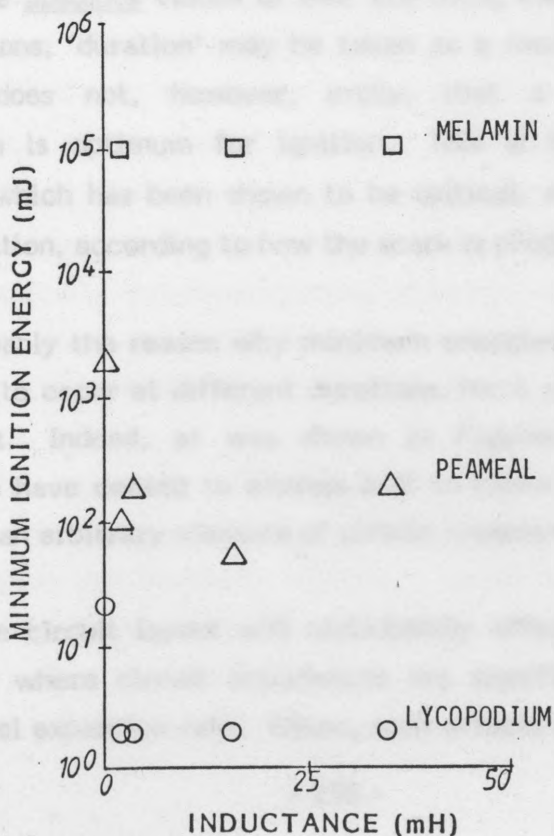


Figure III-59.

Variation in minimum ignition energy for ignition of melamin, peameal and lycopodium clouds, as a function of series inductance. Results from Glarner.

These results have been shown to be quite universal, and in the latter two cases, have led to a European standardisation of the MIE test circuit¹⁴ to include a series inductance. Up until now, the explanation of why inductance (or resistance) serves to decrease the MIE has been stated in terms of the increase in discharge duration. This in turn has been attributed to the losses from the spark kernel during its formation. A quantification of these losses has not, however, been accurately made.

10.2 It would now appear that the direct result of including series impedance in a pure capacitive discharge circuit is to reduce the kernel expansion rate to a value where a critical temperature gradient at its front can be established, and a self-propagating flame initiated. This manifests itself as a slower discharge, but this is a secondary measure and is not the direct reason for a reduction in minimum ignition energy. Optimum conditions exist when the kernel expansion rate is sufficient to fire sufficient dust so that the increase in energy density due to combustion, offsets losses due to quenching terms. As was shown in the previous sections, an optimum value, or range of values of expansion rate will exist, according to the dust and the experimental conditions, such as gap width and method of dispersion.

The use of the term 'spark duration' to define minimum ignition energy is, therefore, quite valid, although it only reflects the change in kernel expansion rate, and cannot be said to directly cause observed changes in MIE. Where absolute values of MIE are being measured, for a given set of test conditions, 'duration' may be taken as a measure of the change in this rate. It does not, however, imply, that a specific energy/duration combination is optimum for ignition. This is because the initial kernel expansion, which has been shown to be critical, may vary for a given spark energy/duration, according to how the spark is produced.

This is probably the reason why minimum energies required for ignition have been found to occur at different durations, for a given dust, according to the test circuit. Indeed, as was shown in Figures III-58 and III-59, many laboratories have ceased to express MIE in terms of discharge duration, but instead use an arbitrary measure of circuit impedance.

Further, the circuit layout will undoubtedly affect the success of ignition, particularly where circuit impedances are significant enough to lead to a slower kernel expansion rate. Often, such effects are difficult to quantify, as

they are distributed in the test circuit, meaning that comparisons between test laboratories is rendered difficult, despite apparently identical circuit conditions. Furthermore, the method of dust dispersion is critical when determining MIE, and this is often very different from laboratory to laboratory. Comparisons are made even more difficult due to possible electrode quenching effects, which, as shown in this work and by Alfert⁶⁰, may exist for dust clouds at electrode distances of less than 4 mm. This is a typical value of electrode spacing used in many test laboratories. Various electrode shapes and materials have also affected quenching losses to an unknown degree, making results all the more difficult to compare.

by electrostatic discharges, then this procedure for evaluating the dusts' sensitivity to ignition may have limited application. This is because the

10.2 Suggestions for a laboratory test method capacitive by nature, and therefore very fast events (typically $< 1 \mu s$). Such fast speeds apply to discharges both

There are two main reasons for measuring MIE in the laboratory. First, the MIE is a measure of the relative sensitivities to ignition of various dust clouds. This is essentially a qualitative process where the ignition source need not be specified. More important, however, the MIE represents an assessment of the electrostatic ignition risk for a given dust cloud. In this case quantitative measurements are required, in order to relate them to specific, potentially hazardous conditions that may exist where the dust is being handled.

nature. In view of the results found both in this work and elsewhere^{1,7,8,9}, this would typically lead to relatively high values of

In the first case, where relative sensitivities are being measured, or worst case conditions are to be simulated for a given dust, the test method for measuring MIE should include some means of varying the discharge energy vs. time profile. Ideally, one should be able to vary discharge duration independently of discharge energy, in order to optimise the rate of spark energy dissipation with time. This may be done crudely, using a simple capacitive circuit, and incorporating inductive or resistive elements, as is widely done. Such a simplified method cannot, however, identify absolute minimum ignition energies for a given dust cloud.

practice may be longer events due to residual resistance or inductance in the

Where absolute minimum values are to be measured, one can only go as far as optimising the energy vs. time profile of a discharge for a given energy/duration combination. 'Absolute' values are clearly hypothetical as they ultimately depend upon the state of movement of the dust cloud at the moment of ignition, which will necessarily vary from one cloud to the next. It may therefore be concluded that for a given set of experimental test

conditions (including dispersion method etc.) qualitative estimates of the sensitivity to ignition of a given dust by electric sparks may be made using a simple test circuit where spark duration can be varied independently of spark energy. Due to the strong dependence of spark duration on MIE observed for some dusts, this duration should be stated as such, and not in terms of a circuit impedance. Furthermore, these values should be established using gap distances greater than the quenching distance for a given dust and electrode materials.

If, on the other hand, one is evaluating the risk of ignition of a particular dust by electrostatic discharges, then this procedure for evaluating the dusts' sensitivity to ignition may have limited application. This is because the majority of discharges in practice are capacitive by nature, and therefore very fast events (typically $\ll 1 \mu\text{s}$). Such fast speeds apply to discharges both from conductor to conductor, and conductor to non-conductor, and cover most of the discharge modes normally arising in practice⁵⁶. These include corona, brush and spark discharges. Such fast events are typified by discharges from a charged insulating surface to a conductor. In this case the discharge of energy in the gap between them may be only a limited fraction of that stored in the field, and event times may be as low as 50 ns ⁶¹. Clearly, any simplified test method that is to simulate such events should be capacitive in nature. In view of the results found both in this work and elsewhere^{1,7,8,9}, this would typically lead to relatively high values of minimum ignition energy compared to those found for ignition sensitivity. Ideally, if one knew the thermalisation times (and thus the kernel expansion rates) for a given discharge type, one would be able to model these accordingly. The closest one has come to such an approach is the concept of 'equivalent energy' as described by Gibson⁶². Further work is clearly necessary to study the thermalisation of rapid discharges, such as brush and propagating brush discharges, in order to establish their relative incendivities.

It has also been argued that 'electrostatic (capacitive) discharges' arising in practice may be longer events due to residual resistance or inductance in the current return path. A classic case is due to poor grounding of conductive objects. This may also apply to the discharges produced from the human body to grounded conductors. Such 'long' discharges are also to be expected from inductive (break flash) circuits. In such cases the nearest estimate to the

hazardous nature of these discharges may be made by measuring the sensitivity to ignition, as described above. It would therefore appear that a dust should be ascribed two MIE values according to its method of handling, and the expected hazardous nature of potential discharges occurring in its vicinity.

Based on a simplified heat energy density equation, the success of ignition of a dust cloud by a transient electric arc-discharge was found to depend upon the rate of expansion of the hot kernel produced by the discharge. This in turn was found to be related to the initial power in the discharge.

For successful ignition to occur, the increase in energy density at the kernel front, as the kernel expands, due to combustion of dust particles, must exceed the loss in energy density from the kernel in the form of quenching and as the spark plasma cools. 'Quenching' losses include conductive losses to the spark electrodes and conductive, radiative and convection losses to the dust-air mixture.

2. For four powders, a commercial dye stabiliser, 'Benzanthron', Lycopodium and PAN, results showed that the energy required for ignition was at a minimum for a given spark duration or range of durations, and for a given gap width. This was expressed in terms of an optimum kernel expansion rate. This value was not determined in this work. This result is expected to apply for any transient ignition source.
3. The values of minimum spark energy for ignition as a function of spark duration, were different for each of the four powders. These values were ultimately dependent upon the chemical composition, state of movement etc. of each powder, and the method of flame propagation and heat transfer in the powder cloud, which were not investigated in this work. The relationship between MIE and duration was, however, similar in form for each of the powders. This general relationship is expected to apply for other powders, allowing for variations in test conditions, in particular the method of dispersion and the type of spark generator circuit used.
4. The times taken from spark discharge to when a self-propagating flame was established, known as the 'critical induction times', were of the

11. SUMMARY OF RESULTS AND CONCLUSIONS

The following conclusions have been drawn from the dust ignition work:

1. Based on a simplified heat energy density equation, the success of ignition of a dust cloud by a transient electric arc-discharge was found to depend upon the rate of expansion of the hot kernel produced by the discharge. This in turn was found to be related to the initial power in the discharge.
For successful ignition to occur, the increase in energy density at the kernel front, as the kernel expands, due to combustion of dust particles, must exceed the loss in energy density from the kernel in the form of quenching and as the spark plasma cools. 'Quenching' losses include conductive losses to the spark electrodes and conductive, radiative and convection losses to the dust-air mixture.
2. For four powders, a commercial dye stabiliser, 'Benzanthron', Lycopodium and PAN, results showed that the energy required for ignition was at a minimum for a given spark duration or range of durations, and for a given gap width. This was expressed in terms of an optimum kernel expansion rate. This value was not determined in this work. This result is expected to apply for any transient ignition source.
3. The values of minimum spark energy for ignition as a function of spark duration, were different for each of the four powders. These values were ultimately dependent upon the chemical composition, state of movement etc. of each powder, and the method of flame propagation and heat transfer in the powder cloud, which were not investigated in this work. The relationship between MIE and duration was, however, similar in form for each of the powders. This general relationship is expected to apply for other powders, allowing for variations in test conditions, in particular the method of dispersion and the type of spark generator circuit used.
4. The times taken from spark discharge to when a self-propagating flame was established, known as the 'critical induction times', were of the

order of 1 - 2 ms for all four powders. These times were measured under low-turbulent conditions. In other tests, where the dust-air mixture was turbulent, this time increased to ~ 5 ms. These times were identified as those at which a critical volume of the kernel was raised to the normal flame temperature. These values, and the size of the kernel at these times, were shown to increase with a decrease in spark duration for a given spark energy. The judgement of ignition success could not, therefore, be based on a 'critical kernel size'. Accurate values of the critical induction times could not be measured using the method adopted in this work. For the stabiliser powder, this time was found to decrease as kernel expansion velocity was reduced, assuming sufficient spark energy for ignition.

7. It was concluded that very rapid discharges (lasting $< 0.1 \mu\text{s}$) such as pure capacitive discharges, would require the longest times, and highest energies, in order to sufficiently raise the energy density of the kernel to ensure ignition. This was confirmed using a simple capacitive discharge circuit.

5. The ultimate success of ignition, for a given spark energy and expansion rate, depends upon the chemical composition of the dust, and in particular the induction times for single particles as a function of temperature. Ignition success is determined at a very early stage, before the spark kernel temperature has fallen below $\sim 1000 \text{ K}$. This time is strongly energy dependent and for the energies used here ($\sim \text{mJ}$) is well within $100 \mu\text{s}$. The increase in energy density due to combustion in this time is therefore decisive, if the kernel is to expand to a self-propagating flame, as is the decrease due to electrode quenching. Where energy is increased, this time is also increased, and so, therefore, is the increase in energy density due to combustion.

6. The kernel expansion rate for a given spark energy was found to be spark-duration dependent. Duration is, however, only an indication of this rate and is not a direct measure. The actual factor governing the rate was previously shown to be the initial power in the spark. For pulse-type discharges, of the form used here, the duration is related to the initial peak spark power. This is also the case for most forms of

discharge circuit where duration is increased using inductive or resistive elements. For these circuit arrangements, however, the relationship between discharge duration and spark power is not as easily defined. Since, in order to reduce ignition energy to a minimum, kernel expansion rate has to be optimised for a given spark energy, it follows that duration is a measure of this optimum rate. One may therefore conclude that the MIE of a given dust is duration-dependent.

The mechanism of kernel expansion was no different from that observed at higher energies.

For common capacitive circuits, where duration is varied as indicated above, the apparent 'duration dependence' will be expected to differ from those measured in this work. This is because of the poorly defined relationship between spark power and discharge duration.

This is reasonable on the grounds of the similarity in the events leading up to 'successful

7. Ignition results using two conditions of dust cloud movement in the spark gap, where average particle velocities were estimated at 1 m.s.^{-1} and 8 m.s.^{-1} , showed a similar trend in the relationship between spark energy and duration, for a given gap width. The results showed that MIE increased by about 10% using the 'faster' dispersion. This was because of a reduction in the energy density of the expanding kernel due to the increase in downstream convection, prior to the formation of a self-propagating flame. These losses caused the time to formation of such a flame to increase from $\sim 1 \text{ ms}$ to $\sim 5 \text{ ms}$. Should dust/air movement increase further, it is expected that these energy losses would eventually lead to much higher spark energies required for ignition. At air velocities as high as 20 m.s.^{-1} , typical of pneumatic transport velocities, the increase in air velocity in the spark gap might also mean that higher voltages would be required to initiate breakdown. In the current work a velocity of 8 m.s.^{-1} was too low to cause such an increase in the breakdown voltage.

Such a value varies from dust to dust, the MIE of a given dust cloud must be measured over a range of spark

8. The effect of increasing the air movement in the spark gap to $\sim 8 \text{ m.s.}^{-1}$ caused an increase in the discharge voltage, and therefore an increase in dissipated energy. This increase was similar to that observed when gap width was increased and was probably due to the elongation or 'bending' of the spark channel. Such increases in energy are expected whenever turbulence exists in the spark gap, due to dust dispersion.

unlikely for low energy sparks ($\sim \text{mJ}$) and that the observed increases in ignition

9. The scatter in ignition probabilities (P) was assumed to be caused by variations in particle size distribution (including the presence of agglomerates) and dust concentration in the gap at the moment of ignition, which inevitably varied from shot to shot. Only at very high spark energies, could such variations be neglected, whereas at energies lying at or near the minimum, these could strongly influence the success of ignition. Where ignition was observed, and $P < 1$, the mechanism of kernel expansion was no different from that observed at higher energies.

be taken when handling this powder.

10. The increase in energy required for ignition using the stabiliser powder, as electrode distance was decreased, indicated that the concept of electrode quenching was valid for dust/air mixtures. This is reasonable on the grounds of the similarity in the events leading up to 'successful ignition' between the four powders tested here, and results for gas mixtures. Under such conditions of quenching, the kernel expansion for a given spark energy/duration, was similar to that of a non-quenched spark of lower energy. This implies that whether effective spark energy is reduced by quenching, or whether the kernel expansion rate is too fast for a given energy, where quenching does not take place, the net effect on the ignition success is the same.

as a fundamental research tool, when studying ignition principles.

For the stabiliser powder, the quenching distance lay between 2 mm and 4 mm.

11. The general observation that MIE decreases with increasing spark duration for the ignition of dust clouds, was interpreted as a decrease in kernel expansion rate to a value suitable for ignition. As very slight increases in series impedance in a conventional capacitive test circuit may cause such a decrease, and such a value varies from dust to dust, the MIE of a given dust cloud must be measured over a range of spark durations. This applies particularly where the 'sensitivity to ignition' is being established, based on the lowest measured energy leading to ignition.

12. The idea that a 'dust-free zone' could be caused by a shock wave emanating from fast sparks ($< 0.1 \mu\text{s}$) was shown to be unlikely for low energy sparks ($\sim \text{mJ}$) and that the observed increases in ignition

energy at such durations were due to the rapid increase in kernel expansion rate. At such fast rates, the increase in energy density due to combustion is too low to offset heat losses from the kernel, and ignition probability is low.

13. The stabiliser powder used in these tests could be ignited using spark energies as low as 0.4 mJ. Such low values would indicate that precautions similar to that for a hydrocarbon/air mixture would have to be taken when handling this powder.
14. It would seem that a given dust should be ascribed two values of MIE according to its method of handling, and the expected hazardous nature of potential discharges occurring in its vicinity. One would be the value obtained using fast capacitive sparks, and the second value would be the value of 'ignition sensitivity' as determined by optimising the kernel expansion rate in a laboratory test.

The first value, using capacitive discharges, would represent an assessment of the potential hazard when handling a dust or powder cloud. The second value would serve as a fundamental research tool, when studying ignition principles.

GENERAL CONCLUSIONS

The work in this thesis has described ignition tests using a 'pulse-type' spark generator, where for arc discharges, duration and energy could be varied independently. The results from these tests, using a single gas mixture and four powders dispersed as clouds, yielded the following conclusions:

1. The rate at which the hot spark kernel expanded following a spark discharge was critical in terms of ensuring ignition. This rate, and the rate of cooling of the kernel, was found to be dependent on the rate at which spark energy was dissipated in the spark gap.

For discharges **III GENERAL CONCLUSIONS** as could be controlled, as in this work, the term 'spark duration' could be used as a measure of the optimum rate of kernel expansion that just led to ignition. That is, an optimum duration, or range of durations, was found at which spark ignition energy was at a minimum.

At durations above and below the 'optimum', the increase in ignition energy was explained in terms of losses from the expanding kernel. At shorter durations, energy losses due to a rapid expansion were assumed to take place. For the gas mixtures, this was thought to be due to a rapid energy dissipation, which could be accompanied by shock, radiation and conductive losses from the kernel. For the powder clouds, this effect was explained by considering the limited contribution of heat energy to the expanding kernel from the particles at the kernel front. At longer durations spark energy was assumed to be wasted, i.e. an inefficient transfer of energy to the combustible medium took place, which was accompanied by a slow kernel expansion.

For the powder clouds, the effect of quenching, leading to an increase in the ignition energy below the optimum duration, was equivalent to an increase in the kernel expansion rate. This was explained in terms of the reduction in the energy density of the expanding kernel.

2. The increase in kernel volume and temperature, eventually leading to a self-propagating flame, was thought to depend upon the expansion time of the kernel, relative to the 'induction times' of the combustible constituents of the medium.

GENERAL CONCLUSIONS

The work in this thesis has described ignition tests using a 'pulse-type' spark generator, where for arc discharges, duration and energy could be varied independently. The results from these tests, using a single gas mixture and four powders dispersed as clouds, yielded the following conclusions:

1. The rate at which the hot spark kernel expanded following a spark discharge was critical in terms of ensuring ignition. This rate, and the rate of cooling of the kernel, was found to be dependent on the rate at which spark energy was dissipated in the spark gap.

For discharges where the rate of energy release could be controlled, as in this work, the term 'spark duration' could be used as a measure of the optimum rate of kernel expansion that just lead to ignition. That is, an optimum duration, or range of durations, was found at which spark ignition energy was at a minimum.

At durations above and below the 'optimum', the increase in ignition energy was explained in terms of losses from the expanding kernel. At shorter durations, energy losses due to a rapid expansion were assumed to take place. For the gas mixture, this was thought to be due to a rapid energy dissipation, which could be accompanied by shock, radiation and conductive losses from the kernel. For the powder clouds, this effect was explained by considering the limited contribution of heat energy to the expanding kernel from the particles at the kernel front. At longer durations spark energy was assumed to be wasted, i.e. an inefficient transfer of energy to the combustible medium took place, which was accompanied by a slow kernel expansion.

For the powder clouds, the effect of quenching, leading to an increase in the ignition energy below the optimum duration, was equivalent to an increase in the kernel expansion rate. This was explained in terms of the reduction in the energy density of the expanding kernel.

2. The increase in kernel volume and temperature, eventually leading to a self-propagating flame, was thought to depend upon the expansion time of the kernel, relative to the 'induction times' of the combustible constituents of the medium.

5. For this reason, optimum spark durations, at which ignition energy was at a minimum, were different for each of the five combustible mixtures. Temperature (in air) would normally fall below the spontaneous ignition
- For the two powder clouds that could be ignited using energies comparable to those for the gas mixture, optimum durations were short, and of the order of 0.2 μ s. For the two other powders, requiring higher ignition energies, these times were increased by 1-2 orders of magnitude. One may conclude, therefore, that where ignition energies for powder clouds are higher than those for gas mixtures, optimum durations will also be higher, due to an increase in the reaction times of individual particles, compared to those on a molecular level for a gas. One would expect these values to increase further with an increase in particle size.
7. Conversely, for an expanding kernel front at a given temperature, one may say that because of increased induction times for powder clouds, compared to gas mixtures, ignition energies and optimum durations are typically higher. magnitude to the reported stored values of MIE for a stoichiometric propane-air mixture. This observation was explained in
3. Discharges from a simple 'capacitive discharge' circuit, were found to be the least efficient ignition sources. For the powder clouds this was explained in terms of the fast kernel expansion caused by the rapid release of spark energy in a short time (typically < 100 ns). This meant that increases in kernel size and temperature were limited by the combustion of particles as the kernel expanded. For the gas mixture, it was assumed that losses, such as those due to expansion and shock wave formation, accounted for the increased ignition energy at such short durations.
10. Further work is necessary to study the 'incondibilities' of other forms of
4. The rate at which energy was discharged in the spark gap, and thus the rate of 'thermalisation' of this energy, influenced the rate of expansion of the hot kernel. As ignition success was found to depend upon the rate of kernel expansion, it was concluded that the rate of energy release, in particular in the initial stages of the discharge when the spark kernel first begins to expand, is a critical factor in determining ignition and may assume an optimum value for a given set of experimental conditions. It was suggested that this criterion be used as a measure of the 'minimum ignition energy' instead of the more diffuse term 'discharge duration'. This is because the rate of energy release is not necessarily fixed as duration is varied, when using capacitive-resistive discharge circuits.

5. 'Ignition success' was found to be governed by events within $\sim 100 \mu\text{s}$ following spark discharge, i.e. within a time at which the spark kernel temperature (in air) would normally fall below the spontaneous ignition temperature of the combustible medium.
6. It was suggested that a gas mixture or dust cloud be assigned two values of 'minimum ignition energy'. One would represent an hazard assessment value, based on ignition by capacitive discharges; the other would represent an 'absolute' value, based on laboratory studies. This second value would be used both for fundamental research purposes, and for hazard assessment where the equivalent discharge circuit is not simply capacitive, and 'worst case' conditions are being sought.
7. The minimum ignition energy (MIE) for the 2.7% propane-air mixture tested here, was an order of magnitude lower than that reported in the literature, and lay at $\sim 0.3 \text{ mJ}$. This energy, measured in the spark gap, was similar in magnitude to the reported stored values of MIE for a stoichiometric propane-air mixture. This observation was explained in terms of a more efficient transfer of spark energy to the gas mixture using the spark generation technique used in this work.
8. For one of the powders tested here, ignition could be obtained using similarly low energies as those required to ignite a 2.7% propane-air mixture ($\sim 0.3 \text{ mJ}$).
9. The concept of a 'quenching distance' for dust clouds was confirmed.
10. Further work is necessary to study the 'incendivities' of other forms of discharges, including glows, coronas, and brush types, and to relate properties of these to the ignition process. This would yield data that would assist both in a further understanding of the ignition of gases and dusts, and in establishing a method of hazard evaluation based on electrostatic discharges.
11. A detailed theoretical treatment of the work presented here is also called for together with measurements of the thermalisation processes, temperature decay times etc. using various spark discharges, so as to predict the optimum conditions for ignition to occur.

REFERENCES

1. van Laar, G.F.M.:
 'Determination of the Minimum Ignition Energy (MIE) - Spark and Hot Spark Energy in the Two-Phase System',
 Prins Maurits Laboratorium, 1984, Report No. 82-20-00001-1-1984.
2. Pollmont, G.:
 'Explosions- und Zündschalter- und Zündkerzen-Combustion und Zündkerzen-Stäuben und Brenngasen',
 Doctoral thesis ETH Nr. 4476, Universität Zürich (1982).
3. Eckhoff, R.K.:
 'Towards Absolute Minimum Ignition Energy for Dust Clouds',
 Combustion and Flame, volume 29, pp. 25-34 (1977).
4. Wolf, I.W. and Burkett, J.:
 'A Method for Determining Minimum Ignition Energy Results for a Neo-pentane-Air Mixture',
 Combustion and Flame, volume 19, pp. 130-135 (1973).
5. Ballal, D.R. and Lefebvre, A.H.:
 'The Influence of Spark Discharge Characteristics on Minimum Ignition Energy in Flowing Gases',
 Combustion and Flame, volume 24, pp. 99-108 (1975).
6. Bartels, A.L. and Riddlestone, H.G.:
 'The Ignition of Methane-air Mixtures by Pulse Discharges',
 The British Electrical and Allied Industries Research Association (BEIRA) Report 3135 (1966).
7. Glaser, T.:
 'Temperatureinflüsse auf Gas-Explosionen - und Zündschalter-Combustion-Stäube',
 Doctoral thesis, ETH Nr. 7130, Eidgenössische Technische Hochschule, Zürich (1985).
8. Boyle, A.R. and Llewellyn, F.J.:
 'The Electrostatic Ignitability of Dust Clouds and Powders',
 Trans. Chem. Ind. volume 47, pp. 372-381 (1958).
9. Linn, L.E. et al.:
 'The Spark Ignition of Dust Clouds',
 J. Phys. Chem. volume 63, pp. 219-224 (1959).
10. Lewis, B. and von Elbe, H.:
 'Combustion, Flames and Explosion of Gases',
 2nd ed., Academic Press (1961).
11. Priede, T.:
 'Initiation of Explosions in Gases',
 Ph.D. Thesis, Universität Zürich (1987).

REFERENCES

REFERENCES

1. van Laar, G.F.M.:
'Determination of the Minimum Ignition Energy (MIE). Gross and Net Spark Energy in the TNO Spark Circuit'.
Prins Maurits Laboratorium, TNO report no. G9548-G0093 (1981).
2. Pellmont, G.:
'Explosions - und Zündverhalten von hybriden Gemischen aus brennbaren Stäuben und Brenngasen'.
Doctoral thesis ETH Nr. 6498, University of Basel (1984).
3. Eckhoff, R.K.:
'Towards Absolute Minimum Ignition Energies for Dust Clouds?'
Combustion and Flame, volume 24, pp. 53-64 (1975).
4. Wolf, I.W. and Burkett, V.T.:
'A Method for Determining Minimum Ignition Energies: Results for a Neo-pentane-Air Mixture'.
Combustion and Flame, volume 19, pp. 330-338 (1957).
5. Ballal, D.R. and Lefebvre, A.H.:
'The influence of Spark discharge Characteristics on Minimum Ignition Energy in Flowing Gases'.
Combustion and Flame, volume 24, pp. 99-108 (1975).
6. Bartels, A.L. and Riddlestone, H.G.:
'The Ignition of Methane-air Mixtures by Pulse Discharges'.
The British Electrical and Allied Industries Research Association (ERA).
Report 5135 (1966).
7. Glarner, T.:
'Temperatureinfluss auf Das Explosions - und Zündverhalten Brennbarer Stäube'.
Doctoral thesis, ETH Nr. 7350, Eidgenoessischen Technischen Hochschule, Zuerich (1983).
8. Boyle, A.R. and Llewellyn, F.J.:
'The Electrostatic Ignitability of Dust Clouds and Powders'.
Trans. Chem. Ind. volume 69, pp. 173-181 (1950).
9. Line, L.E. et al.:
'The Spark Ignition of Dust Clouds'.
J. Phys. Chem. volume 63, pp. 290-294 (1959).
10. Lewis, B. and von Elbe, G.:
'Combustion, Flames and Explosions of Gases'.
2nd ed., Academic Press (1961).
11. Priede, T.:
'Initiation of Explosions in Gases'.
Ph.D. Thesis, University of London (1957).

12. Riddlestone, H.G.:
'The Effect of Series Resistance on the Ignition of Methane-Air Gas Mixtures by Capacitive Discharge'.
ERA report G/T304 (1955).
13. Franke, H.:
'Bestimmung der Mindestzündenergie von Kohlenstäub/Methan/Luft Gemischen (Hybride Gemische)'.
VDI Berichte Nr. 304, pp. 69-72 (1978).
14. Berthold, W.:
'Midestzündenergie - Prüfverfahren'.
VDI-Berichte 494 'Sichere Handhabung brennbarer Stäube'.
VDI conference, Nürnberg (1983).
15. Menown, H. and Newton, B.P.:
'A Multigap, Double-Ended Hydrogen Thyatron'.
Proceedings, Eleventh Modulator Symposium (1973).
16. Glasoe, G.N. and Lebacqz, J.V.:
'Pulse Generators'.
Dover Publications Inc. N.Y. (1965).
17. Molyneux-Berry, R.B.:
'Symmetrical Double-ended Thyatrons in Pulse Modulators'.
Proceedings, Twelfth Modulator Symposium (1976).
18. EEV Handbook:
'Hydrogen Thyatrons'.
English Electric Valve Co. Ltd., Chelmsford, England (1980).
19. Staniforth, J.A.:
'Microwave Transmission'.
English Universities Press (1972).
20. Parker, S.J.:
'An Auto-control Sequencer for Equipment Control'.
CMI-report No. 813301-1, Chr. Michelsen Inst., Bergen (1981).
21. Parker, S.J.:
'An Auto-control Pulse unit for Equipment Control'.
CMI-report No. 823350-2, Chr. Michelsen Inst., Bergen (1982).
22. Thornton, W.M.:
'The Ignition of Gases by Condenser Discharge Sparks'.
Proc. Roy. Soc. London, Ser. A, volume 91, pp. 17-22 (1915).
23. Wheeler, R.V.:
'The Ignition of Gases, Part I. Ignition by the Impulsive Electrical Discharge'.
Chem. Soc. London, Journal, volume 117, pp. 903-917 (1920).
24. Morgan, J.D.:
'Principles of Ignition'.
Sir Isaac Pitman & Sons Ltd., London (1944).

25. Bradford, B.W. and Finch, G.I.:
'The Mechanism of Ignition by Electric Discharges'.
Proceedings, 2nd Symposium on Combustion. Combustion Institute,
Pittsburgh, pp. 112-126 (1965).
26. Finch, G.I. and Sutton, R.W.:
'The Control of Ignition-Coil Discharge Characteristics'.
Proceedings Phys. Soc. of London, volume 45, pp. 288-307 (1933).
27. Parker, S.J.:
'Spark Energy Evaluation using the Tektronix 7612D/4052 Instruments'.
CMI-report No. 833351-2, Chr. Michelsen Inst., Bergen (1983).
28. Maly, R. and Vogel, M.:
'Initiation and Propagation of Flame Fronts in Lean CH₄-Air Mixtures by
the Three Modes of the Ignition Spark'.
Proceedings, 17th Symposium on Combustion, Combustion Institute,
Pittsburgh, pp. 820-831 (1978).
29. Hill, R.D.:
'Thermalisation of A Spark Discharge'.
Journal of Applied Physics, volume 46, no. 7, pp. 2910-2914 (1975).
30. Kono, M. et al.:
'The Optimum Condition for Ignition of Gases by Composite Sparks'.
Proceedings, 16th Symposium on Combustion, Combustion Institute,
Pittsburgh, pp. 757-766 (1976).
31. Riddlestone, H.G.:
'The Ignition of Methane-air Gas Mixtures by Capacitive Spark
Discharges'.
ERA report G/T 278 (1953).
32. Swett, C.C. Jr.:
'Spark Ignition of Flowing Gases, I'.
National Advisory Committee for Aeronautics (NACA) Research
Memorandum RME9E17 (1949).
33. Barreto, E.:
'Ignition by Electric Sparks'.
Inst. Phys. Conf. Ser. No. 48, pp. 135-143 (1979).
34. Ballal, D.R.:
'Ignition and Flame Quenching of Quiescent Dust Clouds of Solid Fuels'.
Proc. Roy. Soc. London, Ser. A, volume 369, pp. 479-500 (1980).
35. Coward, H.F. et al.:
'The Ignition of Electrolytic Gas by the Electric Discharge'.
Chemical Society Journal Volume 101, pp. 2278-2287 (1912).
36. Mole G.:
'The Ignition of Explosive Gases'.
Proceedings, Physical Soc. London, volume 48, pp. 857-864 (1936).
37. Landau, H.G.:
'The Ignition of Gases by Local Sources'.
Chemical Review, volume 21, pp. 245-258.

38. Paterson, C.C. and Campbell, N.:
'Some Characteristics of the Spark Discharge and its Effect in Igniting Explosive Mixtures'.
Proceedings Physical Soc. London, volume 31, pp. 168-229 (1919).
39. Blanc, M.V. et al.:
'Ignition of Explosive Gas Mixtures by Electric Sparks (part I)'.
Journal of Chemical Physics, volume 15, pp. 798-802 (1947).
40. Rose, H.E. and Priede, T.:
'Ignition Phenomena in Hydrogen-Air Mixtures'.
Proceedings 7th Symposium on Combustion, Combustion Institute, Pittsburgh, pp. 436-445 (1958).
41. Watson, E.A.:
'Fuel Control and Burning in Aero-Gas-Turbine Engines'.
Chartered Mech. Eng. volume 3, pp. 91-127 (1956).
42. Eckhoff, R.K. and Enstad, G.:
'Why are 'Long' Electric Sparks more Effective Dust Explosion Initiators than Short Ones?'.
Combustion and Flame, volume 27, pp. 129-131 (1976).
43. Enstad, G.:
'Effect of Shock Wave Emitted from Electric Spark Discharges'.
CMI-report No. 813101-2, Chr. Michelsen Institute, Bergen (1981).
44. Ziegler, F.W. et al.:
'Ignition of Lean Methane-air Mixtures by High Pressure Glow and Arc Discharges'.
Proceedings 20th Symposium on Combustion, Combustion Institute, Pittsburgh (1984).
45. Litchfield, E.L.:
'Chronology and Topography of Sparks at Minimum Energy for Ignition'.
Combustion and Flame, volume 5, pp. 235-241 (1961).
46. Lintin, D.R. and Wooding, E.R.:
'Investigation of the Ignition of a Gas by an Electric Spark'.
British Journal of Applied Physics, volume 10, pp. 159-166 (1959).
47. Friedman, R. and Johnston, W.C.:
'The Wall-quenching of Laminar Propane Flames'.
Journal App. Physics, volume 21, pp. 791-795 (1950).
48. Calcote, H.F. et al.:
'Spark Ignition. Effect of Molecular Structure'.
Proceedings 119th Meeting of American Chemical Society, Cleveland USA, pp. 2656-2445 (1955).
49. Moorhouse, J. et al.:
'An Investigation of the Minimum Ignition Energies of Some C₁ to C₇ Hydrocarbons'.
Combustion and Flame, volume 23, pp. 203-213 (1974).

50. Hay, D.M. and Napier, D.H.:
 "Minimum Ignition Energy of Dust Suspensions".
 I. Chem. Eng. Symposium Series No. 49, pp. 73-79 (1977).
51. Moore, P.W.J. et al.:
 "The Electrostatic Spark Sensitivities of Initiators. Part I".
 Ministry of Supply. E.R.D.E. Report No. 4/R/56 (1956).
52. Roth, W. et al.:
 "Heat Generation by Electric Sparks and Rate of Heat Loss to the Spark Electrodes".
 Journal of Chemical Physics, volume 19, pp. 1530-1535 (1951).
53. Hannes, von H.:
 "Interferometrische Messung der Thermischen Energie von Elektrischen Funken".
 Forschung auf dem Gebiete des Ingenieurwesens, volume 29, no. 6 (1963).
54. Gibson, N.:
 "Characteristics of Powders Processed in the Chemical Industry".
 Proceedings, International Symposium on Dust Explosion Risks in Mines and Industry. ISSA, Karlovy Vary, Czechoslovakia (1972).
55. Dorsett, H.G. et al.:
 "Laboratory Equipment and Test Procedures for Evaluating Explosivity of Dusts".
 U.S. Bureau of Mines, Report of Investigations, 5624 (1960).
56. Glor, M.:
 "Hazards due to Electrostatic Charging of Powders".
 Journal of Electrostatics, volume 16, pp. 175-191 (1985).
57. Marthinen, H. and Tholl, H.:
 "Untersuchung der Temperatur und der Expansion von Funkenkanälen in H₂ bei variabler Energiezufuhr".
 Zeitschrift für Naturforschung, volume 25a, pp. 430-439 (1970).
58. Krauss, L. and Krempl, H.:
 Z. angew. Physik, volume 16, p. 243 (1963).
59. Gibson, N. and Rogers, R.L.:
 "Ignition and Combustion of Dust Clouds in Hot Environments - an Exploratory Study".
 I. Chem. E. Symposium, series no. 58, pp. 209-217 (1980).
60. Alfert, F.:
 "Sicherheitstechnische Kenngrößen von Polynären Brennstoff/Luft-Gemischen und Selbstzerfallenden Stoffen".
 Doctoral thesis, University of Dortmund (1985).
61. Landers, E.U.:
 "Distribution of Charge and Field Strength due to Discharge from Insulating Surfaces".
 Journal of Electrostatics, volume 16, pp. 59-68 (1985).

62. Gibson, N. and Lloyd, F.C.:
British Journal of Applied Physics, volume 16, pp. 1619 (1965).
63. Foucalt, L.:
Ann. Observatoire imp., Paris, volume 5, p. 197 (1859).
64. Toepler, A.:
Ann. Physik und Chem., volume 128, p. 126 (1866).
65. Schardin, H.:
Ergeb. exact. Naturw., volume 20 (1941).
66. Früngel, F.:
'High Speed Pulse Technology'.
Academic Press, New York (1965).
67. Arnold, J.S. and Sherburne, R.K.:
'Observations of the Ignition and Incipient Flame Growth in Hydrocarbon-air Mixtures'.
Proceedings, 4th Symposium on Combustion, The Combustion Institute, Pittsburgh, pp. 139-143 (1953).
68. 'Yu, Y.F.:
'On the Electrostatic Charging of some Finely Divided Materials in Modern Agricultural Pneumatic Transport Systems'.
Journal of Electrostatics, volume 16, pp 209 - 217 (1985).

RESISTORS

R1	7 G Ω	(HV)*	R52	20 Ω	pot
R2	200 M Ω	(HV)*	R53-61	47 k Ω	(1/4 W) MF
R3,4	680 k Ω x 10	(HV)+	R62	100 k Ω	(1/4 W) MF
R5,6	680 Ω	(HV)+	R63	5 M 6	(1/4 W) MF
R7	1 k Ω x 2	(5 W) WW	R64	180 Ω	(1/2 W) C
R8	100 Ω	(2 W) C	R65,66	100 Ω	(1/4 W) C
R9	59 Ω	(2 W) C	R67-70	43 k Ω	(1/4 W) C
R10	1 k Ω	(2 W) C	R71,72	5 M 6	(1/4 W) MF
R11	0.13 Ω	(8 x 1.2 Ω /1 W) WW	R73-82	43 k Ω	(1/4 W) MF
R12	1 k Ω	(5 W) WW	R83,84	560 k Ω	(1/4 W) MF
R13	120 k Ω	(1 W) C	R85	43 k Ω	(1/4 W) C
R14	7 G Ω	(HV)*	R86	560 k Ω	(1/4 W) C
R15,16	680 k Ω x 10	(HV)+	R87-89	43 k Ω	(1/4 W) C
R17,18	680 Ω	(HV)+	R90	68 Ω	(1/2 W) C
R19	1 k Ω x 2	(5 W) WW	R91	39 Ω	(1/2 W) C
R20	100 Ω	(2 W) C	R92	180 Ω	(1/2 W) C
R21	59 Ω	(2 W) C	R93	5 k Ω	pot
R22	1 k Ω	(2 W) C	R94	220 Ω	(1/4 W) C
R23	1 k Ω	(5 W) WW	R95	560 Ω	(1/4 W) C
R24	0.16 Ω	(6 x 1 Ω /1 W) WW	R96	100 Ω	(1/4 W) C
R25	120 k Ω	(1 W) C	R97	560 Ω	(1/4 W) C
R26	59 Ω	(2 W) C	R98	100 Ω	(1/4 W) C
R27	100 Ω	(2 W) C	R99	5 K 6	(1/4 W) C
R28	1 k Ω	(2 W) C	R100	120 k Ω	(1 W) C
R29	10 k Ω	(1 W) C	R101	10 Ω	(1/2 W) WW
R30	22 Ω	(1/4 W) C	R102	100 Ω	(1/4 W) MF
R31	5 K 6	(1/4 W) C	R103,104	1 M Ω	pot
R32	22 Ω	(1/4 W) C	R,R ¹	see text	
R33	470 Ω	(1 W) C			
R34	50 Ω	pot			
R35	470 Ω	(1 W) C			
R36	50 Ω	pot			
R37	120 k Ω	(1 W) C			
R38	10 k Ω	(1 W) C			
R39	200 Ω	pot			
R40	10 k Ω	(1 Ω) C			
R41	100 M Ω	(1/4 W) C			
R42	50 k Ω	pot			
R43	120 k Ω	(1 W) C			
R44	10 k Ω	(1 W) C			
R45	200 Ω	pot			
R46	22 Ω	(1/4 W) C			
R47	10 k Ω	(1 W) C			
R48	22 Ω	(1/4 W) C			
R49	1 k Ω	(1 W) C			
R50	20 Ω	pot			
R51	1 k Ω	(1 W) C			

* High voltage (HV) resistor types Welwyn

T44TUL +/- 5%

+ " " " " " "

T43TUL +/- 5%

All other types either Carbon (C), Metal Film (MF) or Wirewound (WW)

CAPACITORS

C1	100 μ F	250 V	e
C2	200 pF	40 kV	ps
C3	0.1 μ F	1 kV	p
C4,5	100 pF	200 V	c
C6,7	100 μ F	250 V	e
C8	200 pF	40 kV	e
C9	0.1 μ F	1 kV	p
C10,11	100 pF	200 V	c
C12	100 μ F	250 V	e
C13	200 pF	40 kV	ps
C14	1 μ F	1 kV	p
C15	0.1 μ F	1 kV	p
C16	100 μ F	25 V	e
C17	1000 μ F	25 V	e
C18	1 μ F	35 V	t
C19	0.047 μ F	100 V	c
C20	1000 μ F	25 V	e
C21,22	1 μ F	35 V	t
C23	1000 μ F	25 V	e
C24	1 μ F	35 V	t
C25	100 μ F	25 V	e
C26	1000 μ F	25 V	e
C27	1 μ F	35 V	t
C28	1000 μ F	25 V	e
C29	1 μ F	35 V	t
C30	100 μ F	250 V	e
C31	1 μ F	1 kV	p
C32	0.1 μ F	1 kV	p
C33	100 μ F	250 V	e
C34	1 μ F	1 kV	p
C35	0.1 μ F	1 kV	p
C36	100 μ F	250 V	e
C37	1 μ F	35 V	t
C38	1000 μ F	25 V	e
C39	1 μ F	35 V	t
C40,41	1000 μ F	25 V	e

e electrolytic
 ps polystyrene
 p paper
 c ceramic
 t tantalum
 ps polyester

D18	IN4002 x 4		
D19	IN4001		
D20	BTW47/1200R		
C42-49	47 nF	100 V	c
C50	0.47 μ F	50 V	c
C51,52	4.7 μ F	35 V	t
C53,54	39 pF	100 V	ps
C55-62	47 nF	100 V	c
C63-65	0.033 μ F	50 V	c
C66	1000 μ F	25 V	e
C67	1 μ F	35 V	t
C68	100 μ F	25 V	e
C69	0.1 μ F	35 V	ps
C70	0.047 μ F	100 V	c
C71	1 μ F	35 V	t
C72	1 μ F	400 V	p
C73	0.33 μ F	1000 V	p
C74,75	1 μ F	35 V	t
C76	0.47 μ F	50 V	c
C77	0.1-2 μ F	1000 V	p

Q1	LM341P-9
Q2	VN66AF
Q3,4	LM341P-5
Q5	LM341P-12
Q6-9	LM341P-5
Q10-13	MPSA06
Q14	VN66AF
Q15	LM341P-12
Q16,17	VN66AF
Q18	LM341P-5
Q19	LM341P-12
Q20,21	VN66AF
Q22	LM341P-5

IC1	4520B
IC2-5	4518B
IC6	4013B
IC7	4093B
IC8	40102B
IC9	4098B
IC10,11	4093B
IC12	4013B
IC13	4098B
IC14	40102B
IC15,16	4098B
IC17,18	4013B
IC19,20	4093B

TRANSFORMERS

Tr1	220 V - 6.3 V	200 VA (40 kV isolated)
Tr2	N8208	N
Tr3	220 V - 6.3 V	200 VA (40 kV isolated)
Tr4	H8208	N
Tr5	N8640	N
Tr6,7	IT 332	S
Tr8	N6021	N
Tr9	T12	P
Tr10	N8185	N
Tr11	T12	P
Tr12	N8185	N
Tr13	N6021	N
Tr14	T12	P
Tr15	N6039	N
Tr16	T12	P
Tr17	N8626	N
Tr18	T12	P
Tr19	N6039	N
Tr20,21	IT 332	S
Tr22	N8626	N
Tr23,24	IT 332	S
Tr25	N6021	N
Tr26	T22	P
Tr27	N6001	N
Tr28	T22	P
Tr29,30	N6001	N
Tr31,32	T12	P
Tr33	N6037	N
Tr34	N8626	N
Tr35	IT 332	S

N Norsk Transduktor
 P Powerstat
 S Schäffer

SEMICONDUCTOR DEVICES

D1,2	IN4001 x 4
D3	VA30
D4	IN4001 x 4
D5	BTW47/1200R
D6-10	IN4001 x 4
D11,12	IN4001
D13,14	IN4001 x 4
D15	IN4001
D16	VA30
D17	IN4001

D18	IN4002 x 4
D19	IN4001
D20	BTW47/1200R
D21	VA30
D22	BTW47/1200R
D23,24	IN4001 x 4
D25	IN4001
D26	IN4001 x 4
D27	IN4001
D28,29	IN4148
D30	LSM-6LA
D31	IN5349
D32-34	IN4148
D35	LSM-6LA
D36	IN4001 x 4
D37,38	LSM-6LA
D39	IN4001
D40	VS447
D41	BTW47/1200R
D42-49	VA30
D50	IN4148

Q1	LM34IP-9
Q2	VN66AF
Q3,4	LM34IP-5
Q5	LM34IP-12
Q6-9	LM34IP-5
Q10-13	MPSA06
Q14	VN66AF
Q15	LM34IP-12
Q16,17	VN66AF
Q18	LM34IP-5
Q19	LM34IP-12
Q20,21	VN66AF
Q22	LM34IP-5

IC1	4520B
IC2-5	4518B
IC6	4013B
IC7	4093B
IC8	40102B
IC9	4098B
IC10,11	4093B
IC12	4013B
IC13	4098B
IC14	40102B
IC15,16	4098B
IC17,18	4013B
IC19,20	4093B

OTHER COMPONENTS

L1-15 12V 20 mA telephone lamp
R1 Electomatique SA 245 timing switch
V1,2,3 Oltronix LINPAC 40 15 V/2.5 A supply
T1,2 EEV CX1168B thyatron
01 HP HFBR-2201 optical receiver
02 HP HFBR-1201 optical transmitter
03 HP HFBR-1501 optical transmitter
04,4a HP HFBR-2500 optical receiver
05 Vectron crystal oscillator C0536

APPENDIX 2

SPARK ENERGY COMPUTATION PROGRAMME AND LISTING OF VARIABLES

```

80 05H 1000000
90 ON 05H 1000 0500
95 PAGE
100 PAGE
110 PRINT "THE SPARK ENERGY COMPUTATION PROGRAM"
120 PRINT "GIVEN ALL INPUT PARAMETERS"
130 PRINT
140 PRINT
150 PRINT
160 GOTO 1000
170 PRINT "DO YOU WISH TO USE THE DATA DEFINED IN THE PROGRAM?"
180 INPUT A
190 IF A# "Y" GOTO 1000
200 IF A# "N" GOTO 1000
210 PAGE
220 PRINT "GIVEN THE DATA DEFINED IN THE PROGRAM"
230 PRINT "GIVEN THE DATA DEFINED IN THE PROGRAM"
240 PRINT
250 PRINT
260 INPUT B
270 GO TO 1000
280 PAGE
290 PRINT "GIVEN THE DATA DEFINED IN THE PROGRAM"
300 PRINT "GIVEN THE DATA DEFINED IN THE PROGRAM"
310 PRINT
320 PRINT
330 GO TO 1000
340 PAGE
350 PRINT "GIVEN THE DATA DEFINED IN THE PROGRAM"
360 PRINT "GIVEN THE DATA DEFINED IN THE PROGRAM"
370 PRINT
380 PRINT
390 GO TO 1000
400 PRINT "DO YOU WISH TO USE THE DATA DEFINED IN THE PROGRAM?"

```

APPENDIX 2

SPARK ENERGY COMPUTATION PROGRAMME
AND LISTING OF VARIABLES

```

410 PRINT "GIVEN THE DATA DEFINED IN THE PROGRAM"
420 PRINT
430 PRINT
440 PRINT
450 PRINT
460 PRINT
470 PRINT "DO YOU WISH TO USE THE DATA DEFINED IN THE PROGRAM?"
480 INPUT C
490 PRINT
500 PRINT
510 PRINT "DO YOU WISH TO USE THE DATA DEFINED IN THE PROGRAM?"
520 PRINT "Y-YES"
530 INPUT D
540 PRINT "DO YOU WISH TO USE THE DATA DEFINED IN THE PROGRAM?"
550 INPUT E
560 IF E# "Y" GOTO 1000
570 PAGE
580 PRINT
590 PRINT "THE SPARK ENERGY COMPUTATION PROGRAM"
600 INPUT F
610 FOR I=1 TO 1000 STEP 100
620 PRINT
630 PRINT
640 PRINT "WHAT IS THE CHANNEL 1 I-V MEASUREMENT CHANNEL NUMBER?"
650 INPUT G
660 PRINT "WHAT IS THE CHANNEL 2 I-V MEASUREMENT CHANNEL NUMBER?"
670 INPUT H
680 PRINT "GIVE THE TIME PERIOD LENGTH IN SECONDS"
690 INPUT I
700 IF I# "Y" GOTO 1000
710 GOTO 1000
720 PAGE
730 PRINT "DO YOU WISH TO USE THE DATA DEFINED IN THE PROGRAM?"
740 PRINT "THEN PRESS 'Y'"
750 PRINT
760 PRINT "PRESS 'Y' TO USE THE DATA DEFINED IN THE PROGRAM"
770 PRINT "PRESS 'N' TO USE THE DATA DEFINED IN THE PROGRAM"
780 PRINT "NOTE: CHANNEL 1 MEASUREMENT CHANNEL NUMBER IS 1000"
790 INPUT J
800 IF J# "Y" GOTO 1000
810 INPUT K
820 INPUT L
830 INPUT M
840 INPUT N
850 INPUT O
860 INPUT P
870 INPUT Q
880 INPUT R
890 INPUT S
900 INPUT T
910 INPUT U
920 INPUT V
930 INPUT W
940 INPUT X
950 INPUT Y
960 INPUT Z
970 INPUT AA
980 INPUT AB
990 INPUT AC
1000 FOR I=1 TO 1000
1010 FOR J=1 TO 1000
1020 FOR K=1 TO 1000

```

```

30 REM **SPARK INT PROGRAMME WITHOUT BREAKPOINTS, CURVES TOGETHER**
90 ON SRQ THEN 5750
95 U=6
100 PAGE
110 PRINT "NO BREAKPOINT SPARK ENERGY INTEGRATION PROGRAMME"
120 PRINT "WITH ALL CURVES DISPLAYED TOGETHER"
130 PRINT
140 PRINT
150 PRINT
160 DIM Y$(3)
170 PRINT "DO YOU WISH TO VIEW ONLY PART OF THE CURVE? (Y/N)"
180 INPUT Y$
190 IF Y$="N" THEN 280
200 IF Y$="Y" THEN 210
210 PAGE
220 PRINT "BETWEEN WHICH DATA POINTS ?"
230 PRINT "FIRST DATA POINT ....."
240 INPUT W1
250 PRINT "LAST DATA POINT ....."
260 INPUT W2
270 GO TO 300
280 W1=1
290 W2=2048
300 REM **READ NUMBER OF Bk POINTS**
310 PRINT @U,0:"NBPT?"
320 INPUT @U,0:N
330 IF N>1 THEN 350
340 GO TO 440
350 PAGE
360 PRINT "THERE ARE BREAK POINTS IN THE RECORDING. PLEASE WAIT AND"
370 PRINT "SELECT THE RIGHT PROGRAMME"
380 FIND 1
390 WBYTE @20:
400 PRINT "IT MAY NOW BE NECESSARY TO RE-SET THE I/P AMPLIFIERS"
410 PRINT "BEFORE FURTHER DATA AQUISITION"
420 OLD
430 RUN
440 PAGE
450 PRINT "WHAT IS THE PROBE 1 (R1) RATIO ?"
460 INPUT R1
470 PRINT "WHAT IS THE PROBE 2 (R2) RATIO ?"
480 INPUT R2
490 PRINT
500 PRINT
510 PRINT "DO YOU WISH TO USE THE CURVE SATURATION TEST ON CHANNEL B ?"
520 PRINT " (Y/N)"
530 INPUT Z$
540 PRINT "DO YOU WISH TO ZERO THE INITIAL VOLTAGE SPIKE ? (Y/N)"
550 INPUT K$
560 IF K$="N" THEN 610
570 PAGE
580 PRINT
590 PRINT "IS THE SPIKE POS (P) OR NEG(N) ?"
600 INPUT J$
610 REM **READ POS AND SCALE**
620 PRINT
630 PRINT
640 PRINT "WHAT IS THE CHANNEL 1 I/P SETTING (VOLTS/DIVISION) ?"
650 INPUT U1
660 PRINT "WHAT IS THE CHANNEL 2 I/P SETTING (VOLTS/DIVISION) ?"
670 INPUT U2
680 PRINT
690 PRINT "HAVE THE TRACE ZERO LINES BEEN ESTABLISHED? (Y/N)"
700 INPUT Q$
710 IF Q$="Y" THEN 790
720 GOSUB 5130
730 PAGE
740 PRINT "HOW RESET THE I/P AMPS AND RECORD THE WANTED SIGNAL(S)"
750 PRINT "THEN PRESS "RETURN""

760 PRINT "PRESS RUN 790 FOR CONTINUOUS CURVE AQUISITION USING"
770 PRINT "THESE VARIABLES"
775 PRINT "NOTE ZEROING OF CURRENT WAVEFORM RELIES ON 1st 100 POINTS"
780 INPUT F$
790 LET O$="N"
800 PRINT @U,0:"HSFB?"
810 INPUT @U,0:H1,H2,H3,H4,H5
820 DELETE H1,H2,H3,H4
830 PRINT @U,0:"READ A"
840 WBYTE @64+U,96:
850 RBYTE X,X1,X2
860 X3=X1*256+(X2-1)
870 DELETE A
880 DELETE I
885 PAGE
890 DIM A(X3)
900 RBYTE A,X4,X5
910 VIEWPORT 10,60,55,95
920 WINDOW W1,W2,0,255
930 AXIS X3/10,24,255/8,W1,255/2
940 REM **WRITE t**
950 T$="t"
960 MOVE W2,120
970 PRINT "J";
980 PRINT "K";
990 PRINT T$
1000 REM **WRITE SCALE**
1010 FOR I=160 TO 256 STEP 32
1020 MOVE W1-1,I
1030 IF U1*R1->500 THEN 1060
1040 PRINT "HHHH";"+";<I/32-4>*R1*U1;
1050 GO TO 1070
1060 PRINT "HHHH";"+";<I/32-4>*U1;
1070 NEXT I
1080 FOR I=0 TO 96 STEP 32

```

```

1090 MOVE W1-1,I
1100 IF U1*R1=>500 THEN 1130
1110 PRINT "HHHH";(I/32-4)*R1*U1;
1120 GO TO 1140
1130 PRINT "HHHH";(I/32-4)*U1
1140 NEXT I
1150 REM **WRITE U OR KV**
1160 MOVE W1-1,128
1170 PRINT "HHH";"0";
1180 MOVE W1-1,256
1190 IF U1*R1=>500 THEN 1220
1200 PRINT "K";"U";
1210 GO TO 1260
1220 IF R1=1000 THEN 1240
1230 GO TO 1200
1240 PRINT "K";"KV";
1250 REM **WRITE TITLE**
1260 U$="SPARK VOLTAGE"
1270 L$="-----"
1280 MOVE W1+(W2-(W1-1))/2,256
1290 PRINT "L";
1300 FOR T=1 TO LEN(U$)/2
1310 PRINT "H";
1320 NEXT T
1330 PRINT "J";
1340 PRINT L$
1350 MOVE W1+(W2-(W1-1))/2,256
1360 PRINT "K";
1370 FOR T=1 TO LEN(U$)/2
1380 PRINT "H";
1390 NEXT T
1400 PRINT U$;
1410 DELETE T
1420 REM **WRITE TIME SCALE**
1430 S$="TIME SCALE:          PER DIV"

1440 DELETE L$
1450 L$="-----"
1460 MOVE (1+1/11)*W2,0
1470 PRINT "JJ";
1480 FOR T=1 TO LEN(S$)/2
1490 PRINT "H";
1500 NEXT T
1510 PRINT S$;
1520 MOVE (1+1/11)*W2,0
1530 PRINT "JJJ";
1540 FOR T=1 TO LEN(S$)/2
1550 PRINT "H";
1560 NEXT T
1570 PRINT L$;
1580 PRINT "K";
1590 PRINT "HHHHHHHHHHHHHHHHHH";
1600 PRINT H5*2048/10.24;"S"
1610 REM ** A IS NOW POSITIONED CENTRALLY **
1620 REM**A CROSSING POINT IS ESTABLISHED FOR THE ELIMINATION OF**
1630 REM** INTEGRATED DATA BEFORE COMPLETE VOLTAGE BREAKDOWN**
1640 REM**THIS CROSSING Pt IS ARBITRARILY SET AT 5, FOR A NEG**
1650 REM**GOING SPIKE AND AT 250 FOR A POS GOING SPIKE, WHERE**
1660 REM**H5 IS 5 OR 250**
1670 IF K$="N" THEN 1730
1680 IF J$="P" THEN 1710
1690 LET H5=5
1700 GO TO 1720
1710 LET H5=250
1720 CALL "CROSS",A,H5,S,2
1730 FOR I=1 TO X3
1740 A(I)=A(I)-P3*255/8
1750 NEXT I
1751 REM **COMPENSATE FOR 4-POINT DELAY**
1752 DELETE I
1753 FOR I=1 TO X3-4

1754 A(I)=A(I+4)
1755 NEXT I
1760 MOVE W1,A(W1)
1770 FOR I=W1 TO W2
1780 DRAW I,A(I)
1790 NEXT I
1800 PRINT @U,0:"READ B"
1810 WBYTE @64+U,96;
1820 RBYTE Y,Y1,Y2
1830 Y3=Y1*256+(Y2-1)
1840 DELETE B
1850 DIM B(Y3)
1860 RBYTE B,Y4,Y5
1870 VIEWPORT 75,125,55,95
1880 WINDOW W1,W2,0,255
1890 AXIS Y3/10.24,255/8,W1,255/2
1900 MOVE W2,128
1910 PRINT "J";
1920 PRINT "K";
1930 PRINT T$
1940 FOR I=160 TO 256 STEP 32
1950 MOVE W1-1,I
1960 PRINT "HHHH";"+";(I/32-4)*R2*U2;
1970 NEXT I
1980 FOR I=0 TO 96 STEP 32
1990 MOVE W1-1,I
2000 PRINT "HHHH";(I/32-4)*R2*U2;
2010 NEXT I
2020 MOVE W1-1,128
2030 PRINT "HHH";"0";
2040 MOVE W1-1,256
2050 PRINT "K";"A";
2060 DELETE T
2070 I$="SPARK CURRENT"
2080 DELETE L$

```

```

2090 L$="-----"
2100 MOVE W1+(W2-(W1-1))/2,256
2110 PRINT "K";
2120 FOR T=1 TO LEN(I$)/2
2130 PRINT "H";
2140 NEXT T
2150 PRINT I$;
2160 MOVE W1+(W2-(W1-1))/2,256
2170 PRINT "K";
2180 FOR T=1 TO LEN(I$)/2
2190 PRINT "H";
2200 NEXT T
2210 PRINT "J";L$;
2220 DELETE I
2230 REM ** B IS NOW POSITIONED CENTRALLY **
2231 REM **FIRST 100 DATA POINTS TAKEN TO AVERAGE ZERO LINE **
2232 DELETE P4
2233 P4=B(I)/100
2234 FOR I=2 TO 100
2235 P4=P4+B(I)/100
2236 NEXT I
2237 DELETE I
2240 FOR I=1 TO Y3
2250 B(I)=B(I)-P4+127.5
2260 NEXT I
2270 MOVE W1,B(W1)
2280 FOR I=W1 TO W2
2290 DRAW I,B(I)
2300 NEXT I
2310 IF Z$="N" THEN 2390
2320 REM ** B CURVE SATURATION TEST NOW INCORPORATED **
2330 CALL "MAX",B,M5,M6
2340 CALL "MIN",B,M7,M8
2350 M5=M5+P4*32+1
2360 M7=M7+P4*32-1

2370 IF M5=>255 THEN 5700
2380 IF M7<=0 THEN 5700
2390 DELETE C
2400 DELETE D
2410 DELETE I
2420 DELETE K
2430 DELETE L
2440 DELETE M
2450 REM ** A AND B ARE NOW CORRECTED FOR INTEGRATION **
2460 FOR K=1 TO X3
2470 A(K)=A(K)-127.5
2480 NEXT K
2490 FOR K=1 TO X3
2500 IF A(K)=>0 THEN 2530
2510 IF A(K)<0 THEN 2520
2520 A(K)=A(K)*-1
2530 NEXT K
2540 FOR L=1 TO Y3
2550 B(L)=B(L)-127.5
2560 NEXT L
2570 FOR L=1 TO Y3
2580 IF B(L)=>0 THEN 2610
2590 IF B(L)<0 THEN 2600
2600 B(L)=B(L)*-1
2610 NEXT L
2620 REM ** POWER-TIME CURVE NOW OBTAINED AND VOLTAGE SPIKE ZEROED**
2630 IF K$="N" THEN 2680
2640 FOR M=1 TO S
2650 A(M)=0
2660 NEXT M
2670 DELETE M
2680 FOR M=1 TO Y3
2690 A(M)=A(M)*B(M)
2700 A(M)=A(M)*16*R1*R2*U1*U2/127.5^2
2710 NEXT M

2720 REM **DYNAMIC VOLTAGE/CURRENT-TIME CURVE NOW ESTABLISHED**
2730 DELETE M
2740 FOR M=1 TO Y3
2750 IF B(M)>0 THEN 2780
2760 IF B(M)<0 THEN 2780
2770 B(M)=A(M)*10.5*127.5/(100*4*(R1*R2*U1*U2)+0.5)
2780 B(M)=A(M)*127.5^2/(B(M)*16*R1*U1*R2*U2)
2790 B(M)=ABS(B(M))
2800 B(M)=B(M)*R1*U1/(R2*U2)
2810 NEXT M
2820 REM**THIS HAS SET B(M) TO MAX. SCALE VALUE (INF) WHEN B(M)=0**
2830 REM **VERT. SCALE FOUND**
2840 CALL "MAX",A,A1,A2
2850 IF A1<800 THEN 2890
2860 IF A1<8000 THEN 2900
2870 IF A1>8000 THEN 2920
2880 A3=800
2890 GO TO 2930
2900 A3=8000
2910 GO TO 2930
2920 A3=80000
2930 VIEWPORT 10,60,5,40
2940 WINDOW W1,W2,0,A3
2950 AXIS Y3/10.24,A3/8
2960 REM **WRITE t**
2970 MOVE W2,0
2980 PRINT "J";"K";
2990 PRINT I$
3000 REM **WRITE SCALE**
3010 FOR I=0 TO A3 STEP A3/8
3020 MOVE W1-1,I
3030 PRINT "HHHH";I/1000;
3040 NEXT I
3050 MOVE W1-1,A3
3060 PRINT "H";

```

```

3070 PRINT "K";"KVA";
3080 DELETE T
3090 REM **WRITE TITLE**
3100 DELETE L$
3110 L$="-----"
3120 E$="SPARK POWER"
3130 MOVE W1+(W2-(W1-1))/2,A3
3140 PRINT "K";
3150 FOR T=1 TO LEN(E$)/2
3160 PRINT "H";
3170 NEXT T
3180 PRINT E$;
3190 MOVE W1+(W2-(W1-1))/2,A3
3200 PRINT "K";
3210 FOR T=1 TO LEN(E$)/2
3220 PRINT "H";
3230 NEXT T
3240 PRINT "J";
3250 PRINT L$;
3260 DELETE I
3270 MOVE W1,A(W1)
3280 FOR I=W1 TO W2
3290 DRAW I,A(I)
3300 NEXT I
3310 REM **INT NOW PERFORMED**
3320 CALL "INT",A,A
3330 FOR I=1 TO Y3
3340 A(I)=A(I)*H5
3350 NEXT I
3360 REM **VERT. SCALE FOUND**
3370 CALL "MAX",A,C1,C2
3380 C1=C1*1000
3385 IF C1<0.8 THEN 3425
3390 IF C1<9 THEN 3430
3400 IF C1<80 THEN 3450

```

```

3410 IF C1<900 THEN 3470
3420 IF C1<9000 THEN 3490
3425 C3=0.8
3426 GO TO 3500
3430 C3=8
3440 GO TO 3500
3450 C3=80
3460 GO TO 3500
3470 C3=800
3480 GO TO 3500
3490 C3=8000
3500 VIEWPORT 75,125,5,40
3510 WINDOW W1,W2,0,C3/1000
3520 AXIS Y3/10,24,C3/9000
3530 MOVE W2,0
3540 PRINT "J";"K";
3550 PRINT T$
3560 IF C3=8 THEN 3620
3570 FOR I=0 TO C3 STEP C3/8
3580 MOVE W1-1,I/1000
3590 PRINT "HHHH";I;
3600 NEXT I
3610 GO TO 3660
3620 FOR I=0 TO C3 STEP C3/8
3630 MOVE W1-1,I/1000
3640 PRINT "HHH";I;
3650 NEXT I
3660 MOVE W1-1,C3/1000
3670 PRINT "K";
3680 PRINT "H";"MJ";
3690 DELETE T
3700 DELETE L$
3710 L$="-----"
3720 P$="INTEGRATED SPARK ENERGY"
3730 MOVE W1+(W2-(W1-1))/2,C3/1000

```

```

3740 PRINT "K";
3750 FOR T=1 TO LEN(P$)/2
3760 PRINT "H";
3770 NEXT T
3780 PRINT P$;
3790 MOVE W1+(W2-(W1-1))/2,C3/1000
3800 PRINT "K";
3810 FOR T=1 TO LEN(P$)/2
3820 PRINT "H";
3830 NEXT T
3840 PRINT "J";L$;
3850 DELETE I
3860 MOVE W1,A(W1)
3870 FOR I=W1 TO W2
3880 DRAW I,A(I)
3890 NEXT I
3900 DELETE L$
3910 L$="-----"
3920 MOVE W1-1,C1/1000
3930 PRINT L$;
3940 REM **SIG FIG ROUTINE**
3950 DELETE C2
3960 IF C1>99 THEN 4040
3970 C2=INT(C1)
3980 C2=C1-C2
3990 C2=100*C2
4000 C2=INT(C2)
4010 C2=C2/100
4020 C1=INT(C1)+C2
4030 GO TO 4100
4040 C2=INT(C1)
4050 C2=C1-C2
4060 C2=10*C2
4070 C2=INT(C2)
4080 C2=C2/10

```

```

4090 C1=INT(C1)+C2
4100 MOVE W1-1,0
4110 PRINT "J";"HHHHHHHHHHHHHHHHHHHH";
4120 PRINT "SPARK ENERGY =";C1;" mlliJOULES ";
4130 CALL "WAIT",10
4140 COPY
4150 REM**DYNAMIC V/I-t CURVE NOW DRAWN**
4160 PAGE
4170 VIEWPORT 10,125,10,95
4180 WINDOW W1,W2,-1,4
4190 FOR I=1 TO Y3 STEP 204.8
4200 AXIS 0,0,I,0
4210 NEXT I
4220 C4=(W2-W1)*0.02
4230 FOR I=0.1 TO 1 STEP 0.1
4240 MOVE W1,LGT(I)
4250 DRAW I+C4,LGT(I)
4260 NEXT I
4270 FOR I=1 TO 10
4280 MOVE W1,LGT(I)
4290 DRAW I+C4,LGT(I)
4300 NEXT I
4310 FOR I=10 TO 100 STEP 10
4320 MOVE W1,LGT(I)
4330 DRAW I+C4,LGT(I)
4340 NEXT I
4350 FOR I=100 TO 1000 STEP 100
4360 MOVE W1,LGT(I)
4370 DRAW I+C4,LGT(I)
4380 NEXT I
4390 FOR I=1000 TO 10000 STEP 1000
4400 MOVE W1,LGT(I)
4410 DRAW I+C4,LGT(I)
4420 NEXT I
4430 MOVE W1,-1

```

```

4440 DRAW W2-W1,-1
4450 MOVE W1,0
4460 DRAW W2-W1,0
4470 MOVE W1,1
4480 DRAW W2-W1,1
4490 MOVE W1,2
4500 DRAW W2-W1,2
4510 MOVE W1,3
4520 DRAW W2-W1,3
4530 MOVE W2,-1
4540 PRINT "J";"K";
4550 PRINT T$
4560 DELETE T
4570 DELETE L$
4580 L$="-----"
4590 P$="DYNAMIC VOLTAGE/CURRENT"
4600 MOVE W1+(W2-(W1-1))/2,4
4610 PRINT "K";
4620 FOR T=1 TO LEN(P$)/2
4630 PRINT "H";
4640 NEXT T
4650 PRINT P$;
4660 MOVE W1+(W2-(W1-1))/2,4
4670 PRINT "K";
4680 FOR T=1 TO LEN(P$)/2
4690 PRINT "H";
4700 NEXT T
4710 PRINT "J";L$;
4720 REM **WRITE TIME SCALE**
4730 S$="TIME SCALE: PER DIV"
4740 DELETE L$
4750 L$="-----"
4760 MOVE W1+(W2-(W1-1))/2,-1
4770 PRINT "JJ";
4780 FOR T=1 TO LEN(S$)/2

```

```

4790 PRINT "H";
4800 NEXT T
4810 PRINT S$;
4820 MOVE W1+(W2-(W1-1))/2,-1
4830 PRINT "JJ";
4840 FOR T=1 TO LEN(S$)/2
4850 PRINT "H";
4860 NEXT T
4870 PRINT L$;
4880 PRINT "K";
4890 PRINT "HHHHHHHHHHHHHHHHHHHH";
4900 PRINT H5*2048/10.24;"s"
4910 REM **WRITE SCALE**
4920 DELETE I
4930 FOR I=-1 TO 3
4940 MOVE W1-1,I
4950 PRINT "HHHH";10↑I;
4960 NEXT I
4970 MOVE W1-1,4
4980 PRINT "K";"V/I";
4990 MOVE W1-1,3.9
5000 PRINT "HHHH";"10000";
5010 DELETE I
5020 FOR M=1 TO Y3
5030 IF B(M)=0 THEN 5060
5040 B(M)=LGT(B(M))
5050 GO TO 5070
5060 B(M)=-1
5070 NEXT M
5080 MOVE W1,B(W1)
5090 FOR I=W1 TO W2
5100 DRAW I,B(I)
5110 NEXT I
5120 GO TO 5750
5130 REM **ESTABLISH TRACE POSITIONS**

```

```

5140 PAGE
5150 PRINT
5160 PRINT "NOW PRESS "LOCAL", THEN GROUND THE INPUTS, THEN "
5170 PRINT "ARM BOTH CHANNELS AND PRESS "MANUAL TRIGGER.""
5180 PRINT "THEN PRESS "RETURN""
5190 INPUT G$
5200 PRINT @U,0:"READ A"
5210 WBYTE @64+U,96:
5220 RBYTE X,X1,X2
5230 DIM A(2048)
5240 RBYTE A,X4,X5
5250 Z=0
5260 FOR I=1 TO 2048
5270 Z=Z+A(I)
5280 NEXT I
5290 P3=Z/2048
5300 P3=(P3-127.5)/(255/8)
5310 PRINT @U,0:"READ B"
5320 WBYTE @64+U,96:
5330 RBYTE Y,Y1,Y2
5340 DIM B(2048)
5350 RBYTE B,Y4,Y5
5360 Z1=0
5370 FOR I=1 TO 2048
5380 Z1=Z1+B(I)
5390 NEXT I
5400 P4=Z1/2048
5410 P4=(P4-127.5)/(255/8)
5420 PAGE
5430 VIEWPORT 10,60,30,70
5440 WINDOW W1,W2,0,256
5450 AXIS 200,32,W1,128
5460 MOVE 1,A(1)
5470 FOR I=1 TO 2048
5480 DRAW I,A(I)

5490 NEXT I
5500 VIEWPORT 70,120,30,70
5510 WINDOW W1,W2,0,256
5520 AXIS 200,32,W1,128
5530 MOVE 1,B(1)
5540 FOR I=1 TO 2048
5550 DRAW I,B(I)
5560 NEXT I
5570 MOVE 0,256
5580 PRINT "EEEEEE";"HHHHHHHH";"TRACE ZERO LINES";
5590 PRINT "HHHHHHHHHHHHHHHHHHHHHHHHHHHHHHHHHHHHHHHHHHHH";"CHANNEL A";
5600 PRINT " ";"CHANNEL B";
5610 VIEWPORT 0,130,0,100
5620 WINDOW 0,130,0,100
5630 MOVE 5,10
5640 DRAW 125,10
5650 DRAW 125,95
5660 DRAW 5,95
5670 DRAW 5,10
5680 CALL "WAIT",10
5690 RETURN
5700 PAGE
5710 PRINT
5720 PRINT "THE CHANNEL B INPUT SIGNAL MAY HAVE SATURATED THE"
5730 PRINT "INPUT AMPLIFIER ; ADJUST THE VOLTS/DIVISION SETTING"
5740 PRINT "AND/OR THE "POSITION" SETTING IF NECESSARY"
5750 POLL P1,P2;U,0;U,1
5760 RETURN

```

VARIABLES LISTING.

THE FOLLOWING LISTS ALL VARIABLES USED IN PROGRAMMES 1-6. KEY WORDS AND HEADINGS ARE GIVEN FOR GUIDANCE ONLY. PLEASE SEE THE PROGRAMMES FOR THEIR ACTUAL USE. SEE ALSO THE 4052 AND 7612AD MANUALS FOR COMMAND VARIABLE NAMES.

A.....x DATA FROM 7612AD
A1.....MAX VARIABLE USED TO FIND THE VERTICAL "POWER" SCALE
A2.....MAX VARIABLE USED TO FIND THE VERTICAL "POWER" SCALE
A3.....SCALE FACTOR FOR "POWER" CURVE

B.....y DATA FROM 7612AD

C1.....MAX VARIABLE USED TO FIND THE VERTICAL "INT" SCALE
C1.....ALSO THE SPARK ENERGY VALUE
C2.....MAX VARIABLE USED TO FIND THE VERTICAL "INT" SCALE
C2.....ALSO A VARIABLE IN THE SIG FIG ROUTINE
C3.....SCALE FACTOR FOR "INT" CURVE
C4.....A VARIABLE USED FOR LOGARITHMIC SCALING

G1-G9.....a-CHANNEL HORIZONTAL SCALE FACTORS

H1-H5.....a OR b-CHANNEL HORIZONTAL SCALE FACTORS

I.....FOR/NEXT LOOP STEP INTEGER

K.....FOR/NEXT LOOP STEP INTEGER

L.....FOR/NEXT LOOP STEP INTEGER
 M..... FOR/NEXT LOOP STEP INTEGER
 M1-M8.....MAX AND MIN VARIABLES IN THE SATURATION ROUTINE
 N.....NUMBER OF BREAK POINTS
 N5.....CROSSOVER POINT USED IN THE SPIKE-ZEROING ROUTINE
 P1,P2.....POLLING TARGET VARIABLES
 P3.....AVERAGED CHANNEL a ZERO REFERENCE
 P4.....AVERAGED CHANNEL b ZERO REFERENCE
 R.....TIME-SCALE SUBROUTINE ZERO POINT
 R1.....PROBE 1 RATIO
 R2.....PROBE 2 RATIO
 S.....RETURNED CROSSOVER VALUE USED IN SPIKE-ZEROING
 T.....FOR/NEXT LOOP STEP INTEGER
 U.....7612AD GPIB PRIMARY ADDRESS
 U1.....CHANNEL a I/P SENSITIVITY
 U2.....CHANNEL b I/P SENSITIVITY
 W1.....FIRST HORIZONTAL DATA POINT
 W2.....LAST HORIZONTAL DATA POINT
 X1-X5.....READ CHANNEL a DATA
 Y1-Y5.....READ CHANNEL b DATA
 Z.....A VARIABLE USED IN THE ZERO-LINES ROUTINE
 Z1.....CHANNEL a ZERO-VARIABLE
 Z2.....CHANNEL b ZERO-VARIABLE

STRING VARIABLES. SPARK DISCHARGE FORM

E\$...."SPARK POWER"
 F\$...."RETURN" KEY DUPLICATE
 G\$...."RETURN" KEY DUPLICATE
 I\$...."SPARK CURRENT"
 J\$....POS OR NEG SPIKE (P/N) REQUEST
 K\$....YES/NO (Y/N) REQUEST
 L\$....UNDERLINING ARRAYS
 L\$....ALSO ARRAYS USED IN THE VERT PRINT ROUTINES
 M\$....UNDERLINING ARRAY
 N\$....UNDERLINING ARRAY
 P\$...."INTEGRATED SPARK ENERGY"
 P\$....ALSO "DYNAMIC VOLTAGE/CURRENT"
 Q\$....YES/NO (Y/N) REQUEST
 S\$...."TIME SCALE"
 T\$...."t"
 U\$...."SPARK VOLTAGE"
 X\$....VERT PRINT ARRAY
 Y\$....YES/NO (Y/N) REQUEST
 Z\$....YES/NO (Y/N) REQUEST

Discharge phases

When an electric discharge is made to pass between two electrodes, the state of the discharge will pass through a number of stages. These depend upon both the physical gap arrangement and the external circuit. If the gap is raised to or above its breakdown potential, using a capacitor-discharge circuit for example, then the discharge voltage and current will typically take the forms shown in Figures A1 and A2. The complete process may progress through the following stages:

- (1) Pre-discharge phase
- (2) Breakdown phase
- (3) Transition region
- (4) Arc phase
- (5) Arc/glow transition
- (6) Glow phase

APPENDIX 3

NOTES ON SPARK DISCHARGE FORM

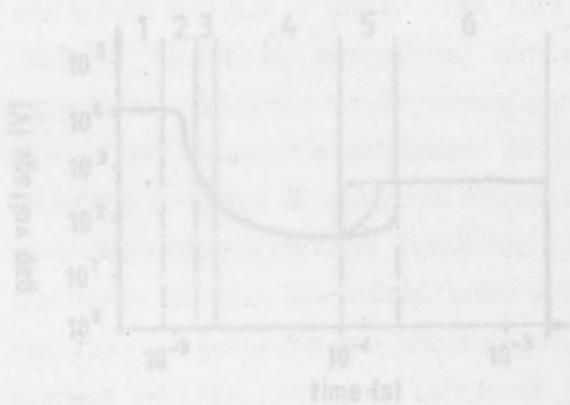


Figure A1. Discharge voltage curve showing the 6 basic discharge phases.

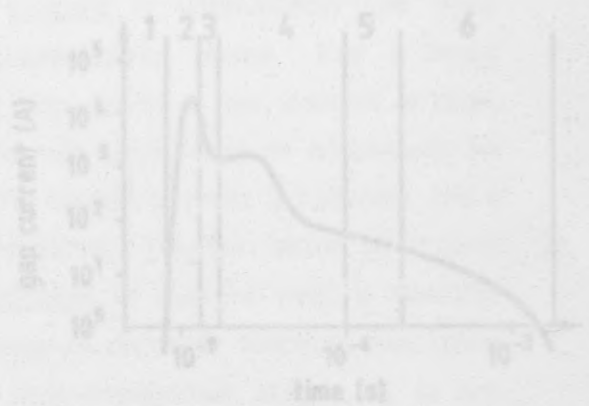


Figure A2. Discharge current curve showing the 6 basic discharge phases.

According to this simplified process, a discharge, or 'spark' is usually classified in terms of the post-breakdown phase and may be termed an 'arc' or 'glow' type.

The breakdown phase is essentially initiated by the spark-gap capacitance. This phase is typically very short in duration (< 10 ns) and creates the conductive path prior to the formation of an arc or glow. The temperatures reached in the breakdown channel may reach $\sim 60,000$ K, and energy is transferred to the plasma almost without loss. Energy is stored by the gas molecules in the channel by ionization and dissociation.

Discharge phases

When an electric discharge is made to pass between two electrodes, the state of the discharge will pass through a number of stages. These depend upon both the physical gap arrangement and the external circuit. If the gap is raised to or above its breakdown potential, using a capacitor-discharge circuit for example, then the discharge voltage and current will typically take the forms shown in Figures A1 and A2. The complete process may progress through the following stages²⁸:

- (1) Pre-discharge phase
- (2) Breakdown phase
- (3) Transition region
- (4) Arc phase
- (5) Arc/glow transition
- (6) Glow phase

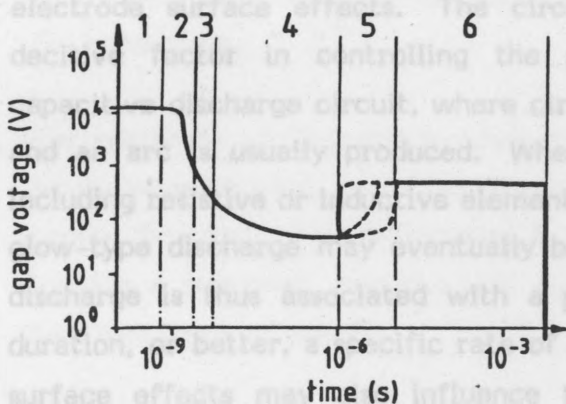


Figure A1. Discharge voltage curve showing the 6 basic discharge phases.

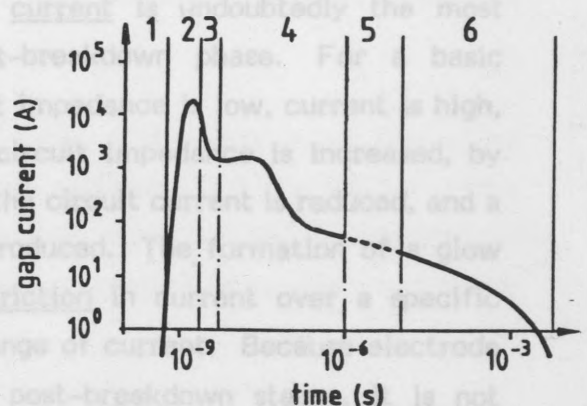


Figure A2. Discharge current curve showing the 6 basic discharge phases.

According to this simplified process, a discharge, or 'spark' is usually classified in terms of the post-breakdown phase and may be termed an 'arc' or 'glow' type.

The breakdown phase is essentially initiated by the spark-gap capacitance. This phase is typically very short in duration (< 10 ns) and creates the conductive path prior to the formation of an arc or glow. The temperatures reached in the breakdown channel may reach $\sim 60,000$ K, and energy is transferred to the plasma almost without loss. Energy is stored by the gas molecules in the channel by ionization and dissociation.

The arc phase typically shows a low voltage drop of ~ 100 V and the current may reach some kA, according to the external circuit. Voltage falls at the cathode and anode constitute the greater part of the overall voltage drop, and significant losses may be incurred at the electrodes. Equilibrium gas temperatures are limited to ~ 6000 K, and expansion occurs due to heat conduction and mass diffusion.

The glow phase typically shows a higher voltage drop than the arc (300 - 1000 V) and a low current of < 500 mA. The voltage fall at the cathode may constitute the greater part of the overall drop, and losses are higher than for the arc. Equilibrium temperatures may reach ~ 3000 K, and despite lower ionization and dissociation in the gap, expansion is similar to the arc phase.

(this is the static breakdown voltage)

Not all discharges proceed to stages 5 or 6, and some do not appear to pass through the arc stage (4). The appearance of one phase or another, or of a transition between the two, is mainly controlled by the external circuit, and electrode surface effects. The circuit current is undoubtedly the most decisive factor in controlling the post-breakdown phase. For a basic capacitive discharge circuit, where circuit impedance is low, current is high, and an arc is usually produced. Where circuit impedance is increased, by including resistive or inductive elements, the circuit current is reduced, and a glow-type discharge may eventually be produced. The formation of a glow discharge is thus associated with a restriction in current over a specific duration, or better, a specific rate of change of current. Because electrode surface effects may also influence the post-breakdown stages, it is not always possible to predict a given discharge type, particularly where current is limited. For this reason spark current and voltage should be measured to help ascertain a discharge phase, particularly when circuit impedance is increased. The appearance of a glow is often more diffuse than for an arc, which may also help in classifying the post-breakdown phase.

Intermediate phases may also be observed, where current falls slowly, and a transition from arc to glow takes place (phase 4). This was observed when attempting to increase discharge duration in Part 1 of this work.

Most workers studying spark ignition have used capacitive circuits where arc discharges were produced. Where discharge duration has been studied, however, and circuit impedances arbitrarily altered, the form of the

discharge has not always been held constant, making interpretations difficult. In addition, breakdown energy has usually been neglected or not measured.

Gap pulsing

When the voltage across a spark gap is raised slowly, a sheath of positive ions will tend to form around the positive electrode. This represents a process which can be seen as small 'corona' stabilisations. Because of the long times involved, this, together with a similar process at the cathode, may tend to restrict breakdown. Thus a high voltage is required for breakdown of the gap (this is the static breakdown voltage.) When instead, a fast pulse is used, then depending upon the pulse speed, the ions will not have time to form, and a streamer may form across the gap, leading to breakdown. The formation of a streamer depends upon electrode surface effects; pointed electrodes will tend to promote the streamer mechanism, allowing lower voltages to be used for breakdown.

For electrode configurations other than points, a streamer is not formed so easily when pulsing, and lower breakdown voltages than the 'static' value cannot be used. This is because a sufficient electric field is required to initiate a streamer, and this will decrease dramatically as electrode shape becomes more spherical.

The schlieren principle

The principle of schlieren operation used here was the same as that developed by Foucault⁶³ in 1859, often referred to as the "knife-edge test". This was elaborated upon some few years later by Toepler⁶⁴ and amplified extensively by Schardin⁶⁵. The principle is outlined in Figure A3⁶⁶. A light source is placed at a distance $2F$ from the concave schlieren lens of focal length F . When the eye is placed at L' , distance $2F$ from the other side of the lens, the whole lens will appear to radiate light. If a straight edge is now moved across point L' , then a certain point will be reached where rays refracted due to a disturbance in the viewed field S cause an addition or subtraction to or from the total illumination. That is, rays are refracted either towards or away from the edge at L' , and thus a part of the field will appear bright or dark. The variations in brightness depend on differences in the gradients of refractive index in the schlieren field S .

APPENDIX 4

SCHLIEREN TECHNIQUES USED IN THIS WORK

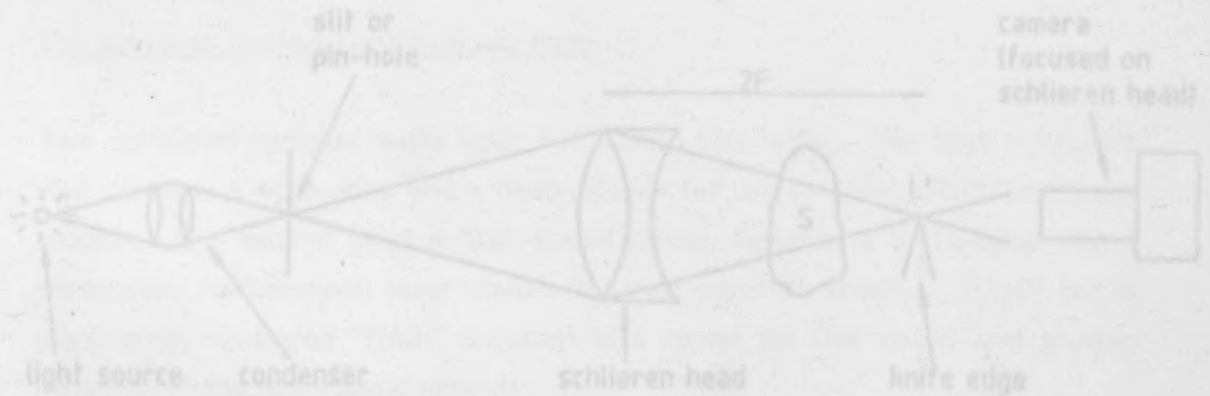


Figure A3. Basic schlieren set-up.

This basic approach was elaborated upon in the current work. Similar approaches have also been used by a number of other workers when studying spark and explosion phenomena^{6,10,45}

The schlieren principle

The principle of schlieren operation used here was the same as that developed by Foucault⁶³ in 1859, often referred to as the "knife-edge test". This was elaborated upon some few years later by Toepler⁶⁴ and amplified extensively by Schardin⁶⁵. The principle is outlined in Figure A3⁶⁶. A light source is placed at a distance $2F$ from the concave schlieren lens of focal length F . When the eye is placed at L' , distance $2F$ from the other side of the lens, the whole lens will appear to radiate light. If a straight edge is now moved across point L' , then a certain point will be reached where rays refracted due to a disturbance in the viewed field S cause an addition or subtraction to or from the total illumination seen at L' . That is, rays are refracted either towards or away from the edge at L' , and thus a part of the field will appear bright or dark. An image is therefore formed, wherein the variations in brightness depend on differences in the gradients of refractive index in the schlieren field S .

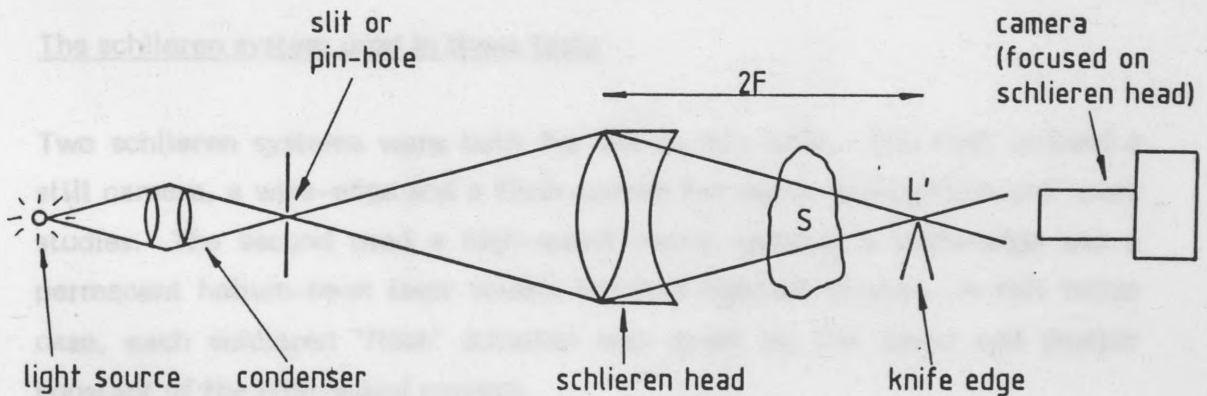


Figure A3. Basic schlieren set-up.

This basic approach was elaborated upon in the current work. Similar approaches have also been used by a number of other workers when studying spark and explosion phenomena^{6,10,45}.

These workers all used a similar method to observe the disturbances produced by a spark or an explosion around a pair of electrodes. The spark gap is first triggered, and a spark produced, leading to ignition. After a chosen delay, the schlieren light source is triggered, creating a short-duration high intensity light flash, which passes through the schlieren field (i.e., spark or explosion chamber) and is focused on the knife-edge. The position of the knife edge is carefully adjusted to give a high-definition refraction pattern of the schlieren field. This positioning is critical.

Four factors are of utmost importance in the alignment of the light-refraction system. First, the light-lens-chamber-camera combination must be carefully aligned and free from vibration. Secondly, the light-flash duration should be as short as possible compared with the event time in the schlieren field. Thirdly, the light from the flash-source should be carefully collimated into a narrow, well defined beam. Lastly, the distances involved may be critical when viewing small changes in refractive index and should be kept as short as possible, particularly the distance from the viewing field to the camera.

The schlieren system used in these tests

Two schlieren systems were built for use in this work. The first utilised a still camera, a wire-edge and a flash-source for use in gas-ignition and spark studies. The second used a high-speed movie camera, a knife-edge and a permanent helium-neon laser source for dust-ignition studies. In this latter case, each schlieren 'flash' duration was given by the speed and shutter constant of the high-speed camera.

Schlieren system using a still camera

The light source used in these studies was a xenon flashtube which could yield a wide variety of light-flash intensities and durations. This flashtube (EG + G type FX265) could produce 500 ns, 5W light discharges with a low time jitter of less than 200 ns.

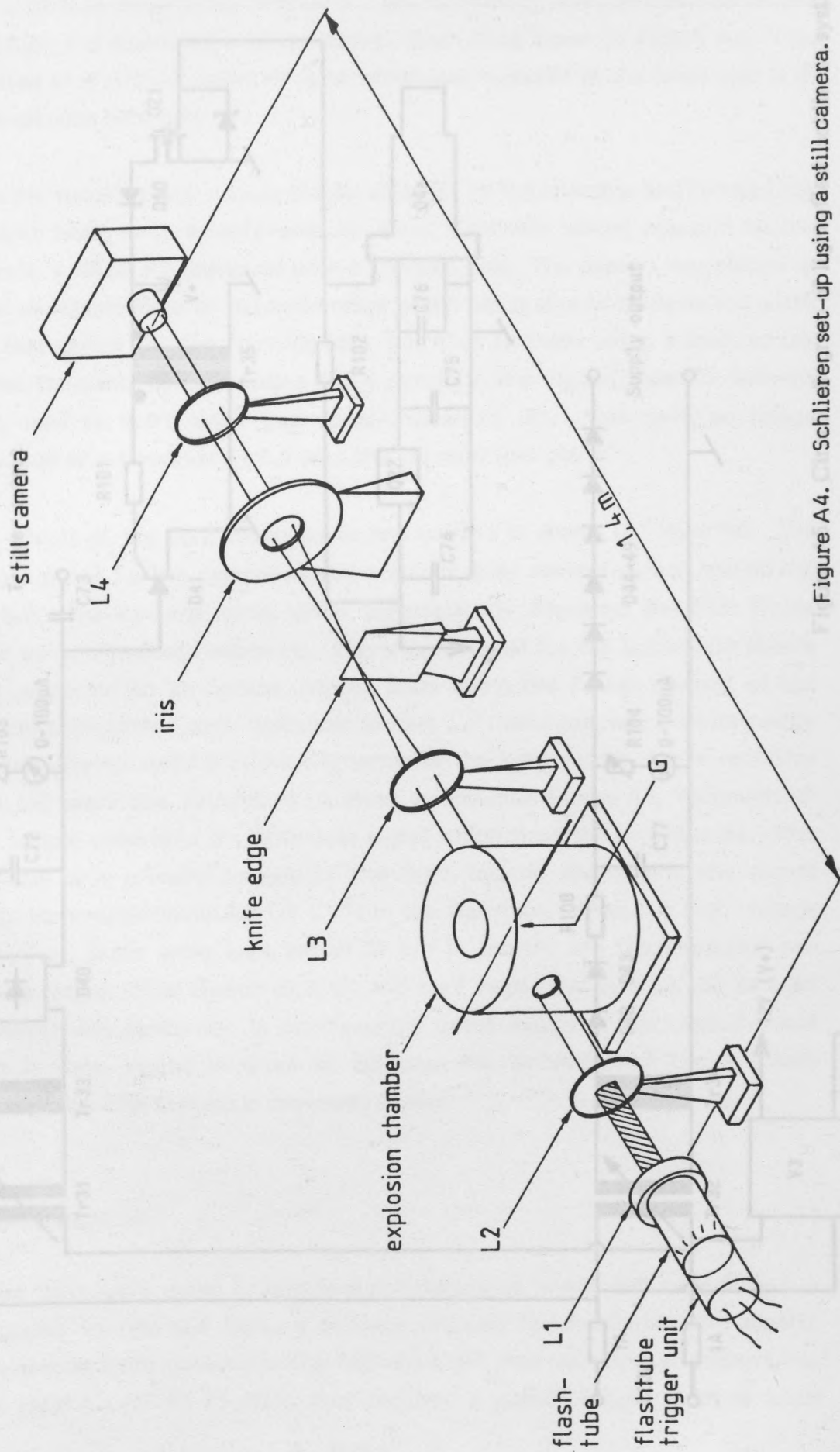


Figure A4. Schlieren set-up using a still camera.

The light was collimated, first by a 2 cm cylindrical lens L1, mounted on the flashtube and finally by a 10 cm convex lens L2, as shown in Figure A4. This resulted in a circular beam of light which was directed at the spark gap G in the explosion chamber.

A 16 cm focusing lens L3 was placed adjacent to the chamber and focused the incident beam onto a knife-edge or wire. This was placed adjacent to the camera, a Nikon F3, equipped with a 105 mm lens. The camera was placed as close as was possible to the knife-edge whilst being able to focus on the spark gap through L4 and the focusing lens, L3. Due to there being a limit to the lowest focusable distance using a 105 mm lens, the closest possible distance from lens to knife edge was approximately .5 cm. This gave an image reduction of approximately 0.5 onto the (35 mm) film plane.

The circuit of the light flash source and camera is shown in Figure A5. The trigger signal for the camera closed a pair of relay contacts which opened the shutter. The camera motor-drive automatically advanced the film frame after each 1/2 second exposure. The trigger signal for the light-flash source was converted to an optical trigger pulse using the fourth channel of the 'optical transmitter' unit, described in Part 1. This signal was transmitted by optical fiber to avoid spurious triggering of the light source due to radiation from the spark gap. An optical receiver, as shown in Figure A5, 'reconverted' this trigger pulse into a 12V trigger signal which fired the thyristor T1. This resulted in a primary trigger of the light source, discharging the stored capacitor energy (given by $1/2 CV^2$) in the flashtube. When the high voltage (capacitor) leads were kept below 50 cm in length, and the capacitor and voltage values were chosen as 2 μF and 1 kV respectively, a 1J, 0.5 μs light discharge was produced. In practice, the exact values of the capacitor and voltage were varied in order to optimise the definition of the schlieren photograph. This process is described below.

Initial test set-up

Initial tests were made to optimise positioning of lenses and camera and in particular to find the lighting settings suitable for particular film-speeds. Best results were obtained using high-contrast poor-sensitivity orthographic film (AGFA ORTHO 25 ASA) that required a powerful light flash of some

Joules to give any exposure. Such a film was also insensitive to any explosion radiation that might otherwise obscure the clarity of the schlieren image. It was also of a very fine grain, meaning a greater quality of enlargement compared to more sensitive film types.

The system was fully aligned by recycling the ACS (timing unit) to produce a continuous flashing of the light-source. This enabled the fine positioning of the schlieren stop (usually a wire as proposed by Arnold and Sherburne⁶⁷). For stability, all components were mounted on optical benches placed on either side of the explosion chamber. To keep exposure time (flash-time) to a minimum, voltage V was varied and capacitance C was kept as low as possible for a fixed discharge energy. The final choice of values yielded a light flash of some 2 Joules with a duration of $0.6 \mu\text{s}$.

Schlieren system using a high-speed camera

This system was a modified version of the first and used a permanent light source in the form of a helium-neon laser instead of a flash-source. Such a system had to be constructed for use with dust-ignition experiments, where ignition phenomena were not reproducible in space between shots. The system is shown schematically in Figure A6.

The output beam of the laser was expanded and collimated by the beam expander unit L1. This provided a well defined beam of 2.5 cm diameter aimed at the spark gap G.

A 16 cm focusing lens L3 was placed adjacent to the chamber, as before, and focused onto a knife-edge. An electronic shutter was placed between this and a Hitachi 'Hymac' high-speed camera equipped with the same Nikon 105 mm lens as used in the first system. This lens was focused on the spark gap through the schlieren lens L3. With the distances given in Figure A6, an image reduction of approximately 0.1 was achieved onto the (16 mm) film plane. This whole system relied upon careful triggering of the dust dispersion, spark gap, electronic shutter and camera with respect to one another. The electronic shutter was important as a means of utilising the full 38 meter film length. By reversing a film and using it over again and selecting various shutter opening times, up to four sequences of some 80 ms

duration could be recorded on the same film using a camera speed of 9000 frames per second. This reduced film wastage considerably, as it was necessary to accelerate some 25 metres of the film before the desired speed of 9000 frames per second was reached. In these tests, the film was reversed and two segments run on each 13 metre end section.

Timing functions were controlled by the ACPU and ACS timing units, which switched camera shutter, spark discharge and dispersion in a fixed sequence according to the film segment being used.

Initial test set-up

Initial tests were made at 9000 fps (close to the maximum speed of the camera) to establish:

- a) optimum laser intensity
- b) optimum film type (black and white)
- c) optimum camera positioning and lens aperture
- d) optimum knife-edge settings for use with either sparks only or with a dust cloud present in the explosion vessel
- e) timing settings to allow for shutter opening delay and film acceleration

Results indicated a laser intensity of 7mW using Kodak RAR 2749 film with the camera positioned as shown in Figure A6. Final system sensitivity was variable using the knife-edge. A 'dark' schlieren field was used for tests using sparks only, and a brighter field was used with dust in the chamber (which tended to attenuate and diffuse the incident laser beam). The equivalent 'flash duration' (the exposure time) was given by the camera shutter constant (≈ 5). This gave an exposure time of 22 μ s per frame. Due to vibrations transmitted during acceleration from the camera housing along the optical bench to other components, the camera was mounted on a 75 kg steel base plate, and four 10 mm rubber isolators placed between the base plate and bench. This is shown in Figure A6.

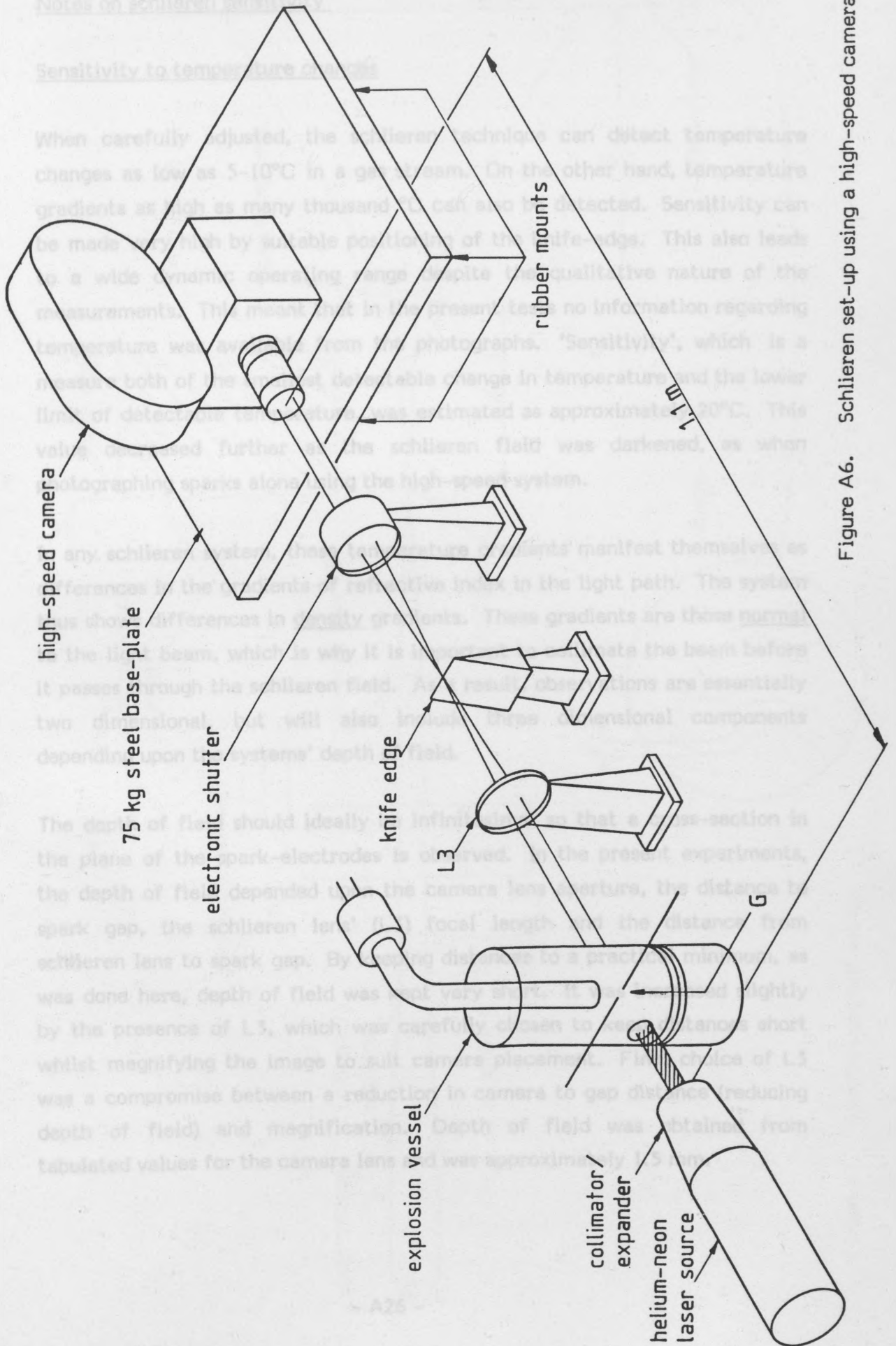


Figure A6. Schlieren set-up using a high-speed camera.

Notes on schlieren sensitivity

Sensitivity to temperature changes

When carefully adjusted, the schlieren technique can detect temperature changes as low as 5–10°C in a gas stream. On the other hand, temperature gradients as high as many thousand °C can also be detected. Sensitivity can be made very high by suitable positioning of the knife-edge. This also leads to a wide dynamic operating range despite the qualitative nature of the measurements. This meant that in the present tests no information regarding temperature was available from the photographs. 'Sensitivity', which is a measure both of the smallest detectable change in temperature and the lower limit of detectable temperature, was estimated as approximately 20°C. This value decreased further as the schlieren field was darkened, as when photographing sparks alone using the high-speed system.

In any schlieren system, these temperature gradients manifest themselves as differences in the gradients of refractive index in the light path. The system thus shows differences in density gradients. These gradients are those normal to the light beam, which is why it is important to collimate the beam before it passes through the schlieren field. As a result, observations are essentially two dimensional, but will also include three dimensional components depending upon the systems' depth of field.

The depth of field should ideally be infinitesimal so that a cross-section in the plane of the spark-electrodes is observed. In the present experiments, the depth of field depended upon the camera lens aperture, the distance to spark gap, the schlieren lens' (L3) focal length and the distance from schlieren lens to spark gap. By keeping distances to a practical minimum, as was done here, depth of field was kept very short. It was increased slightly by the presence of L3, which was carefully chosen to keep distances short whilst magnifying the image to suit camera placement. Final choice of L3 was a compromise between a reduction in camera to gap distance (reducing depth of field) and magnification. Depth of field was obtained from tabulated values for the camera lens and was approximately 1.5 mm.

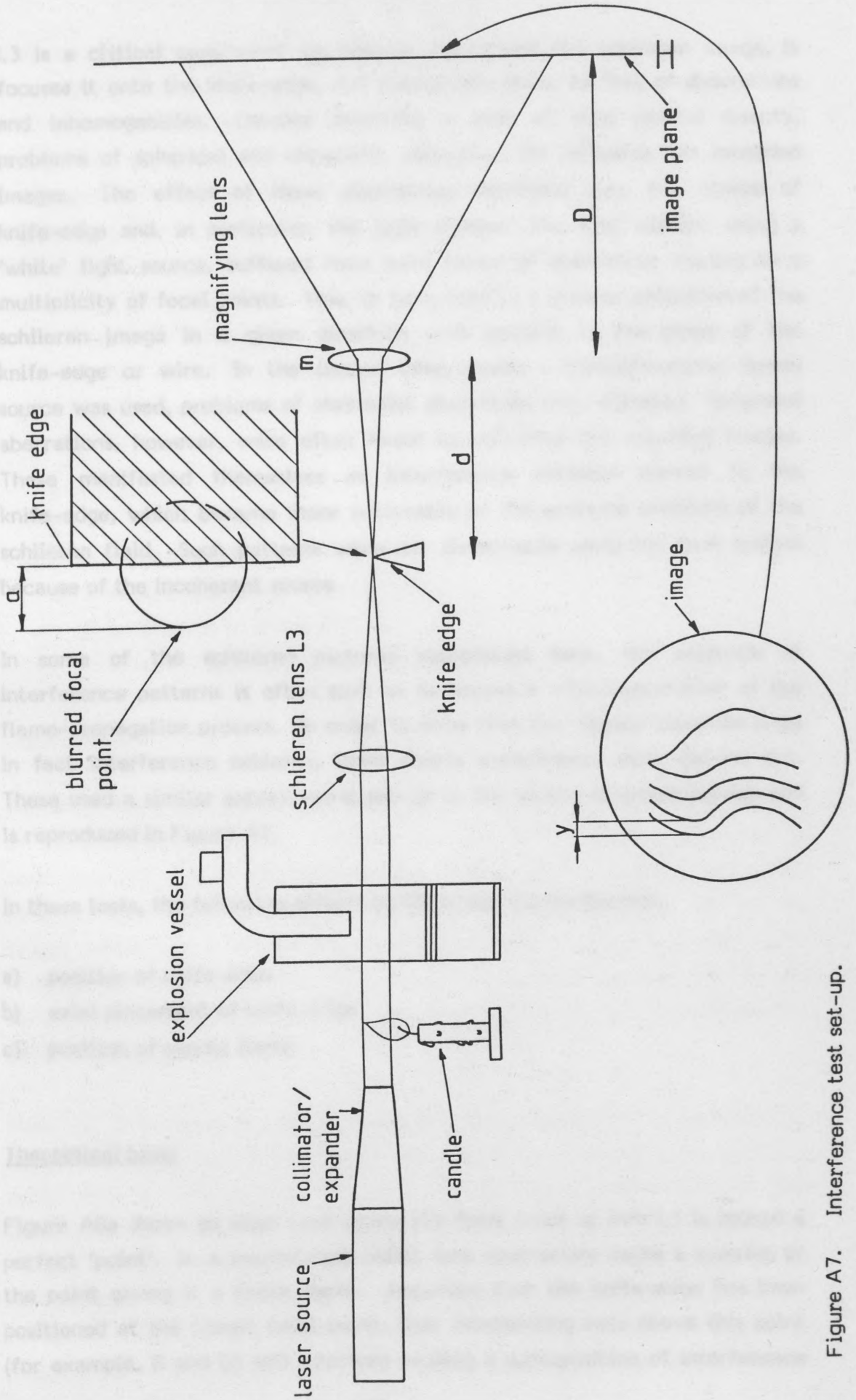


Figure A7. Interference test set-up.

L3 is a critical component as, besides magnifying the schlieren image, it focuses it onto the knife-edge. L3 should, therefore, be free of aberrations and inhomogenities. Despite selecting a lens of good optical quality, problems of spherical and chromatic aberration did influence the recorded images. The effect of these aberrations depended upon the choice of knife-edge and, in particular, the light source. The first system, using a 'white' light source, suffered from both forms of aberration, leading to a multiplicity of focal points. This, in turn, lead to a greater definition of the schlieren image in a given direction with respect to the plane of the knife-edge or wire. In the second case, where a monochromatic (laser) source was used, problems of chromatic aberration were obviated. Spherical aberrations, however, were often found to influence the recorded images. These manifested themselves as interference patterns normal to the knife-edge, which became more noticeable at the extreme positions of the schlieren field. Such patterns were not discernable using the first system because of the incoherent source.

In some of the schlieren pictures reproduced here, the presence of interference patterns is often such as to invoke a misinterpretation of the flame-propagation process. In order to show that the 'layers' observed were in fact interference patterns, some simple experiments were carried out. These used a similar experimental set-up to the second schlieren system and is reproduced in Figure A7.

In these tests, the following effects on the image I were studied:

- a) position of knife-edge
- b) axial placement of knife-edge
- c) position of candle flame

Theoretical basis

Figure A8a shows an ideal case where the focal point of lens L3 is indeed a perfect 'point'. In a second case (A8b), lens aberrations cause a blurring of the point giving it a finite depth. Assuming that the knife-edge has been positioned at the (ideal) focal point, then intersecting rays above this point (for example, B and D) will interfere causing a superposition of interference

lines on the image plane. If, in addition, these rays should be refracted prior to reaching their points of focus (i.e., in the schlieren field) then the position of these lines on the film plane will change. Clearly this interference phenomena is directional, so that for a horizontal positioning of the knife-edge interference will be observed above the edge. This is shown in Figure A8c, where three rays are incident on the plane of the knife-edge. Ray F meets the knife itself and, unless refracted upwards by the schlieren field, does not contribute to the image. An 'ideal' ray B meets the knife-edge at P, whilst ray A meets the knife-edge plane at Q. It may then be shown that A and B interfere, giving image lines separated by distance 'y' where 'y' is given by:

$$y = \frac{\lambda D m}{a} \quad (1)$$

where a is distance PQ

λ is light wavelength ($6.32 \cdot 10^{-7}$ m)

D is distance to image (0.2m)

m is lens magnification (see figure A5) = 10

Experiments

The knife-edge was adjusted using a micrometer so that incremental changes in the knife-edge position could be measured. The knife-edge could be positioned and turned vertically or horizontally. Positioning the knife-edge centrally and horizontally gave interference lines in the top half of the image, which were clearer at the image edge. Rotating the knife-edge reversed the position of the lines. Placing the edge centrally and in the vertical plane caused the patterns to spread across the left or right half of the image plane.

With the knife-edge positioned centrally, either vertically or horizontally, image line separation 'y' was measured using a candle flame in the schlieren field. With a distance 'a' of 0.1 mm, 'y' was approximately 1.1 cm. This value compared well with a theoretical value of 1.26 cm (from formula 1). Moving the knife-edge across its plane and reducing 'a' to 0.05 mm darkened the schlieren field almost completely but doubled the line separations as was expected. The few observable lines were now concentrated in the outer image area. The optimum position for interference lines was central, where

the schlieren effect was also optimum. Brightening the field reduced the sensitivity of the schlieren effect, whereas a darkening increased it but only at the field extremes. This was confirmed first by moving the position of the candle flame, and then by replacing this with a smouldering match. With the match placed at position A, as shown in Figures A9a and b, a very dim image resulted, but at position B, interference lines were observed. At C, a schlieren image was observed without interference lines.

Positioning of the knife-edge was, therefore, a compromise between sensitivity and unavoidable interference effects. In the ignition experiments, the knife-edge was repositioned for each film sequence and thus slight variations in image quality were observed. For example where sensitivity was low, as for photographing sparks only, interference effects were not visible, but for other sequences the knife-edge position often gave noticeable interference lines. These were visible not least because of the very high magnifications used to view the gap area.

Choice and positioning of knife-edge

Because of the widening and deepening of the focal point due to lens inhomogeneities, a particular positioning of the knife-edge often gave increased sensitivity in one half of the image plane. For a centrally and horizontally placed edge, this occurred in the top half of the image. An attempt was made in the first test run (propane-air ignitions) to eliminate this problem, using a thin wire instead of a knife-edge. This acted as two knife-edges back-to-back. Positioning and thickness were critical and often gave increased sensitivity in one half of the image. In some of the later tests, a knife-edge or thicker wire was used, which gave an increased sensitivity in one direction only.

In the second test run using dusts, a vertical knife-edge was used. This had to be positioned so as to reduce the laser intensity to avoid over-exposure of the high-speed film. Correct positioning was found experimentally and depended on whether dust was present (which also reduced the transmitted light through the schlieren field). In all cases, positioning was such as to give an increased sensitivity in one direction only. This direction was normal to the knife-edge (into free space). This effect was confirmed first by rotating the knife edge and then by placing it horizontally. In both cases, recorded images were observed normal to the edge only (into free space).

Figure A8. Effects of schlieren lens L3 aberrations.

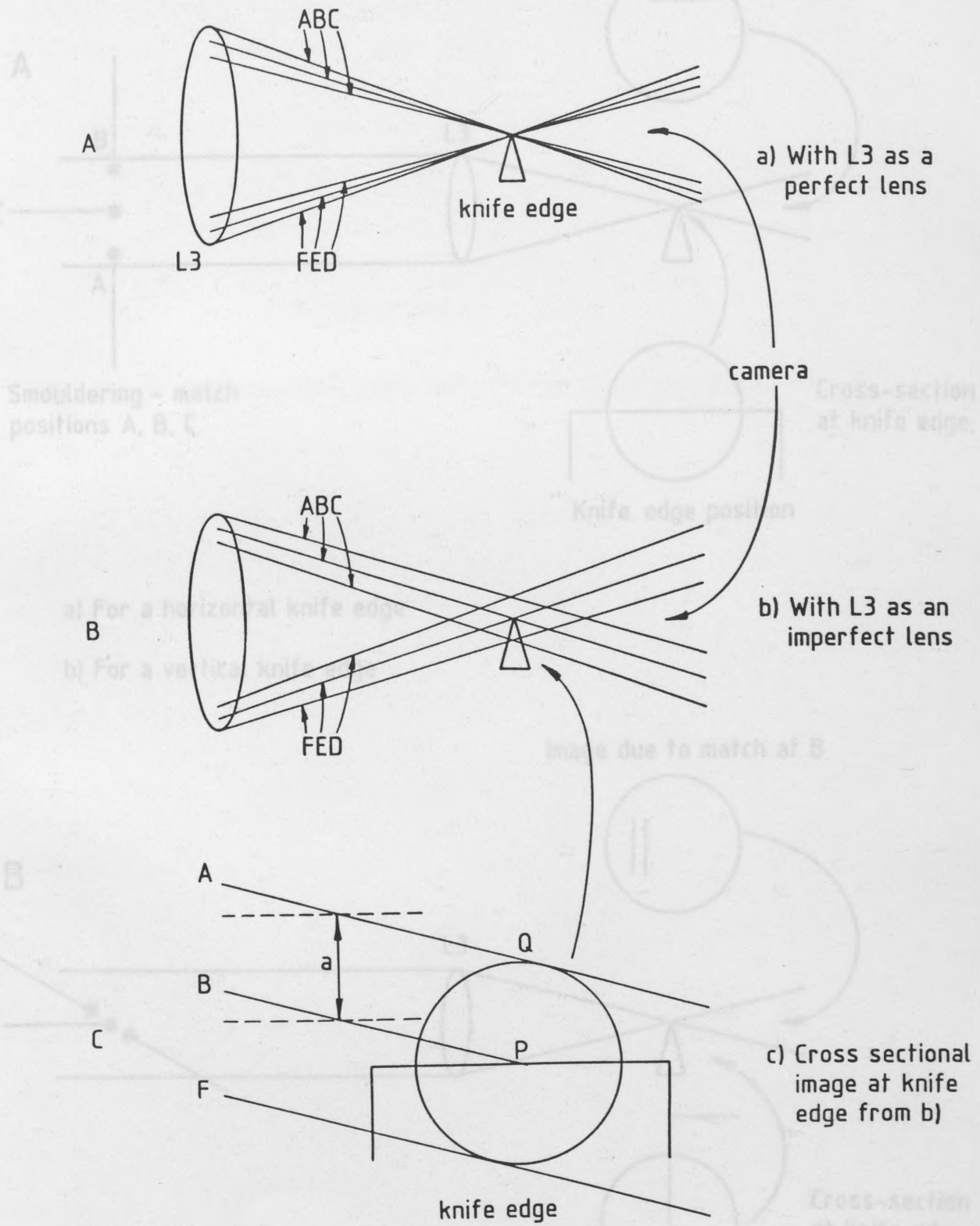
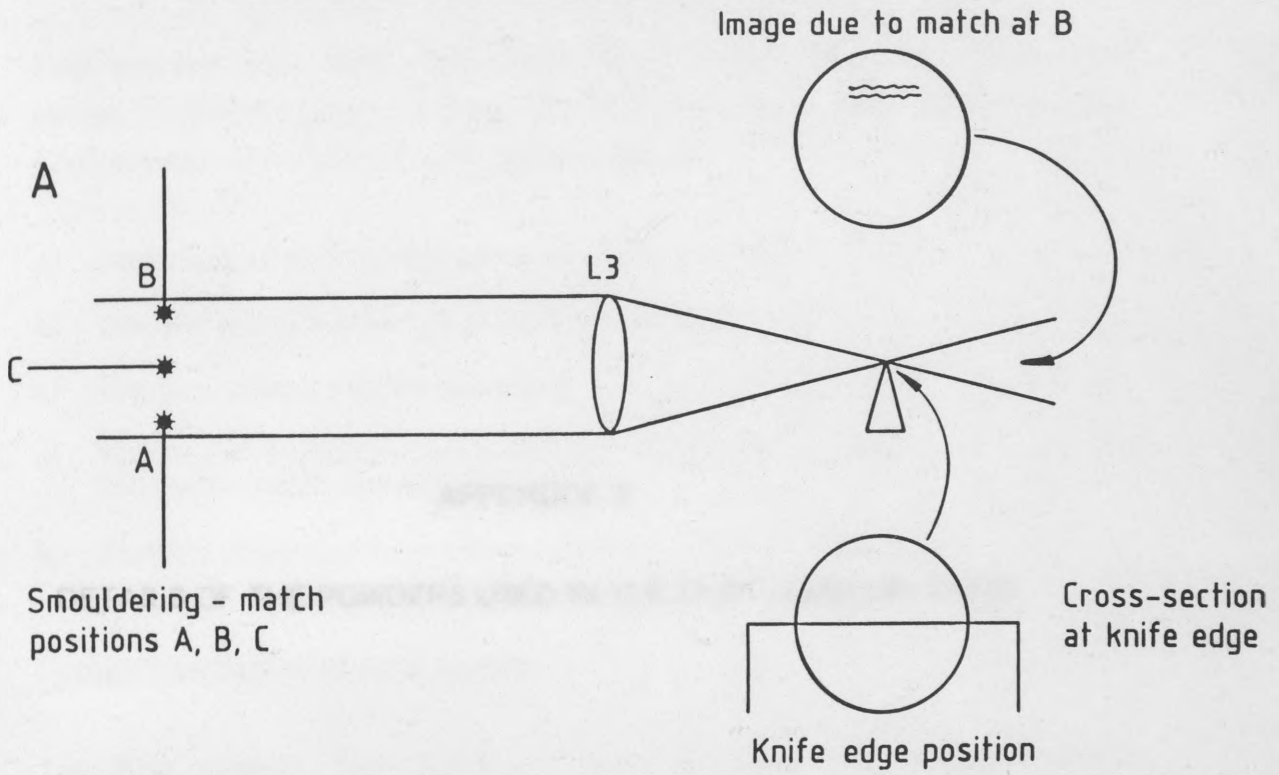
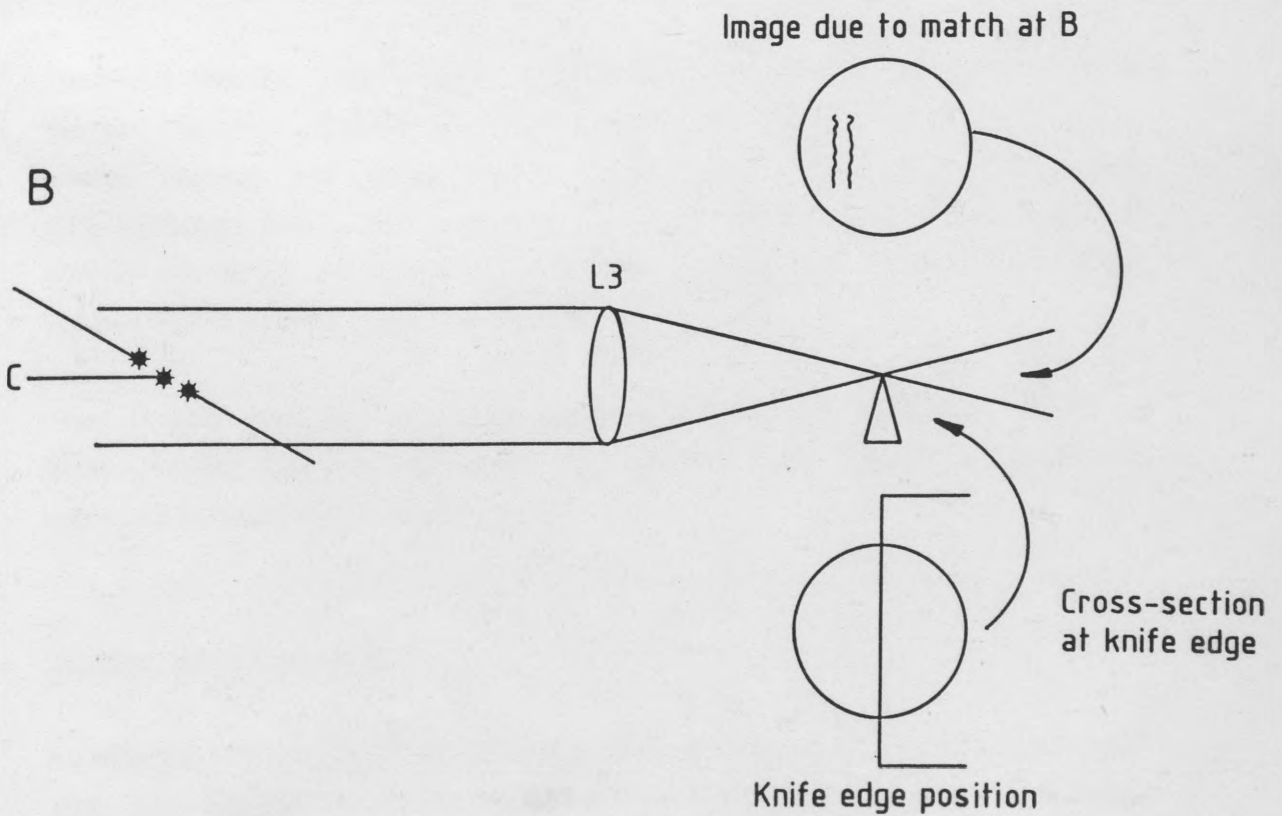


Figure A9. Test set-up showing the appearance of interference lines.



a) For a horizontal knife edge

b) For a vertical knife edge



Analysis of the powders

Four powders were used in the dust ignition tests in this work. These were named 'Stabiliser powder', Benzenethron, Lycopodium and Polyacrylonitrile. Each powder was analysed in the following tests:

- a) Particle size distribution using a Coulter counter
- b) Specific surface area using the Ströhlein apparatus
- c) Density, using an air pycnometer
- d) Maximum explosion pressure and rate of pressure rise in the Hertmann-bomb apparatus
- e) Particle shape and form using a scanning electron microscope

APPENDIX 5

DETAILS OF THE POWDERS USED IN THE DUST-IGNITION TESTS

General description of each powder

The first powder, the 'stabiliser', was obtained from a West-German chemical company, and was developed as a polymer stabiliser. No details of chemical composition could be obtained for this powder.

The second powder, Benzenethron, was also a West-German product, and like the first, no details could be procured concerning its chemical composition.

The third powder, Lycopodium, was obtained from Norges Medicinaldepot in Bergen, Norway. Earlier chemical analysis of other, similar lycopodium spores⁹ showed that lycopodium is essentially composed of ~ 65% carbon, 10% hydrogen and ~ 25% oxygen. The standance of lycopodium spores of similar chemical and physical properties would imply that this analysis applies to the sample used in this work.

The fourth powder, Polyacrylonitrile (PAN), was obtained from a West-German chemical company. No details of its method of production were available at the time of testing.

Coulter counter analyses

Results from the Coulter analyses are given in Figures A10 to A13. Values of 10%, 50% and 90% undersize, μ - A33 - from these figures, are given in Table A1.

Analyses of the powders

Four powders were used in the dust ignition tests in this work. These were named 'Stabiliser powder', Benzanthron, Lycopodium and Polyacrylonitrile. Each powder was analysed in the following tests:

- a) Particle size distribution using a Coulter counter
- b) Specific surface area using the Ströhlein apparatus
- c) Density, using an air pichnometer
- d) Maximum explosion pressure and rate of pressure rise in the Hartmann-bomb apparatus
- e) Particle shape and form using a scanning electron microscope

General description of each powder

The first powder, the 'stabiliser', was obtained from a West-German chemical company, and was developed as a polymer stabiliser. No details of chemical composition could be obtained for this powder.

The second powder, Benzanthron, was also a West-German product, and like the first, no details could be procured concerning its chemical composition.

The third powder, Lycopodium, was obtained from Norges Medisinaldepot in Bergen, Norway. Earlier chemical analysis of other, similar lycopodium spores⁹ showed that lycopodium is essentially composed of ~ 65% carbon, 10% hydrogen and ~ 25% oxygen. The abundance of lycopodium spores of similar chemical and physical properties would imply that this analysis applies to the sample used in this work.

The fourth powder, Polyacrylonitrile (PAN), was obtained from a West-German chemical company. No details of its method of production were available at the time of testing.

Coulter counter analyses

Results from the Coulter analyses are given in Figures A10 to A13. Values of 10%, 50% and 90% undersize, obtained from these figures, are given in Table A1.

Particle size μm			
Powder	d_{10}	d_{50}	d_{90}
Stabiliser	2.4	7	20
Benzanthron	5.6	21	50
Lycopodium	~ 24	~ 26	~ 27
PAN	5.8	18	35

Table A1. Coulter-counter undersize measurements.

Specific surface area and density measurements

Results from the Ströhlein and density measurements are given below in Table A2.

Powder	True density, gcm^{-3}	Specific surface m^2g^{-1}
Stabiliser	1.10	4.714
Benzanthron	1.38	0.548
Lycopodium	1.09	0.805
PAN	1.22	7.33

Table A2. Ströhlein and density measurements.

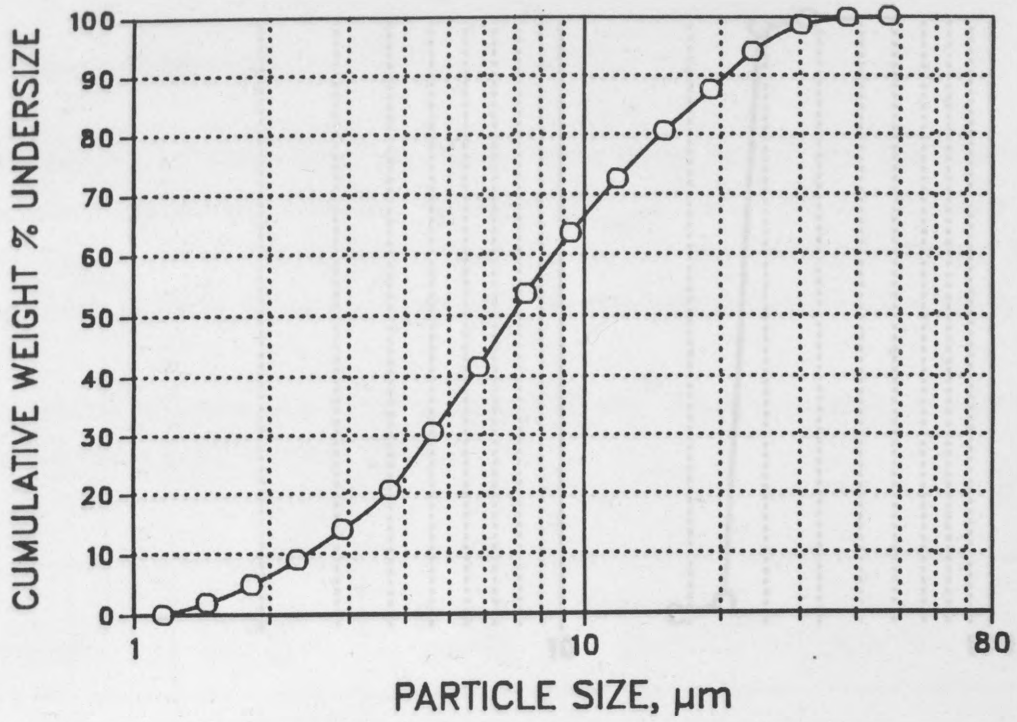


Figure A10. Coulter-counter results for the stabiliser powder.

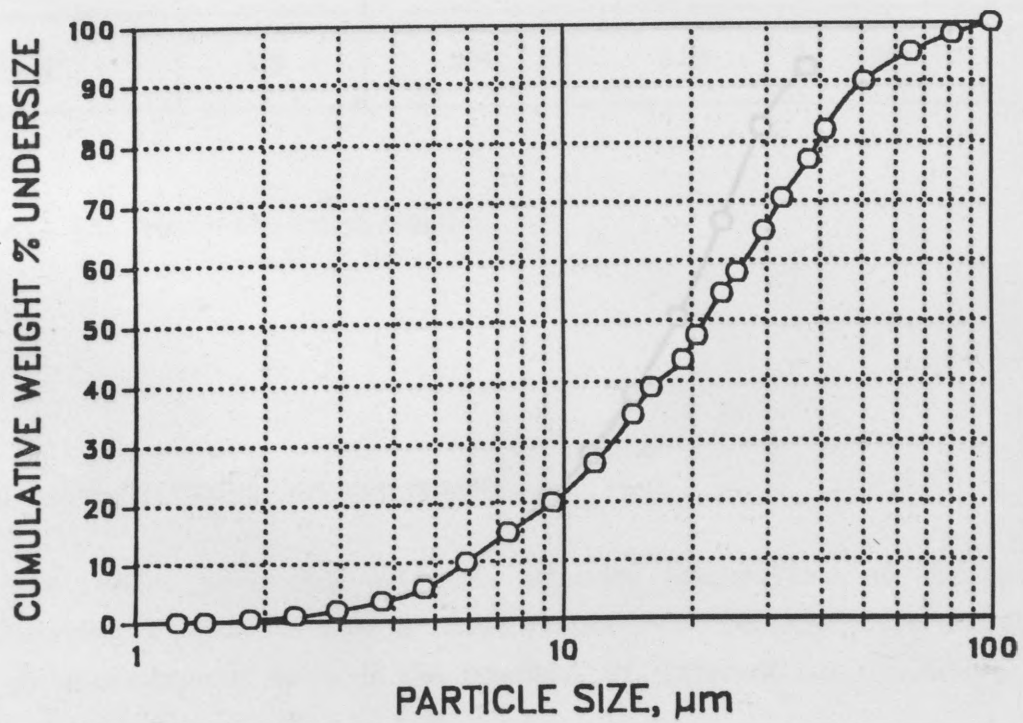


Figure A11. Coulter-counter results for the Benzanthron powder.

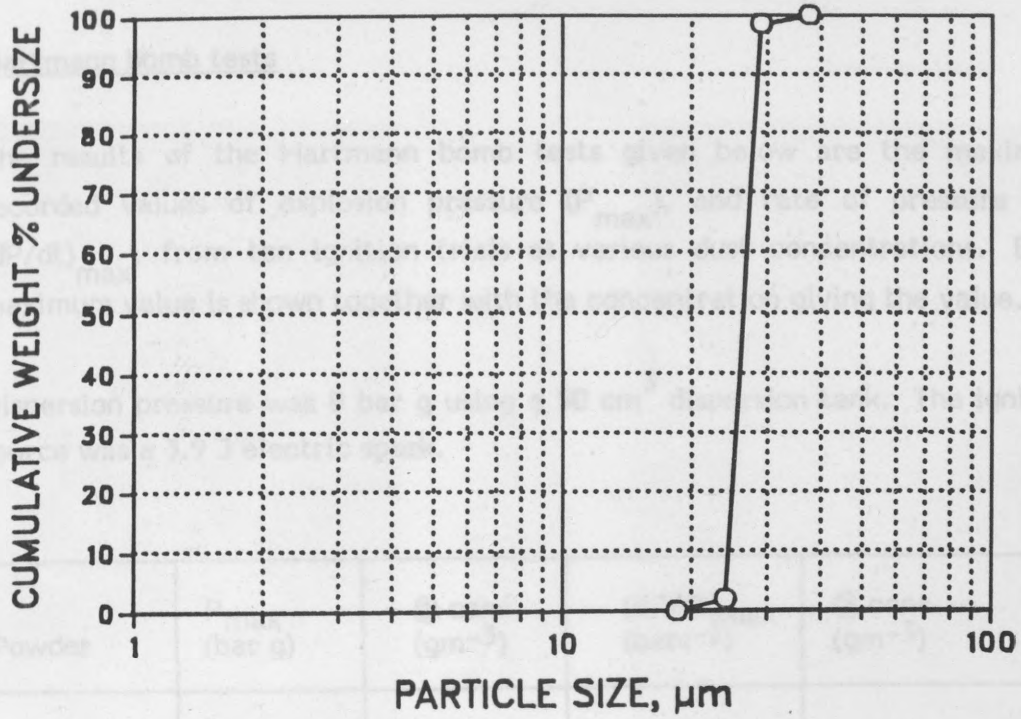


Figure A12. Coulter-counter results for the Lycopodium powder.

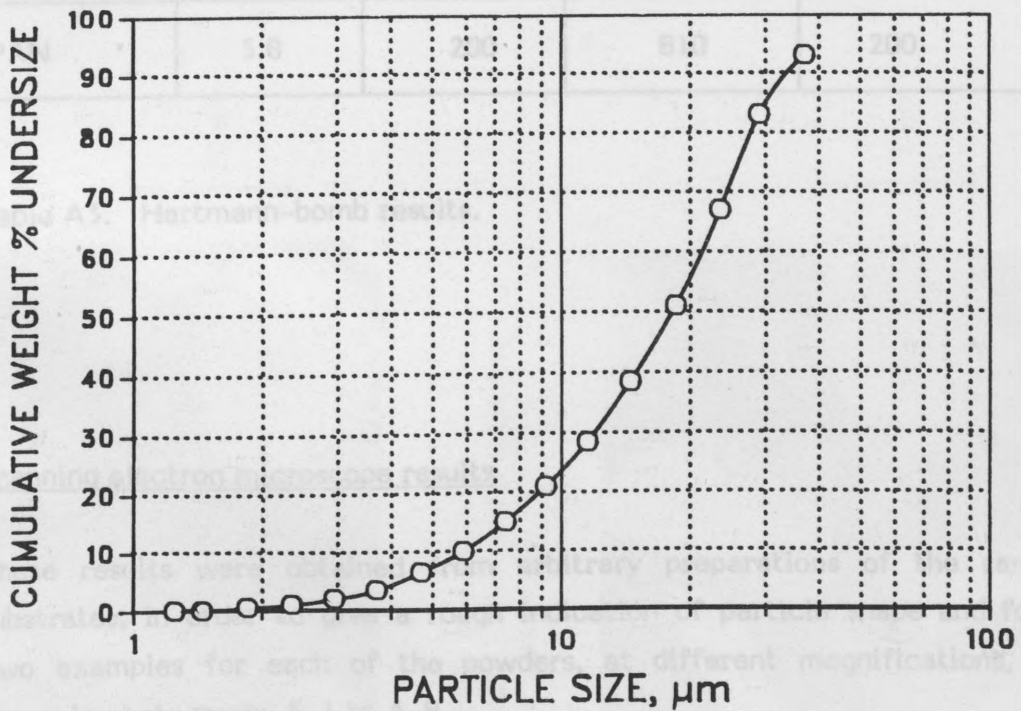


Figure A13. Coulter-counter results for the PAN powder.

Hartmann bomb tests

The results of the Hartmann bomb tests given below are the maximum recorded values of explosion pressure (P_{\max}), and rate of pressure rise $(dP/dt)_{\max}$, from ten ignition trials at various dust concentrations. Each maximum value is shown together with the concentration giving the value.

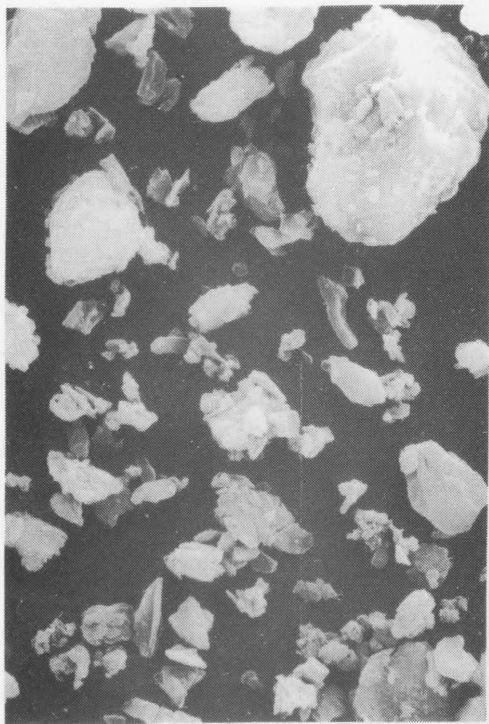
Dispersion pressure was 8 bar g using a 50 cm³ dispersion tank. The ignition source was a 3.9 J electric spark.

Powder	P_{\max} (bar g)	@ conc. (gm ⁻³)	$(dP/dt)_{\max}$ (bars ⁻¹)	@ conc. (gm ⁻³)
Stabiliser	6.3	250	1220	250
Benzanthron	4.7	300	560	300
Lycopodium	4.9	150	480	200
PAN	5.8	200	810	200

Table A3. Hartmann-bomb results.

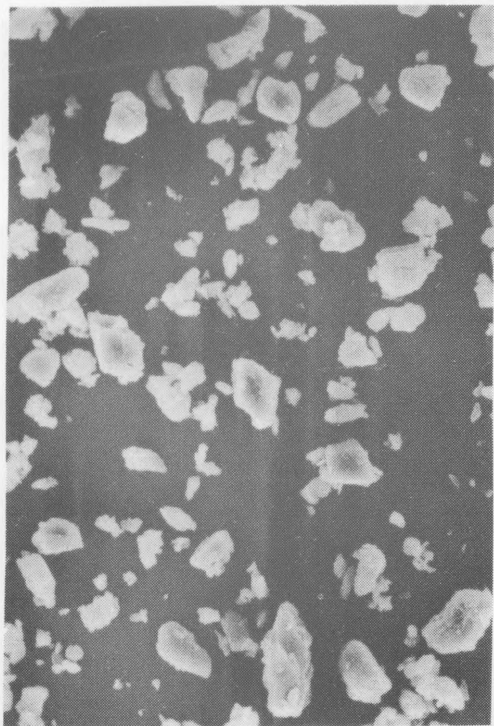
Scanning electron microscope results

These results were obtained from arbitrary preparations of the sample substrates, in order to give a rough indication of particle shape and form. Two examples for each of the powders, at different magnifications, are shown in photographs A-1 to A-8.



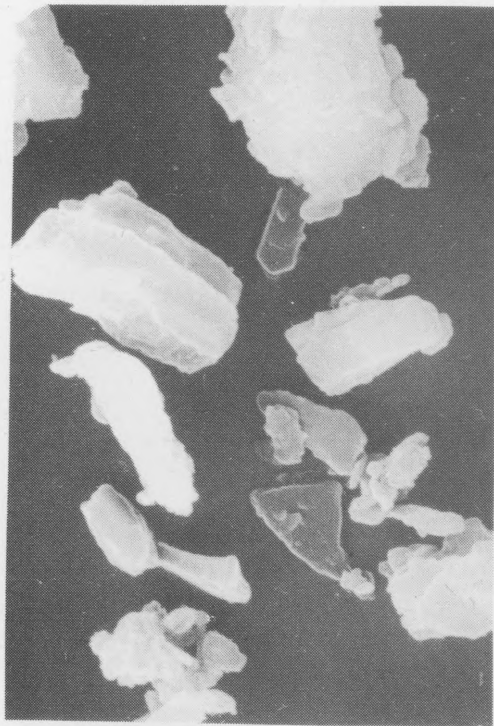
20 μm

Photograph A-1.
'Stabiliser' 1000 X under scanning electron microscope.



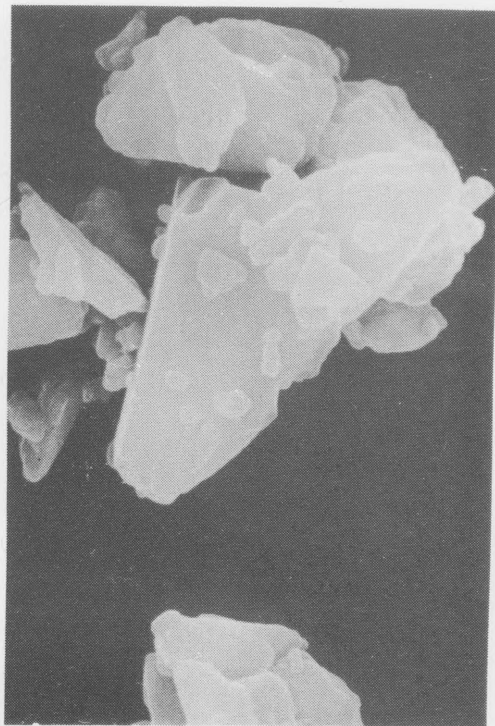
70 μm

Photograph A-3.
'Benzanthron' 300 X under scanning electron microscope.



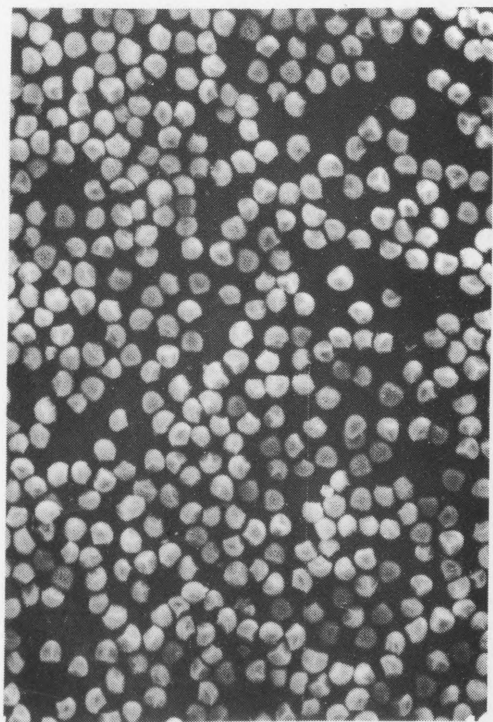
7 μm

Photograph A-2.
'Stabiliser' 3000 X under scanning electron microscope.

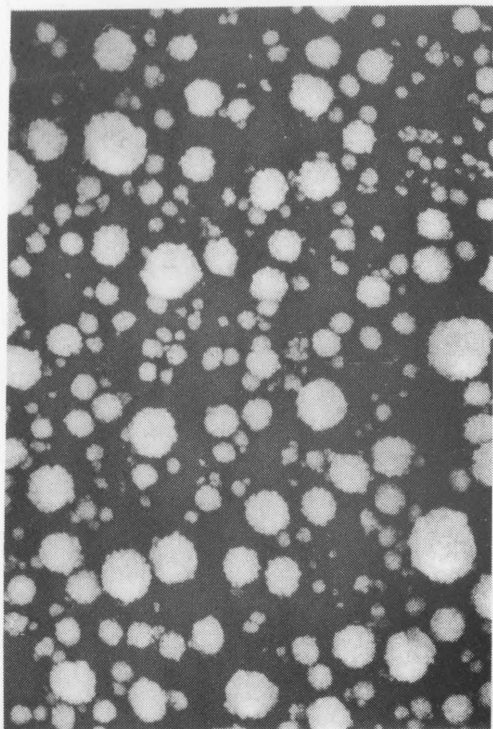


7 μm

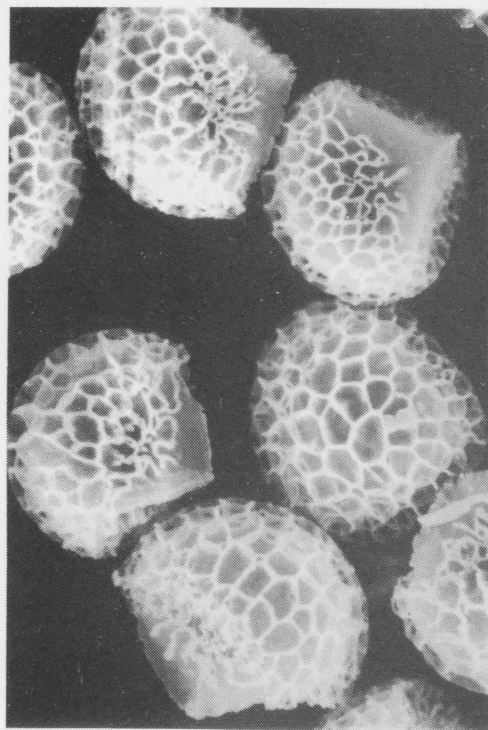
Photograph A-4.
'Benzanthron' 3000 X under scanning electron microscope.



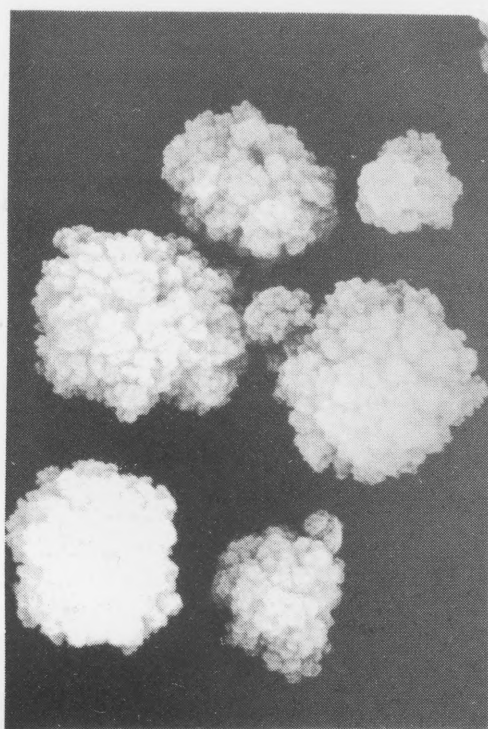
Photograph A-5.
'Lycopodium' 100 X under
scanning electron microscope.



Photograph A-7.
'PAN' 300 X under scanning
electron microscope.



Photograph A-6.
'Lycopodium' 1000 X under
scanning electron microscope.



Photograph A-8.
'PAN' 3000 X under
scanning electron microscope.